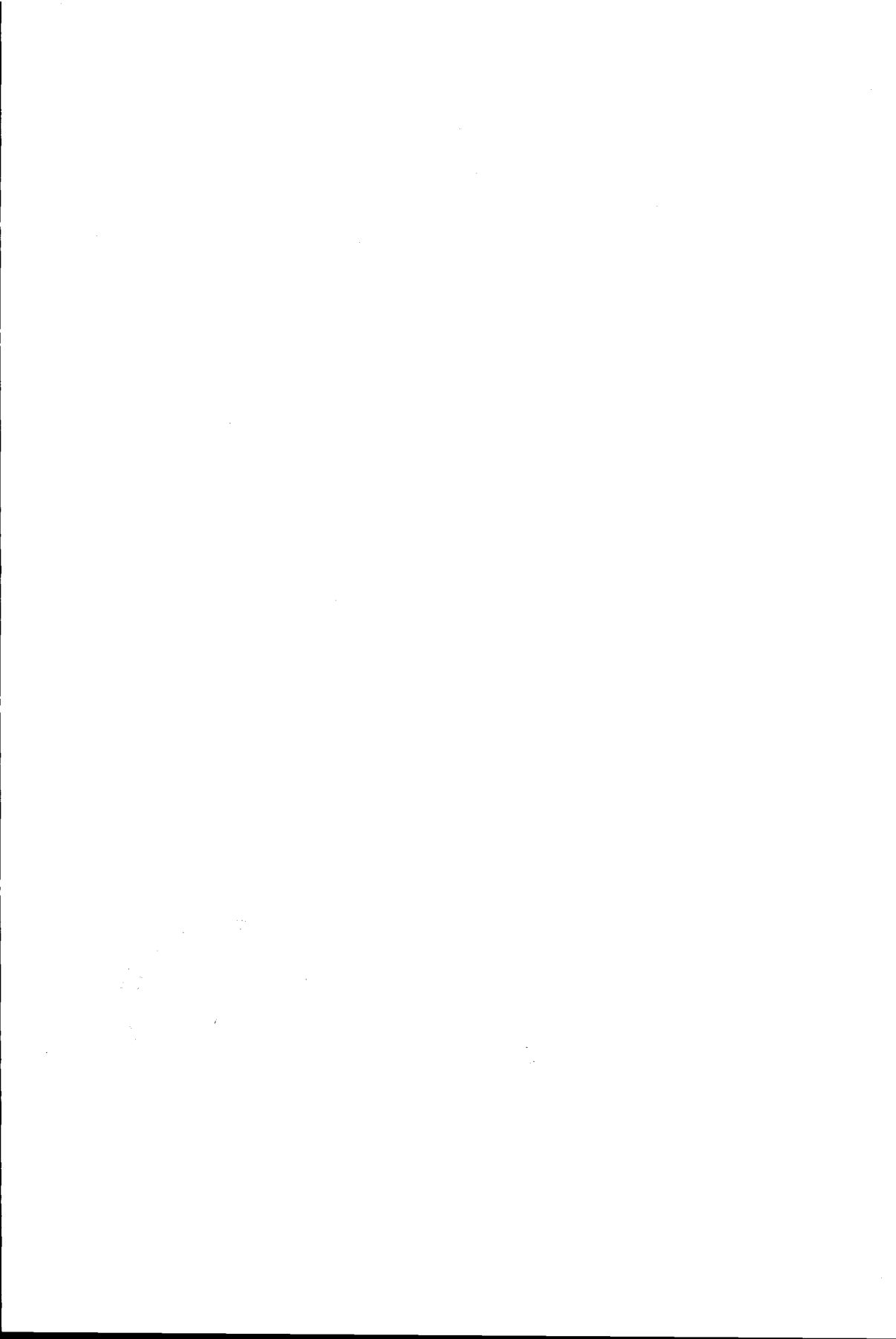


668231  
2269929  
TR diss 2016

**TR diss  
2816**

# **Dynamics of Belt Systems**

**G. LODEWIJKS**



# Dynamics of Belt Systems

PROEFSCHRIFT

ter verkrijging van de graad van doctor  
aan de Technische Universiteit Delft,  
op gezag van de Rector Magnificus Prof. ir. K.F. Wakker,  
in het openbaar te verdedigen ten overstaan van een commissie,  
door het College van Dekanen aangewezen,  
op maandag 14 oktober 1996 te 13.30 uur  
door

Gabriël LODEWIJKS

werktuigkundig ingenieur,  
geboren te Apeldoorn.



Dit proefschrift is goedgekeurd door de promotoren:

Prof. ir. M. van Holst

Prof. dr. ir. P. Meijers

Samenstelling promotiecommissie:

Rector Magnificus, voorzitter

Prof. ir. M. van Holst, promotor Technische Universiteit Delft

Prof. dr. ir. P. Meijers, promotor Technische Universiteit Delft

Prof. Dr.-Ing. W.H.F. Deleroi Technische Universiteit Delft

Prof. dr. ir. H. B. Pacejka Technische Universiteit Delft

Prof. dr. ir. K. van de Werff Technische Universiteit Delft

Prof. Dr.-Ing. M. Hager Universität Hannover

Dr. ir. J.P. Meijaard Technische Universiteit Delft

CIP-DATA KONINKLIJKE BIBLIOTHEEK, DEN HAAG

Lodewijks, Gabriël

Dynamics of Belt Systems / Gabriël Lodewijks. - Delft : Delft University of Technology, Faculty of Mechanical Engineering and Marine Technology. - Ill.

Thesis Technische Universiteit Delft. - With ref.

ISBN 90-370-0145-9

Subject headings: belt conveyors / dynamics / finite element method / simulation.

Copyright © 1996 by Gabriël Lodewijks

All rights reserved. No part of this publication may be reproduced, stored in a retrieval system, or transmitted, in any form or by any means, electronic, mechanical, photocopying, recording, or otherwise, without the prior permission of the author.

PRINTED IN THE NETHERLANDS  
BY UNIVERSITEITSDRUKKERIJ, DELFT



to my father and my son



# Summary

---

This thesis focuses on the dynamics of belt systems for bulk solids transport. Starting from a number of specific belt parameters, the dynamic behaviour of a belt system is mathematically described using an analytical as well as a discrete, or finite element, approach. The analytical approach is only applicable to describe the dynamic behaviour of a simplified belt system during stationary operation whereas the discrete approach is the only approach for real complicated systems to describe both the stationary and the non-stationary operation.

The analysis of the stationary operation of belt systems focuses on the determination of the amplitudes of transverse vibration of belt spans supported by two rolls. For this purpose a system of two coupled equations of motion is derived. The amplitude of transverse vibration of a belt span is normally small and the linear solution of the equations of motion is accurate. However, if a belt span is excited in or near a resonance frequency due to direct or parametric excitation, this amplitude can increase considerably and only the non-linear solution is accurate. An asymptotic non-linear solution, based on a perturbation method, is given and has been verified by experiments. Based on the results of this verification, criteria have been set up to design so-called resonance free belt supports.

The analysis of the non-stationary operation of belt systems focuses on the question whether the transient belt tension is admissible and whether the performance of the system is acceptable. A software system called **TUDBELT**, based on the finite element method, has been developed for this purpose. The structure of **TUDBELT** is object-oriented and includes a description of all major components of belt conveyer systems. With this software system calculations can be performed to simulate the non-linear dynamic behaviour of a belt system. The finite element description also includes a detailed description of the motion resistances of the belt and the dynamics of the drive system. A number of simulations have been performed to determine the influence of the start-up procedure, specified in velocity profile and duration of the procedure, on the maximum belt tension and the performance of the belt system. The results of these simulations are compared with the results of simplified analyses.

As an example a horizontal belt conveyor system of 1 kilometre length driven by an induction motor, controlled by a static power converter (SPC), has been chosen. The shortest start-up time can be obtained when the acceleration of the drive pulley is kept constant and the start-up supply frequency of the SPC is about 10 to 20 % of the stationary supply frequency. A good estimation of the upper limit of the start-up time for the considered conveyor in case of a start-up with constant acceleration can be achieved using the maximum belt force during stationary operation, the maximum acceleration force, the required safety factors on the belt tension during stationary and non-stationary operation and the stationary belt speed.

# Samenvatting

---

In dit proefschrift ligt het accent op de dynamica van bandtransporteurs. Uitgaande van een aantal karakteristieke bandparameters, is het dynamisch gedrag een bandsysteem wiskundig beschreven volgens zowel een analytische als een discrete, of eindige elementen, benadering. De analytische benadering is alleen bruikbaar voor de beschrijving van het dynamisch gedrag van een vereenvoudigd bandsysteem tijdens de stationaire toestand. De discrete benadering daarentegen, is de enige benadering waarmee het dynamisch gedrag van gecompliceerde bandsystemen tijdens zowel de stationaire als de instationaire toestand beschreven kan worden.

Bij de analyse van de stationaire toestand gaat de aandacht met name uit naar de amplitudes van transversale trillingen in bandsegmenten ondersteund door twee rollen. Hiervoor is een gekoppeld stelsel van twee bewegingsvergelijkingen afgeleid. Normaal zijn de trillingsamplituden klein en is de lineaire oplossing van het stelsel van bewegingsvergelijkingen nauwkeurig. In geval van directe of parametrische excitatie van een bandsegment in of dichtbij een eigenfrequentie kunnen deze amplitudes aanzienlijk zijn en is alleen de niet-lineaire oplossing nauwkeurig. Een asymptotische, niet-lineaire oplossing, gebaseerd op een perturbatie methode, is gegeven en geverifieerd met behulp van experimenten. Op grond van de deze verificatie zijn criteria opgesteld waarmee zogenaamde "resonantie vrije bandondersteuning" ontworpen kunnen worden.

De analyse van de niet stationaire toestand is vooral gericht op de vraag of de bandspanningen tijdens die toestand toelaatbaar zijn en of het bandsysteem op acceptabele wijze functioneert. Voor deze analyse is het computerprogramma **TUDBELT** geschreven, gebaseerd op een eindige elementen model. De structuur van **TUDBELT** is object georiënteerd en bevat een beschrijving van alle belangrijke componenten van een bandtransporteur. Met dit programma kunnen berekeningen worden uitgevoerd waarmee het niet-lineaire dynamisch gedrag van een bandsysteem gesimuleerd kan worden. Bij de eindige elementen beschrijving van de bandtransporteur is ook aandacht besteed aan de bewegingsweerstand die een band ondervindt en de dynamica van de elektrische aandrijving. Met het computerprogramma zijn een aantal simulaties uitgevoerd om de invloed van de aanlooppprocedure, gespecificeerd door snelheidsprofiel en tijdsduur, te onderzoeken

op de maximale bandspanning en het functioneren van een bandtransporteur. De resultaten van deze simulaties zijn vergeleken met de resultaten van vereenvoudigde berekeningsmethoden.

Als voorbeeld is gekozen voor een horizontale, 1 kilometer lange transporteur die wordt aangedreven door een elektromotor gestuurd door een frequentieregelaar. Gebleken is dat de kortste aanlooptijd gerealiseerd kan worden wanneer de versnelling van de aandrijftrommel constant wordt gehouden en de frequentieregelaar een startfrequentie heeft van ongeveer 10 tot 20 % van de stuurfrequentie tijdens stationair bedrijf. Tevens is gebleken dat in dit geval, uitgaande van de maximale bandkracht tijdens stationair bedrijf, de maximale acceleratiekracht, de veiligheidsfactoren op de bandspanning tijdens stationair en instationair bedrijf en de bandsnelheid tijdens stationair bedrijf, een goede bovengrens voor de tijdsduur van de aanlooptprocedure met constante versnelling gevonden kan worden.

# Contents

---

<b>Summary</b>	<b>vii</b>
<b>Samenvatting</b>	<b>x</b>
<b>Nomenclature</b>	<b>xvii</b>
<b>Chapter 1 Introduction</b>	<b>1</b>
1.1 Aim and scope of the study	3
1.2 Contents of the thesis	4
<b>Chapter 2 General theory</b>	<b>7</b>
2.1 Mathematical background and techniques	7
2.2.1 Matrices and vectors	7
2.2.2 Vector valued functions and maps	8
2.2 Finite element techniques	11
2.2.1 Finite element description	11
2.2.2 Transfer functions	13
2.2.3 The equations of motion	17
2.2.4 Kinematic analysis	18
2.2.5 Kinetostatic analysis	20
2.3 Software engineering	21
2.3.1 Object oriented software engineering	21
2.3.2 TAKEOFF	22
2.3.3 FLIGHT	28
2.3.4 LANDING	28
2.4 References	29

<b>Chapter 3 Belt properties</b>	<b>31</b>
3.1 Carcass properties	31
3.1.1 Unit strength	32
3.1.2 Young's modulus	34
3.1.3 Bending stiffness	37
3.1.4 Belt tension related parameters	39
3.2 Cover properties	42
3.3 References	46
<b>Chapter 4 Analytical modelling of belt systems</b>	<b>49</b>
4.1 Introduction	49
4.1.1 String-like systems	50
4.1.2 Beam-like systems	51
4.2 Dynamics of a stationary moving belt	52
4.2.1 Deformation of the belt	52
4.2.2 Equations of motion	54
4.2.3 Linear solution	58
4.2.3.1 Axial vibration	58
4.2.3.2 Transverse vibration of a string	60
4.2.3.3 Transverse vibration of a beam	62
4.2.3.4 Transverse vibration of a beam with string effect	63
4.2.4 Nonlinear solution	64
4.2.4.1 Method of solution	64
4.2.4.2 Non moving belt	68
4.2.4.3 Stationary moving belt	74
4.2.5 Parametric excitation	76
4.3 References	77
<b>Chapter 5 Motion resistances of belt conveyors</b>	<b>81</b>
5.1 The rolling resistance	81
5.1.1 The indentation rolling resistance	82
5.1.2 The inertia of the idlers	91
5.1.3 The rolling resistance of the bearings	91
5.1.4 The total rolling resistance	91
5.2 Motion resistance of horizontally curved belt sections	92
5.3 References	96



---

<b>Chapter 6 The belt conveyor drive system</b>	<b>97</b>
6.1 Technical requirements of a drive system	97
6.1.1 Starting and stopping procedures	97
6.1.2 Overload protection	100
6.1.3 Drive requirements	101
6.2 Components of a drive system	101
6.3 Static power converter	103
6.4 Induction motor	103
6.4.1 The electromagnetic couple	104
6.4.2 Induction motor parameters	111
6.4.3 Steady state torque of an induction motor	112
6.4.4 Simulation of a start of an induction motor	114
6.5 Fluid coupling	115
6.6 Drum brake	117
6.7 Reduction box	118
6.8 Disc pack	119
6.9 References	121
<b>Chapter 7 Discrete modelling of belt systems</b>	<b>123</b>
7.1 Introduction	123
7.2 Finite element models of belt conveyors	126
7.2.1 Belt elements	130
7.2.1.1 Truss	130
7.2.1.2 Truss with belt sag	131
7.2.1.3 Beam	133
7.2.1.4 Idler supported beam	135
7.2.1.5 Pulley supported beam	136
7.2.1.6 Plate supported beam	138
7.2.2 Dynamic characteristics	138
7.2.3 Electrical and mechanical elements of belt conveyor systems	144
7.2.3.1 Torsion	144
7.2.3.2 Induction motor	144
7.2.3.3 Fluid coupling	145
7.2.3.4 Drum brake and back stop	145
7.2.3.5 Reduction box	145
7.2.3.6 Pulley transition	146
7.3 References	146

---

<b>Chapter 8 Numerical results of belt conveyor simulations</b>	<b>151</b>
8.1 Problem description	151
8.2 Calculation according to DIN 22101	152
8.3 Finite element models	157
8.4 Model implications	159
8.4.1 Frequency of axial vibration	159
8.4.2 Frequency of transverse vibration	161
8.4.3 Wave propagation	166
8.4.4 Bulk solid material stream	168
8.5 Start-up of an inextensible conveyor belt	171
8.6 Start-up of an elastic conveyor belt	174
8.6.1 Direct start	174
8.6.2 Velocity controlled start	179
8.6.2.1 Linear offset start-up procedure	179
8.6.2.2 Alternative velocity controlled start-ups	184
8.6.3 Estimation of the start-up time	186
8.6.3 Application of beam elements	189
8.7 Conclusions	192
8.8 References	194
<b>Chapter 9 Experimental analysis of transverse belt vibrations</b>	<b>195</b>
9.1 Introductory experiment	195
9.2 Test facility	200
9.2.1 Acoustic displacement meter	202
9.2.2 Idler spacing adjustment	202
9.2.3 Belt tension adjustment	202
9.2.4 Belt speed adjustment	204
9.2.5 Signal processing	205
9.3 Experimental program	205
9.3.1 Experimental data	205
9.3.2 Installed conveyor belts	207
9.4 Results of the experiments	207
9.5 Application of the experimental results	212
9.6 References	214
<b>Chapter 10 Design aspects, conclusions and recommendations</b>	<b>215</b>
10.1 Stationary operation	215
10.2 Non-stationary operation	216
10.3 Calculation methods	217

10.4	Belt parameters	219
10.5	Conclusions on the developed software system	220
10.6	Recommendations on model development	221
<i>Appendix A</i>	<b>Distribution of the belt and bulk mass</b>	<b>223</b>
<i>Appendix B</i>	<b>Experimental data</b>	<b>227</b>
	B.1 Experimental data conveyor belt EP 120/1	228
	B.2 Experimental data conveyor belt EP 200/2	231
	B.3 Experimental data conveyor belt EP 240/2	234
	B.4 Experimental data conveyor belt EP 360/3	237
<i>Appendix C</i>	<b>Computational data</b>	<b>241</b>
<i>Appendix D</i>	<b>Measured belt properties</b>	<b>245</b>
	<b>Acknowledgements</b>	<b>251</b>
	<b>Curriculum Vitae</b>	<b>253</b>



# Nomenclature

---

## Capitals

A	cross sectional area of the belt	[m <sup>2</sup> ]
A <sub>bulk</sub>	cross sectional area of the bulk solid material	[m <sup>2</sup> ]
A <sub>C</sub>	cross sectional area of a steelcord	[m <sup>2</sup> ]
A <sub>M</sub>	cross sectional area of a steelcord carcass	[m <sup>2</sup> ]
B	belt width	[m]
C <sub>des</sub>	design capacity of a belt conveyor system	[kg.s <sup>-1</sup> ]
C <sub>L</sub>	mass ratio of a loaded belt	[-]
C <sub>U</sub>	mass ratio of an unloaded belt	[-]
C <sub>i</sub>	reference configuration	[-]
D	diameter of an idler roll	[m]
D <sub>0</sub>	diameter of an idler roll accounting for the curvature of the belt	[m]
D <sub>i</sub> /D <sub>i</sub>	linear/nonlinear deformation function	[-]
E'	storage modulus	[N.m <sup>-2</sup> ]
E''	loss modulus	[N.m <sup>-2</sup> ]
E*	lateral flexibility	[N.m <sup>-3</sup> ]
E <sub>b</sub>	effective Young's modulus of a belt	[N.m <sup>-2</sup> ]
E <sub>c</sub>	Young's modulus of a carcass	[N.m <sup>-2</sup> ]
E <sub>d</sub>	dynamic Young's modulus of a belt	[N.m <sup>-2</sup> ]
E <sub>m</sub>	Young's modulus of the matrix material	[N.m <sup>-2</sup> ]
E <sub>s</sub>	Young's modulus of a steelcord	[N.m <sup>-2</sup> ]
E <sub>1,2</sub>	Young's moduli of the three parameter solid model	[N.m <sup>-2</sup> ]
F <sub>B</sub>	breaking strength of a yarn or cable	[N]
F <sub>d</sub>	drive force	[N]
F <sub>G</sub>	belt guiding force due to vertical belt and bulk material load	[N]
F <sub>i</sub>	indentation rolling resistance force per unit width	[N.m <sup>-1</sup> ]
F <sub>i</sub>	kinematic transfer function	[-]
F <sub>R</sub>	belt guiding force due to friction	[N]
F <sub>T</sub>	traction force	[N]
F <sub>Z</sub>	vertical belt load per unit width	[N.m <sup>-1</sup> ]
I <sub>n</sub>	nominal motor current	[A]
I <sub>roll</sub>	moment of inertia of an idler roll	[m <sup>4</sup> ]
I <sub>y</sub>	moment of inertia of a belt with respect to the x-axis	[m <sup>4</sup> ]
K <sub>A</sub>	start-up factor	[-]
K <sub>S</sub>	static belt sag ratio	[-]

## Nomenclature

---

$L$	idler spacing	[m]
$L_{\text{conv}}$	conveyor length	[m]
$L_r$	rotor inductance	[ $\Omega$ ]
$L_s$	stator inductance	[ $\Omega$ ]
$L_{\text{conv}}$	length of the belt conveyor system	[m]
$M$	mass matrix	[-]
$M_f$	resistance moment of a bearing of an idler roll	[N.m]
$M_r$	mutual inductance between two rotor phases	[ $\Omega$ ]
$M_s$	mutual inductance between two stator phases	[ $\Omega$ ]
$M_{sr}$	mutual inductance between a stator and a rotor phase	[ $\Omega$ ]
$N$	matrix of shape functions	[-]
$N_c$	number of steelcords per mm belt width	[m <sup>-1</sup> ]
$N_f$	number of fabric plies in a carcass	[-]
$N_y$	number of yarns per mm fabric width	[m <sup>-1</sup> ]
$P_0^2$	dimensionless flexural stiffness	[-]
$P_1^2$	inverse initial static strain	[-]
$P_{cr}$	Euler buckling load	[N]
$R$	radius of an idler roll	[m]
$R_r$	rotor resistance	[ $\Omega$ ]
$R_s$	stator resistance	[ $\Omega$ ]
$R_{ch}$	radius of a horizontal curve	[m]
$S$	actual safety factor	[-]
$S_A$	safety factor of a nonstationary moving belt	[-]
$S_B$	safety factor of a stationary moving belt	[-]
$S$	matrix of elasticity constants	[-]
$S_d$	matrix of damping constants	[-]
$T$	belt tension	[N]
$T_a$	start-up time	[s]
$U$	dimensionless axial displacement	[-]
$U_n$	nominal motor voltage	[V]
$V$	dimensionless transverse displacement	[-]
$V_b$	belt speed	[m.s <sup>-1</sup> ]
$V_C$	volume fraction of carcass material in a belt	[-]
$X$	dimensionless axial co-ordinate	[-]
$Z$	nominal impedance	[ $\Omega$ ]

## Non capitals

$a$	dimensionless amplitude	[-]
$c_1$	longitudinal wave speed	[m.s <sup>-1</sup> ]
$c_2$	axial propagation speed of transverse waves	[m.s <sup>-1</sup> ]
$b_s$	total thickness of the side covers of a belt	[m]
$d_b$	total thickness of a belt	[m]
$d_c$	thickness of a carcass	[m]
$d_f$	thickness of a fabric ply	[m]

$d_l$	thickness of lower belt cover	[m]
$d_m$	mean tickness of a belt cover	[m]
$d_u$	thickness of upper belt cover	[m]
$\mathbf{f}$	force vector	[-]
$f_a$	acceleration rolling resistance factor	[-]
$f_{ar}$	horizontal curve resistance factor	[-]
$f_b$	bearing rolling resistance factor	[-]
$f_c$	steel cord fill factor	[-]
$f_i$	indentation rolling resistance factor	[-]
$f_s$	correction factor for the indentation rolling resistance factor	[-]
$f_t$	total rolling resistance factor	[-]
$h$	thickness of visco-elastic belt under cover	[m]
$i_s$	supply current	[A]
$i_y$	radius of gyration	[m]
$\mathbf{i}$	vector of phase currents	[-]
$k_B$	bending rigidity parameter	[-]
$k_C$	unit strength of a carcass	[N.mm <sup>-1</sup> ]
$k_F$	unit fabric strength	[N.mm <sup>-1</sup> ]
$k_N$	standarised unit strength of a belt	[N.mm <sup>-1</sup> ]
$l$	length of a deformed element	[m]
$l_0$	initial length of an element	[m]
$m'_{belt}$	belt mass per unit of length	[kg.m <sup>-1</sup> ]
$m'_{bulk}$	mass of the bulk material on the belt per unit of length	[kg.m <sup>-1</sup> ]
$m'_{roll}$	reduced mass of the idlers per unit of length	[kg.m <sup>-1</sup> ]
$m_{red}$	reduced mass of an idler	[kg]
$n$	number of revolutions of a shaft	[rpm]
$p$	number of pole pairs	[-]
$q$	distibuted belt load	[N.m <sup>-1</sup> ]
$q_i$	component of the vector of independent nodal co-ordinates and deformations	[-]
$r$	internal roll radius	[m]
$r_{0,1,2}$	reduction factor of the safety factor	[-]
$s$	slip	[-]
$t$	time	[s]
$u$	axial displacement	[m]
$\mathbf{u}$	vector of phase voltages	[-]
$u_s$	supply voltage	[V]
$v$	transverse displacement	[m]
$x$	cartesian co-ordinate	[-]
$x_i$	nodal co-ordinate	[-]
$y$	cartesian co-ordinate	[-]
$z$	cartesian co-ordinate	[-]

## Nomenclature

---

### Greek capitals

$\Gamma$	load ratio	[-]
$\Phi$	retardation function	[-]
$\Psi$	relaxation function	[N.m <sup>-2</sup> ]
$\Omega$	dimensionless frequency	[-]

### Greek non capitals

$\alpha_{1,2}$	trough angles	[-]
$\beta$	speed ratio	[-]
$\gamma$	deformation tensor	[-]
$\delta$	loss angle	[-]
$\delta_s$	inclination angle of a belt conveyor system	[-]
$\varepsilon$	strain	[-]
$\varepsilon_i$	generalised strain	[-]
$\eta$	damping factor	[N.m <sup>-2</sup> .s]
$\eta_{cf}$	fabric strength efficiency in a carcass	[-]
$\eta_{fc}$	steel wire efficiency in a steelcord	[-]
$\eta_{fy}$	yarn strength efficiency in fabric	[-]
$\vartheta$	tilt angle of an idler station	[-]
$\theta$	super elevation angle of an idler station (Chapter 5) / rotor angle (Chapter 6)	[-]
$\kappa$	ratio between the stiffness of the belt tensioner and that of the belt	[-]
$\mu$	perturbation parameter	[-]
$\mu_{br}$	friction coefficient between belt and idler roll	[-]
$\nu$	Poisson's ratio	[-]
$\xi$	length co-ordinate	[-]
$\rho$	density of the belt material	[kg.m <sup>-3</sup> ]
$\rho_{bulk}$	density of the bulk solid material	[kg.m <sup>-3</sup> ]
$\sigma$	stress	[N.m <sup>-2</sup> ]
$\sigma_i$	generalised stress	[N.m]
$\tau$	relaxation time	[s]
$\varphi_0$	angle of surcharge	[-]
$\psi_{1,2}$	alignment angles	[-]
$\omega$	frequency	[s <sup>-1</sup> ]



# Chapter 1

## Introduction

---

**B**elts, tapes and cables, just as beams and rods in general, have in common that the dimension in one direction, referred to as the axial direction, is much larger than in the other two directions. In many cases a one-dimensional approach is eligible for a proper description of the configuration. If belts, tapes and cables are applied in mechanical systems like belt conveyors, tape recorders and monocabable ropeways, they are often referred to as axially moving materials or axially moving continua. In this thesis the name axially moving materials is adopted. Other examples of the application of axially moving materials encompasses mechanical systems such as high-speed magnetic and paper tapes, cable tramways, skilifts, band saws, axially moving threadlines, strings, wires and fibres, pipes that contain flowing fluid and power transmission chains and belts.

In this thesis systems that combine a belt and a supporting structure to transport information, energy and/or materials are called belt systems. In belt systems the belt may be supported by rolls or wheels and plates or bars, or by an air film. The belt may be endless and can be used as a carrier of information or materials, or the belt itself can be transported. In general an endless belt is a permanent part of a system whereas a non endless belt is mostly not a permanent part of a system.

The dynamic behaviour of a belt system depends on the belt load, the properties of the belt, the characteristics of the support structure, including the drive system, and the interaction between belt and support structure. Important properties of the belt, which also determine the propagation speed of stress waves in the belt and its energy consumption, include the density of the belt material, Young's modulus, the flexural rigidity and the visco-elastic properties of the belt covers. The characteristics of the belt support structure include the drive characteristics, the rotational inertia of the rolls and pulleys, and the friction in their bearings. The interaction between the belt and the support structure is mainly determined by the belt tensioner, the roll or idler spacing, the roll diameters and the belt speed.

The dynamic behaviour of a belt system can be ascertained by determination of vibrations of the belt and the belt tensioner. Severe belt vibrations should be

prevented since they cause operational and maintenance problems, including excessive wear of the belt and the support components, and an increase of the energy consumption of the system. The frequencies of transverse vibrations of the belt, however, indicate the belt tension and its condition and therefore these frequencies can be used in monitoring systems. The analysis of the vibrations and the dynamic stability of belt systems and also the prediction of the response to general excitation are essential to the optimal design of a broad class of technical devices. A distinction can be made between the dynamic behaviour of belt segments or belt spans and that of the entire belt system.

If the dynamic behaviour of one belt span is of interest it may be considered as uncoupled and isolated from the remainder of the system by its support by wheels, rolls, pulleys or guide bearings, assuming high wheel inertia, infinite rigidity of the supporting structure and negligible belt sag compared to the roll or idler spacing. Excitation of transverse vibrations caused by the interaction of the belt and its supports is common and significant. Roll eccentricities and belt imperfection, in particular those in the belt splice, are major causes of these excitations. During the manufacturing process a number of imperfections will be introduced into the belt. These imperfections may be geometric in nature, such as thickness or width variations, or possibly changes in the mechanical properties of the cross section. Resonance phenomena occur when the excitation frequency approaches a natural frequency of the moving supported belt span. In addition to resonance due to direct excitation, axially moving materials may exhibit instabilities due to parametric excitations caused by belt tension fluctuations. The natural frequencies of transverse vibration of an axially moving belt decrease with increasing belt speed. At a critical belt speed these frequencies are zero. This critical speed increases with increasing longitudinal velocity of the transverse waves.

Transverse vibrations of an endless belt couple the response of the entire belt to that of the support rolls or wheels. The model describing the motion of one span cannot be uncoupled from the remainder of the system without loss of model validity. The static belt sag couples the different spans and the wheels. Wheel or roll inertia, stiffness of the belt tensioner and the belt tension and speed are other parameters that govern the degree of coupling. Besides the resonance phenomena mentioned above, tensioner resonance may also occur in a belt system when the excitation frequency is equal to the natural frequency of the (spring) tensioner system.

The travelling flexible string and the travelling, tensioned Euler-Bernoulli beam are the most common models of axially moving materials. Due to the simplicity of the linear models that are usually used, their responses to general excitation and given initial conditions do not represent the true responses in case of low belt tension or large belt sag which cause large amplitudes of vibration. Analytical studies of non-linear models based on a perturbation method can be used to improve the solution obtained from the linear approach. To determine the response of a total belt system,

including the support rolls or wheels, models based on the finite element method (FEM) are best suitable.

## 1.1 Aim and scope of the study

This study focuses on the application of models of belt systems used in the field of bulk solids transport. In view of their world-wide use and proven reliability, belt conveyors are of considerable importance for continuous transport of bulk solids. Due to improvements in design procedures and in the manufacturing of belt conveyor systems, the use of belt conveyors is no longer restricted to in-plant movement of bulk solid materials and they are now used for long distance overland transportation as well.

Current belt conveyor research and development cover the following areas:

- 1) belt conveyor dynamics, including:
  - design of starting and stopping procedures
  - determination of dynamic belt stresses
  - transverse vibrations of conveyor belts and the influence of idler spacing and troughing configuration
  - stability of motion of belts and the bulk solid on conveyor belts
  - booster drives to reduce belt tensions and permit longer individual span length
- 2) belt monitoring, including:
  - belt tension monitoring employing acoustic and electro-magnetic devices
  - belt crack detection employing ultra-sonic devices
- 3) conveyor belt performance and economics, including:
  - calculation of the rolling resistance, taking into account belt rubber hardness, sag, troughing configuration, idler/belt interaction and ambient operating temperature
  - conveyor belt/drive drum friction, taking into account rubber hardness, surface roughness and wrap angle
- 4) design of transition geometries, including:
  - design of horizontal and vertical curves
  - design of troughing zones
- 5) splice design and analysis
- 6) belt cleaning including carry-back measurement and development of improved cleaning efficiencies
- 7) improved quality control in belt and component manufacturing

The first three subjects are considered in this thesis. Starting from finite element (FE) models of belt conveyors described in the literature, a new FE-model has been developed. Current FE-models of belt conveyors can only simulate the axial elastic response of the belt to general excitation and given initial conditions. However, an important aspect of modern belt conveyor design is the analysis of resonance phenomena in an axially moving belt span supported by two idlers. To consider both axial and transverse elastic response of the belt, the new FE-model permits simulation of the transverse elastic response and coupling of the axial and transverse responses. This allows the design of belt supports that prevent resonance of transverse vibration of the belt, the so-called resonance free belt supports, and the solution of operational problems including the lifting of the belt from its supports. To determine the nature of transverse belt vibrations and the parameters which govern these vibrations an analytical approach is used. The accuracy of the results obtained from this approach has been verified by experiments. During the design process of a belt conveyor system the choice of the type of the conveyor belt to be used is important since the dynamic performance of the belt mainly depends on its mechanical properties. These properties were included in the model to enable comparison between different types of belts. To maintain a consistent level of accuracy of the total model this demanded the development of accurate models of the drive system and the resistances met by the belt during motion through the conveyor. To facilitate the application of the knowledge gained in this research project, simulation tools have been developed which can be used in the design stage of belt conveyor systems.

## 1.2 Contents of the thesis

Chapter 2 is devoted to essential aspects of the mathematical and finite element techniques, and to software engineering.

In Chapter 3 the material properties of belts are highlighted. A number of characteristic ratios have been derived which enable a quick comparison of the relevant properties of different types of belts. These ratios are used in the following chapters.

Chapter 4 addresses the analytical modelling of general belt systems. An overview of models described in the literature is given and a model which can be used to determine the transverse vibration of a belt span has been derived.

Chapter 5 deals with the motion resistance of belt conveyors, in particular the indentation rolling resistance of the belt and the resistance in horizontal curves.

In Chapter 6 the components of a drive system are highlighted. An explanation of the components that are used and the criteria that affect the selection of these components is given.

Chapter 7 is devoted to the discrete modelling of belt systems. A finite element representation of the belt and the drive components is presented. The results from simulations with this model are shown in Chapter 8.

In Chapter 9 the transverse vibrations of belt spans are investigated. The relation between the frequency of transverse vibration and the axial belt speed is shown and its practical relevance is illustrated. The results obtained from experiments are used to verify the theoretical models derived in previous chapters.

Chapter 10 is devoted to the conclusions, design aspects and practical recommendations. In particular, methods to select an optimal start-up procedure of belt conveyor systems and the design of resonance free belt supports are considered.



## Chapter 2

# General theory

---

In this chapter the mathematical background and techniques, the finite element techniques and the software engineering used in this study are considered. The definitions given are used in the following chapters.

### 2.1 Mathematical background and techniques

In this section some aspects of the elementary matrix and vector theory are highlighted.

#### 2.1.1 Matrices and vectors

A matrix, denoted by a bold capital, is a rectangular array of real or complex numbers. With the numbers  $A_{ij}$ , also called the elements or components of  $\mathbf{A}$ , an  $M \times N$  matrix  $\mathbf{A}$  can be written as [Bowen and Wang, 1976]:

$$\mathbf{A} = \begin{bmatrix} A_{11} & A_{12} & \cdots & A_{1N} \\ A_{21} & A_{22} & \cdots & A_{2N} \\ \vdots & \vdots & \ddots & \vdots \\ A_{M1} & A_{M2} & \cdots & A_{MN} \end{bmatrix} \quad (2.1)$$

This matrix can be subdivided into a number of submatrices, for example:

$$\mathbf{A} = \begin{bmatrix} \mathbf{A}_{11} & \mathbf{A}_{12} \\ \mathbf{A}_{21} & \mathbf{A}_{22} \end{bmatrix} \quad (2.2)$$

If two square matrices  $\mathbf{A}$  and  $\mathbf{B}$  are of the same order and such that  $\mathbf{AB} = \mathbf{BA} = \mathbf{I}$  then  $\mathbf{B}$  is called the inverse of  $\mathbf{A}$  and can be written as  $\mathbf{B} = \mathbf{A}^{-1}$ . If  $\mathbf{A}$  has an inverse then it

is said to be nonsingular. If  $\mathbf{A}$  and  $\mathbf{B}$  are both nonsingular matrices then  $(\mathbf{AB})^{-1} = \mathbf{B}^{-1}\mathbf{A}^{-1}$ . The matrix of order  $N \times M$  obtained by interchanging the rows and columns of the  $M \times N$  matrix  $\mathbf{A}$  is called the transpose of  $\mathbf{A}$  and is denoted by  $\mathbf{A}^T$ . It can easily be shown that  $(\mathbf{AB})^T = \mathbf{B}^T\mathbf{A}^T$ .

A vector, denoted by a bold lower case, is a one-dimensional array of real or complex numbers. For example the vector  $\mathbf{b}$  can be written as:

$$\mathbf{b} = \begin{bmatrix} b_1 \\ b_2 \\ \vdots \\ b_M \end{bmatrix} = [b_1 \quad b_2 \quad \cdots \quad b_M]^T \quad (2.3)$$

If the elements of a vector or matrix are time dependent then their differentiation is defined as the vector or matrix of the differentiated elements. For example:

$$\frac{d\mathbf{A}(t)}{dt} = \dot{\mathbf{A}}(t) = \begin{bmatrix} \dot{A}_{11} & \dot{A}_{12} & \cdots & \dot{A}_{1N} \\ \dot{A}_{21} & \dot{A}_{22} & \cdots & \dot{A}_{2N} \\ \vdots & \vdots & \ddots & \vdots \\ \dot{A}_{M1} & \dot{A}_{M2} & \cdots & \dot{A}_{MN} \end{bmatrix} \quad (2.4)$$

The integration of a vector or matrix is defined as the vector or matrix of the integrated elements. For example:

$$\int \mathbf{A}(t)dt = \begin{bmatrix} \int A_{11}dt & \int A_{12}dt & \cdots & \int A_{1N}dt \\ \int A_{21}dt & \int A_{22}dt & \cdots & \int A_{2N}dt \\ \vdots & \vdots & \ddots & \vdots \\ \int A_{M1}dt & \int A_{M2}dt & \cdots & \int A_{MN}dt \end{bmatrix} \quad (2.5)$$

### 2.1.2 Vector valued functions and maps

Let  $X$  and  $Y$  be two vector spaces and  $\mathbf{x}$  and  $\mathbf{y}$  two vectors,  $\mathbf{x} \in X$  and  $\mathbf{y} \in Y$ . Linear mappings between vector spaces will be denoted by capitals and the corresponding matrices by bold face capitals. If  $F$  is a linear mapping then it is defined by:

$$F: X \rightarrow Y \text{ or } \mathbf{y} = \mathbf{F}\mathbf{x}, \quad \mathbf{x} \in X, \mathbf{y} \in Y \quad (2.6)$$



where  $F$  is a matrix. However, linear mappings are sometimes too restrictive. Therefore also non-linear mappings, for which the relation between  $x$  and  $y$  is non-linear, are considered. Non-linear mappings are denoted by capital italics and the corresponding non-linear functions by bold face capital italics. If  $F$  is a non-linear mapping then it is defined by:

$$F: X \rightarrow Y \text{ or } y = F(x), \quad x \in X, y \in Y \quad (2.7)$$

Manifolds may be defined as subsets of an  $m$ -dimensional space  $R^m$  in which the manifolds are embedded. The manifolds considered in this thesis are defined by  $m-n$  algebraic equations as:

$$F(x) = 0 \quad (2.8)$$

where  $F$  is an  $(m-n)$ -dimensional vector valued function of  $x \in R^m$  which is sufficiently many-times differentiable. The manifold is now an  $n$ -dimensional surface in the space  $R^m$ . Let  $F$  be a non-linear map of a manifold  $M(X)$  into a manifold  $M(Y)$ ,

$$F: M(X) \rightarrow M(Y) \text{ or } y = F(x), \quad x \in M(X), y \in M(Y) \quad (2.9)$$

$F$  is differentiable at a point if its local representative is differentiable. The components of the derivative map  $DF$ , that are partial derivatives of  $F$  at  $x = x_0$ , can be associated with the so-called Jacobian matrix of  $F$  at  $x_0$ :

$$D_j F_i(x_0) = F_{i,j}(x_0) = \left. \frac{\partial F_i}{\partial x_j} \right|_{x_0} \quad (2.10)$$

If there is no possibility of confusion then the point of application  $x_0$  may be omitted. The components of the second order derivative  $D^2 F$  can be associated similarly with the second order partial derivatives of the vector function  $F$ :

$$D_{jk} F_i = F_{i,jk} = \frac{\partial}{\partial x_k} \left( \frac{\partial F_i}{\partial x_j} \right) \quad (2.11)$$

Let  $X, Y$  and  $Z$  be three vector spaces,  $G$  a mapping of  $X$  into  $Y$  and  $F$  a mapping of  $Y$  into  $Z$ , then  $H: X \rightarrow F(G(X))$  is a mapping of  $X$  into  $Z$ , which is said to be composed of  $F$  and  $G$  (in that order), and denoted by  $H = F \circ G$ . The components of the derivative map  $DH$  are defined by:

$$D_i H = D_i(F \circ G) = DF \cdot D_i G \quad (2.12)$$

The components of the second order derivative map  $D^2 H$  follow from the chain rule:

$$D_{ij} H = D_{ij}(F \circ G) = (D^2 F \cdot D_i G) \cdot D_j G + DF \cdot D_{ij} G \quad (2.13)$$

It is often convenient to think of  $X$  as a mapping from  $I(R^1)$  into  $U(R^3)$ :

$$X: I \rightarrow U \text{ or } x = X(t), x \in U, t \in I \quad (2.14)$$

The image of  $I$  under the mapping  $X$  is called a trajectory. If  $F$  is a mapping from  $U(R^3)$  into  $V(R^3)$  then the mapping  $Y$ , which is composed of  $X$  and  $F$ , can be written as:

$$Y: I \rightarrow V \text{ or } y = Y(t) = F \circ X(t), y \in V, t \in I \quad (2.15)$$

From equation (2.14) the derivative map  $DX$  is defined by:

$$DX: I \rightarrow TU \text{ or } \dot{x} = DX(t), \dot{x} \in TU, t \in I \quad (2.16)$$

where  $TU$  is the so-called tangent space to  $U$ . With the equations (2.12) and (2.15) the derivative map  $DY = D(F \circ X)$  is:

$$DY: I \rightarrow TV \text{ or } \dot{y} = DY(t) = DF \cdot DX(t) = DF \cdot \dot{x}, \dot{y} \in TV, t \in I \quad (2.17)$$

The second order derivative map  $D^2 X$  follows from equation (2.16):

$$D^2 X: I \rightarrow T^2 U \text{ or } \ddot{x} = D^2 X(t), \ddot{x} \in T^2 U, t \in I \quad (2.18)$$

where  $T^2 U$  is the tangent space to  $TU$ . From the equations (2.17) and (2.18), the second order derivative map  $D^2 Y$  is given by :

$$\begin{aligned} D^2 Y: I \rightarrow T^2 V \text{ or } \ddot{y} &= (D^2 F \cdot DX(t)) \cdot DX(t) + DF \cdot D^2 X(t) \\ &= (D^2 F \cdot \dot{x}) \cdot \dot{x} + DF \cdot \ddot{x}, \ddot{y} \in T^2 V, t \in I \end{aligned} \quad (2.19)$$

## 2.2 Finite element techniques

A specific finite element theory for the analysis of multibody systems was initiated and developed by Besseling [1977 and 1982], Van der Werff [1977] and Jonker [1988]. It was originally designed for the kinematic and dynamic analysis of mechanisms and manipulators with a number of flexible links. The description starts from the expressions of the element deformation modes, the so-called generalised strains, as non-linear functions of the nodal co-ordinates. This is an algebraic analogue to the continuous field description of deformations. The deformation of an element is taken into account in case of a flexible element whereas it is zero in case of a rigid element. Deformable elements are handled by allowing non-zero deformation parameters for these elements and by specifying constitutive equations relating the deformation and the dual stress parameters. Instead of imposing constraint equations for the connection between different parts of a mechanism, permanent contact between the parts or elements is achieved by letting the elements have displacements and certain rotations of the nodal points in common.

The usefulness of this approach for the dynamic analysis of (flexible) belt systems can be illustrated by consideration of the description of the contact between a roll support and the belt. If constraint equations are used to account for the (sliding) contact between the belt and a roll then these equations have to be adjusted continuously, depending on the time dependent position of the belt on the roll. This adjustment can be omitted by application of a special roll supported belt element, with extra zero deformation modes, that accounts for the contact between the roll and the belt. Therefore the application of special elements, of which the deformation modes represent the physical character of a coupling, enable an efficient finite element description of a belt system.

### 2.2.1 Finite element description

The global position of each element, denoted with a superscript  $e$ , is specified by a set of nodal co-ordinates,  $\mathbf{x}^e \in X^e$ , which may be Cartesian co-ordinates or co-ordinates that describe an orientation. The assembly of the co-ordinate subspaces  $X^e$  form the configuration space  $X$  of the entire belt system:

$$X = \sum_e X^e \quad (2.20)$$

The generalised strains,  $\boldsymbol{\varepsilon}^e \in E^e$ , are defined as (non-linear) functions of the nodal co-ordinates:

$$\varepsilon^e = D^e(x^e) \quad (2.21)$$

The configuration space, defined in (2.20), is the sum of overlapping co-ordinate subspaces since the elements can share nodal points. Since elements never share deformation modes the intersection of the deformation spaces of two elements is the null space. Therefore the deformation space of the system  $E$  is the direct sum of the deformation spaces of the elements:

$$E = \bigoplus_e E^e \quad (2.22)$$

The deformation functions can be taken together in a continuity map for the entire system:

$$D: X \rightarrow E, \varepsilon = D(x) \quad (2.23)$$

The map (2.23) constitutes the basic equations for the kinematic analysis. Kinematic constraints can be imposed by giving nodal co-ordinates or deformations prescribed values.

The spaces  $X$  and  $E$  can both be partitioned in agreement with the constraint conditions and the choice of generalised co-ordinates as

$$X = X^o \oplus X^c \oplus X^m; E = E^o \oplus E^c \oplus E^m \quad (2.24)$$

The superscript  $o$  denotes the fixed (invariant) nodal co-ordinates or deformations,  $c$  the dependent nodal co-ordinates or deformations and  $m$  the independent (or generalised) nodal co-ordinates or deformations. Let  $n_x$  be the total number of nodal co-ordinates  $x_i$ ,  $n_{x^o}$  the number of fixed support co-ordinates  $x_i^o$ ,  $n_{x^c}$  the number of dependent nodal co-ordinates  $x_i^c$  and  $n_{x^m}$  the number of independent nodal co-ordinates  $x_i^m$ . Also let  $n_\varepsilon$  be the total number of deformation mode co-ordinates  $\varepsilon_i$ ,  $n_{\varepsilon^o}$  the number of fixed prescribed deformation mode co-ordinates (constraint conditions)  $\varepsilon_i^o$ ,  $n_{\varepsilon^c}$  the number of dependent deformation mode co-ordinates  $\varepsilon_i^c$  and  $n_{\varepsilon^m}$  the number of independent or generalised deformations  $\varepsilon_i^m$ . The number of degrees of freedom of the belt system is  $n = n_x - n_{x^o} - n_{\varepsilon^o} = n_{x^m} + n_{\varepsilon^m}$ . Since  $n_x = n_{x^o} + n_{x^c} + n_{x^m}$  it follows that  $n_{x^c} - n_{\varepsilon^o} = n_{\varepsilon^m}$ .

### 2.2.2 Transfer functions

The nodal co-ordinates and deformations can be determined as non-linear functions of the independent co-ordinates, [Jonker, 1988]:

$$\begin{bmatrix} \mathbf{x}^o \\ \mathbf{x}^c \\ \mathbf{x}^m \\ \boldsymbol{\varepsilon}^o \\ \boldsymbol{\varepsilon}^m \\ \boldsymbol{\varepsilon}^c \end{bmatrix} = \begin{bmatrix} \mathbf{F}^{xo}(\mathbf{x}^m, \boldsymbol{\varepsilon}^m) \\ \mathbf{F}^{xc}(\mathbf{x}^m, \boldsymbol{\varepsilon}^m) \\ \mathbf{F}^{xm}(\mathbf{x}^m, \boldsymbol{\varepsilon}^m) \\ \mathbf{F}^{eo}(\mathbf{x}^m, \boldsymbol{\varepsilon}^m) \\ \mathbf{F}^{em}(\mathbf{x}^m, \boldsymbol{\varepsilon}^m) \\ \mathbf{F}^{ec}(\mathbf{x}^m, \boldsymbol{\varepsilon}^m) \end{bmatrix} \quad (2.25a)$$

Summarised:

$$\begin{bmatrix} \mathbf{x} \\ \boldsymbol{\varepsilon} \end{bmatrix} = \begin{bmatrix} \mathbf{F}^x(\mathbf{q}) \\ \mathbf{F}^e(\mathbf{q}) \end{bmatrix} = \mathbf{F}(\mathbf{q}) \quad (2.25b)$$

where  $\mathbf{q} = \left[ (\mathbf{x}^m)^T \quad (\boldsymbol{\varepsilon}^m)^T \right]^T$ . The non-linear vector functions  $\mathbf{F}^x$  and  $\mathbf{F}^e$  are called the geometric transfer functions of the belt system and  $\mathbf{F}$  the kinematic transfer function. With equation (2.25a) the velocity vector can be determined as:

$$\begin{bmatrix} \dot{\mathbf{x}}^o \\ \dot{\mathbf{x}}^c \\ \dot{\mathbf{x}}^m \\ \dot{\boldsymbol{\varepsilon}}^o \\ \dot{\boldsymbol{\varepsilon}}^m \\ \dot{\boldsymbol{\varepsilon}}^c \end{bmatrix} = \begin{bmatrix} D\mathbf{F}^{xo}(\mathbf{q}) \\ D\mathbf{F}^{xc}(\mathbf{q}) \\ D\mathbf{F}^{xm}(\mathbf{q}) \\ D\mathbf{F}^{eo}(\mathbf{q}) \\ D\mathbf{F}^{em}(\mathbf{q}) \\ D\mathbf{F}^{ec}(\mathbf{q}) \end{bmatrix} \cdot \dot{\mathbf{q}} \quad (2.26a)$$

where the operator D represents partial differentiation with respect to the generalised co-ordinates. Summarised:

$$\begin{bmatrix} \dot{\mathbf{x}} \\ \dot{\boldsymbol{\varepsilon}} \end{bmatrix} = \begin{bmatrix} D\mathbf{F}^x(\mathbf{q}) \\ D\mathbf{F}^e(\mathbf{q}) \end{bmatrix} \cdot \dot{\mathbf{q}} = D\mathbf{F}(\mathbf{q}) \cdot \dot{\mathbf{q}} \quad (2.26b)$$

The deformation modes are also functions of the nodal co-ordinates, with equation (2.23):

$$\begin{bmatrix} \dot{\varepsilon}^o \\ \dot{\varepsilon}^m \\ \dot{\varepsilon}^c \end{bmatrix} = \begin{bmatrix} D^o(x) \\ D^m(x) \\ D^c(x) \end{bmatrix} \quad (2.27)$$

The superscripts o, c and m combined with the operator D are introduced to indicate partial differentiation with respect to the corresponding co-ordinates. The deformation rates are obtained from equation (2.27):

$$\begin{bmatrix} \dot{\varepsilon}^o \\ \dot{\varepsilon}^m \\ \dot{\varepsilon}^c \end{bmatrix} = \begin{bmatrix} D^o D^o(x) & D^c D^o(x) & D^m D^o(x) \\ D^o D^m(x) & D^c D^m(x) & D^m D^m(x) \\ D^o D^c(x) & D^c D^c(x) & D^m D^c(x) \end{bmatrix} \begin{bmatrix} \dot{x}^o \\ \dot{x}^c \\ \dot{x}^m \end{bmatrix} \quad (2.28a)$$

which can be summarised in:

$$\dot{\varepsilon} = DD(x) \cdot \dot{x} \quad (2.28b)$$

The matrix  $\left[ (D^c D^o)^T \quad (D^c D^m)^T \right]^T$  is an (neo+nem) x (nxc) matrix which is square since nxc=neo+nem, as is explained in section (2.2.1). From their definitions it follows that:

$$\dot{x}^o = DF^{xo} \cdot \dot{q} = \begin{bmatrix} \mathbf{0} & \mathbf{0} \end{bmatrix} \cdot \dot{q}; \quad \dot{x}^m = DF^{xm} \cdot \dot{q} = \begin{bmatrix} \mathbf{I} & \mathbf{0} \end{bmatrix} \cdot \dot{q} \quad (2.29a)$$

$$\dot{\varepsilon}^o = DF^{eo} \cdot \dot{q} = \begin{bmatrix} \mathbf{0} & \mathbf{0} \end{bmatrix} \cdot \dot{q}; \quad \dot{\varepsilon}^m = DF^{em} \cdot \dot{q} = \begin{bmatrix} \mathbf{0} & \mathbf{I} \end{bmatrix} \cdot \dot{q} \quad (2.29b)$$

thus with equation (2.28a) it follows that:

$$\begin{aligned} \begin{bmatrix} \dot{x}^c \\ \dot{x}^m \end{bmatrix} &= \begin{bmatrix} \left[ D^c D^o \right]^{-1} & \mathbf{0} \\ \left[ D^c D^m \right] & \mathbf{I} \end{bmatrix} \begin{bmatrix} -D^m D^o & \mathbf{0} \\ -D^m D^m & \mathbf{I} \\ \mathbf{I} & \mathbf{0} \end{bmatrix} \cdot \dot{q} = \Sigma^o \Delta^o \dot{q} \\ &= \begin{bmatrix} \left[ D^c D^o \right]^{-1} & \mathbf{0} \\ \left[ D^c D^m \right] & \mathbf{I} \end{bmatrix} \begin{bmatrix} -D^m D^o & \mathbf{0} \\ -D^m D^m & \mathbf{I} \\ \mathbf{I} & \mathbf{0} \end{bmatrix} \begin{bmatrix} \dot{x}^m \\ \dot{\varepsilon}^m \end{bmatrix} = Z^* \dot{q} \end{aligned} \quad (2.30)$$

With equation (2.30) the first order transfer functions  $DF^{xc}$  are determined:

$$\dot{\mathbf{x}}^c = \mathbf{DF}^{xc} \cdot \dot{\mathbf{q}} = \begin{bmatrix} D^c D^o \\ D^c D^m \end{bmatrix}^{-1} \begin{bmatrix} -D^m D^o & \mathbf{0} \\ -D^m D^m & \mathbf{I} \end{bmatrix} \cdot \dot{\mathbf{q}} \quad (2.31)$$

With the equations (2.28a) and (2.30) the time derivatives of  $\varepsilon^c$ , which also determine the first order transfer functions  $\mathbf{DF}^{bc}$ , are:

$$\dot{\varepsilon}^c = \mathbf{DF}^{bc} \cdot \dot{\mathbf{q}} = \begin{bmatrix} D^c D^c & D^m D^c \end{bmatrix} \begin{bmatrix} \dot{\mathbf{x}}^c \\ \dot{\mathbf{x}}^m \end{bmatrix} = \begin{bmatrix} D^c D^c \cdot \mathbf{DF}^{xc} + D^m D^c \cdot \mathbf{DF}^{xm} \end{bmatrix} \cdot \dot{\mathbf{q}} \quad (2.32)$$

To find the second order derivatives equation (2.28a) is differentiated with respect to time from which it follows that:

$$\begin{bmatrix} \ddot{\varepsilon}^o \\ \ddot{\varepsilon}^m \\ \ddot{\varepsilon}^c \end{bmatrix} = \begin{bmatrix} (D^2 D^o(\mathbf{x}) \cdot \dot{\mathbf{x}}) \cdot \dot{\mathbf{x}} \\ (D^2 D^m(\mathbf{x}) \cdot \dot{\mathbf{x}}) \cdot \dot{\mathbf{x}} \\ (D^2 D^c(\mathbf{x}) \cdot \dot{\mathbf{x}}) \cdot \dot{\mathbf{x}} \end{bmatrix} + \begin{bmatrix} D^o D^o(\mathbf{x}) & D^c D^o(\mathbf{x}) & D^m D^o(\mathbf{x}) \\ D^o D^m(\mathbf{x}) & D^c D^m(\mathbf{x}) & D^m D^m(\mathbf{x}) \\ D^o D^c(\mathbf{x}) & D^c D^c(\mathbf{x}) & D^m D^c(\mathbf{x}) \end{bmatrix} \begin{bmatrix} \ddot{\mathbf{x}}^o \\ \ddot{\mathbf{x}}^c \\ \ddot{\mathbf{x}}^m \end{bmatrix} \quad (2.33a)$$

In short:

$$\ddot{\varepsilon} = (D^2 D(\mathbf{x}) \cdot \dot{\mathbf{x}}) \cdot \dot{\mathbf{x}} + \mathbf{DD}(\mathbf{x}) \cdot \ddot{\mathbf{x}} \quad (2.33b)$$

Similar to the derivation of equation (2.30) it can be shown that:

$$\begin{bmatrix} \ddot{\mathbf{x}}^c \\ \ddot{\mathbf{x}}^m \end{bmatrix} = \begin{bmatrix} \begin{bmatrix} D^c D^o \\ D^c D^m \\ \mathbf{0} \end{bmatrix}^{-1} & \mathbf{0} \\ \mathbf{0} & \mathbf{I} \end{bmatrix} \begin{bmatrix} \begin{bmatrix} -D^m D^o & \mathbf{0} \\ -D^m D^m & \mathbf{I} \\ \mathbf{I} & \mathbf{0} \end{bmatrix} \begin{bmatrix} \ddot{\mathbf{x}}^m \\ \ddot{\varepsilon}^m \end{bmatrix} - \begin{bmatrix} (D^2 D^o \cdot \dot{\mathbf{x}}) \cdot \dot{\mathbf{x}} \\ (D^2 D^m \cdot \dot{\mathbf{x}}) \cdot \dot{\mathbf{x}} \\ \mathbf{0} \end{bmatrix} \end{bmatrix} \quad (2.34a)$$

In short:

$$\begin{bmatrix} \ddot{\mathbf{x}}^c \\ \ddot{\mathbf{x}}^m \end{bmatrix} = \mathbf{Z}^* \ddot{\mathbf{q}} + \Sigma^o \mathbf{g}^{2om} \quad (2.34b)$$

where:

$$\Sigma^o = \begin{bmatrix} \begin{bmatrix} D^c D^o \\ D^c D^m \\ \mathbf{0} \end{bmatrix}^{-1} & \mathbf{0} \\ \mathbf{0} & \mathbf{I} \end{bmatrix} \text{ and } \mathbf{g}^{2om} = - \begin{bmatrix} (D^2 D^o \cdot \dot{\mathbf{x}}) \cdot \dot{\mathbf{x}} \\ (D^2 D^m \cdot \dot{\mathbf{x}}) \cdot \dot{\mathbf{x}} \\ \mathbf{0} \end{bmatrix} \quad (2.35)$$

Note that:

$$\ddot{\mathbf{x}} = (D^2 F^x \cdot \dot{\mathbf{q}}) \cdot \dot{\mathbf{q}} + D F^x \cdot \ddot{\mathbf{q}} \quad (2.36)$$

From the equations (2.34) and (2.36) the components of the second order geometric transfer functions  $D^2 F^{xc}$  can be obtained:

$$D_{ij} F^{xc} = - \begin{bmatrix} D^c D^o \\ D^c D^m \end{bmatrix}^{-1} \begin{bmatrix} (D^2 D^o \cdot D_i F^x) \cdot D_j F^x \\ (D^2 D^m \cdot D_i F^x) \cdot D_j F^x \end{bmatrix} \quad (2.37)$$

The components of  $D^2 F^{xo}$  and  $D^2 F^{xm}$  are zero. The time derivatives of  $\dot{\epsilon}^c$  are:

$$\ddot{\epsilon}^c = \begin{bmatrix} D^c D^c & D^m D^c \end{bmatrix} \begin{bmatrix} \ddot{\mathbf{x}}^c \\ \ddot{\mathbf{x}}^m \end{bmatrix} + (D^2 D^c \cdot \dot{\mathbf{x}}) \cdot \dot{\mathbf{x}} \quad (2.38a)$$

or

$$\ddot{\epsilon}^c = \begin{bmatrix} D^c D^c & D^m D^c \end{bmatrix} Z^* \ddot{\mathbf{q}} + \mathbf{g}^{2c} \quad (2.38b)$$

where

$$\begin{aligned} \mathbf{g}^{2c} &= \begin{bmatrix} D^c D^c & D^m D^c \end{bmatrix} \Sigma^0 \mathbf{g}^{2om} + (D^2 D^c \cdot \dot{\mathbf{x}}) \cdot \dot{\mathbf{x}} \\ &= -D^c D^c \begin{bmatrix} D^c D^o \\ D^c D^m \end{bmatrix}^{-1} \begin{bmatrix} (D^2 D^o \cdot \dot{\mathbf{x}}) \cdot \dot{\mathbf{x}} \\ (D^2 D^m \cdot \dot{\mathbf{x}}) \cdot \dot{\mathbf{x}} \end{bmatrix} + (D^2 D^c \cdot \dot{\mathbf{x}}) \cdot \dot{\mathbf{x}} \end{aligned} \quad (2.39)$$

Note that:

$$\ddot{\epsilon} = (D^2 F^e \cdot \dot{\mathbf{q}}) \cdot \dot{\mathbf{q}} + D F^e \cdot \ddot{\mathbf{q}} \quad (2.40)$$

The components of  $D^2 F^{ec}$  can be obtained after differentiation of equation (2.32) with respect to time:

$$D_{ij} F^{ec} = (D^2 D^c \cdot D_i F^x) \cdot D_j F^x + D^c D^c \cdot D_{ij} F^{xc} \quad (2.41)$$

The components of  $D^2 F^{eo}$  and  $D^2 F^{em}$  are zero. Expressions for the vector functions  $D$  are given in Chapter 7.



### 2.2.3 The equations of motion

The equations of motion of a belt system can be derived with the aid of the principle of virtual power (Jourdain's principle), [Davies, 1982]. According to this principle the virtual power of the external forces that act on a body is zero for all the virtual velocities with zero rate of deformation. So,

$$\delta \dot{\mathbf{x}}^T (\mathbf{f}(\mathbf{x}, \dot{\mathbf{x}}, t) - \mathbf{M}(\mathbf{x}, \dot{\mathbf{x}}, t) \ddot{\mathbf{x}} - (\mathbf{N} \cdot \dot{\mathbf{x}}) \cdot \dot{\mathbf{x}}) = \mathbf{0} \quad \forall \delta \dot{\mathbf{x}} \in \{ \delta \dot{\mathbf{x}} \mid \delta \dot{\boldsymbol{\varepsilon}} = \mathbf{D}\mathbf{D}(\mathbf{x}) \cdot \delta \dot{\mathbf{x}} = \mathbf{0} \}$$

(2.42)

With the aid of a vector of multipliers of Lagrange  $\boldsymbol{\sigma}$  this leads to

$$\delta \dot{\mathbf{x}}^T (\mathbf{f} - \mathbf{M} \ddot{\mathbf{x}} - (\mathbf{N} \cdot \dot{\mathbf{x}}) \cdot \dot{\mathbf{x}}) = \boldsymbol{\sigma}^T (\mathbf{D}\mathbf{D} \cdot \delta \dot{\mathbf{x}})$$

(2.43a)

or,

$$\mathbf{M} \ddot{\mathbf{x}} = \mathbf{f} - (\mathbf{N} \cdot \dot{\mathbf{x}}) \cdot \dot{\mathbf{x}} - \mathbf{D}^T \boldsymbol{\sigma}$$

(2.43b)

where

$$\mathbf{D} = \mathbf{D}\mathbf{D}(\mathbf{x})$$

(2.44)

The components of the vector of multipliers of Lagrange  $\boldsymbol{\sigma}$  may be interpreted as the generalised stresses dual to the generalised strains defined in (2.23). The equations of motion are reduced to a minimal set of equations by means of the transfer functions  $F$  and its derivatives. Substitution of equation (2.36) in equation (2.43b) yields:

$$\left[ (\mathbf{D}\mathbf{F}^x)^T \mathbf{M} \mathbf{D}\mathbf{F}^x \right] \ddot{\mathbf{q}} = (\mathbf{D}\mathbf{F}^x)^T \left[ \mathbf{f} - (\mathbf{N} \cdot (\mathbf{D}\mathbf{F}^x \cdot \dot{\mathbf{q}})) \cdot (\mathbf{D}\mathbf{F}^x \cdot \dot{\mathbf{q}}) - \mathbf{D}^T \boldsymbol{\sigma} - \mathbf{M} \left( (\mathbf{D}^2 \mathbf{F}^x \cdot \dot{\mathbf{q}}) \cdot \dot{\mathbf{q}} \right) \right]$$

(2.45a)

If  $\ddot{\mathbf{x}}^0$  is left out, since it is zero, and equation (2.34) is used then the following set of equations of motion is obtained:

$$\left[ \mathbf{Z}^{*T} \mathbf{M} \mathbf{Z}^* \right] \ddot{\mathbf{q}} = \mathbf{Z}^{*T} \left[ \mathbf{f} - \mathbf{f}_n - \mathbf{D}^T \boldsymbol{\sigma} - \mathbf{M} \boldsymbol{\Sigma}^0 \mathbf{g}^{2om} \right]$$

(2.45b)

where

$$\mathbf{f}_n = (\mathbf{N} \cdot (\mathbf{D}\mathbf{F}^x \cdot \dot{\mathbf{q}})) \cdot (\mathbf{D}\mathbf{F}^x \cdot \dot{\mathbf{q}})$$

(2.46)

Equation (2.45) can be written in a compact form as:

$$\mathbf{M}_o(\mathbf{q}, \dot{\mathbf{q}}, t) \ddot{\mathbf{q}} = \mathbf{F}_o(\mathbf{q}, \dot{\mathbf{q}}, t) \quad (2.47)$$

where

$$\mathbf{M}_o = [\mathbf{Z}^{*T} \mathbf{M} \mathbf{Z}^*], \quad \mathbf{F}_o = \mathbf{Z}^{*T} [\mathbf{f} - \mathbf{f}_n - \mathbf{D}^T \boldsymbol{\sigma} - \mathbf{M} \Sigma^o \mathbf{g}^{2om}] \quad (2.48)$$

or in a state space form as

$$\frac{d}{dt} \begin{bmatrix} \mathbf{q} \\ \dot{\mathbf{q}} \end{bmatrix} = \begin{bmatrix} \dot{\mathbf{q}} \\ \mathbf{M}_o^{-1} \mathbf{F}_o \end{bmatrix} \quad (2.49a)$$

which may be reduced to:

$$\dot{\mathbf{y}}(t) = \mathbf{f}^*(t, \mathbf{y}) \quad (2.49b)$$

where  $\mathbf{y} = [\mathbf{q}^T \quad \dot{\mathbf{q}}^T]^T$ . The equations of motion (2.49) are integrated numerically by a Runge-Kutta procedure with variable stepsize [Press et al., 1992]. The constitutive equations are given in Chapter 7.

### 2.2.4 Kinematic analysis

Starting from a known configuration  $[\mathbf{x}_{(n)}^T \quad \boldsymbol{\varepsilon}_{(n)}^T]^T$  at time  $t=t_n$  of a belt system, the instantaneous vectors  $\mathbf{q}_{(n+\#)}$ ,  $\dot{\mathbf{q}}_{(n+\#)}$  and  $\ddot{\mathbf{q}}_{(n+\#)}$  are obtained after numerical integration of the equations of motion (2.49). The new instantaneous configuration of the belt system at time  $t=t_{n+1}$  is determined by:

$$\begin{bmatrix} \mathbf{x}_{(n+\#)} \\ \boldsymbol{\varepsilon}_{(n+\#)} \end{bmatrix} = \begin{bmatrix} \mathbf{F}_{(n+\#)}^x(\mathbf{q}_{(n+\#)}) \\ \mathbf{F}_{(n+\#)}^\varepsilon(\mathbf{q}_{(n+\#)}) \end{bmatrix} \quad (2.50)$$

However, this configuration cannot be determined directly from equation (2.50) since the kinematic transfer functions  $[(\mathbf{F}_{(n+\#)}^x)^T \quad (\mathbf{F}_{(n+\#)}^\varepsilon)^T]^T$ , contrary to the first and second order transfer functions, are unknown. Therefore the first and second order transfer functions, as described in Section 2.2.2, are used to calculate a second order

prediction of  $\left[ \mathbf{x}_{(n+1)}^T \quad \boldsymbol{\varepsilon}_{(n+1)}^T \right]^T$  accounting for the first and second order terms of the Taylor series expansion at  $\left[ \mathbf{x}_{(n)}^T \quad \boldsymbol{\varepsilon}_{(n)}^T \right]^T$ . This is written as follows:

$$\begin{bmatrix} \mathbf{x}_{(n+1)} \\ \boldsymbol{\varepsilon}_{(n+1)} \end{bmatrix} = \begin{bmatrix} \mathbf{x}_{(n)} \\ \boldsymbol{\varepsilon}_{(n)} \end{bmatrix} + \begin{bmatrix} D\mathbf{F}_{(n)}^x \cdot \Delta \mathbf{q}_{(n+1)} \\ D\mathbf{F}_{(n)}^e \cdot \Delta \mathbf{q}_{(n+1)} \end{bmatrix} + \frac{1}{2} \begin{bmatrix} (D^2 \mathbf{F}_{(n)}^x \cdot \Delta \mathbf{q}_{(n+1)}) \cdot \Delta \mathbf{q}_{(n+1)} \\ (D^2 \mathbf{F}_{(n)}^e \cdot \Delta \mathbf{q}_{(n+1)}) \cdot \Delta \mathbf{q}_{(n+1)} \end{bmatrix} \quad (2.51)$$

where

$$\Delta \mathbf{q}_{(n+1)} = \mathbf{q}_{(n+1)} - \mathbf{q}_{(n)} \quad (2.52)$$

To guarantee that

$$D(\mathbf{x}_{(n+1)}) = \boldsymbol{\varepsilon}_{(n+1)} \quad (2.53)$$

an iteration process is applied. A solution for this system of equations is determined by using an iterative correction routine based on the Newton-Raphson method which takes only the first order terms of the Taylor series expansion of  $D(\mathbf{x})$  into account [Bathe, 1985]. The iterative approximation is as follows:

$$\mathbf{x}_{(i+1)}^c = \mathbf{x}_{(i)}^c + \delta \mathbf{x}_{(i)}^c \quad (2.54)$$

where the residual vector  $\delta \mathbf{x}_{(i)}^c$  is the correction at step  $i$ , calculated from the linear system of equations

$$\delta \mathbf{x}_{(i)}^c = - \begin{bmatrix} D^o D^c \\ D^m D^c \end{bmatrix}^{-1} \begin{bmatrix} \delta \boldsymbol{\varepsilon}_{(i)}^o \\ \delta \boldsymbol{\varepsilon}_{(i)}^m \end{bmatrix} \quad (2.55)$$

where the residual deformations are obtained from the continuity equations

$$\begin{bmatrix} \delta \boldsymbol{\varepsilon}_{(i)}^o \\ \delta \boldsymbol{\varepsilon}_{(i)}^m \end{bmatrix} = \begin{bmatrix} D^o(\mathbf{x}_{(i)}) \\ D^m(\mathbf{x}_{(i)}) - \boldsymbol{\varepsilon}_{(i)}^m \end{bmatrix} \quad (2.56)$$

The correction routine (2.54) ends if the final solution  $\left[ \mathbf{x}_{(i)}^T \quad \boldsymbol{\varepsilon}_{(i)}^T \right]^T$  is sufficiently accurate. This is verified by

$$\begin{Bmatrix} \delta \varepsilon_{(i)}^o \\ \delta \varepsilon_{(i)}^m \end{Bmatrix} < \delta^* \quad (2.57)$$

where  $\delta^* > 0$  is a prescribed threshold value. This iteration process converges if the approximation  $[\mathbf{x}_{(i)}^T \ \varepsilon_{(i)}^T]^T$  is sufficiently close to the final solution  $[\mathbf{x}_{(n)}^T \ \varepsilon_{(n)}^T]^T$  [Jonker, 1988].

### 2.2.5 Kinetostatic analysis

The internal stress distribution and the unknown reaction forces of the belt system can be calculated with a kinetostatic analysis after the motion of the system is known. If the total forces are defined by:

$$\mathbf{f}^{\text{tot}} = \mathbf{f} - \mathbf{M}\ddot{\mathbf{x}} - (\mathbf{N} \cdot \dot{\mathbf{x}}) \cdot \dot{\mathbf{x}} = \mathbf{f} + \mathbf{f}^{\text{in}} \quad (2.58)$$

where the superscript  $\text{in}$  denotes the inertia forces, then the virtual power equation can be written as:

$$\delta \dot{\mathbf{x}}^T \mathbf{f}^{\text{tot}} = \delta \dot{\varepsilon}^T \boldsymbol{\sigma} \quad \forall \delta \dot{\mathbf{x}} \in \{ \delta \dot{\mathbf{x}} \mid \delta \dot{\varepsilon} = \mathbf{D}\mathbf{D}(\mathbf{x}) \cdot \delta \dot{\mathbf{x}} \} \quad (2.59a)$$

The inertia forces  $\mathbf{f}^{\text{in}}$  have been obtained from the preceding dynamic analysis. Equation (2.59a) can also be written as:

$$\mathbf{f} + \mathbf{f}^{\text{in}} = \mathbf{D}\mathbf{D}^T \boldsymbol{\sigma} \quad (2.59b)$$

From equation (2.59b) the internal stress distributions  $\boldsymbol{\sigma}^o$  and  $\boldsymbol{\sigma}^m$ , that must be calculated before the reaction forces can be calculated, can be obtained:

$$\begin{Bmatrix} \boldsymbol{\sigma}^o \\ \boldsymbol{\sigma}^m \end{Bmatrix} = \left[ (\mathbf{D}^o \mathbf{D}^o)^T (\mathbf{D}^c \mathbf{D}^m)^T \right]^{-1} \left( \mathbf{f}^c + \mathbf{f}^{c,\text{in}} - (\mathbf{D}^c \mathbf{D}^c)^T \boldsymbol{\sigma}^c \right) \quad (2.60)$$

where the vector  $\mathbf{f}^c$  contains the prescribed forces and the vector of dependent stresses  $\boldsymbol{\sigma}^c$  is determined from a constitutive law. Finally the vector of reaction forces  $\mathbf{f}^o$  and the vector of driving forces  $\mathbf{f}^m$  can be obtained from:

$$\begin{bmatrix} \mathbf{f}^o \\ \mathbf{f}^m \end{bmatrix} = \begin{bmatrix} -\mathbf{f}^{o,in} \\ -\mathbf{f}^{m,in} \end{bmatrix} + \begin{bmatrix} (D^o D^o)^T & (D^o D^m)^T & (D^o D^c)^T \\ (D^m D^o)^T & (D^m D^m)^T & (D^m D^c)^T \end{bmatrix} \begin{bmatrix} \boldsymbol{\sigma}^o \\ \boldsymbol{\sigma}^m \\ \boldsymbol{\sigma}^c \end{bmatrix} \quad (2.61)$$

## 2.3 Software engineering

Starting from a correct mathematical model of a physical process or system, a software system can be designed to perform simulation of that process or system. A software system consists of a computer program and its documentation. The development or engineering of a software system should be a systematic process. According to the definition of Jalote [1991] software engineering is the systematic approach to the development, operation, maintenance and retirement of software. It can be considered as a combination of structured programming, structured documentation and structured management. In particular structured programming is important considering its influence on the maintainability and in particular the extensibility of the software system. In this chapter the structure of the simulation software system **TUBBELT** is considered. **TUBBELT** has been developed to perform simulations of the dynamic behaviour of belt systems. The computer program of **TUBBELT** is written in the object oriented computer language C++. Object oriented programming has some advantages for finite element analysis and multibody system dynamics as will be indicated in the next section, [Forde et al., 1990], [Lodewijks, 1991], [Zimmermann et al., 1992], [Dubois-Pelerin and Zimmermann, 1993] and [Koh and Park, 1994].

### 2.3.1 Object oriented software engineering

In the finite element analysis of a belt system the system is decomposed in finite elements. A similar approach is obtained from the object-oriented analysis of a belt system where the system is decomposed in objects. These objects are defined within the scope of the problem domain and represent physical parts of the system. The advantage of applying the object oriented approach in finite element analysis is that it provides an overlay in which the object oriented decomposition covers the finite

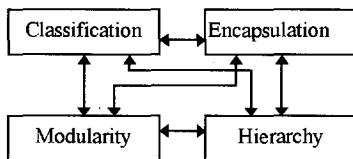


Figure 2.1: Elements of an object model.

element decomposition. The description of the objects can include the description of finite elements thus creating a compact data structure. This is provided by the four elements that form an object model: classification, encapsulation, modularity and hierarchy. A classification denotes the essential

characteristics of an object that distinguish it from all other kinds of objects thus providing crisply defined conceptual boundaries, relative to the perspective of the viewer [Booch, 1994]. A classification serves to separate an object's essential behaviour from its implementation by focusing on the outside view of an object. A complementary concept is encapsulation that focuses on the implementation that gives rise to the object's behaviour. Encapsulation is the process of compartmentalising the elements of a class that constitute its structure and behaviour; encapsulation serves to separate the contractual interface of a class and its implementation [Booch, 1994]. To reduce the complexity of a system it can be decomposed into sets of coupled modules. This modularity creates a number of *well-defined and documented* boundaries within a program. To rank the objects a hierarchy can be developed that orders and links the classifications.

The computer program **TUDBELT** is built up of three modules. The first module, **TAKEOFF**, reads the model data from an input data file and builds the finite element model according to predefined rules. The second module, **FLIGHT**, starts, controls and stops the simulation process. The third module, **LANDING**, prepares the graphical presentation of the simulation results. The objects that are used within these modules represent components of the modelled belt system, including an induction motor and a pulley, and components that are used during the calculation process, including matrices and vectors. The modules and the objects are discussed in the next three sections.

### 2.3.2 TAKEOFF

Prior to a computer session the user has to discretise the belt system into a number of discrete elements and give the initial position, displacements, velocities and accelerations of the nodal points. Based on this information the user has to define the elements and give the element type, the nodal point numbers of the elements and specific element data including the cross-sectional area, the specific weight, Young's modulus and the bending stiffness. He also has to give the position, the magnitude and the direction of the prescribed forces and the constraint conditions. The constraint conditions include information of the type: initial state and position of the motor, the gear box, the tensioning system, the pulleys and the idlers. Finally the user has to give specific calculation process data including the minimum stepsize, the required accuracy, the maximum number of steps and the calculation time interval. The information about the nodal points, elements, prescribed forces, constraints and calculation process data is stored in the data file MODEL.TXT.

After start-up of **TUDBELT** the module **TAKEOFF** reads the data file MODEL.TXT. To enable further processing and easy access to the most important

data stored in this file, four objects are used. These objects are decomposed in such a way that they cover the finite element decomposition. In other words the four objects store and represent the nodal points, elements, prescribed forces and constraints. The objects, which are defined by corresponding classes, point to four data lists which are automatically initiated by the module **TAKEOFF** after reading the dimension, or the number of items, of a list. See Table 2.1 and Figure 2.2.

class name	object name	dimension
NodalPoint	NoList	nno
Element	EIList	nel
Constraint	CoList	nco
Force	FoList	nfo

Table 2.1: Data lists classes

As a result, the dimension of for example the *NoList* is equal to the number of nodal points. During the initialisation process, each component of the *EIList*, that is also an object of the class *Element*, is connected to the *NoList* by two pointers that point to the nodal points of the corresponding element, see Figure 2.3. This figure also shows the contents of the objects of the classes *Element* and *NodalPoint*. The contents of objects of the class *Element* include the deformation parameters, the generalised stresses and the two pointers. The contents of the class *NodalPoint* include the position (x,y,z,a), the displacements (u,v,w,f), the velocities (ud,vd,wd,fd), the accelerations (udd,vdd,wdd,fd) and the number of degrees of freedom (nvrij). After initialisation of the four data lists, the *CoList* is considered to determine the positions of the pulleys and idlers. If a pulley is detected then an additional nodal point is created. The position of this nodal point is equal to the position of the axis of the pulley. The positions of the pulley and idlers are compared

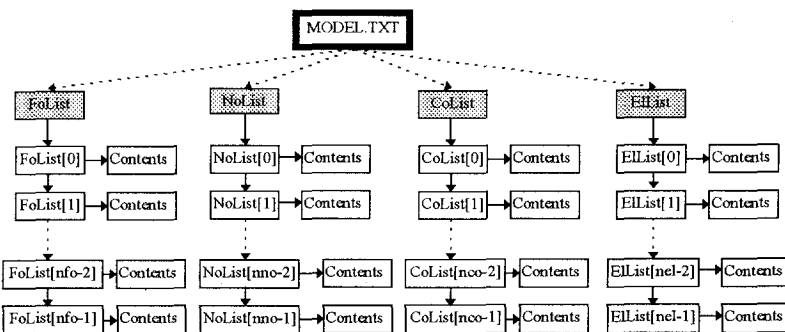


Figure 2.2: Initiation of the data lists.

to the positions of the nodal points to detect the elements that are supported by a pulley or an idler. If an element is supported by a pulley or an idler then the parameter *rolnr* indicates the position of the object in the *CoList* that stores the data of the specific pulley or idler. If a nodal point is supported by a pulley then the switch *on\_pulley* of the nodal points is set to 1 instead of 0. After consideration of the *CoList*, the *NoList* is considered. If a nodal point is supported by a pulley, which can be learned from the switch *on\_pulley*, then an additional element is created that connects the nodal point of the belt element with the nodal point that represents the axis of the pulley. The switch *original* of the objects *Element* is 1 for elements that are defined by the user and 0 for elements defined by the module **TAKEOFF**. After consideration of the *NoList* the whole belt system has been discretised into finite elements.

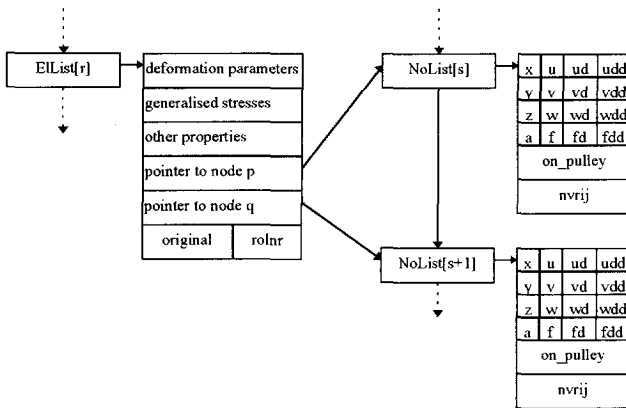


Figure 2.3: Connection between the *EList* and the *NoList*.

Although all the information of (discretised) components of the belt system is stored in the four data lists *NoList*, *EList*, *CoList* and *FoList*, this storage does not always enable easy access of specific information of, for example, the induction motor or a pulley. If information is required about the motor or a specific pulley then the *CoList* has to be

searched for this information. This information may be stored in the last object of the *CoList* which makes this search process very time consuming. Therefore objects have been defined in such a way that they provide an overlay in which the object oriented decomposition covers the component decomposition of a belt system, see Figure 2.4. These belt system components will be discussed in the Chapters 3 and 6. If a specific part of a belt system is considered then this part may contain a drive system, a belt, a pulley, an idler and bulk solid material. To enable access to a specific part of a belt system the class *BeltSys* has been defined. An object of this class is not used to store data but it inherits the data structure from classes that represent physical components of a belt system. These classes are *DriveSystem*, *TensionSystem*, *Belt*, *Pulley*, *Idler* and *BulkSolid*. The classes *DriveSystem*, *Belt* and *Idler* inherit a part of their data structure from classes that represent parts of the components. For the class *DriveSystem* these classes are *IndMotor*, *ReductionBox*, *FluidCoupling*, *SPC* (Static



Power Converter), *CST* (Controlled Start Transmission), *DiskBrake* and *HoldBack*. For the class *Belt* these classes are *Cover* and *Carcass* and for the class *Idler* they are *Roll* and *Frame*. Besides information that is obtained from linkage by pointers to objects of the four data lists, the objects of these classes also contain new data and procedures. For example, the class *IndMotor* provides a procedure to calculate the motor torque. To enable easy access to objects of the classes *IndMotor* and *FluidCoupling*, which is required to enable a fast calculation of the motor torque and fluid coupling torque, the objects of the class *IndMotor* are linked to each other in the list *MoList* and the objects of the class *FluidCoupling* in the list *FiList*.

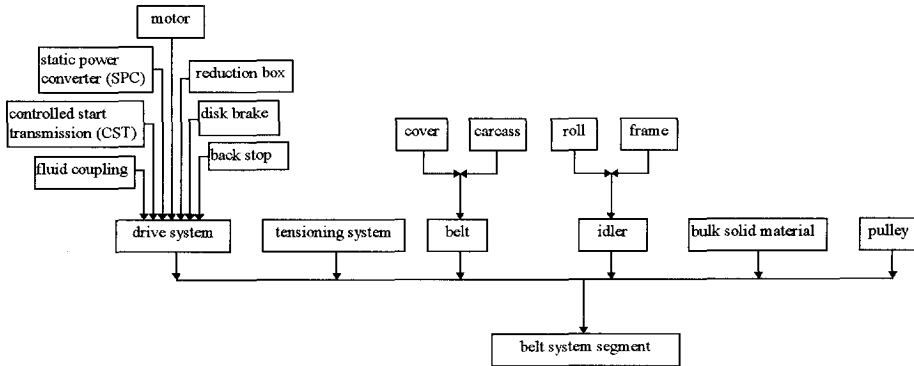


Figure 2.4: Decomposition to belt system segments.

Overlays that cover the finite element decomposition and the component decomposition of a belt system are provided by the two decompositions described above. However, the application of objects of these decompositions is not suitable for covering the mathematical decomposition of the belt system. In other words, no part of these objects can directly be used in the numerical solution of the equations of motion of the belt system. Therefore objects have been defined in such a way that they provide an overlay in which the object oriented decomposition covers the mathematical decomposition of a belt system. In Section 2.2.1 the partitioning of the spaces  $X$  and  $E$  in three sub spaces was described. This partitioning is also used in the

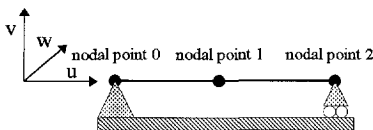


Figure 2.5: Two element finite element model.

module **TAKEOFF**. Since all the necessary information is already stored in the *NoList* and *ELList*, and also accessible via the component decomposition, only six lists of pointers are required to perform the partitioning of the nodal point co-ordinates

and the deformation parameters. The class *SubSpaceElem* is used for this purpose. The objects of this class only contain a pointer and specific information about the object data they are pointing to. In the module **TAKEOFF** six objects of the class *SubSpaceElem* are defined, *XO*, *XC*, *XM*, *E0*, *EC* and *EM*, which represent the vectors  $\mathbf{x}^o$ ,  $\mathbf{x}^c$ ,  $\mathbf{x}^m$ ,  $\boldsymbol{\varepsilon}^o$ ,  $\boldsymbol{\varepsilon}^c$  and  $\boldsymbol{\varepsilon}^m$  respectively. The partitioning of the nodal point co-ordinates and the deformation parameters, and thus the distribution of the co-ordinates and parameters over the six pointer lists, is automatically performed in accordance with rules prescribed by the user. As an example the partitioning of the nodal co-ordinates of the finite element model shown in Figure 2.5 is shown in Figure 2.6.

The partitioning implies that matrices and vectors have to be built up in accordance with the partitioning. For example the matrix **M** and the columns of matrix **D** are built up in accordance with the partitioning of *X* where the rows of **D** are built up in accordance with the partitioning of *E*. The most simple way to build the matrices and vectors is by accessing the nodal co-ordinates and the deformation parameters through the *NoList* and the *ELList*. However, these data lists are not partitioned. Therefore the pointer lists are used to sort the matrices and vectors according to the sub space partitioning. After the partitioning process the module **TAKEOFF** defines the matrices and vectors used in the numerical solution of the equations of motion and determines the initial position of the belt system, in particular the position of the belt on the supports.

The main steps performed by the module **TAKEOFF** then can be summarised in:

- step 1. Read model data from the input file and store these in data lists.
- step 2. Scan the data lists of the elements, nodal points and boundary conditions, and define, in case of elements that represent a supported belt part, additional elements, nodal points and deformation modes. Partition the nodal co-ordinates and the deformation modes and make the vectors  $\mathbf{x}^o$ ,  $\mathbf{x}^c$ ,  $\mathbf{x}^m$ ,  $\boldsymbol{\varepsilon}^o$ ,  $\boldsymbol{\varepsilon}^c$  and  $\boldsymbol{\varepsilon}^m$ .
- step 3. Define the matrices **D**, **Z**<sup>\*</sup>, **Σ**<sup>o</sup>, **M** and **M**<sub>0</sub> and the vectors **y**, **σ**, **g**<sup>2om</sup> and **F**<sub>0</sub>.
- step 4. Determine the initial position of the belt on the supports.
- step 5. Set the timestep counter to the initial time :  $t = t_0$ .

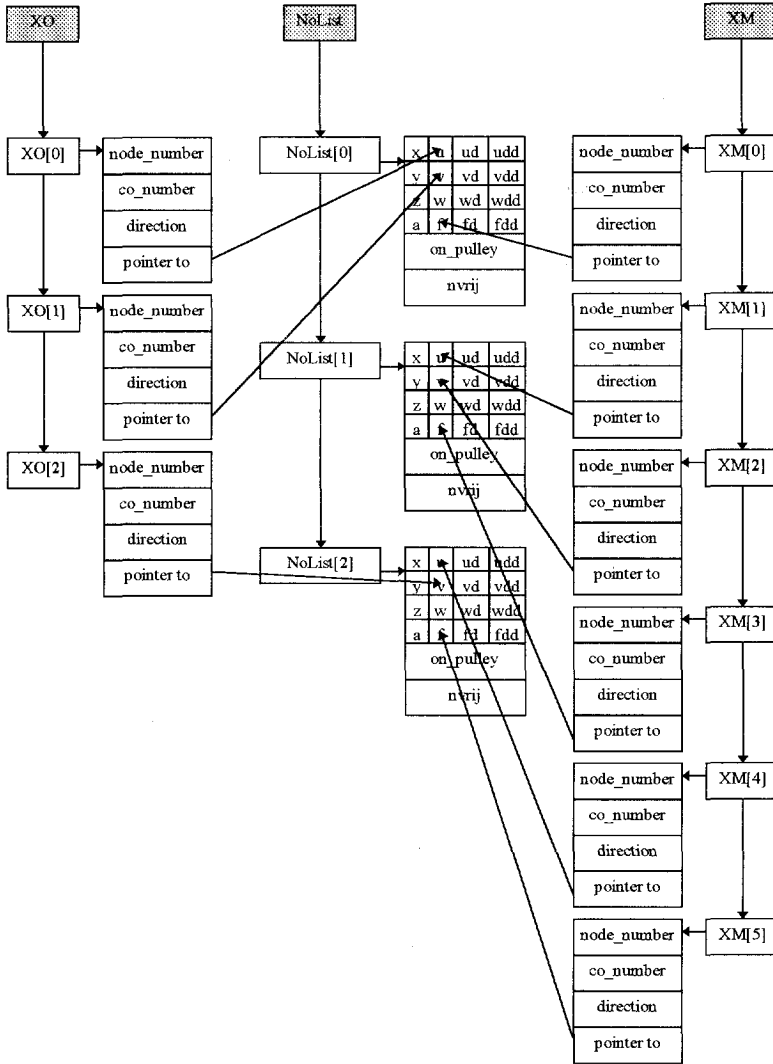


Figure 2.6: Distribution of the nodal co-ordinates over the pointer lists  $XO$  and  $XM$  in accordance with the sub space partitioning.

### 2.3.3 FLIGHT

The module **FLIGHT** starts, controls and stops the simulation process. The main steps of this process are summarised by:

- step 1. Update the state of the belt system including the drive system, the bulk solid material stream etc. for time  $t$ .
- step 2. Calculate the deformation parameters and the generalised stresses. Make the matrices  $\mathbf{D}$ ,  $\mathbf{Z}^*$ ,  $\Sigma^o$  and the vectors  $\mathbf{f}$ ,  $\mathbf{g}^{2om}$  and  $\sigma$ . Evaluate the system mass matrix  $\mathbf{M}$ . Make the matrix  $\mathbf{M}_0$ , the vectors  $\mathbf{F}_0$  and  $\mathbf{f}^*$ . To obtain  $\mathbf{M}_0^{-1}$  use Gauss-Jordan elimination with full pivoting [Press et al. (1992)].
- step 3. Calculate the generalised stress vectors  $\sigma^o$  and  $\sigma^m$  and the force vectors  $\mathbf{f}^o$  and  $\mathbf{f}^m$ . If the final time is reached,  $t > t_{stop}$ , or if the motion of a belt element is such that a constraint condition should be removed, then stop.
- step 4. Apply a fourth order Runge-Kutta method with variable stepsize [Press et al. (1992)] to integrate  $\dot{\mathbf{y}}_i$  to obtain  $\mathbf{y}_{t+\Delta t}$ . Before each integration step, step 2 is repeated starting from the second integration step. After each integration step the new configuration of the belt system is calculated by a kinematic analysis, see equation (2.53).
- step 5. Store the timestep data. Increment the timestep counter,  $t \rightarrow t + \Delta t$ , go to step 1.

### 2.3.4 LANDING

The module **LANDING** prepares the graphical presentation of the simulation results. The main steps performed in this module are:

- step 1. create two output files DATA.TXT and RESULT.TXT. The lay-out of the latter is equal to the lay-out of MODEL.TXT. DATA.TXT can be used as input file for the graphical procedures of the software package Matlab®.
- step 2. delete all the used data structures.
- step 3. if the simulation process was stopped before  $t > t_{stop}$ , then rename RESULT.TXT to MODEL.TXT and restart the module **TAKEOFF** else terminate **TUDBELT**.

---

## 2.4 References

- Bathe, K.J. (1985), *Finite element procedures in engineering analysis*, Prentice Hall, Inc., Englewood Cliffs, New Jersey.
- Besseling, J.F. (1977), "Derivatives of deformation parameters for bar elements and their use in buckling and postbuckling analysis", *Comp. Meth. in Applied Mechanics and Engineering* **12**, pp. 97-124.
- Besseling, J.F. (1982), "Non-linear theory for elastic beams and rods and its finite element representation", *Comp. Meth. in Applied Mechanics and Engineering* **31**, pp. 205-220.
- Booch, G. (1994), *Object oriented analysis and design with applications*, second edition, The Benjamin/Cummings Publishing Company Inc., Redwood City.
- Bowen, R.M. and Wang, C.C. (1976), *Introduction to vectors and tensors*, Plenum press, New York.
- Davies, G.A.O. (1982), *Virtual work in structural analysis*, John Wiley & Sons, Chichester.
- Dubois-Pelerin Y. and Zimmermann, T. (1993), "Object-oriented finite element programming: III, an efficient implementation in C++", *Comp. Meth. in Applied Mechanics and Engineering* **108**, pp. 165-183.
- Forde, B.W.R., Forschi, R.O., and Stierner, S.F. (1990), "Object-oriented finite element analysis", *Computers & Structures* **34**, pp. 355-374.
- Jalote, P. (1991), *An integrated approach to software engineering*, Springer-Verlag, Berlin.
- Jonker, B. (1988), *A finite element dynamic analysis of flexible spatial mechanisms and manipulators*, Ph.D. thesis, Delft University of Technology, Delft.
- Koh, A.S. and Park, J.P. (1994), "Object oriented dynamics simulator", *Computational Mechanics* **14**, pp. 277-287.
- Lodewijks, G. (1991), *Object oriented programming in C++*, reportno. 91.3.TT.2886, Delft University of Technology, Delft.
- Press, W.H., Teukolsky, S.A., Vetterling, W.T. and Flannerly, B.P. (1992), *Numerical recipes in C, the art of scientific computing*, Cambridge University Press, Cambridge.
- Werff, K. van der (1977), *Kinematic and Dynamic Analysis of Mechanisms, a Finite Element Approach*, Ph.D. thesis, Delft University of Technology, Delft.
- Zimmermann, T., Dubois-Pelerin, Y. and Bomme, P. (1992), "Object oriented finite element programming: I, governing principles", *Comp. Meth. in Applied Mechanics and Engineering* **98**, pp. 291-303.



# Chapter 3

## Belt properties

---

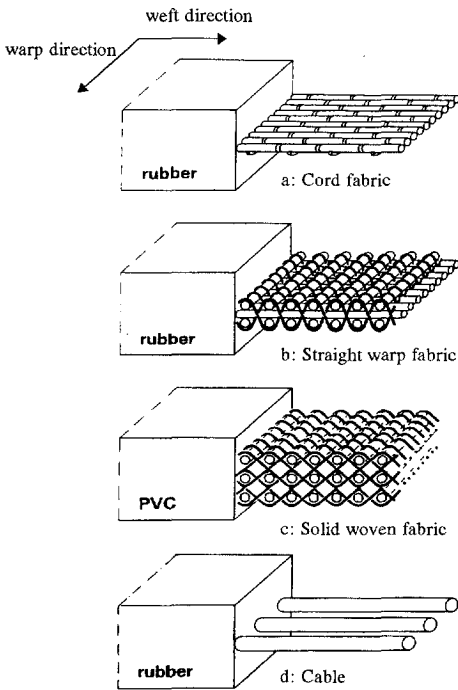


Figure 3.1: Carcass types .

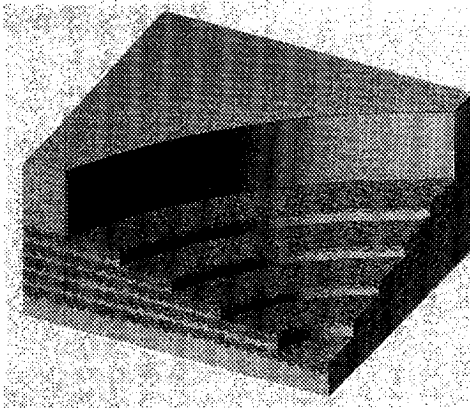
provide the necessary strength and stiffness in the weft (axial) direction of the belt. Figure 3.1a shows the mono-ply cord fabric whereas the multi-ply cord fabric is shown in Figure 3.2. To provide bending stiffness in the warp direction of the belt, warp cords are included in the carcass as is shown in the straight warp fabric of Figure 3.1b. To combine a high carcass strength and high warp bending stiffness, the

Since most belts used in the Netherlands are reinforced by fabric carcasses, this chapter focuses on the properties of fabric belts. These properties mainly determine the belt's dynamic behaviour and can be defined by a number of quantities. The carcass properties are highlighted in Section 3.1 and the belt cover properties in Section 3.2. Properties of steelcords and steelcord belts are given for comparison.

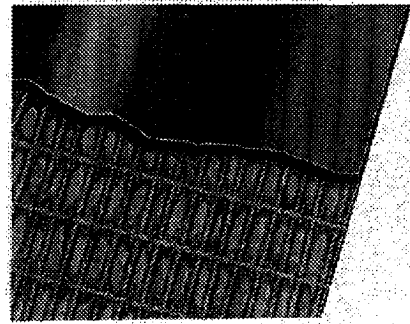
### 3.1 Carcass properties

The carcass, which is the reinforcement of the belt, can consist of a (multi) ply or solid woven fabric or of aramide or steelcord cables. Figure 3.1 shows the four typical carcass structures. The simplest carcass structure is the cord fabric where the cords, which can be made of polyester (E), polyamide (P) or aramide (A),

solid woven fabric can be used as shown in Figure 3.1c. If aramide cords or steelcords are used as reinforcement, the carcass structure can be like shown in Figure 3.1d. In practice the cables are held together by warp cables like shown in Figure 3.3.



**Figure 3.2:** Multi ply cord fabric belt, [Breidenbach, 1995].



**Figure 3.3:** Steel cord belt, [Breidenbach, 1995].

A fabric is built up of yarns that are twined bundles of fibres. For the application in the carcass of a belt, the usefulness of different reinforcement yarns is compared on the basis of three criteria. Firstly, the yarns must have a low density to minimise the specific mass of the belt. Secondly, the yarns must have a high specific strength to minimise the number of yarns and thus the thickness of the carcass. Thirdly, the stiffness of the yarns should limit the elongation of the carcass to maximal 1.5 % to reduce the size of the belt tensioner.

### 3.1.1 Unit strength

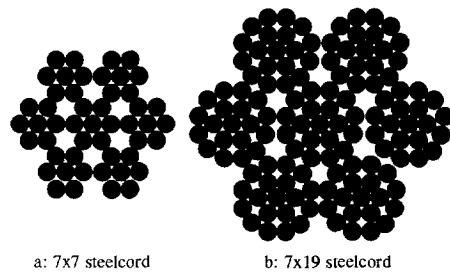
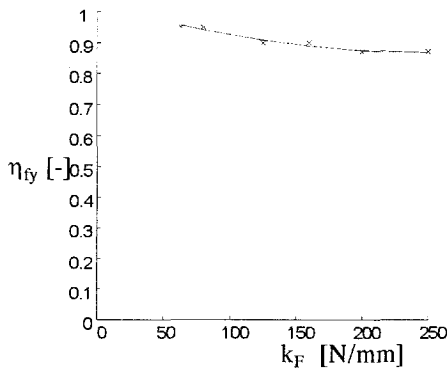
In structural elements like rods, the breaking strength of an element can be calculated by multiplying the cross-sectional area and the breaking stress of the material. In the field of conveyor belts, however, this approach is not useful since only the carcass and not the belt covers contribute to the belt strength. Therefore the breaking strength of a belt with a specific width  $B$  is calculated by multiplying the breaking strength per unit width of the carcass, also called the unit carcass strength, and the belt width. The tensile strength per unit fabric width, or unit fabric strength,  $k_F$ , can be calculated from the breaking strength of a yarn,  $F_B$ , the number of yarns per mm fabric width,  $N_y$ , and the yarn strength efficiency in fabric,  $\eta_{fy}$ , [Lodewijks, 1990]:



$$k_F = \eta_{fy} N_y F_B, \quad [\text{N} \cdot \text{mm}^{-1}] \quad (3.1a)$$

The number of yarns varies from 50 to 225 per 100 mm in the weft and from 30 to 100 per 100 mm in the warp direction of a ply. The yarn strength efficiency in fabrics made of polyester yarns in the weft and polyamide yarns in the warp direction, the so-called EP fabrics, is about 0.92 as is depicted in Figure 3.4. In the same way, the unit strength of a steelcord ply,  $k_F$ , can be calculated from the breaking strength of a steelcord,  $F_B$ , the number of steelcords per mm belt width,  $N_c$ , and the steel wire efficiency in steelcord,  $\eta_{fc}$ , [Lodewijks, 1990]:

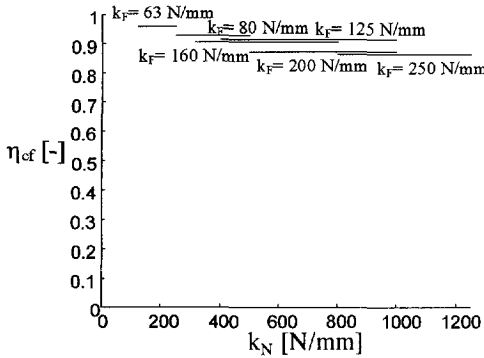
$$k_F = \eta_{fc} N_c F_B \quad (3.1b)$$



**Figure 3.4:** Yarn strength efficiency in EP fabric, [Lodewijks, 1990]. **Figure 3.5:** Typical steelcord structure.

The steelcords used in a steelcord belt are made of 7 smaller cables each made of 7 or 19 steel wires, see Figure 3.5. Also in this case the strength of one steelcord is less than the sum of the strengths of the smaller cables whose strength in turn is less than the sum of the strengths of the steel wires. The efficiency of the wires in a 1x7 cable and a 1x19 cable is approximately 0.90 and 0.88 respectively. A good estimate of the efficiency,  $\eta_{fc}$ , of the steel wires in a 7x7 and a 7x19 steelcord, as depicted in Figure 3.5, is 0.84 and 0.80 respectively, [Feyrer, 1994]. The number of steelcords varies from 6 till 10 per 100 mm belt width. The unit strength of a multi-ply EP carcass,  $k_C$ , is defined by:

$$k_C = \eta_{cf} N_r k_F \quad (3.2)$$



**Figure 3.6:** Fabric strength efficiency in a carcass, [Lodewijks, 1990].

where  $\eta_{cf}$  is the fabric strength efficiency in a carcass and  $N_f$  the number of fabric plies. Figure 3.6 shows the fabric strength efficiency  $\eta_{cf}$  of a carcass, made of fabric plies with different unit fabric strengths<sup>1</sup>  $k_F$ , as a function of the standardised unit strength  $k_N$ . The standardised unit strength, which indicates the minimum unit strength of a carcass, is used for classification of carcasses in a number of categories. These categories indicate the field of application of a carcass.

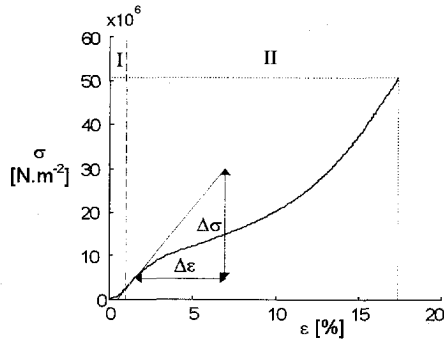
### 3.1.2 Young's modulus

To find the static Young's modulus of an EP belt from experiments, a tensile test as described in DIN standard 22102 can be used. The speed of the traverse of the tensile testing machine is, as is prescribed by that standard, 100 mm/min yielding a strain rate of about  $0.017 \text{ s}^{-1}$  for a sample with standardised length of 100 mm. A typical stress-strain curve that can be obtained from a tensile test is shown in Figure 3.7. In this figure two zones can be distinguished. In zone I the woven structure of the belt's fabric is stretched. This process is irreversible which results in a permanent strain of the belt and explains why this zone does not occur in a tensile test of a used belt. In zone II the real tensile test begins. Under normal operational conditions the maximum strain of a belt is smaller than 1.5 %. In that case the belt material is almost linear elastic and Young's modulus of the belt is constant. It can be obtained from Figure 3.7 by:

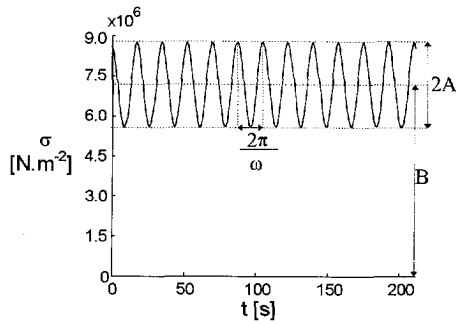
$$E_b = \frac{\Delta\sigma}{\Delta\varepsilon} \tag{3.3}$$

The value of Young's modulus of a belt obtained from a tensile test is dependent on the strain rate during that test. Although the static Young's modulus can be used for a statically loaded belt, it can not be used for a dynamically loaded belt.

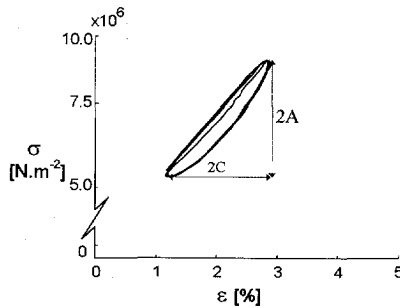
<sup>1</sup> Note that this efficiency is independent of the number of fabric plies in the carcass and of the thickness of the rubber plies between the fabrics plies.



**Figure 3.7:** Stress-strain curve of an EP 500/3 belt, [Lodewijks, 1991].



**Figure 3.8:** Sinusoidal belt load applied to an EP 500/3 belt during hysteresis experiment with frequency of 0.05 Hz, [Lodewijks, 1991].



**Figure 3.9:** Belt load/strain curve of an EP 500/3 belt during hysteresis experiment with frequency of 0.05 Hz, [Lodewijks, 1991].

To obtain Young's modulus for a dynamically loaded belt, a hysteresis test is performed where a sinusoidal load is applied to the belt as is shown in Figure 3.8. The time dependent stress is prescribed by the following equation:

$$\sigma(t) = A\sin(\omega t) + B \quad (3.4)$$

where A is the amplitude of stress variation,  $\omega$  the circular frequency of deformation and B the mean stress. The visco-elastic response, shown in Figure 3.9, is equal to [Struik and van den Berg, 1989]:

$$\varepsilon(t) = C\sin(\omega t + \delta) + D \quad (3.5)$$

where D is the mean strain,  $\delta$  is the phase angle here called the loss angle,  $A/C = E_d$  the dynamic Young's modulus,  $E_d \cos \delta = E'(\omega)$  the storage modulus and  $E_d \sin \delta = E''(\omega)$  the loss modulus. The loss factor is defined by  $\tan \delta = E''/E'$ . If the mean load, the load amplitude and frequency are known in advance, the dynamic Young's modulus  $E_d$  should be used instead of the static Young's modulus  $E_b$  to determine the correct elastic response. As an example, the static Young's modulus of an EP 500/3 belt, which can be obtained from the stress/strain curve as shown in Figure 3.7,  $E_b = 244.14 \text{ N.mm}^{-2}$  whereas the dynamic Young's modulus, which can be obtained from Figure 3.9,  $E_d = 286.93 \text{ N.mm}^{-2}$ .

To calculate the static Young's modulus of the belt in case no experimental data are available, the Gough-Tangorra formulas, that are based on the classical laminate theory, can be used [Hsieh, 1985]:

$$E_b = V_c E_c + (1 - V_c) E_m \quad (3.6)$$

where  $V_c$  is the volume fraction of carcass material,  $E_c$  the static Young's modulus of the carcass material and  $E_m$  the static Young's modulus of the matrix material that protects the carcass. In cases where equation (3.6) yields inaccurate moduli, more sophisticated formulas are available, [Kittredge, 1991]. However, from experiments it follows that the moduli obtained from equation (3.6) are accurate in most cases. The static Young's modulus of a fabric carcass ply normally follows from experiments since it is not very convenient to define a formula for this modulus considering the many different carcass structures. However, in case of a cord reinforced carcass, the static Young's modulus can be determined from the geometry of the cords. The static Young's modulus of an 1xN steelcord can be calculated by [Feyrer, 1994]:

$$E_s = \frac{1}{A_M} \sum_{i=0}^n \frac{z_i \cos^3 \alpha_i}{1 + \nu_i \sin^2 \alpha_i} E_i A_i \quad (3.7)$$

where  $A_M$  is the total cross sectional area of all the wires in the cable,  $z_i$  the number of wires in the  $i^{\text{th}}$  layer around the core of the cable,  $\alpha_i$  the twist angle of the wires in the  $i^{\text{th}}$  layer,  $\nu_i$  Poisson's ratio of these wires,  $E_i$  the static Young's modulus of the wires in the  $i^{\text{th}}$  layer and  $A_i$  the cross sectional area of the wires in that layer.

In case of a multi-ply cord fabric carcass the volume fraction of carcass material can be obtained from:

$$V_c = \frac{B - b_s}{B} \frac{N_f d_f}{d_b} \quad (3.8a)$$

where  $B$  is the belt width,  $b_s$  the total thickness of the belt's side covers,  $N_f$  the number of plies,  $d_f$  the thickness of each fabric ply and  $d_b$  the thickness of the belt. The volume fraction of carcass material of a (mono-ply) steelcord belt can be obtained from :

$$V_c = \frac{B - b_s}{B} \frac{A_c N_c}{d_b} f_c \quad (3.8b)$$

where  $N_c$  the number of steel cables per unit belt width,  $A_c$  is the cross sectional area of a steelcord and  $f_c$  the fill factor.

### 3.1.3 Bending stiffness

The effective bending stiffness of a belt with respect to the neutral axis can be calculated by:

$$(E_b I_y)_{\text{eff}} = \int E(y, z) z^2 dA \quad (3.9)$$

With use of equation (3.9) and the dimensions given in Figure 3.10, the effective Young's modulus, with respect to the  $y$ -axis as indicated in Figure 3.10, of a belt with upper cover, lower cover and side covers, is equal to:

$$(E_b I_y)_{\text{eff}} = \left[ \frac{E_c(B - b_s)}{12} + \frac{E_m b_s}{12} \right] \left[ d_c(4d_c^2 - 6d_b d_c + 3d_b^2 - 12d_b d_l + 12d_l d_c + 12d_l^2) \right] + \frac{E_m B}{12} \left[ d_u(4d_u^2 - 6d_b d_u + 3d_b^2) + d_l(4d_l^2 - 6d_b d_l + 3d_b^2) \right] \quad (3.10a)$$

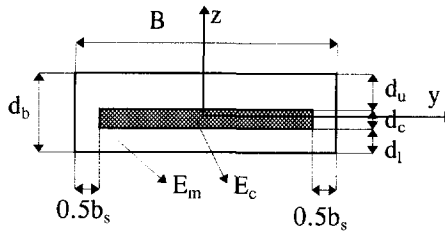


Figure 3.10: Cross section of a belt.

The effective bending stiffness, in case of a one-ply cord fabric belt with belt width  $B$ , no side covers ( $b_s=0$ ) and two covers with thickness  $d_m$  ( $d_l=d_u=d_m$ ;  $d_b=2d_m+d_c$ ), calculated with respect to the  $y$ -axis as indicated in Figure 3.10 (which in this case is the neutral axis), is:

$$(E_b I_y)_{\text{eff}} = E_c \frac{B d_c^3}{12} + E_m B \left( \frac{2}{3} d_m^3 + d_m^2 d_c + \frac{1}{2} d_m d_c^2 \right) \quad (3.10b)$$

Normally the average Young's modulus of the belt,  $E_b$  or  $E_d$ , is known instead of Young's moduli of the carcass  $E_c$  and of the belt cover, or matrix material,  $E_m$ . However, the carcass delivers the largest contribution to the effective bending stiffness since Young's modulus of for example a rubber belt cover is about  $1 \text{ N.mm}^{-2}$  whereas the average static Young's modulus of for example an EP 500/2 belt is  $250 \text{ N.mm}^{-2}$ . Therefore, if  $E_b$  or  $E_d$  is known instead of  $E_c$  and  $E_m$ , then the effective bending stiffness can be calculated with use of equation (3.10) taking  $E_c$  equal to  $E_b$  or  $E_d$  and  $E_m$  zero. In case of a troughed belt also the trough shape has to be accounted for, see [Harrison, 1984] and [Lodewijks, 1994].

To determine whether or not the bending stiffness significantly influences the dynamic behaviour of a belt, a bending rigidity parameter  $k_B$  is defined<sup>2</sup>:

<sup>2</sup> This parameter will be derived in Section 4.2.3.4.

$$k_B = \sqrt{1 + n^2 \pi^2 \frac{E_b I_y}{TL^2}}, \quad n = 1, 2, \dots \quad (3.11)$$

where  $n$  is the wave number of the transverse vibrations,  $T$  the belt tension and  $L$  the idler spacing. If  $k_B$  differs significantly from 1 then the belt's bending stiffness must be taken into account.

### 3.1.4 Belt tension related parameters

For design purposes, standards like DIN 22101, ISO 5048 and CEMA provide safety factors that limit the allowable belt load. The safety factor that has to be taken into account on the stationary stresses in a belt,  $S_B$ , is defined by:

$$S_B = \frac{1}{1 - (r_0 + r_1 + r_2)} \quad (3.12a)$$

and the safety factor on the non-stationary stresses in the belt,  $S_A$ , is equal to:

$$S_A = \frac{1}{1 - (r_0 + r_1)} \quad (3.12b)$$

where  $r_0$  accounts for the reduction of the strength of the belt (splices) due to fatigue,  $r_1$  takes into account the extra forces that act on the belt in transition zones and on pulleys etc., whereas  $r_2$  accounts for the extra dynamic stresses in the belt during starting and stopping. The values of these reduction factors can be found in Table 3.1. Some conveyor belt manufacturers allow for lower safety factors on the stationary belt stresses, see Table 3.2.

Carcass material	operational condition	$r_0$	$r_1$	$r_2$	$S_A$	$S_B$
B (Cotton)	light	≥0.691	≥0.100	≥0.060	≥4.8	≥6.7
P (Polyamide)	normal	≥0.715	≥0.100	≥0.060	≥5.4	≥8.0
E (Polyester)	heavy	≥0.734	≥0.100	≥0.060	≥6.0	≥9.5
ST (Steelcord belt)	light	≥0.641	≥0.150	≥0.060	≥4.8	≥6.7
	normal	≥0.665	≥0.150	≥0.060	≥5.4	≥8.0
	heavy	≥0.684	≥0.150	≥0.060	≥6.0	≥9.5

Table 3.1: Reduction factors and safety factors according to DIN 22101.

Carcass material	operational condition	$S_{B,min1}$	$S_{B,min2}$
B (Cotton)	light	3.0	3.2
P (Polyamide)	normal	-	3.5
E (Polyester)	heavy	3.6	3.7
ST (Steelcord belt)	light	2.5	2.8
	normal	-	3.0
	heavy	3.0	3.2

**Table 3.2:** Minimum safety factors  $S_{B,min}$  on the stationary stresses in a belt according to ContiTech Transportbandsysteme GmbH ( $S_{B,min1}$ ) and Dunlop-Enerka B.V. ( $S_{B,min2}$ ).

This reduction is not only based on improved belt and splice design but also on the increased experience with the design of transition zones and with starting and stopping procedures, also see [Lodewijks, 1995a]. The existing, or actual, safety factor  $S$  in a belt section is defined by:

$$S = \frac{k_N B}{T} \tag{3.13}$$

where  $T$  is the belt tension in that section. Note that  $T$  and  $S$  are variable along the belt length. According to DIN 22101 it is required that  $S > S_A$  during starting and stopping and that  $S > S_B$  during normal operation. A typical value for  $S$  during normal stationary operation is 8.

A sufficiently accurate approximation of the static belt sag ratio  $K_s$ , which is the ratio between the static belt sag and the idler spacing, is:

$$K_s = \frac{m'g L}{8T} \tag{3.14}$$

where  $m'g$  is the distributed belt and bulk weight in  $N.m^{-1}$ . In correctly designed belt conveyor systems  $K_s$  is smaller than 0.015, although some designers accept ratios of about 0.05.

For the design of starting and stopping procedures it is important to know at what speed stress waves travel through a belt. Two wave speeds can be defined:

$$c_1 = \sqrt{\frac{E_b}{\rho}} ; c_2 = \sqrt{\frac{\sigma}{\rho}} = \sqrt{\frac{T}{\rho A}} \tag{3.15}$$



where  $\rho$  is the density and  $A$  the cross sectional area of the belt material. The first parameter  $c_1$  is the longitudinal wave speed that governs the frequencies of axial vibrations of a belt. The second,  $c_2$ , is the axial propagation speed of transverse waves that governs the frequencies of transverse vibrations of a belt span without bending stiffness and supported by two idlers. Table 3.3 shows the wave speeds for two belts loaded at  $S=10$ .

Belt type	$c_1$ [m/s]	$c_2$ [m/s]
EP 1000/5	804.3	80.0
St 1000	1637.4	76.0

Table 3.3: Wave speeds for three different belts, [Lodewijks, 1990].

The wave speeds however, depend not only on the density of the belt material but, in case of a conveyor belt, on the mass of the bulk material on the belt as well. The longitudinal wave speed also depends on the load of the (reduced) masses of the supporting idlers. If the two wave speeds are rewritten to:

$$c_1 = \sqrt{\frac{E_b}{\rho}} = \sqrt{\frac{E_b A}{m'_{\text{belt}}}}; c_2 = \sqrt{\frac{T}{\rho A}} = \sqrt{\frac{T}{m'_{\text{belt}}}} \quad (3.16)$$

where  $m'_{\text{belt}}$  is the belt mass per unit of length, then the effective wave speeds for an unloaded, supported belt can be written as follows:

$$c_{1,\text{effU}} = \sqrt{\frac{E_b A}{m'_{\text{belt}} + m'_{\text{roll}}}} = \sqrt{\frac{m'_{\text{belt}}}{m'_{\text{belt}} + m'_{\text{roll}}}} c_1 = C_{U1} c_1; c_{2,\text{effU}} = c_2 \quad (3.17)$$

where  $m'_{\text{roll}}$  is the reduced mass of the idlers per unit of length, and for a loaded, supported belt:

$$c_{1,\text{effL}} = \sqrt{\frac{E_b A}{m'_{\text{belt}} + m'_{\text{bulk}} + m'_{\text{roll}}}} = \sqrt{\frac{m'_{\text{belt}}}{m'_{\text{belt}} + m'_{\text{bulk}} + m'_{\text{roll}}}} c_1 = C_{L1} c_1 \quad (3.18)$$

$$c_{2,\text{effL}} = \sqrt{\frac{T}{m'_{\text{belt}} + m'_{\text{bulk}}}} = \sqrt{\frac{m'_{\text{belt}}}{m'_{\text{belt}} + m'_{\text{bulk}}}} c_2 = C_{L2} c_2$$

where  $m'_{\text{bulk}}$  is the mass of bulk material on the belt per unit of length. In practice the equations (3.18) represent the lower limits of the wave speeds whereas the equations

(3.17) represent the upper limits. The ratio between the wave speeds for a loaded and an unloaded belt can be obtained from the equations (3.17) and (3.18):

$$c_{1,\text{effL}} = \sqrt{\frac{m'_{\text{belt}} + m'_{\text{roll}}}{m'_{\text{belt}} + m'_{\text{bulk}} + m'_{\text{roll}}}} c_{1,\text{effU}} = \frac{C_{L1}}{C_U} c_{1,\text{effU}}$$

$$c_{2,\text{effL}} = \sqrt{\frac{m'_{\text{belt}}}{m'_{\text{belt}} + m'_{\text{bulk}}}} c_{2,\text{effU}} = C_{L2} c_{2,\text{effU}}$$
(3.19)

### 3.2 Cover properties

Most belt covers are made of rubber or polyester material. The constitutive behaviour of these materials is visco-elastic as can be learned from the time-dependency of the stress-strain relations, [Lodewijks, 1990 & 1995b]. The most important environmental parameters that affect the dynamic response of visco-elastic materials are temperature, frequency and the amplitude of an imposed load, see for example [Eirich, 1978]. It is also important to know the exact compound of the material. In rubber for example the amount of carbon black influences the material properties considerably, [Mey and Van Amerongen, 1969].

The constitutive equation for an isotropic linear visco-elastic material can be written in general tensor form [Flügge, 1975], [Struik and Van den Berg, 1989]:

$$\sigma^d(t) = \int_{-\infty}^t \Psi(t-t') \frac{\partial \gamma^d(t')}{\partial t'} dt' \quad (3.20)$$

in which  $\sigma^d = \sigma - (\frac{1}{3} \text{tr} \sigma) \mathbf{I}$  is the deviatoric stress tensor and  $\gamma^d = \gamma - (\frac{1}{3} \text{tr} \gamma) \mathbf{I}$  the deviatoric strain tensor. The fourth order tensor function  $\Psi(t)$  is called the relaxation function and specifies the stress response to a unit strain increment. It can be written as :

$$\Psi(t) = \Psi_{\infty} + \int_0^{\infty} g(\tau) \exp(-\frac{t}{\tau}) d\tau \quad (3.21)$$

where  $g(\tau)$  is the relaxation spectrum which can be discrete or continuous and  $\tau$  the relaxation time. If in the uniaxial case a pulse-spectrum  $g(\tau) = \sum_{j=1}^N g_j \delta(\tau - \tau_j)$  is used then the relaxation function is equal to:

$$\Psi(t) = \Psi_{\infty} + \sum_{j=1}^N g_j \exp\left(-\frac{t}{\tau_j}\right) \quad (3.22)$$

This material model is known as the generalised Maxwell model. Figure 3.11 shows this uniaxial case. In this model a number of damping coefficients  $\eta_i$  is used which are related to specific relaxation times  $\tau_i$ , in order to be able to represent the constitutive behaviour of a material for a wide range of loading frequencies.

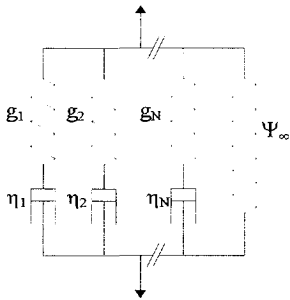


Figure 3.11: Generalised uniaxial Maxwell model.

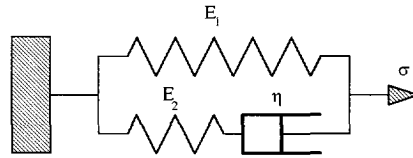


Figure 3.12: Three parameter Maxwell model (standard linear solid model).

If this range is relatively small for a specific application then it is sufficient to use one relaxation time which fits for that range. In such a case a three parameter Maxwell model, or a so called standard linear solid model, results, which is the simplest model that can describe the relaxation of a material and situations of constant stress or high strain rates, see Figure 3.12.

The relaxation function of the three parameter model is :

$$\Psi(t) = E_1 + E_2 \exp\left(-\frac{t}{\tau}\right) \quad (3.23)$$

where the relaxation time  $\tau = \frac{\eta}{E_2}$ . For a three parameter Maxwell model the storage modulus is:

$$E'(\omega) = \frac{E_1 E_2^2 + \omega^2 \eta^2 (E_1 + E_2)}{E_2^2 + \omega^2 \eta^2} \quad (3.24)$$

where  $\omega$  is the circular frequency of deformation. The loss factor  $\tan\delta$  is in this case defined by:

$$\tan\delta = \frac{E''}{E'} = \frac{\omega\eta E_2^2}{E_1 E_2^2 + \omega^2 \eta^2 (E_1 + E_2)} \quad (3.25)$$

The damping factor  $\eta$  of the three parameter Maxwell model can then be written in terms of the loss factor:

$$\eta(\delta) = \frac{2\pi \tan\delta}{2 + (\pi + 2\delta)\tan\delta} \quad (3.26)$$

From experiments it can be learned that a real rubber cannot be modelled with one relaxation time. However, if the differences in belt speed are not too large, in fact the belt speed of conveyor belts varies from 0.1 m/s to 10 m/s, then it is sufficient to choose one relaxation time. This relaxation time must be chosen in agreement with the time it takes for a material point of the belt cover to pass the contact zone between belt and roll.

As an example, the storage modulus, the loss modulus and the loss factor of an SBR rubber have been obtained from experiments using a Dynaliser™ [Lodewijks, 1995b]. The Dynaliser™ is used to perform a strain controlled relaxation test by imposing a known deformation on a sample and measuring the variation of the reaction force as a function of time. The testpiece is deformed by fast penetration of a spherical indenter. The indentation is kept constant for the minute or less required for the test and an integrally mounted transducer produces the data for a force relaxation curve. A computer then calculates the storage modulus  $E'$ , the loss modulus  $E''$  and the loss factor  $\tan\delta$  [Smith, 1993]. With these moduli and factor being known, the equations (3.24)-(3.26) can be used to determine the parameters  $E_1, E_2$  and  $\eta$  of the three parameter Maxwell model. The results of the experiments are depicted in the Figures 3.13 - 3.15 as a function of temperature and deformation rate. In Figure 3.15 it can be seen that the loss factor passes through a maximum. This maximum is the so-called transition point which is about  $-40^\circ\text{C}$  for the considered SBR rubber. The temperature zone around the transition point is called the transition region. The temperature zone below the transition region is called the glassy region whereas the temperature zone above the transition region is called the rubbery region [Brown, 1996].

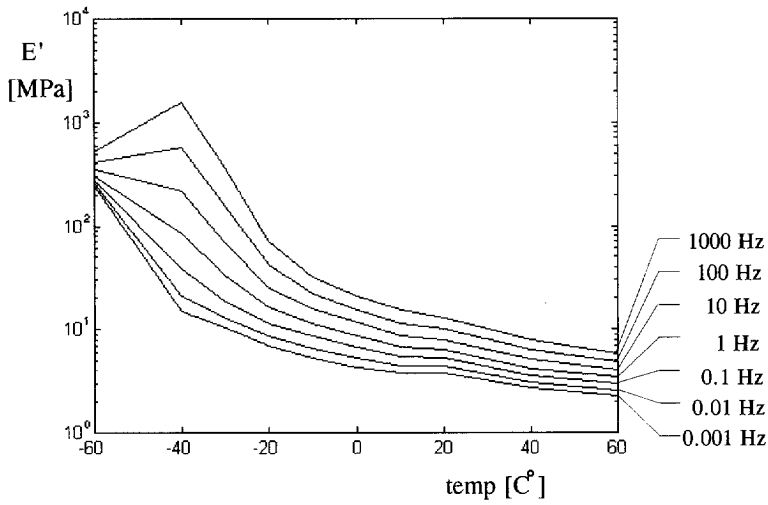


Figure 3.13: The storage-modulus as a function of temperature and deformation rate, [Lodewijks, 1995b].

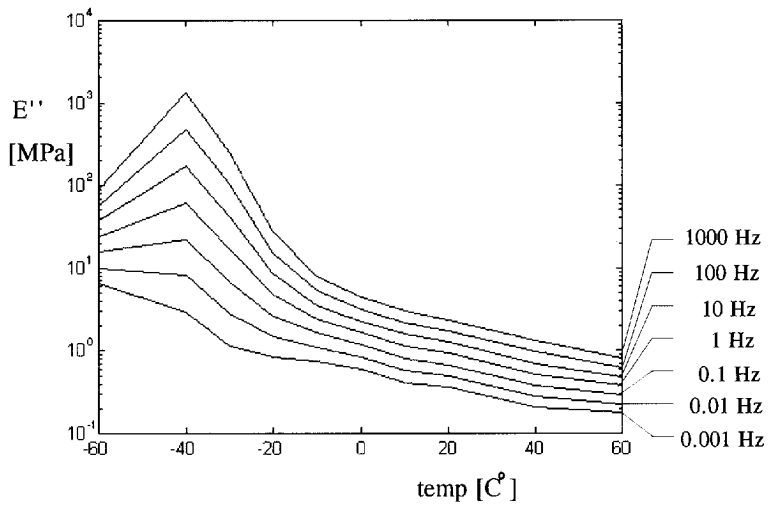


Figure 3.14: The loss-modulus as a function of temperature and deformation rate, [Lodewijks, 1995b].

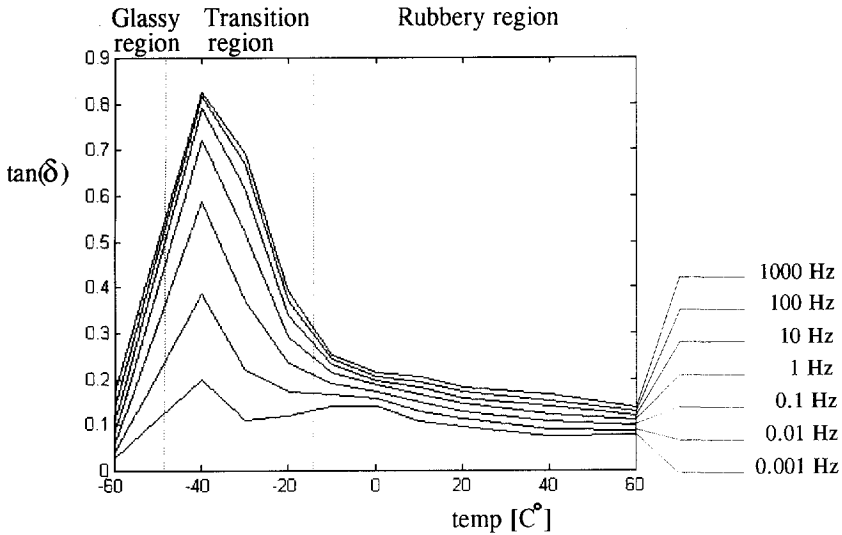


Figure 3.15: The loss-factor as a function of temperature and deformation rate, [Lodewijks, 1995b].

### 3.3 References

- Breidenbach, H. (1995), *Fördergurt-Technik, Projektierung und Berechnung*, BTR Dunlop Belting Group, Drachten.
- DIN - Taschenbuch 44 (1973), *Normen über Hebezeuge und Fördermittel*, Deutsche Normenausschuß, Berlin.
- Brown, R. (1996), *Physical testing of rubber*, Chapman and Hall, London.
- Eirich, R.F. (1978), *Science and Technology of Rubber*, Academic Press, London.
- Feyrer, K (1994), *Drahtseile, Bemessung, Betrieb, Sicherheit*, Springer-verlag, Berlin.
- Flügge, W. (1975), *Viscoelasticity*, Springer-Verlag, Berlin.
- Harrison, A. (1984), "Flexural behaviour of tensioned conveyor belts", *Bulk Solids Handling* 4, pp. 333-337.
- Hsieh, K.T. (1985), *Modelling of cord-reinforced rubber laminates*, Ph.D. thesis, University of Texas, Austin.
- Kittredge, C.A. (1991), *Static response of cord composite plates*, Ph.D. thesis, University of Illinois, Urbana-Champaign.
- Lodewijks, G. (1990), *Stageverslag Dunlop-Enerka (in Dutch)*, Twente University, Enschede.

Lodewijks, G. (1991), *Experimenteel onderzoek van transportbandmonsters ter determinatie van de dynamische eigenschappen (in Dutch)*, Reportno. 91.3.TT.2916, Section Transporttechnology, Delft University of Technology.

Lodewijks, G. (1994), *Transverse vibrations in flexible belt systems*, Reportno. 94.3.TT.4270, Section Transporttechnology, Delft University of Technology.

Lodewijks, G. (1995a), "De levensduur van transportbanden (in Dutch)", *Bulk* 3(1), pp. 16-19.

Lodewijks, G. (1995b), "The rolling resistance of conveyor belts", *Bulk Solids Handling* 15, pp. 15-22.

Mey, S. and Amerongen, G.J. van (1969), "Mechanic-Dynamic Characteristics of Rubber Compounds", *Rubber Chemistry and Technology* 21, pp. 1215-1232.

Smith, L.P. (1993), *The Language of Rubber*, Butterworth-Heinemann Ltd, Oxford.

Struik, L.C.E. and Berg, J.W.A. van den (1989), *Kunststoffen (in Dutch)*, Lecture book, Twente University, Enschede.





## *Chapter 4*

# **Analytical modelling of belt systems**

---

**I**n most belt systems the belt is vibrating transversely with a small amplitude in its lowest natural frequency. This amplitude increases considerably when the belt is excited in the resonance frequency by the supports or the tensioning system. Severe transverse vibration of a belt is often the cause of costly breakdowns in large belt conveyor systems [Harrison, 1992]. In band saws, vibration results in waste of raw material, reduced tool life, and poorer dimensional accuracy and surface quality in the product. [Ulsoy and Mote, 1982]. Therefore, knowledge of the natural frequencies of transverse vibration of belt parts is important for the design of a support structure which will not cause belt excitation, a so-called resonance free belt support.

In this chapter the analytical determination of the natural frequencies of transverse vibration of a moving flat belt span, supported by two pulleys or idlers, is discussed. The dependence of these frequencies on the belt material parameters, the belt speed and the stiffness of the tensioning system will be shown. The interaction between different belt parts or between the belt and the tensioning system is mostly modelled by a discrete approach. This approach will be discussed in Chapter 7. The design of resonance free belt supports will be discussed in Chapter 9.

### **4.1 Introduction**

Belt systems can be divided into two categories: the string-like systems (second order systems) and the beam or plate-like systems (fourth order systems). If the bending stiffness of an axially moving material can be neglected then the system is classified as a string-like system otherwise it is classified as a beam-like system [Wickert and Mote, 1988].

### 4.1.1 String-like systems

The transverse vibration of moving string-like systems was first investigated by Skutch (1897) who calculated the fundamental vibration frequency of a string travelling between two fixed supports. Subsequent fundamental research on linear vibrations yielded three major conclusions [Archibalt and Emslie, 1958; Swope and Ames, 1963]. Firstly, if  $c_2$  is the propagation speed of transverse waves at zero transport speed and  $V_b$  is the axial transport speed, then disturbances propagate in the up- and downstream directions at speeds  $c_2 - V_b$  and  $c_2 + V_b$ , respectively, relative to a fixed observer. Secondly, this speed difference renders a motion of the travelling string of non-constant phase; disturbances that travel upstream are retarded in phase relative to those that propagate downstream. Thirdly, the natural frequencies of the oscillations decrease monotonically as the transport speed increases. All frequencies vanish when  $V_b = c_2$  and instability results. Archibalt and Emslie (1958) noted the similarity between the axially moving string vibration problem and that of a pipe containing a flowing fluid.

The accuracy of the linear theory was investigated through inclusions of several forms of non-linearity in the equations of motion (cf. [Carrier, 1945; Lee, 1958; Vicario, 1958; Zaiser, 1964; Mote, 1966]). Simplifications such as relatively small transverse displacements and constant axial velocity and mass density were used to calculate approximate solutions for the non-linear planar motion. This showed the limitations of the linear theory. Tension variation during oscillation with sufficiently large amplitudes affects the response, and the linear theory is rendered inapplicable. This effect becomes more pronounced when  $\beta = V_b/c_2$  increases [Thurman and Mote, 1969].

Axially-moving string-like materials interact with other components of the system which has been analysed in several recent studies (cf. [Rhodes, 1970; Mote and Wu, 1985; Ulsoy et al., 1985; Majewski, 1986; Wang and Mote, 1986; Fujino et al., 1993; Hwang et al., 1994]).

All axially-moving materials accelerate and decelerate axially, and some systems, such as magnetic tapes and aerial tramways, do so frequently. Miranker (1960) first introduced variable transport speed in a model. Acceleration has a stabilising effect on transverse vibration but deceleration has a destabilising effect [Mote, 1968].

Although the influence of damping on the vibrations can be considerable, only a few studies consider this. Linear damping forces of the form  $Cv_{,t}$  (cf. [Sack, 1954; Mahalingam, 1957; Mote, 1968]) where  $v$  is the transverse displacement,  $C(v_{,t} + V_b v_{,x})$  (cf. [Mahalingam, 1957; Ulsoy and Mote, 1982]) and  $C_1 v_{,t} + C_2 V_b v_{,x}$  [Ulsoy and Mote, 1982] where included in the equation of transverse motion. Here  $v_{,t} + V_b v_{,x}$  represents the transverse velocity of a string particle as measured by a

fixed observer;  $v_1$  is that velocity measured by an observer moving axially with the string with a speed  $V_b$ .

The influence of sag of an axial moving cable was first recognised by Simpson (1972). He analysed the free, in-plane vibrations of an elastic, axially-moving cable, that passes through fixed eyelets at the same elevation. His model assumed both small displacements and small equilibrium cable sag (also see [Soler, 1970; Irvine, 1980; Luongo et al., 1984]). Triantafyllou (1984&1985) later considered in-plane vibrations of axially moving cables with support eyelets at different elevation and cables with either very small or very large sag. Perkins and Mote (1987) developed a non-linear three-dimensional cable dynamics theory. Recently, periodic solutions of some large amplitude forced belt vibrations were given by Blom (1994).

### 4.1.2 Beam-like systems

Early analysis of the vibration and stability of axially-moving beam-like materials focused on the linear transverse vibration of an axially-moving Euler-Bernoulli beam (cf. [Mote, 1965; Barakat, 1967; Chubachi, 1958]). Simpson (1973) first derived the equations of motion of a travelling Timoshenko beam.

The stability of travelling beams excited parametrically either by periodic tension variation or periodic edge loading has been analysed by Mote (1968) (see also Buffington and Kane, 1985). Wheel eccentricity, variations in band stiffness, and pinch roller or guide friction forces produce periodic axial tension. Periodic axial motion is another source of parametric excitation (cf. [Wickert and Mote, 1990; Abrate, 1992; Asokanathan and Ariaratnam, 1994]).

Motivated by high-velocity computer tapes that travel over guides and read-write heads, several investigators have analysed the steady-state displacement of materials that travel over a rigid discontinuous surface [Ono, 1979; Majewski, 1986]. In most applications, the axially-moving beam is supported at two points and the transverse motion of the beam within the span interior is of interest. The dynamics of a cantilever beam, which is ejected from a single fixed support was studied by Mansfield and Simmonds (1987). Development of this model was motivated by the development of long, slender spacecraft antennas [Weeks, 1986] and by paper transport in copying machines [Mansfield and Simmonds, 1987].

A band and pulley system consists of two band spans and two pulleys. The earliest models considered vibration of only one span; because of the inertia and dissipation associated with the pulleys, the vibration of the considered span was assumed uncoupled from the motion of the other span and the pulleys. However, transverse vibration of the endless band loop couples response of the entire band to that of the pulleys, and in general, the model describing the motion of one span cannot be decoupled from the remainder of the system without loss of model accuracy. Band-pulley coupling has some important implications for vibration control.

In some instances active control of one span motion can be achieved through application of control forces to the other span, the pulleys or the support structure (cf. [Mote, 1965; Rhodes, 1970; Mote and Wu, 1985; Wang and Mote, 1986; Wang and Mote, 1987; Abrate, 1992; Asokanathan and Ariaratnam, 1994]).

## 4.2 Dynamics of a stationary moving belt

In this section the motion of a homogeneous belt span supported by two rolls or pulleys is considered. The frequencies of axial and transverse vibration are derived accounting for the influence of the belt speed, the belt material parameters and the stiffness of the tensioning system. The interaction between adjacent belt parts is not considered.

### 4.2.1 Deformation of the belt

Consider a belt supported by two pulleys as depicted in Figure 4.1. The belt will be pre-tensioned and has an initial strain  $\epsilon^0$  in the reference configuration  $C_0$ . The configuration of static equilibrium under gravity load is  $C_1$  in which  $\epsilon^1$  is the additional deformation of the middle surface of the belt.  $C_2$  indicates the configuration of the belt during motion in which the strain additional to  $\epsilon^1$  is  $\epsilon^2$ . Starting from the reference configuration  $C_0$  the square of the length of an infinitesimal pre-tensioned belt part  $ds$  is equal to, see also Figure 4.2:

$$(ds)^2 = (dx)^2 \tag{4.1}$$

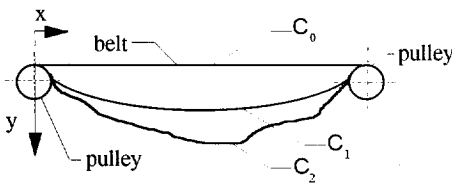


Figure 4.1: Belt configurations.

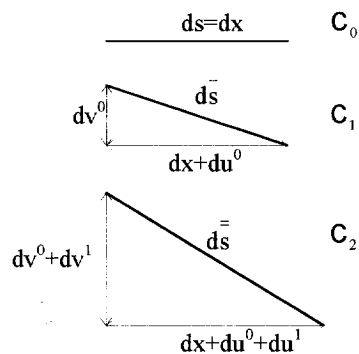


Figure 4.2: Deformation of an infinitesimal belt segment.

The square of the length of the infinitesimal belt part,  $d\bar{s}$ , in configuration  $C_1$  is equal to:

$$(d\bar{s})^2 = (dx + du^0)^2 + (dv^0)^2 = \left[ (1 + u_{,x}^0)^2 + (v_{,x}^0)^2 \right] (dx)^2 = [1 + 2\gamma_{11}^1] (dx)^2 \quad (4.2)$$

where  $\gamma_{11}^1$  is a component of the deformation tensor  $\gamma$  in  $C_1$  which is:

$$\gamma_{11}^1 = u_{,x}^0 + \frac{1}{2} \left[ (u_{,x}^0)^2 + (v_{,x}^0)^2 \right] \quad (4.3)$$

Note that the initial belt sag is not a function of time. The square of the length of the infinitesimal part in configuration  $C_2$ ,  $d\bar{s}$ , is equal to:

$$\begin{aligned} (d\bar{s})^2 &= (dx + du^0 + du^1)^2 + (dv^0 + dv^1)^2 \\ &= \left[ (1 + u_{,x}^0 + u_{,x}^1)^2 + (v_{,x}^0 + v_{,x}^1)^2 \right] (dx)^2 = [1 + 2\gamma_{11}^2] (dx)^2 \end{aligned} \quad (4.4)$$

where  $\gamma_{11}^2$  is a component of the deformation tensor  $\gamma$  in  $C_2$ :

$$\gamma_{11}^2 = u_{,x}^0 + u_{,x}^1 + \frac{1}{2} \left[ (u_{,x}^0 + u_{,x}^1)^2 + (v_{,x}^0 + v_{,x}^1)^2 \right] \quad (4.5)$$

If the belt strains are small, the axial strain can be divided into the following two terms:

$$\begin{aligned} \varepsilon^1 &= \frac{d\bar{s} - ds}{ds} = \sqrt{1 + 2\gamma_{11}^1} - 1 \\ \varepsilon^2 &= \frac{d\bar{s} - d\bar{s}}{ds} = \sqrt{1 + 2\gamma_{11}^2} - \sqrt{1 + 2\gamma_{11}^1} \end{aligned} \quad (4.6)$$

Substituting the equation (4.3) and (4.5) in equation (4.6), and considering the pre-strain  $\varepsilon_0$ , yields:

$$\begin{aligned} \varepsilon^0 &= \frac{T_0}{E_b A} \quad ; \quad \varepsilon^1 = \sqrt{(1 + u_{,x}^0)^2 + (v_{,x}^0)^2} - 1 \\ \varepsilon^2 &= \sqrt{(1 + u_{,x}^0 + u_{,x}^1)^2 + (v_{,x}^0 + v_{,x}^1)^2} - \sqrt{(1 + u_{,x}^0)^2 + (v_{,x}^0)^2} \end{aligned} \quad (4.7)$$

where  $T_0$  is the initial belt tension whereas  $E_b$  and  $A$  are Young's modulus and the cross sectional area of the belt. The average belt stress in the deformed configuration  $C_2$  then is:

$$\sigma = E_b(\varepsilon^0 + \varepsilon^1 + \varepsilon^2) = E_b\varepsilon \quad (4.8)$$

where

$$\varepsilon = \frac{T_0}{E_b A} + \sqrt{(1 + u^0_{,x} + u^1_{,x})^2 + (v^0_{,x} + v^1_{,x})^2} - 1 \quad (4.9)$$

### 4.2.2 Equations of motion

To obtain the transverse and longitudinal or axial equations of motion of a belt span supported by two frictionless guides, it is useful to use the following co-ordinates:

$$\tilde{\mathbf{x}} = \begin{bmatrix} x + \tilde{u} \\ \tilde{v} \end{bmatrix} = \begin{bmatrix} x + u^0(x) + u^1(x, t) \\ v^0(x) + v^1(x, t) \end{bmatrix} \quad (4.10)$$

With these co-ordinates the velocities are:

$$\dot{\tilde{\mathbf{x}}} = \begin{bmatrix} \dot{x}_{,t} + u^0_{,x}\dot{x}_{,t} + u^1_{,x}\dot{x}_{,t} + \dot{u}^1_t \\ \dot{v}^0_{,x}\dot{x}_{,t} + v^1_{,x}\dot{x}_{,t} + \dot{v}^1_t \end{bmatrix} = \begin{bmatrix} \dot{u}^1_t + V_b(1 + \tilde{u}_{,x}) \\ \dot{v}^1_t + V_b\tilde{v}_{,x} \end{bmatrix} \quad (4.11)$$

where  $V_b$  is the belt speed:

$$V_b = x_{,t} \quad (4.12)$$

The accelerations are:

$$\ddot{\tilde{\mathbf{x}}} = \begin{bmatrix} \ddot{u}^1_{,tt} + 2V_b\dot{u}^1_{,xt} + V_b^2\ddot{u}_{,xx} \\ \ddot{v}^1_{,tt} + 2V_b\dot{v}^1_{,xt} + V_b^2\ddot{v}_{,xx} \end{bmatrix} \quad (4.13)$$

Just as in Chapter 2, the equations of motion are obtained with aid of the principle of virtual power:

$$\int_0^L \delta \dot{\epsilon}^T \sigma dx = \int_0^L \delta \ddot{\mathbf{x}}^T (\mathbf{f} - \rho A \ddot{\mathbf{x}}) dx \quad (4.14)$$

where  $L$  is the pulley spacing and

$$\int_0^L \delta \dot{\epsilon}^T \sigma dx = E_b A \int_0^L \epsilon \delta \dot{\epsilon} dx + E_b I_y \int_0^L \ddot{v}_{,xx} \delta \dot{v}_{,xx} dx \quad (4.15)$$

With equation (4.9),

$$\delta \dot{\epsilon} = \left[ (1 + \tilde{u}_{,x}) \delta \tilde{u}_{,x} + \tilde{v}_{,x} \delta \dot{\tilde{v}}_{,x} \right] \left[ (1 + \tilde{u}_{,x})^2 + (\tilde{v}_{,x})^2 \right]^{-\frac{1}{2}} \quad (4.16)$$

The force vector  $\mathbf{f}$  is equal to:

$$\mathbf{f} = \begin{bmatrix} 0 \\ -q(x,t) \end{bmatrix} \quad (4.17)$$

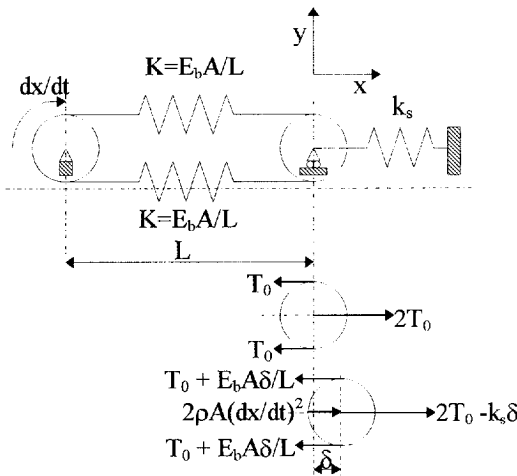


Figure 4.3: Belt support interaction.

Assume that the belt is supported by a spring tensioning system as is depicted in Figure 4.3 and that the pre tension of the belt is  $T_0$ . When the belt is moving, a displacement from the static equilibrium position is caused by the centrifugal force. The equilibrium position of the tension pulley can be obtained from force equilibrium neglecting the resistance between the pulley wheels and the guide rails:

$$2 \left( T_0 + \frac{E_b A}{L} \delta \right) = 2 \rho A (x_1)^2 + 2 T_0 - k_s \delta \Rightarrow \delta = \frac{\rho A V_b^2}{\frac{E_b A}{L} + \frac{k_s}{2}} \quad (4.18)$$

which yields the total belt tension  $T_b$  of both spans:

$$T_b = T_0 + \delta \frac{E_b A}{L} = T_0 + \eta \rho A V_b^2 \quad (4.19)$$

where

$$\eta = \left( 1 + \frac{k_s L}{2E_b A} \right)^{-1} \quad (4.20)$$

The parameter  $\eta$  depends on the relative stiffness of the support and the belt. For locked centre pulleys with very rigid shafts and supports,  $\eta=0$ . When the support stiffness vanishes as is the case when the belt tension is applied by a dead weight,  $\eta=1$ .

Substitution of the equations (4.9), (4.15), (4.16) and (4.19) in (4.14) yields:

$$\int_0^L \frac{\left[ (1 + \tilde{u}_{,x}) \delta \tilde{u}_{,x} + \tilde{v}_{,x} \delta \tilde{v}_{,x} \right] \left[ T_b - E_b A + E_b A \sqrt{(1 + \tilde{u}_{,x})^2 + (\tilde{v}_{,x})^2} \right]}{\sqrt{(1 + \tilde{u}_{,x})^2 + (\tilde{v}_{,x})^2}} dx \quad (4.21)$$

$$+ \int_0^L E_b I_y \tilde{v}_{,xx} \delta \tilde{v}_{,xx} dx = \int_0^L \delta \tilde{x} (\mathbf{f} - \rho A \ddot{\tilde{x}}) dx$$

Substituting the equations (4.11) and (4.13) in equation (4.21) yields:

$$\int_0^L \left\{ \begin{aligned} & \rho A \left[ u_{,tt}^1 + 2V_b u_{,xt}^1 + V_b^2 \tilde{u}_{,xx} \right] \\ & - \left( \frac{\left[ T_b - E_b A + E_b A \sqrt{(1 + \tilde{u}_{,x})^2 + (\tilde{v}_{,x})^2} \right] [1 + \tilde{u}_{,x}]}{\sqrt{(1 + \tilde{u}_{,x})^2 + (\tilde{v}_{,x})^2}} \right)_{,x} \end{aligned} \right\} \delta \tilde{u} dx +$$

$$\int_0^L \left\{ \begin{aligned} & \rho A \left[ v_{,tt}^1 + 2V_b v_{,xt}^1 + V_b^2 \tilde{v}_{,xx} \right] - q \\ & - \left( \frac{\left[ T_b - E_b A + E_b A \sqrt{(1 + \tilde{u}_{,x})^2 + (\tilde{v}_{,x})^2} \right] \tilde{v}_{,x}}{\sqrt{(1 + \tilde{u}_{,x})^2 + (\tilde{v}_{,x})^2}} \right)_{,x} + E_b I_y \tilde{v}_{,xxxx} \end{aligned} \right\} \delta \tilde{v} dx = 0 \quad (4.22)$$



This equation yields the two equations of motion. The equation of motion for the axial direction is:

$$u_{,tt}^1 + 2V_b u_{,xt}^1 + (V_b^2 - c_1^2) \tilde{u}_{,xx} = c_1^2 \left( 1 - \frac{T_b}{E_b A} \right) \left( \frac{(1 + \tilde{u}_{,x}) \tilde{v}_{,x} \tilde{v}_{,xx} - \tilde{v}_{,x}^2 \tilde{u}_{,xx}}{[(1 + \tilde{u}_{,x})^2 + (\tilde{v}_{,x})^2]^{\frac{3}{2}}} \right) \quad (4.23a)$$

where  $c_1$  is the wave speed for longitudinal waves defined in equation (3.15). The equation of motion for the transverse direction is:

$$v_{,tt}^1 + 2V_b v_{,xt}^1 + (V_b^2 - c_1^2) \tilde{v}_{,xx} + E_b I_y \tilde{v}_{,xxxx} = c_1^2 \left( \frac{T_b}{E_b A} - 1 \right) \left( \frac{(1 + \tilde{u}_{,x})^2 \tilde{v}_{,xx} - (1 + \tilde{u}_{,x}) \tilde{u}_{,xx} \tilde{v}_{,x}}{[(1 + \tilde{u}_{,x})^2 + (\tilde{v}_{,x})^2]^{\frac{3}{2}}} \right) + \frac{q}{\rho A} \quad (4.23b)$$

In the following, terms with  $u_{,x}^0$  are neglected compared to terms with  $u_{,x}^1$  and the superscript 1 of  $u^1$  is dropped. The following dimensionless parameters are introduced:

$$\begin{aligned} X &= \frac{x}{L} & U &= \frac{u}{L} & \tilde{V} &= \frac{\tilde{v}}{L} \\ \tau &= \frac{c_2 t}{L} & \beta &= \frac{V_b}{c_2} & \Gamma &= \frac{qL}{T_0} \\ P_0^2 &= \frac{E_b I}{T_0 L^2} & P_1^2 &= \frac{E_b A}{T_0} & \kappa &= 1 - \eta \end{aligned} \quad (4.24)$$

With these parameters and neglecting terms  $O(\tilde{V}^4)$  and  $O(U^2) = O(\tilde{V}^4)$ , equation (4.23a) reduces to:

$$U_{,xx} + 2\beta U_{,x\tau} + (\beta^2 - P_1^2) U_{,xx} = (P_1^2 - 1 - \eta\beta^2) \tilde{V}_{,x} \tilde{V}_{,xx} \quad (4.25a)$$

Equation (4.23b) reduces to:

$$\begin{aligned} &\tilde{V}_{,\tau\tau} + 2\beta \tilde{V}_{,x\tau} + (\kappa\beta^2 - 1) \tilde{V}_{,xx} + P_0^2 \tilde{V}_{,xxxx} \\ &= (P_1^2 - 1 - \eta\beta^2) \left( \frac{3}{2} \tilde{V}_{,x}^2 \tilde{V}_{,xx} + U_{,x} \tilde{V}_{,xx} + \tilde{V}_{,x} U_{,xx} \right) + \Gamma \end{aligned} \quad (4.25b)$$

The motion of the belt on top of the pulleys is constrained. The simple support boundary conditions are assumed to be:

$$\tilde{V}(0, \tau) = \tilde{V}(1, \tau) = 0 ; \tilde{V}_{,xx}(0, \tau) = \tilde{V}_{,xx}(1, \tau) = 0 ; U(0, \tau) = U(1, \tau) = 0 \quad (4.26)$$

### 4.2.3 Linear solution

Before the nonlinear equations (4.25a&b) are considered, four special cases of vibration, which are frequently used in literature, are derived from the following linear differential equations:

$$U_{,tt} + 2\beta U_{,xt} + (\beta^2 - P_1^2)U_{,xx} = 0 \quad (4.27a)$$

$$\tilde{V}_{,tt} + 2\beta\tilde{V}_{,xt} + (\kappa\beta^2 - 1)\tilde{V}_{,xx} + P_0^2\tilde{V}_{,xxxx} = \Gamma \quad (4.27b)$$

The four cases of free vibrations are:

1. the axial vibration of a belt
2. the transverse vibration of a string
3. the transverse vibration of a beam
4. the transverse vibration of a beam with string effect.

#### 4.2.3.1 Axial vibration

The linear differential equation (4.27a) can be rewritten in the original parameters:

$$u_{,tt} + 2V_b u_{,xt} + (V_b^2 - c_1^2)u_{,xx} = 0 \quad (4.28)$$

If the belt vibrates harmonically in a natural frequency, the motion in the longitudinal direction is:

$$u(x, t) = \hat{u}(x) \cos(\omega t + \varphi) \quad (4.29)$$

where  $\varphi$  is the phase shift which in case of a moving belt depends on the position on the belt and is equal to:

$$\varphi = \frac{\omega(x - L)}{V_b^*} \quad (4.30)$$

where

$$V_b^* = \frac{c_1^2 - V_b^2}{V_b} = V_b \left( \frac{c_1^2}{V_b^2} - 1 \right) \quad (4.31)$$

Substitution of the equations (4.29)-(4.31) in (4.28) shows that the amplitude function  $\hat{u}(x)$  has to satisfy the following equation:

$$\hat{u}_{,xx} + \frac{c_1^2 \omega^2}{(c_1^2 - V_b^2)^2} \hat{u} = 0 \quad (4.32)$$

The solution for  $\hat{u}(x)$  then is:

$$\hat{u}(x) = C_1 \sin\left(\frac{\omega x}{c^*}\right) + C_2 \cos\left(\frac{\omega x}{c^*}\right) \quad (4.33)$$

where

$$c^* = \frac{c_1^2 - V_b^2}{c_1} = c_1 \left( 1 - \frac{V_b^2}{c_1^2} \right) \quad (4.34)$$

If the belt is clamped at  $x=0$ :

$$\hat{u}(0, t) = 0 \quad (4.35a)$$

and harmonically excited at the other end:

$$\hat{u}(L, t) = u_0 \cos(\omega t) \quad (4.35b)$$

then substitution of these boundary conditions yields the constants of equation (4.33):

$$C_1 = \frac{u_0}{\sin\left(\frac{\omega L}{c^*}\right)} ; C_2 = 0 \quad (4.36)$$

The constants  $V_b^*$  and  $c^*$  are called the apparent belt speed and the apparent wave speed respectively. From equation (4.36) it can be seen that resonance occurs when:

$$\frac{\omega L}{c^*} = n\pi, \quad n = 1, 2, 3, \dots \quad (4.37)$$

hence the natural frequencies are:

$$\omega = \frac{n\pi}{L} c_1 \left( 1 - \frac{V_b^2}{c_1^2} \right), \quad n = 1, 2, 3, \dots \quad (4.38)$$

Since  $c_1$  is usually large with respect to  $V_b$ , see for example Table 3.3, the influence of the belt speed on the axial natural frequencies is normally neglected.

#### 4.2.3.2 Transverse vibration of a string

When the belt stress due to the pre-stressing of the belt is high compared to the additional stress caused by the transverse vibration of the belt, it is justified to assume the pre-stress constant and linearise the equations of motion. If in addition the strain energy due to bending deformation is small with respect to the strain energy due to axial deformation, the bending term in equation (4.27b) may be omitted. In case of a stationary moving belt with a spring tensioning system, the following equation is obtained from (4.27b) omitting the tilde:

$$v_{,tt} + 2V_b v_{,xt} + (\kappa V_b^2 - c_2^2) v_{,xx} = 0 \quad (4.39)$$

in case the belt load  $\Gamma=0$ . If one belt end, at  $x=0$ , is clamped and the other, at  $x=L$ , is subjected to harmonic displacement:

$$v(L, t) = v_0 \cos(\omega t) \quad (4.40)$$

the solution of the equation of motion (4.39) may be written as:

$$v(x, t) = \hat{v}(x) \cos(\omega t + \frac{\omega}{V_b^*} (x - L)) \quad (4.41)$$

where  $\hat{v}(x)$  has to satisfy the equation:

$$\hat{v}_{,xx} + \frac{(c_2^2 + (1 - \kappa)V_b^2)}{(c_2^2 - \kappa V_b^2)^2} \omega^2 \hat{v} = 0 \quad (4.42)$$

and

$$V_b^* = \frac{c_2^2 - \kappa V_b^2}{V_b} = V_b \left( \frac{1}{\beta^2} - \kappa \right) \quad (4.43)$$

The general solution of equation (4.42) is:

$$\hat{v}(x) = C_1 \sin\left(\frac{\omega x}{c^*}\right) + C_2 \cos\left(\frac{\omega x}{c^*}\right) \quad (4.44)$$

where

$$c^* = \frac{c_2^2 - \kappa V_b^2}{\sqrt{c_2^2 + (1 - \kappa)V_b^2}} = c_2 \frac{1 - \kappa\beta^2}{\sqrt{1 + (1 - \kappa)\beta^2}} \quad (4.45)$$

Substitution of the boundary conditions in equation (4.44) yields the constants:

$$C_1 = \frac{v_0}{\sin\left(\frac{\omega L}{c^*}\right)} ; C_2 = 0 \quad (4.46)$$

The final solution is:

$$v(x,t) = v_0 \frac{\sin\left(\frac{\omega x}{c^*}\right)}{\sin\left(\frac{\omega L}{c^*}\right)} \cos\left(\omega \left(t + \frac{x-L}{V_b^*}\right)\right) \quad (4.47)$$

From equation (4.47) it can be seen that resonance occurs when:

$$\frac{\omega L}{c^*} = n\pi, \quad n = 1, 2, 3, \dots \quad (4.48)$$

hence the natural frequencies are:

$$\omega = \frac{n\pi}{L} c_2 \frac{1 - \kappa\beta^2}{\sqrt{1 + (1 - \kappa)\beta^2}}, \quad n = 1, 2, 3, \dots \quad (4.49)$$

Equation (4.49) indicates that the frequencies vanish when  $V_b = c_2/\sqrt{\kappa}$ . This belt speed is called the critical belt speed. Note that with decreasing stiffness ratio  $\kappa$  the critical speed increases. This critical belt speed is also called the divergence speed. If the belt speed tends to the critical speed, the requirements to linearise the equations of motion will no longer be fulfilled.

In case of a non moving belt equation (4.49) is reduced to:

$$\omega = \frac{n\pi}{L} c_2, \quad n = 1, 2, 3, \dots \quad (4.50)$$

The existence of a critical speed, which is in this case  $V_b = c_2$ , has no implications for belt conveyor systems since the belt speed never approaches the critical speed. However, for high speed belt-systems like band saws, it should be remembered that the belt speed of systems tensioned by spring tensioners can easily approach the critical belt speed.

#### 4.2.3.3 Transverse vibration of a beam

When during vibration the strain energy due to pre-stressing is negligible compared to the strain energy due to bending, it is justified to neglect the pre-stress terms in equation (4.27b). In case of a non moving belt and omitting the tilde, the following equation remains:

$$v_{,tt} + \frac{E_b I_y}{\rho A} v_{,xxxx} = 0 \quad (4.51)$$

After substituting

$$v(x, t) = \hat{v}(x) \cos(\omega t + \varphi) \quad (4.52)$$

in (4.51) the following differential equation is found:

$$\frac{d^4 \hat{v}}{dx^4} - \mu^4 \hat{v} = 0 \quad (4.53)$$

where

$$\mu = \left( \frac{\rho A \omega^2}{E_b I} \right)^{\frac{1}{4}} \quad (4.54)$$

The general solution of (4.53) is:

$$\hat{v}(x) = C_1 \cosh(\mu x) + C_2 \sinh(\mu x) + C_3 \cos(\mu x) + C_4 \sin(\mu x) \quad (4.55)$$

The four integration constants have to satisfy the boundary conditions. In case of a simply supported belt they are:

$$\hat{v}(0) = \hat{v}(L) = \hat{v}_{,xx}(0) = \hat{v}_{,xx}(L) = 0 \quad (4.56)$$

Substitution of the boundary conditions yields the following natural frequencies:

$$\omega = \frac{n^2 \pi^2}{L^2} \sqrt{\frac{E_b I_y}{\rho A}}, \quad n = 1, 2, 3, \dots \quad (4.57)$$

#### 4.2.3.4 Transverse vibration of a beam with string effect

If both the pre-stress and the bending stiffness influence the belt vibration, the full differential equation (4.27b) must be used, omitting the tilde:

$$v_{,tt} + 2V_b v_{,xt} + (kV_b^2 - c_2^2) v_{,xx} + \frac{E_b I_y}{\rho A} v_{,xxxx} = 0 \quad (4.58)$$

For a non-moving belt, the displacement function:

$$v(x, t) = C \sin\left(\frac{n\pi x}{L}\right) \exp(i\omega t) \quad (4.59)$$

satisfies the boundary conditions of a simply supported belt. Substitution in (4.58) yields the natural frequencies:

$$\omega^2 = \left(\frac{n\pi}{L}\right)^2 c_2^2 + \left(\frac{n\pi}{L}\right)^4 \frac{E_b I_y}{\rho A} \quad (4.60a)$$

or

$$\omega = \frac{n\pi}{L} c_2 \sqrt{1 + \frac{P_{ct}}{T_0}} \quad (4.60b)$$

where  $T_0$  is the pre-stress load and  $P_{ct}$  the  $n^{\text{th}}$  Euler buckling load for a simply supported ideal column:

$$P_{c_2} = \frac{n^2 \pi^2 E_b I_y}{L^2} \quad (4.61)$$

To estimate the effect of neglecting the bending stiffness of a belt, the parameter  $k_B$ , which has been defined in (3.11), can be used in equation (4.60):

$$\omega = \frac{n\pi}{L} c_2 k_B \quad (4.62)$$

For a stationary moving belt the exact solution of (4.58) is obtained by assuming a solution in the form:

$$v(x, t) = \hat{v}(x) \exp\left(i \frac{n}{L} (x - V_b t)\right) \quad (4.63)$$

After substitution into equation (4.58) the following natural frequencies for a belt supported by non-centre locked pulleys can be obtained, [Abrate, 1992]:

$$\omega = \frac{n\pi}{L} \left[ -V_b \pm \sqrt{\eta V_b^2 + \frac{T_0}{\rho A} + \left(\frac{n\pi}{L}\right)^2 \frac{E_b I_y}{\rho A}} \right] \quad (4.64)$$

Neglecting the Coriolis acceleration term  $2V_b v_{,xt}$  in equation (4.58) yields the following result for the square of the natural frequencies:

$$\omega^2 = \frac{n^2 \pi^2}{L^2} c_2^2 (1 - \kappa \beta^2)^2 + \frac{n^4 \pi^4}{L^4} \frac{E_b I_y}{\rho A} \quad (4.65)$$

This equation gives results in good agreement with experimental values [Abrate, 1992].

## 4.2.4 Nonlinear solution

### 4.2.4.1 Method of solution

If the amplitudes  $U$  and  $\tilde{V}$  are small as has been assumed, the governing equations (4.25) are weakly non-linear. The nonlinear terms in those equations are of order  $\tilde{V}^2$  or  $\tilde{V}^3$ . Therefore, a perturbation method is well suited. In [Thurman and Mote,



1969] a combination of the methods of Lindstedt and Krylov-Bogoliubov is used. Power series expansions for  $U$ ,  $\tilde{V}$  and  $\tau$  in a small parameter  $\mu$  are introduced into the two partial differential equations (4.25) and thus an arbitrariness will appear in the approximation following the solution of the linear equations. This arbitrariness allows the selection of available coefficients in order to eliminate the secular terms in the subsequent approximations. This is done by selecting the undetermined coefficients in such a way that the non-homogeneous perturbation term is orthogonal, on the average, to the linear solution. To reduce the increasing amount of calculations, only those longitudinal vibrations will be considered that are caused by transverse vibrations (particular solution of equation (4.25a)).

Substitute the following functions into the equations (4.25):

$$\begin{aligned} U &= U_0 + \mu U_1 + \mu^2 U_2 + \dots \\ \tilde{V} &= \tilde{V}_0 + \mu \tilde{V}_1 + \mu^2 \tilde{V}_2 + \dots \\ \tau &= \frac{T}{\Omega_0} (1 + \mu h_1 + \mu^2 h_2 + \dots) \end{aligned} \quad (4.66)$$

where  $\mu$  is a small and as yet undefined parameter,  $h_i$  are constants to be determined and

$$\Omega_0 = \frac{\omega L}{c_2} \quad (4.67)$$

which is the dimensionless lowest frequency of the linear solution. Equating the coefficients of equal powers of  $\mu$  to zero, the nonlinear problem is reduced to a sequence of linearised equations in each of which the nonlinear terms are known from the solutions of the equations of lower order in  $\mu$ . When the transport speed is constant these are:

$$L_0 \tilde{V}_0 = \Gamma \quad (4.68)$$

$$L_1 U_0 = (P_1^2 - 1 - \eta \beta^2) \tilde{V}_{0,x} \tilde{V}_{0,xx} \quad (4.69)$$

$$L_0 \tilde{V}_1 = F_1 - 2h_1 [\beta \Omega_0 \tilde{V}_{0,xT} + (\kappa \beta^2 - 1) \tilde{V}_{0,xx} + P_0^2 \tilde{V}_{0,xxxx} - \Gamma] \quad (4.70)$$

$$\begin{aligned}
 L_1 U_1 &= (P_1^2 - 1 - \eta\beta^2)(\tilde{V}_{1,x}\tilde{V}_{0,xx} + \tilde{V}_{0,x}\tilde{V}_{1,xx}) \\
 &- 2h_1[\beta\Omega_0 U_{0,xT} + (\beta^2 - P_1^2)U_{0,xx} - (P_1^2 - 1 - \eta\beta^2)\tilde{V}_{0,x}\tilde{V}_{0,xx}]
 \end{aligned} \tag{4.71}$$

$$\begin{aligned}
 L_0 \tilde{V}_2 &= F_2 - 2h_2[\beta\Omega_0 \tilde{V}_{0,xT} + (\kappa\beta^2 - 1)\tilde{V}_{0,xx} + P_0^2 \tilde{V}_{0,xxxx} - \Gamma] \\
 &- h_1^2[(\kappa\beta^2 - 1)\tilde{V}_{0,xx} + P_0^2 \tilde{V}_{0,xxxx} - \Gamma] \\
 &- 2h_1[\beta\Omega_0 \tilde{V}_{1,xT} + (\kappa\beta^2 - 1)\tilde{V}_{1,xx} + P_0^2 \tilde{V}_{1,xxxx} - F_1]
 \end{aligned} \tag{4.72}$$

$$\begin{aligned}
 L_1 U_2 &= (P_1^2 - 1 - \eta\beta^2)(\tilde{V}_{1,x}\tilde{V}_{1,xx} + \tilde{V}_{0,x}\tilde{V}_{2,xx} + \tilde{V}_{2,x}\tilde{V}_{0,xx}) \\
 &- 2h_2[\beta\Omega_0 U_{0,xT} + (\beta^2 - P_1^2)U_{0,xx} - (P_1^2 - 1 - \eta\beta^2)\tilde{V}_{0,x}\tilde{V}_{0,xx}] \\
 &- h_1^2[(\beta^2 - P_1^2)U_{0,xx} - (P_1^2 - 1 - \eta\beta^2)\tilde{V}_{0,x}\tilde{V}_{0,xx}] \\
 &- 2h_1[\beta\Omega_0 U_{0,xT} + (\beta^2 - P_1^2)U_{1,xx} - (P_1^2 - 1 - \eta\beta^2)(\tilde{V}_{1,x}\tilde{V}_{0,xx} + \tilde{V}_{0,x}\tilde{V}_{1,xx})]
 \end{aligned} \tag{4.73}$$

$$\begin{aligned}
 L_0 \tilde{V}_3 &= F_3 - 2h_3[\beta\Omega_0 \tilde{V}_{0,xT} + (\kappa\beta^2 - 1)\tilde{V}_{0,xx} + P_0^2 \tilde{V}_{0,xxxx} - \Gamma] \\
 &- 2h_1 h_2[(\kappa\beta^2 - 1)\tilde{V}_{0,xx} + P_0^2 \tilde{V}_{0,xxxx} - \Gamma] \\
 &- h_1^2[(\kappa\beta^2 - 1)\tilde{V}_{1,xx} + P_0^2 \tilde{V}_{1,xxxx} - F_1] \\
 &- 2h_2[\beta\Omega_0 \tilde{V}_{1,xT} + (\kappa\beta^2 - 1)\tilde{V}_{1,xx} + P_0^2 \tilde{V}_{1,xxxx} - F_1] \\
 &- 2h_1[\beta\Omega_0 \tilde{V}_{2,xT} + (\kappa\beta^2 - 1)\tilde{V}_{2,xx} + P_0^2 \tilde{V}_{2,xxxx} - F_2]
 \end{aligned} \tag{4.74}$$

where

$$L_0 = \Omega_0^2 \frac{\partial^2}{\partial T^2} + 2\beta\Omega_0 \frac{\partial^2}{\partial X \partial T} + (\kappa\beta^2 - 1) \frac{\partial^2}{\partial X^2} + P_0^2 \frac{\partial^4}{\partial X^4} \tag{4.75}$$

$$L_1 = \Omega_0^2 \frac{\partial^2}{\partial T^2} + 2\beta\Omega_0 \frac{\partial^2}{\partial X \partial T} + (\beta^2 - P_1^2) \frac{\partial^2}{\partial X^2} \tag{4.76}$$

$$F_1 = \frac{1}{\mu} (P_1^2 - 1 - \eta\beta^2) (\frac{3}{2} \tilde{V}_{0,x} \tilde{V}_{0,xx} + U_{0,x} \tilde{V}_{0,xx} + \tilde{V}_{0,x} U_{0,xx}) \tag{4.77}$$

$$F_2 = \frac{1}{\mu} (P_1^2 - 1 - \eta\beta^2) \left( \frac{3}{2} \tilde{V}_{0,X}^2 \tilde{V}_{1,XX} + 3 \tilde{V}_{1,X} \tilde{V}_{0,X} \tilde{V}_{0,XX} \right. \\ \left. + U_{0,X} \tilde{V}_{1,XX} + \tilde{V}_{1,X} U_{0,XX} + U_{1,X} \tilde{V}_{0,XX} + \tilde{V}_{0,X} U_{1,XX} \right) \quad (4.78)$$

$$F_3 = \frac{1}{\mu} (P_1^2 - 1 - \eta\beta^2) \left[ \begin{aligned} & \frac{3}{2} \tilde{V}_{0,X}^2 \tilde{V}_{1,XX} + \frac{3}{2} \tilde{V}_{0,X}^2 \tilde{V}_{2,XX} + 3 \tilde{V}_{0,X} \tilde{V}_{2,X} \tilde{V}_{0,XX} + \\ & 3 \tilde{V}_{1,X} \tilde{V}_{0,X} \tilde{V}_{1,XX} + U_{2,X} \tilde{V}_{0,XX} + U_{1,X} \tilde{V}_{1,XX} + U_{0,X} \tilde{V}_{2,XX} \\ & + U_{0,XX} \tilde{V}_{2,X} + U_{1,XX} \tilde{V}_{1,X} + U_{2,XX} \tilde{V}_{0,X} \end{aligned} \right] \quad (4.79)$$

The solution procedure is systematic. Solving equation (4.68) yields the linear, generating solution,  $\tilde{V}_0$ , and the first linear natural frequency  $\Omega_0$ . Using  $\tilde{V}_0$  and  $\Omega_0$ , equation (4.69) can be solved for the particular solution  $U_0$ . With  $\tilde{V}_0$  and  $U_0$ ,  $F_1$  can be calculated using equation (4.77). After substitution of  $\tilde{V}_0$  and  $F_1$ , the right hand side of equation (4.70) will contain some terms of the same frequency as  $\tilde{V}_0$ . To obtain a periodic solution for  $\tilde{V}_1$ , the influence of these terms must be minimised. Therefore, the right hand side of (4.70) is constructed orthogonal to the linear solution,  $\tilde{V}_0$ , by appropriately selecting the as yet undetermined constant  $h_1$ . This factor becomes:

$$h_1 = \frac{\int_0^1 \int_0^{2\pi} \tilde{V}_0 F_1 dT dX}{2 \int_0^1 \int_0^{2\pi} \tilde{V}_0 [\beta \Omega_0 \tilde{V}_{0,XT} + (\kappa \beta^2 - 1) \tilde{V}_{0,XX} + P_0^2 \tilde{V}_{0,XXXX} - \Gamma] dT dX} \quad (4.80)$$

The first nonlinear approximation to the circular frequency is:

$$\Omega = \frac{\Omega_0}{1 + \mu h_1} \quad (4.81)$$

Now determine the particular solution  $\tilde{V}_1$  from equation (4.70).  $U_1$  is obtained from (4.71) and  $F_2$  from (4.78). Similarly the right hand side of equation (4.72) is constructed orthogonal to the linear solution  $\tilde{V}_0$ . The second constant  $h_2$  is:

$$\begin{aligned}
 h_2 = & \frac{\int_0^1 \int_0^{2\pi} \tilde{V}_0 F_2 dT dX}{2 \int_0^1 \int_0^{2\pi} \tilde{V}_0 [\beta \Omega_0 \tilde{V}_{0,XT} + (\kappa \beta^2 - 1) \tilde{V}_{0,XX} + P_0^2 \tilde{V}_{0,XXXX} - \Gamma] dT dX} + \\
 & h_1^2 \left( 2 - \frac{\int_0^1 \int_0^{2\pi} \tilde{V}_0 [(\kappa \beta^2 - 1) \tilde{V}_{0,XX} + P_0^2 \tilde{V}_{0,XXXX} - \Gamma] dT dX}{2 \int_0^1 \int_0^{2\pi} \tilde{V}_0 [\beta \Omega_0 \tilde{V}_{0,XT} + (\kappa \beta^2 - 1) \tilde{V}_{0,XX} + P_0^2 \tilde{V}_{0,XXXX} - \Gamma] dT dX} \right) \quad (4.82)
 \end{aligned}$$

The first nonlinear approximation to  $U$  and  $\tilde{V}$  and the second approximation to  $\Omega$  are:

$$U = U_0 + \mu U_1 ; \tilde{V} = \tilde{V}_0 + \mu \tilde{V}_1 ; \Omega = \frac{\Omega_0}{1 + \mu h_1 + \mu^2 h_2} ; \mu = P_1^2 a^2 \quad (4.83)$$

Proceeding in the same manner would yield higher order approximations which improve the accuracy. However, the accuracy of the second approximation on  $\Omega$  is already satisfying [Thurman and Mote, 1969].

#### 4.2.4.2 Non moving belt

To illustrate the solution method for the nonlinear equations of motion, the first ( $n=1$ ) nonlinear frequency of transverse vibration of a non-moving belt ( $\beta=0$ ) without bending stiffness ( $P_0^2 = 0$ ) and supported by locked centre pulleys ( $\kappa=1$ ) is shown in this section. The linear solution for this case was determined in Section 4.2.3.2 and given in equation (4.50). In dimensionless form this frequency is  $\Omega_0 = \pi$ . The dimensionless displacement function, see also equation (4.47), is:

$$\tilde{V}_0(X, T) = a \sin(\pi X) \cos(T) \quad (4.84)$$

However, this displacement function was determined without accounting for the weight of the belt. To determine the displacement function which accounts for this effect, the displacement function is written in terms of the eigenfunctions,  $\chi$  and  $\psi$  [Meirovitch, 1974]:

$$\tilde{V}_0(X, T) = \xi(T)\chi(X) + \zeta(T)\psi(X) \quad (4.85)$$

The generalised co-ordinates  $\xi$  and  $\zeta$  are [Meirovitch, 1975]:

$$\begin{aligned}\xi(T) &= \int_0^T \left[ \tilde{F}(t') \cos(\Omega(T-t')) + \tilde{\tilde{F}}(t') \sin(\Omega(T-t')) \right] dt' + \xi(0) \cos(\Omega T) + \zeta(0) \sin(\Omega T) \\ \zeta(T) &= \int_0^T \left[ \tilde{\tilde{F}}(t') \cos(\Omega(T-t')) - \tilde{F}(t') \sin(\Omega(T-t')) \right] dt' + \zeta(0) \cos(\Omega T) - \xi(0) \sin(\Omega T)\end{aligned}\quad (4.86)$$

where  $\tilde{F}$  and  $\tilde{\tilde{F}}$  are the generalised forces:

$$\tilde{F}(T) = -\Omega \int_0^1 \psi(X) q(X, T) dX ; \quad \tilde{\tilde{F}}(T) = \Omega \int_0^1 \chi(X) q(X, T) dX \quad (4.87)$$

The distributed belt load  $q(X, T)$  is equal to the belt weight  $\Gamma$ . The components of the orthonormal eigenfunctions are [Wickert and Mote, 1990]:

$$\chi = \frac{1}{\pi} \sqrt{\frac{2}{1-\kappa\beta^2}} \sin(\pi X) \cos(\pi\beta X) ; \quad \psi = \frac{1}{\pi} \sqrt{\frac{2}{1-\kappa\beta^2}} \sin(\pi X) \sin(\pi\beta X) \quad (4.88)$$

In case of a non moving belt ( $\beta=0$ ) and the first natural frequency ( $n=1$ ) the components of the orthonormal eigenfunctions reduce to:

$$\chi = \frac{\sqrt{2}}{\pi} \sin(\pi X) ; \quad \psi = 0 \quad (4.89)$$

Substitution of these eigenfunctions in equation (4.87) yields the generalised forces  $\tilde{F}$  and  $\tilde{\tilde{F}}$ :

$$\tilde{F} = 0 ; \quad \tilde{\tilde{F}} = \frac{2\sqrt{2}}{\pi} \Gamma \quad (4.90)$$

Substitution of these forces in equation (4.86) yields:

$$\xi(T) = \frac{\tilde{\tilde{F}}}{\Omega} (1 - \cos(T)) ; \quad \zeta(T) = 0 \quad (4.91)$$

Substitution of the equations (4.89) and (4.91) in (4.85) then yields the displacement function:

$$\tilde{V}_0(X, T) = \frac{4\Gamma}{\pi^3} \sin(\pi X)(1 - \cos(T)) = \frac{4qL}{\pi^3 T_0} \sin(\pi X)(1 - \cos(T)) \quad (4.92)$$

The static belt sag at  $X=0.5$  is approximated by  $K_s = \frac{4qL}{\pi^3 T_0}$ . This is comparable with the approximation of DIN 22101 standard obtained by using a parabolic displacement field,  $\frac{qL}{8T_0}$ , which was given in equation (3.14).

Following the perturbation method as described in Section 4.2.4.1, the first approximation of the axial motion  $U_0$  is determined from:

$$\Omega_0^2 U_{0,TT} - P_1^2 U_{0,XX} = (P_1^2 - 1) \tilde{V}_{0,X} \tilde{V}_{0,XX} \quad (4.93)$$

With the displacement function given in equation (4.92), the particular solution of this equation is given by:

$$U_0 = \frac{\Gamma^2}{\pi^5} \sin(2\pi X) \left[ -3 \left( \frac{P_1^2 - 1}{P_1^2} \right) + 16 \left( \frac{P_1^2 - 1}{4P_1^2 - 1} \right) \cos(T) - \cos(2T) \right] \quad (4.94a)$$

For practical applications  $P_1^2 \gg 1$  and in that case the result reduces to:

$$U_0 = \frac{\Gamma^2}{\pi^5} \sin(2\pi X) [-3 + 4\cos(T) - \cos(2T)] \quad (4.94b)$$

If the effect of the belt weight, and thus the static belt sag, is negligible ( $\Gamma=0$ ), then the displacement function given in equation (4.84) is used to calculate the particular solution of (4.93) which in that case is:

$$U_0 = \frac{\pi a^2}{16} \sin(2\pi X) \left[ -\frac{P_1^2 - 1}{P_1^2} - \cos(2T) \right] \quad (4.95a)$$

If  $P_1^2 \gg 1$  this reduces to:

$$U_0 = \frac{\pi a^2}{16} \sin(2\pi X) [-1 - \cos(2T)] \quad (4.95b)$$

The function  $\mu F_1$  can be determined from equation (4.77) and  $\mu h_1$  from equation (4.80) which, in case of zero bending stiffness  $P_0^2 = 0$ , can be rewritten to:

$$\mu h_1 = \frac{\int_0^1 \int_0^{2\pi} \tilde{V}_0 \mu F_1 dT dX}{2 \int_0^1 \int_0^{2\pi} V_0 [-V_{0,XX}] dT dX} \quad (4.96)$$

This can be calculated with use of the symbolic manipulator program Maple V. Starting from (4.92), the belt sag equation, the result is:

$$\mu h_1 = -\frac{(P_1^2 - 1)\Gamma^2 \left(1920 P_1^2 + 288 - \frac{96}{P_1^2}\right)}{64 \pi^4 (4P_1^2 - 1)} \approx -\frac{7.5}{\pi^4} P_1^2 \Gamma^2 \quad (4.97a)$$

and starting from (4.84), the amplitude equation, the result is:

$$\mu h_1 = -\frac{\pi^2 a^2 (6 P_1^2 + 1)(P_1^2 - 1)}{64 P_1^2} \approx -\frac{3}{32} \pi^2 P_1^2 a^2 \quad (4.97b)$$

With these coefficients, the first approximation of the lowest nonlinear fundamental frequency is, in case of belt sag:

$$\Omega = \frac{\pi}{1 - \frac{(P_1^2 - 1)\left(1920 P_1^2 + 288 - \frac{96}{P_1^2}\right)\Gamma^2}{64 \pi^4 (4P_1^2 - 1)}} \approx \frac{\pi}{1 - \frac{7.5}{\pi^4} P_1^2 \Gamma^2} \quad (4.98a)$$

and for free vibrations:

$$\Omega = \frac{\pi}{1 - \frac{\pi^2 (6 P_1^2 + 1)(P_1^2 - 1)a^2}{64 P_1^2}} \approx \frac{\pi}{1 - \frac{3}{32} \pi^2 P_1^2 a^2} \quad (4.98b)$$

Proceeding in a systematic manner to calculate the second approximation,  $F_1$ ,  $h_1$  and  $\tilde{V}_0$  are substituted in the right hand side of equation (4.70). If the restriction is made to cases for what  $P_1^2 \gg 1$ , the following particular solutions can be found. For belt sag:

$$\tilde{V}_1(X, T) = \frac{\Gamma P_1^2}{\pi^7} \sin(\pi X) [-40 + 8\cos(2T) - 0.5\cos(3T)] \quad (4.99a)$$

and in case of free vibrations:

$$\tilde{V}_1(X, T) = \frac{a}{4\pi^2} \sin(\pi X) \cos(3T) \quad (4.99b)$$

Accordingly solving equation (4.71) yields, in case of belt sag [Serckx, 1995]:

$$U_1(X, T) = \frac{\Gamma^2 P_1^2}{\pi^9} \sin(2\pi X) \left[ 40 - 36\cos(T) - \frac{33}{4} \cos(2T) + \frac{9}{2} \cos(3T) - \frac{1}{4} \cos(4T) \right] \quad (4.100a)$$

and for free vibrations [Thurman and Mote, 1969]:

$$U_1(X, T) = \frac{-1}{32\pi} a^2 \sin(2\pi X) \left[ \left( 1 + \frac{2(6P_1^2 + 1)}{P_1^2(P_1^2 - 1)} \right) \cos(2T) + \frac{(P_1^2 - 1)}{(P_1^2 - 4)} \cos(4T) \right] \quad (4.100b)$$

$$\approx -\frac{1}{32\pi} a^2 \sin(2\pi X) [\cos(2T) + \cos(4T)]$$

The functional  $\mu F_2$  is formed by substitution of the appropriate functions into equation (4.78) and  $\mu h_2$  from equation (4.82). In case of belt sag:

$$\mu^2 h_2 = \frac{3}{2} \left( \frac{(P_1^2 - 1)\Gamma^2 \left( 1920 P_1^2 + 288 - \frac{96}{P_1^2} \right)}{64 \pi^4 (4P_1^2 - 1)} \right)^2 \quad (4.101a)$$

$$+ \frac{(P_1^2 - 1)\Gamma^4 (8832000P_1^4 - 3037440P_1^2)}{15360\pi^8 (4P_1^2 - 1)} \approx \frac{1825P_1^4 \Gamma^4}{8\pi^8}$$

and in case of free vibrations:

$$\mu^2 h_2 = \frac{\pi^4 a^4 (P_1^2 - 1)^2}{1024} \left( \left( \frac{6P_1^2 + 1}{2P_1^2} \right)^2 - \frac{3}{4} \right) \approx \frac{33}{4096} \pi^4 P_1^4 a^4 \quad (4.101b)$$



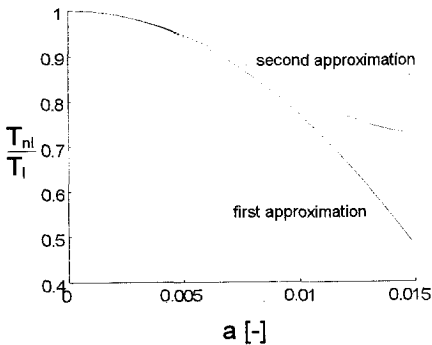
With the coefficients  $h_1$  and  $h_2$ , the second approximation to the lowest nonlinear fundamental frequency is, in case of belt sag:

$$\Omega = \frac{\pi}{1 - \frac{7.5}{\pi^4} P_1^2 \Gamma^2 + \frac{1825}{8\pi^8} P_1^4 \Gamma^4} \quad (4.102a)$$

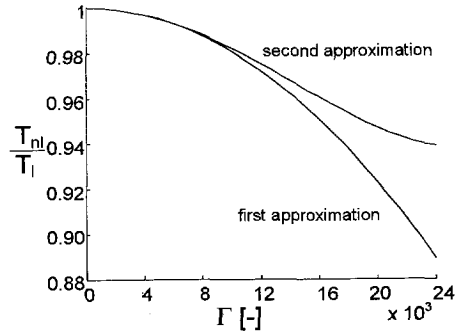
and for free vibrations:

$$\Omega = \frac{\pi}{1 - \frac{3}{32} \pi^2 P_1^2 a^2 + \frac{33}{4096} \pi^4 P_1^4 a^4} \quad (4.102b)$$

The ratio between the linear and the nonlinear frequency applying equations (4.98a) and (4.102a) is depicted in Figure 4.3. Figure 4.4 shows this ratio applying equation (4.98b) and (4.102b). Note that  $\Gamma$  is  $\pi^3/4 \approx 8$  times the static belt sag  $K_s$ . To obtain approximations to the nonlinear period of an axially moving belt, the same procedure can be used. Some results for free vibrations are given by Thurman and Mote [1969].



**Figure 4.3:** Ratio between the nonlinear,  $T_{nl}$ , and linear,  $T_l$ , period versus vibration amplitude for  $P_1=50$ .



**Figure 4.4:** Ratio between the nonlinear,  $T_{nl}$ , and linear,  $T_l$ , period versus belt load for  $P_1=50$ .

#### 4.2.4.3 Stationary moving belt

To determine an approximate solution of the equation of transverse motion of an axially moving belt, Bapat and Srinivasan [1967] neglected the coupling between the axial and transverse motion of a moving belt by assuming that the belt tension force is constant. The nonlinear equation of transverse motion (4.25b) of a belt, supported by locked centre pulleys ( $\kappa=1$ ) and neglecting the bending stiffness ( $P_0=0$ ), then reduces to:

$$\tilde{V}_{,\pi\pi} + 2\beta\tilde{V}_{,\pi x} + (\beta^2 - 1)\tilde{V}_{,xx} = \frac{3}{2}(P_1^2 - 1)\tilde{V}_{,x}^2\tilde{V}_{,xx} \quad (4.103)$$

Bapat and Srinivasan [1967] used the method of harmonic balance to obtain a solution of this equation. Their result can easily be extended to predict all natural frequencies [Abrate, 1992]:

$$\Omega_n = n\pi\sqrt{1 - \beta^2} \sqrt{1 + \frac{9}{32(1 - \beta^2)} n^2 \pi^2 P_1^2 a^2}, \quad n = 1, 2, 3, \dots \quad (4.104)$$

This equation indicates that, with the same vibration amplitude, the non-linear effects are more pronounced for high values of  $\beta$  and higher modes. Non-linear effects can be neglected only for small amplitudes and high tension levels. Figure 4.5 shows the period ratio for different values of  $\beta$  using equation (4.104).

Korde [1985] also considered this problem and he obtained a correction factor for equation (4.107):

$$\Omega_1^K = \Omega_1 \left[ 1 + \frac{1}{48} \left( 1 + \frac{32(1 - \beta^2)}{9\pi^2 P_1^2 a^2} \right)^{-2} \right]^{-1} \quad (4.105)$$

The two approximations of Thurman and Mote for the nonlinear/linear period ratio as given in the equations (4.98b) and (4.102b), and the approximations of Bapat and Srinivasan, equation (4.104), and of Korde, equation (4.105), are compared in Figure 4.6.

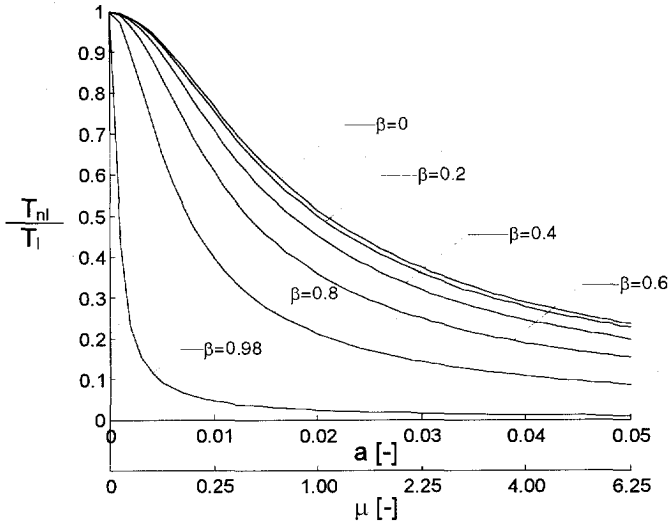


Figure 4.5: Period variation versus amplitude for different values of  $\beta$  and  $P_1=50$ .

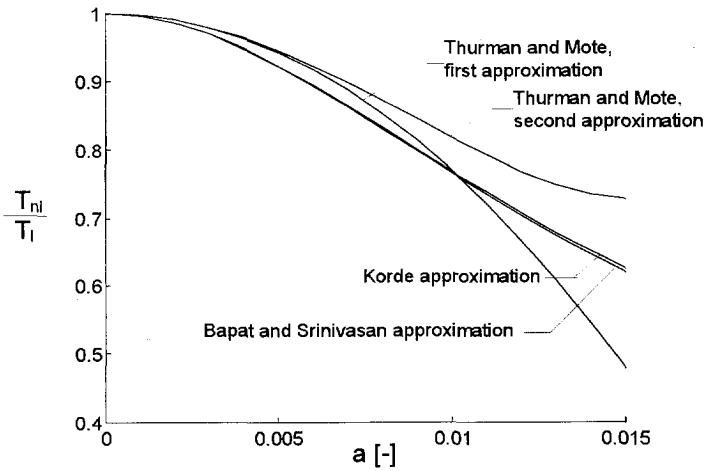


Figure 4.6: Period ratio versus vibration amplitude for four different approximations ( $\beta=0$ ,  $P_1=50$ ).

### 4.2.5 Parametric excitation

There are two principal mechanisms that may drive a running belt spanning two pulleys into transverse vibration. The first mechanism of excitation, at a frequency close to a natural frequency of transverse vibration of the belt, is direct transverse excitation of the belt end by pulley runout or another irregularity. Pulley eccentricity or passage of the belt splice over the pulleys can directly excite the belt. The second mechanism of excitation, at a frequency close to twice a natural frequency, is through the tension or the edge loading being periodically driven. Pulley eccentricity, variations in belt thickness or stiffness, passage of a splice over the pulleys and pinch roller or guide friction forces produce periodic axial tension.

Besides these direct excitation sources there is a mechanism of parametric self-excitation [Rhodes, 1970]. If a belt is vibrating transversely the length of the vibrating span changes at twice the frequency of the belt vibration and with the length, the tension has also an alternating component at twice the belt frequency. When the belt winds onto the pulley, the varying tension on the moving belt will be recorded as a strain or stress pattern in the belt, assuming the belt does not slip on the pulley surface. When the belt pays off the pulley onto the next span, this stress pattern causes a corresponding tension variation on that span. The process repeats around the next pulley introducing into the original span a replica of the original tension variation but delayed in time and reduced in amplitude. If the delay has a proper relation to the belt vibration period, then this fed-around tension can sustain or increase the vibration.

A rough generalisation is that metallic belts, of which the axial tension may change markedly when either a pulley or belt irregularity is encountered, tend to be excited parametrically. Belts of more compliant materials, like rubber or leather, tend to be excited directly.

The principle of parametric excitation of a non-moving belt was explained by Kauderer (1958). Abrate (1987) analysed the vibration due to manufacturing imperfections of V-belts. The imperfections were shown to be detectable by a Fourier series analysis of the ride-out variations during a standard belt inspection test. Ride out is defined as the radial motion of the belt in a pulley groove. An experimental investigation of a V-belt drive by Kozhevnikov (1982) indicated that splices in the belt due to manufacturing imperfections can be a significant source of vibration. The bending stiffness in the joint area is in general greater than in the rest of the belt which gives additional dynamic loads. The response of a band/pulley system under impulsive boundary conditions due to the passage of welds was investigated by Wang and Mote (1987). As the weld enters or leaves a span, an impulse to the transverse displacement was observed. A mathematical model for this system consisting of two coupled spans and accounting for the inertia of the pulleys and flexibility of the supports has been presented. Koyama (1990) showed experimentally that tension

variations generated by pulley eccentricity can reduce the amplitude of vibration of timing belts for which tooth impacts are the major source of excitation. It was also shown that adding material to the back of the belt along half of its length so as to change its density will also help to reduce vibration amplitudes near resonance peaks. Analyses of a moving string subjected to a force excitation representing tooth-sprocket impacts were presented by Watanabe et al. (1990) for the case of variable tension and variable density.

### 4.3 References

- Abbate, S. (1992), "Vibrations of Belts and Belt Drives", *Mech. Mach. Theory* **27**, pp. 645-659.
- Ames, W.F., Lee, S.Y., Zaiser, J.N. (1968), "Non-linear Vibration of a Travelling Threadline", *Non-Linear Mechanics* **3**, pp. 449-468.
- Archibald, F.R., Emslie, A.G. (1958), "The Vibration of a String Having a Uniform Motion along its Length", *Applied Mechanics* **25**, pp. 347-348.
- Asokanathan, S.F., Ariaratnam, S.T. (1994), "Flexural Instabilities in Axially Moving Bands", *Vibration and Acoustics* **116**, pp. 275-279.
- Bapat, V.A. and Srinivasan, P. (1967), "Nonlinear Transverse Oscillations in Travelling Strings by the Method of Harmonic Balance", *Applied Mechanics* **34**, pp. 775-777.
- Barakat, R. (1967), "Transverse Vibrations of a Moving Thin Rod", *J. Acoust. Soc. Amer.* **43**, pp. 533-539.
- Blom, C.J. (1994), *Time-periodic Solutions of Some Forced Nonlinear Wave Equations*, Ph.D. thesis, Delft University of Technology.
- Buffington, K.W., Kane, T.R. (1985), "Dynamics of a Beam Moving over Supports", *Solid Structures* **21**, pp. 617-643.
- Carrier, G.F. (1945), "On the Non-Linear Vibration Problem of the Elastic String", *Applied Mechanics* **12**, pp. 157-165.
- Chubachi, T. (1958), "Lateral Vibrations of Axially Moving Wire or Belt Form Materials", *Bull. JSME* **1**, pp. 24-25.
- Fujino, Y., Warnitchai, P., Pacheco, B.M. (1993), "Active Stiffness Control of Cable Vibration", *Applied Mechanics* **60**, pp.948-953.
- Harrison, A. (1992), "Modern Design of Belt Conveyors in the Context of Stability Boundaries and Chaos", *Phil. Trans. R. Soc. Lond.* **338**, pp. 491-502.
- Hwang, S.J., Perkins, N.C., Ulsoy, A.G. (1994), "Rotational Response and Slip Prediction of Serpentine Belt Drive Systems", *Vibration and Acoustics* **116**, pp. 71-78.
- Irvine, H.M. (1980), "Energy Relations for a Suspended Cable", *Quarterly Mechanics and Applied Mathematics* **33**, pp. 227-234.
- Kauderer, H. (1958), *Nichtlineare Mechanik*, Springer Verlag, Berlin.

- Korde, K.R. (1985), "On Nonlinear Oscillation of Moving String", *Applied Mechanics* **52**, pp. 493-494.
- Koyoma, T., Watanabe, K., Nagai, K. and Kagotani, M. (1990), *J. Mech. Des.* **112**, pp. 419-423.
- Kozhevnikov, S.N. et al. (1982), *Soviet Engng. Res.* **2(5)**, pp. 33-34.
- Lee, S.Y. (1958), *Wave Propagation and Vibration of a String Undergoing Axial Motion*, Ph.D. thesis, University of Delaware, Newark, Delaware.
- Luongo, A., Rega, G., Vestroni, F. (1984), "Planar Non-Linear Free Vibrations of an Elastic Cable", *Non-Linear Mechanics* **19**, pp. 39-52.
- Mahalingam, S. (1957), "Transverse Vibrations of Power Transmission Chains", *British Journal of Applied Physics* **8**, pp. 347-348.
- Majewski, T. (1986), "Audio Signal Modulation Caused by Self-Excited Vibrations of Magnetic Tape", *Sound and Vibration* **105**, pp. 17-25.
- Mansfield, L., Simmonds, J.G. (1987), "The Reverse Spaghetti Problem: Drooping Motion of an Elastica Issuing from a Horizontal Guide", *Applied Mechanics* **54**, pp. 147-150.
- Meirivitch, L. (1974), "A New Method of Solution of the Eigenvalue Problem for Gyroscopic Systems", *ALAA J.* **12**, pp. 1337-1342.
- Meirovitch, L. (1975), "A Modal Analysis for the Response of Linear Gyroscopic Systems", *Applied Mechanics* **42**, pp. 446-450.
- Miranker, W.L. (1960), "The Wave Equation in a Medium in Motion", *IBM Research & Development* **4**, pp. 36-42.
- Mote, C.D. (1965), "A Study of Band Saw Vibrations", *Franklin Institute* **279**, pp. 430-444.
- Mote, C.D. (1966), "On the Non-Linear Oscillation of an Axially Moving String", *Applied Mechanics* **33**, pp. 463-464.
- Mote, C.D. (1968), "Dynamic Stability of an Axially Moving Band", *Franklin Institute* **285**, pp. 329-346.
- Mote, C.D., Wu, W.Z. (1985), "Vibration Coupling in Continuous Belt and Band Systems", *Sound and Vibration* **102**, pp. 1-9.
- Ono, K. (1979), "Lateral Motion of an Axially Moving String on a Cylindrical Guide Surface", *Applied Mechanics* **46**, pp. 905-912.
- Perkins, N.C., Mote, C.D. (1987), "Three Dimensional Vibration of Travelling Elastic Cables", *Sound and Vibrations* **114**, pp. 325-340.
- Rhodes, J.E. (1970), "Parametric Self-Excitation of a Belt into Transverse Vibration", *Applied Mechanics* **37**, pp. 1055-1060.
- Sack, R.A. (1954), "Transverse Oscillations in Travelling Strings", *British Applied Physics* **5**, pp. 224-226.
- Serckx, T. (1995), *Non-linear Vibrations of an Axially Moving Strip*, Reportno. 1057, Laboratory for Engineering Mechanics, Delft University of Technology.
- Simpson, A. (1972), "On the Oscillatory Motions of Translating Elastic Cables", *Sound and Vibration* **20**, pp. 177-189.

- Simpson, A. (1973), "Transverse Modes and Frequencies of Beams Translating between Fixed End Supports", *J. Mech. Engrg. Sci.* **15**, pp. 159-164.
- Skutch, R. (1897), "Über die Bewegung eines gespannten Fadens, welche gezwungen ist, durch zwei feste Punkte, mit einer konstanten Geschwindigkeit zu gehen und zwischen den Selben in transversal Schwingungen von geringer Amplitude versetzt wird", *Annalen der Physik und Chemie* **61**, pp. 190-195.
- Soler, A.I. (1970), "Dynamic Response of Single Cables with Initial Sag", *Franklin Institute* **290**, pp. 377-387.
- Swope, R.D., Ames, W.F. (1963), "Vibrations of a Moving Threadline", *Franklin Institute* **275**, pp. 36-55.
- Triantafyllou, M.S. (1984), "The Dynamics of Taut Inclined Cables", *Quarterly Mechanics and Applied Mathematics* **37**, pp. 421-440.
- Triantafyllou, M.S. (1985), "The Dynamics of Translating Cables", *Sound and Vibration* **103**, pp. 171-182.
- Thurman, A.L., Mote, C.D. (1969), "Free, Periodic, Nonlinear Oscillation of an Axially Moving Strip", *Applied Mechanics* **36**, pp. 83-91.
- Ulsoy, A.G., Mote, C.D. (1982), "Vibrations of Wide Band Saw Blades", *Engineering for Industry* **104**, pp. 71-78.
- Ulsoy, A.G., Whitesell, J.E., Hooven, M.D. (1985), "Design of Belt-Tensioner Systems for Dynamic Stability", *Vibration, Acoustics, Stress and Reliability in Design* **107**, pp. 282-290.
- Vicario, A.A. (1958), *Longitudinal Wave Propagation on a Travelling String*, Ph.D. thesis, University of Delaware, Newark, Delaware.
- Wang, K.W., Mote, C.D. (1986), "Vibration Coupling Analysis of Band/Wheel Mechanical Systems", *Sound and Vibration* **109**, pp. 237-258.
- Wang, K.W., Mote, C.D. (1987), "Band/Wheel System Vibration under Impulsive Boundary Excitation", *Sound and Vibration* **115**, pp. 203-216.
- Watanabe, K, Koyoma, T., Nagai, K. and Kagotani, M. (1990), "", *Mechanical Design* **112**, 424-429.
- Weeks, G.E. (1986), "Dynamic Analysis of a Deployable Space Structure", *Spacecraft Rockets* **23**, pp. 102-107.
- Wickert, J.A., Mote, C.D. (1988), "Current Research on the Vibration and Stability of Axially-Moving Materials", *Shock and Vibration Digest* **20**, pp. 3-13
- Wickert, J.A., Mote, C.D. (1990), "Classical Vibration Analysis of Axially Moving Continua", *Applied Mechanics* **57**, pp. 738-744.
- Zaiser, J.N. (1964), *Non-Linear Vibrations of a Moving Threadline*, Ph.D. thesis, University of Delaware, Newark, Delaware.





## *Chapter 5*

# **Motion resistances of belt conveyors**

---

**T**o obtain accurate results and get full advantage of modern simulation techniques using discrete models of belt systems, it is important to be able to model not only the belt properly, but the interaction between the belt and the supporting structure as well. In this chapter the mathematical formulations of a number of resistance forces encountered by a conveyor belt during motion will be given. The underlying phenomena which cause the resistances differ. Some are caused by the visco-elastic behaviour of the belt cover material whereas others are caused by the friction between the belt and the supporting structure.

### **5.1 The rolling resistance**

The rolling resistance accounts for the major part of all motion resistances. The parameters which determine the rolling resistance of the belt are the belt speed, the diameter and material of the rolls, the belt parameters such as width, material, temperature, tension, lateral load, idler spacing and trough angle.

In this section an approximate formulation of the rolling resistance is derived for a flat belt. However, the equations can easily be extended to troughed belts. The important energy dissipating sources are: the time dependent indentation rolling resistance, the rotation inertia of the rolls of the idlers and the friction of the bearings of the idler rolls. Each source is considered separately and the contribution to the rolling resistance is given. The results obtained are compared to those of Jonkers (1980) and Spaans (1991).

### 5.1.1 The indentation rolling resistance

The rolls of the idlers are made of a relatively hard material like steel or aluminium whereas the belt covers are made of much softer material like rubber and PVC. Therefore the belt cover is indented by the roll due to the weight of the belt and the bulk material when the belt moves over a roll. Due to the visco-elastic properties of the cover material the recovery of the compressed part will take some time. This results in an asymmetrical stress distribution between the belt and the roll which yields a resultant resistance force; the indentation rolling resistance force. The magnitude of this resistance force depends on the constitutive behaviour of the cover material, the radius of the idler roll, the vertical force due to the weight of the belt and the bulk solid material, and the radius of curvature of the belt in curves in the vertical plane.

To reduce the investment and operating costs of a belt-conveyor system it is important to identify the influences of the plant parameters on the energy consumption. In terms of the indentation rolling resistance this implies that the dependence of this resistance on the roll radius, idler spacing, belt speed and radius of curvature should be known. It is also important to know the influence of the belt material and belt structure on the indentation rolling resistance and therefore on the energy consumption of the belt. For example, the resistances of steelcord belts and EP belts differ due to the difference in carcass structure, [Greune and Hager, 1993] and [Hager and Hintz, 1993]. Here the differences in belt structure are not taken into account.

The constitutive behaviour of the rubber belt cover material is described by a three parameter Maxwell model as described in Section 3.2. This model is used by a number of researchers, see for example [May et al., 1959], [Hunter, 1961], [Jonkers, 1980] and [Johnson, 1985]. Morland (1962) uses a model with more relaxation times.

The various sources of energy dissipation in rolling may be classified into those which arise through micro-slip and friction, those which are due to inelastic properties of the material and those due to roughness of the (rolling) surfaces. In this section the restriction is made to the rolling friction due to the inelastic properties of the belt cover material which is the largest contribution, [Johnson, 1985].

During rolling the material lying in front of the contact zone between belt and roll is being compressed whilst that at the rear is being relaxed. In case of conveyor belts, the visco-elastic cover material relaxes more slowly than it is compressed so that the belt and the roll separate at a point ( $x = -b$ ) closer to the centre line ( $x = 0$ ) than the point where they first make contact ( $x = a$ ), see Figure 5.1. In the figures the belt and the roll are depicted upside down which is done for simplicity only. The asymmetrical contact-phenomenon and the resulting asymmetrical stress distribution result in a resistance force.

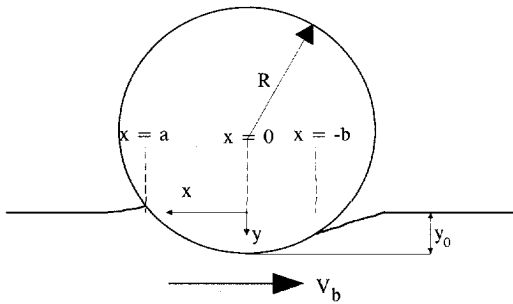


Figure 5.1: Idler rolling over a rubber half space.

If the maximum indentation, which is a function of the belt speed  $V_b$ , is  $y_0$  and the radius of the roll is  $R$  then at any point  $P(x,y)$  within the contact area the indentation can be approximated by :

$$y = y_0 - \frac{x^2}{2R} \quad (5.1)$$

provided that  $y_0 \ll R$ . If point  $P$  enters the contact zone at  $t=0$  with a constant speed  $V_b$  and the process is stationary then

$$a - x = V_b t \quad (5.2)$$

Combining the equations (5.1) and (5.2) yields :

$$(a - V_b t)^2 = 2R(y_0 - y) \quad (5.3)$$

Assuming  $a^2 = 2Ry_0$  which is correct for an independent spring support, a so-called Winkler foundation see Figure 5.2, the indentation written in terms of time  $t$  is given by [May et al., 1959]:

$$y = \frac{V_b}{2R} (2at - V_b t^2) \quad (5.4)$$

Finding the pressure distribution between a rigid cylinder and a visco-elastic layer requires the solution of an integral equation. This procedure is followed by Hunter (1961). The solution from this approach is relatively complicated and cannot be used directly in this case because Hunter considers the problem that the indentation depth  $y_0$ , and not the resultant vertical force, is prescribed. A more convenient approach is to assume that the belt covers can be modelled by a simple visco-elastic Winkler foundation model rather than by a visco-elastic layer, see Figure 5.2. The visco-elastic foundation of depth  $h$ , rests on a rigid base and is compressed by the rigid roller. Since there is no interaction between the springs of the foundation this implies a.o. that shear between adjacent elements of the model is ignored. The inertia of the foundation material is also neglected.

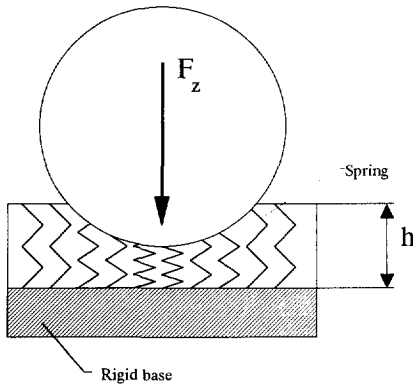


Figure 5.2: Winkler foundation model.

If the indentation depth is small compared to the thickness of the belt cover and it may be assumed that the carcass material is indeed undeformable, then the visco-elastic Winkler model can be applied to approximate the strain of the belt covers due to the indentation of the roll. Therefore, this deformation is given by:

$$\gamma = \frac{y}{h} = \frac{V_b}{2Rh} (2at - V_b t^2) \quad (5.5)$$

(compression strain is taken positive here) and the deformation rate is equal to:

$$\dot{\gamma} = \frac{V_b}{Rh} (a - V_b t) \quad (5.6)$$

If a Maxwell model with one relaxation time (three parameter solid) is chosen to model the constitutive behaviour of the belt cover material then substitution of the equations (5.5) and (5.6) in equation (3.20) yields the stress distribution:

$$\sigma(t) = \frac{E_1 V_b}{2Rh} (2at - V_b t^2) + \frac{E_2 V_b \tau}{Rh} \left[ (a + V_b t) \left( 1 - \exp\left(-\frac{t}{\tau}\right) \right) - V_b t \right], \quad 0 \leq t \leq \frac{a + b}{V_b} \quad (5.7)$$

Substituting  $\frac{a-x}{V_b}$  for  $t$  yields the following equation :

$$\sigma(x) = a^2 \left\{ \frac{E_1}{2Rh} \left( \frac{a-x}{a} \right) \left( \frac{a+x}{a} \right) + \frac{E_2 k}{Rh} \left[ (1+k) \left( 1 - \exp\left(-\frac{1}{k} \frac{(a-x)}{a}\right) \right) - \left( \frac{a-x}{a} \right) \right] \right\} \quad (5.8)$$

where

$$k = \frac{V_b \tau}{a} \quad (5.9)$$

The ratio  $b/a$  can be obtained from equation (5.8) since  $\sigma(-b) = 0$ . If the belt moves at a constant speed then the distributed vertical force per unit width may be obtained by integrating equation (5.8) which yields :

$$F_z = \int_{-b}^a \sigma(x) dx = \frac{E_1 a^3}{6Rh} \left[ -\left(\frac{b}{a}\right)^3 + 3\left(\frac{b}{a}\right) + 2 \right] + \frac{E_2 k a^3}{Rh} \left[ (1+k) \left\{ \left(\frac{a+b}{a}\right) + k \left( \exp\left(-\frac{1}{k} \left(\frac{a+b}{a}\right)\right) - 1 \right) \right\} - \frac{1}{2} \left(\frac{a+b}{a}\right)^2 \right] \quad (5.10)$$

Since  $F_z$  is constant for a stationary moving belt and the ratio  $b/a$  is known from equation (5.8), the length  $a$  can be calculated from equation (5.10). This leads to:

$$a = \frac{F_z^{1/3}}{\left[ \frac{E_1}{6Rh} \left[ -\left(\frac{b}{a}\right)^3 + 3\left(\frac{b}{a}\right) + 2 \right] + \frac{E_2 k}{Rh} \left[ (1+k) \left\{ \left(\frac{a+b}{a}\right) + k \left( \exp\left(-\frac{1}{k} \left(\frac{a+b}{a}\right)\right) - 1 \right) \right\} - \frac{1}{2} \left(\frac{a+b}{a}\right)^2 \right] \right]^{1/3}} \quad (5.11)$$

To calculate the rolling resistance, the moment has to be taken about the centre of the roller:

$$M = \int_{-b}^a \sigma(x) x dx \quad (5.12)$$

The total resistance force per unit width is:

$$F_i = \frac{M}{R} = \frac{E_1 a^4}{8R^2 h} \left[ 1 - 2\left(\frac{b}{a}\right)^2 + \left(\frac{b}{a}\right)^4 \right] + \frac{E_2 a^4 k}{R^2 h} \left[ k^3 - \frac{k}{2} \left( 1 + \left(\frac{b}{a}\right)^2 \right) + \frac{1}{3} \left( 1 + \left(\frac{b}{a}\right)^3 \right) - k(1+k) \left( k + \frac{b}{a} \right) \exp\left(-\frac{1}{k} \left(\frac{a+b}{a}\right)\right) \right] \quad (5.13)$$

Finally, the indentation rolling resistance factor, defined as used in DIN 22101, is equal to:

$$f_{im} = \frac{F_i}{F_z} = \frac{F_z^{1/3} h^{1/3}}{D^{2/3}} F_{RM} \left( k, \frac{a}{b}, E_1, E_2 \right) \quad (5.14)$$

in which  $D$  is the diameter of the roll. The derivation of the indentation rolling resistance factor (5.14) is the same as given by May et al. (1959). However, in the application May assumes that the indentation depth  $h$  is independent of the belt speed. As a result, starting from a specific belt speed  $V_{bm}$ , the vertical force in the model of May increases with increasing belt speed. In the above consideration the vertical load  $F_Z$  is taken constant which results in a decreasing indentation of the belt with increasing belt speed. Therefore, the indentation rolling resistance factor found by May et al. (1959) is higher than  $f_{im}$  for belt speeds above  $V_{bm}$  and lower than  $f_{im}$  for belt speeds below  $V_{bm}$ .

Spaans (1991) and Jonkers (1980) also use the Winkler foundation model instead of a layer to model the visco-elastic response of the belt. To determine the indentation rolling resistance they use a formulation for the energy loss due to hysteresis losses of the cover material. Spaans assumes that the visco-elastic response of the belt material can be modelled by a combination of linear elastic belt material and a coefficient of energy loss due to indentation that accounts for the visco-elastic behaviour. He arrives at :

$$f_{is} = 0.5\eta \frac{F_Z^{1/3}}{\left(\frac{2}{3}\right)^{4/3} E^{*1/3} D_0^{2/3} (1 + (1 - \eta_i)^{3/4})^{4/3}} \quad (5.15)$$

where  $E^*$  is the lateral flexibility of the belt which is equal to the dynamic Young's modulus of the total belt divided by the belt thickness and can be determined from a hysteresis test. This test also yields the loss factor  $\eta$ . The diameter  $D_0$  accounts for the diameter of the roll and the radius of curvature of the belt. It is defined by:

$$\frac{1}{D_0} = \frac{1}{D} + \frac{1}{2R_c} \quad (5.16)$$

where  $R_c$  is the radius of curvature of the belt on top of the roll. The lateral flexibility and the loss factor are determined from a hysteresis test performed at a specific frequency. Therefore equation (5.15) is only valid for a specific belt speed. To compare Spaans' equation with equation (5.14), equation (5.15) has to be adapted. As mentioned above the lateral flexibility of the belt is equal to the dynamic Young's modulus of the total belt divided by the belt thickness. Here only the belt cover is considered. The lateral flexibility is therefore equal to:

$$E^* = \frac{E_d}{h} = \frac{E'(\omega)}{h \cos(\delta)} \quad (5.17)$$

where  $E'$  is the storage modulus and  $\delta$  the loss angle of the belt cover material which, for the three parameter Maxwell model, are given in the equations (3.24) and (3.25) respectively. With this result and the loss factor as given in equation (3.26), the indentation rolling resistance factor becomes :

$$f_{is}^* = 0.5\eta(\delta) \frac{F_Z^{1/3} h^{1/3}}{\left(\frac{2}{3}\right)^{4/3} E_d^{1/3} D_0^{2/3} [1 + (1 - \eta_i(\delta))^{3/4}]^{4/3}} \quad (5.18)$$

Jonkers also relates the indentation rolling resistance directly to the hysteresis losses due to the indentation of the belt cover. He assumes that the development of the indentation depth  $y$  along the contact line can be approximated by a sinusoidal instead of a parabolic function (equation (5.4)):

$$y = y_0 \sin(\omega t) \quad (5.19)$$

where

$$\omega = \frac{\pi V_b}{a + b} \quad (5.20)$$

Jonkers uses the three parameter Maxwell model to determine the hysteresis losses. He arrives at :

$$f_{ij} = 0.5 \pi \tan\delta \left[ \frac{(\pi + 2\delta)\cos\delta}{4\sqrt{1 + \sin\delta}} \right]^{4/3} \frac{F_Z^{1/3} h^{1/3}}{E^{1/3} D_0^{2/3}} \quad (5.21)$$

The contact length  $(a+b)$  depends on the storage modulus. The storage modulus, however, depends on the deformation rate which depends on the contact length. Therefore, to calculate the deformation rate an iterative procedure using a predictor  $2a_0$  for the contact length has to be used which follows from the Winkler model, [Johnson, 1985]:

$$a_0^3 = \frac{3 F_Z D h}{4 E_1} \quad (5.22)$$

The correct deformation rate and storage modulus are obtained after a number of predictor-corrector steps.

For the calculation of the maximum indentation depth, both Jonkers and Spaans assume that the indentation of the belt by the roll is symmetrical with respect

to the centre line of the roll. However, with increasing belt speed, and hence increasing deformation rate, the indentation profile becomes more asymmetrical.

The drawback to these theories is twofold. Firstly, the hysteresis loss factor (equation 3.26) is generally not a material constant. Secondly, the hysteresis loss factor in rolling cannot be identified with the loss factor in a simple tension or compression cycle. The latter effect can be estimated by comparing the results obtained by Hunter (1961) and May (1959). In both analyses the indentation depth is prescribed instead of the vertical belt load.

Hunter starts from the retardation equation instead of the relaxation equation (3.23):

$$\Phi(t) = \frac{1}{\mu_D} \left[ 1 + f^* \left( 1 - \exp\left(-\frac{t}{\tau}\right) \right) \right] \quad (5.23)$$

In case of the three parameter Maxwell model the modulus  $\mu_D$  and the retardation coefficient  $f^*$  are:

$$\mu_D = E_1 + E_2, f^* = \frac{E_2}{E_1} \quad (5.24)$$

The indentation rolling resistance according to Hunter is:

$$f_{\text{th}}^* = \frac{1}{R} \left[ V_b \tau \left( 1 - \frac{1}{1 + f^*} \right) + \Gamma_1 \left( 1 - \left( \frac{a}{a_0} \right)^2 \right) \right] \quad (5.25)$$

where:

$$a_0^2 = \frac{2(1-\nu)(1+f^*) R F_z}{\pi \mu_D} \quad (5.26)$$

$$\left( \frac{a_0}{a} \right)^2 = 1 + \frac{2f^* / h^*}{K_0(\frac{1}{k}) / K_1(\frac{1}{k}) + I_0(h^*) / I_1(h^*)} \quad (5.27)$$

$$\Gamma_1 = a \left( -\frac{1}{h^*} - \frac{1}{2} \left[ \left( \frac{a_0}{a} \right)^2 - 1 \right] \frac{I_0(h^*)}{I_1(h^*)} \right) \quad (5.28)$$

and

$$h^* = (1+f^*)k \quad (5.29)$$



The functions  $K_0, K_1, I_0, I_1$  are zero and first order (modified) Bessel functions [Watson, 1952].

The vertical belt load,  $F_z^*$ , and the indentation rolling resistance force,  $F_i^*$ , according to May can be obtained from the equations (5.10) and (5.13) by substitution of  $a_0$ , see equation (5.26), for  $a$ . Note that in this case the indentation depth is prescribed and not the vertical belt load. The indentation factor according to May is:

$$f_{im}^* = \frac{F_i^*}{F_z^*} \quad (5.30)$$

If a correction factor is defined by:

$$f_s = \frac{f_{ih}^*}{f_{im}^*} \quad (5.31)$$

which indicates the accuracy of the Winkler model, then the proposed total indentation resistance factor is:

$$f_i = f_s f_{im} \quad (5.32)$$

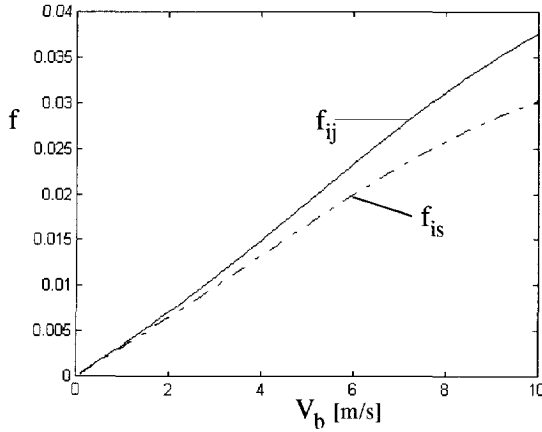
Besides Spaans, Jonkers, May and Hunter, other researchers developed models to determine the indentation rolling resistance force. A survey is given in [Lodewijks, 1995].

If the radius of the roll  $R=0.0795$  m, the thickness of the belt cover  $h=0.008$  m, the vertical force  $F_z=2000$  N/m, the belt speed varies from 0.1 to 10 m/s and the cover material is the SBR rubber of Section 3.2, then the following three parameters can be used :

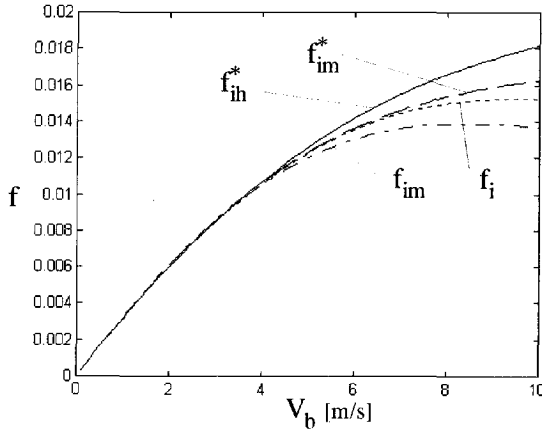
$$E_1 = 7.10^6 \text{ Nm}^{-2}, E_2 = 2,5.10^8 \text{ Nm}^{-2}, \eta = 1875 \text{ Nm}^{-2}\text{s}$$

With these belt parameters the different results for the indentation rolling resistance factors are given in the Figures 5.3 and 5.4. As can be seen in the Figures 5.3 and 5.4 the indentation rolling resistance factors calculated with the equations of Hunter, equation (5.25), May, equation (5.30), Jonkers, equation (5.21), and Spaans, equation (5.18), are higher than those calculated with the equations (5.14) and (5.32). The differences between the factors shown in Figure 5.4 are caused by differences in the formulation of the problem. Hunter and May prescribe the indentation depth whereas in case of equation (5.14) and (5.32) the vertical belt load is prescribed. The indentation rolling resistance factor obtained from the moment  $M$ , which is the result

of the asymmetrical stress distribution, is about half the factor which is obtained from calculation of the indentation rolling resistance force using the loss factor. This explains the differences between the factors shown in the Figures 5.3 and 5.4. In **TUDBELT** the indentation rolling resistance factor given in equation (5.32) is used.



**Figure 5.3:** Indentation rolling resistance factor according to Jonkers (solid line, equation (5.21)) and Spaans (dashdot line, equation (5.18)).



**Figure 5.4:** Indentation rolling resistance factor according to Hunter (solid line, equation (5.25)), May et al. (dashed line, equation (5.30)), equation (5.14) (dashdot line) and equation (5.32) (dotted line).

### 5.1.2 The inertia of the idlers

When the belt is not moving at a stationary speed then the rotation inertia of the idlers and the bearings should be taken into account. This inertia can be accounted for by the following acceleration rolling resistance factor :

$$f_a = \frac{m_{red} \frac{dV_b}{dt}}{F_z B} \quad (5.33)$$

where B is the belt width and  $m_{red} = \frac{I_{roll}}{R^2}$  the reduced mass of the idler rolls. The moment of inertia of an idler roll, neglecting the end disks, is equal to:

$$I_{roll} = \frac{1}{2} \rho \pi b_{roll} (R^4 - r^4) \quad (5.34)$$

where  $b_{roll}$  is the roll width, R the external and r the internal roll radius.

### 5.1.3 The rolling resistance of the bearings

The rolling resistance of the bearings of an idler roll, which is the resistance of those bearings to rotation in steady state, can be defined by :

$$f_b = \frac{M_f}{F_z B R} \quad (5.35)$$

where  $M_f$  is the resistance moment. This resistance moment includes a load independent and a load dependent component, and depending on the bearing type, it can also include a contribution of the sealings. These components are normally given by the bearing manufacturer.

### 5.1.4 The total rolling resistance

Finally, the total rolling resistance factor is defined by:

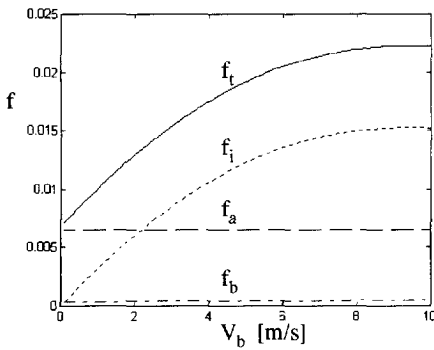
$$f_t = f_i + f_a + f_b \quad (5.36)$$

Typical data of an idler roll are:

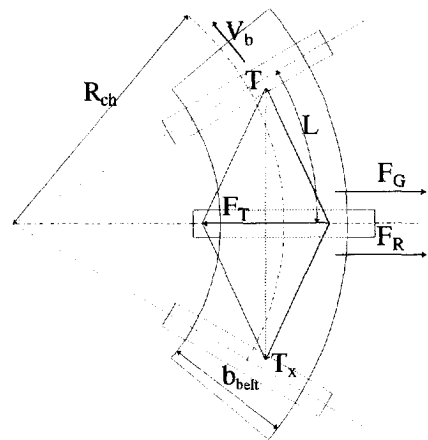
$$R = 0.0795 \text{ m} , r = 0.0775 \text{ m} , \rho = 7850 \text{ kg.m}^{-3} , b_{\text{roll}} = 1.150 \text{ m}$$

$$B = 1 \text{ m} , F_z = 2000 \text{ N.m}^{-1} , \frac{dV_b}{dt} = 1.5 \text{ m.s}^{-2}$$

With these data the acceleration rolling resistance factor is equal to  $f_a = 0.0065$ . In Figure 5.5 the bearing rolling resistance factor of an SKF bearing type 6305 is shown. This figure also shows the acceleration rolling resistance factor,  $f_a$ , of the above mentioned roll in case the acceleration of the belt is  $1.5 \text{ m.s}^{-2}$ , the indentation rolling resistance factor,  $f_i$ , and the total rolling resistance factor  $f_t$ .



**Figure 5.5:** The total rolling resistance factor (solid line), the bearing rolling resistance factor (dash-dot line), the indentation rolling resistance factor (dotted line) and the acceleration resistance factor (dashed line).



**Figure 5.6:** Forces acting on a belt travelling through a horizontal curve.

## 5.2 Motion resistance of horizontally curved belt sections

In comparison with straight belt conveyors there are two aspects of horizontal, curved conveyors that need to be considered: the traction force  $F_T$  directed to the inside of the curve and the in-plane bending stresses, see also Figure 5.6. In this section only the first aspect will be considered.

When a belt runs through a horizontal curve, a component of the tensile force of the belt is directed to the inside of the curve of the supporting frame [Weigel, 1976],[ Grimmer and Kessler, 1992]:

$$F_T = \frac{TL}{R_{ch}} \tag{5.37}$$

assuming that  $L \ll R_{ch}$ . To prevent run-off, the belt supports must exert forces on the belt which counteract this traction force  $F_T$ . These forces are obtained as a result of the weight of the belt and the bulk material, summarised in the force  $F_G$ , and the friction between the idlers and the belt, summarised in the force  $F_R$ .  $F_G$  and  $F_R$  are called the horizontal belt guide forces. For the extreme situations where the belt is located on the inside or the outside of the curve, a run-off can only be prevented if the following condition is satisfied:

$$F_{Go} + F_{Ro} < F_T < F_{Gi} + F_{Ri} \tag{5.38}$$

where the index  $i$  denotes the inside and  $o$  the outside of the curve. From equation (5.38) the conclusion can be drawn that the guide forces must decrease from the inside of the curve to the outside of the curve. The guide force  $F_G$  results from the distribution of the gravitational force over the three idler rolls depending on the position of the belt and the super-elevation angle of the idler. The force  $F_{G,belt}$  results from the total belt material weight,  $F_{TG,belt}$ , whereas  $F_{G,bulk}$  results from the total bulk material weight,  $F_{TG,bulk}$ , see Appendix A and Figure 5.7.

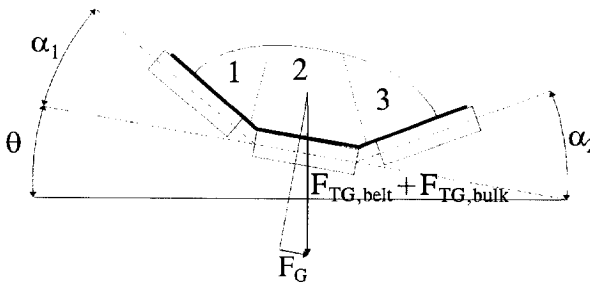
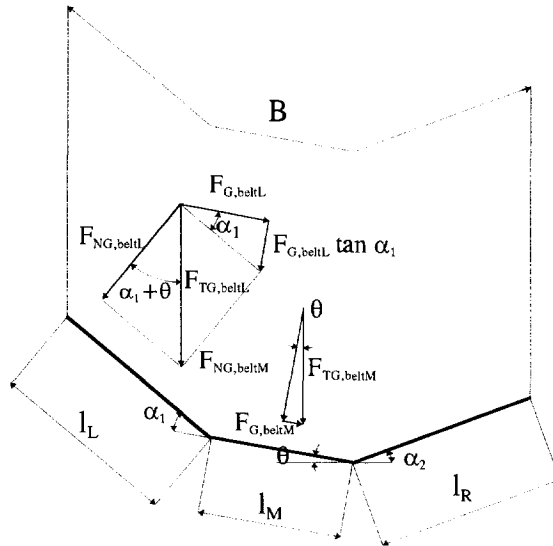


Figure 5.7: Guide force resulting from the weight of the belt and the bulk material.

The guide force  $F_G$  can be divided into three parts corresponding to the three idler rolls:

$$F_G = F_{GL} + F_{GM} + F_{GR} \quad (5.39)$$

where the indices L, M and R indicate the left, middle and right idler roll respectively.



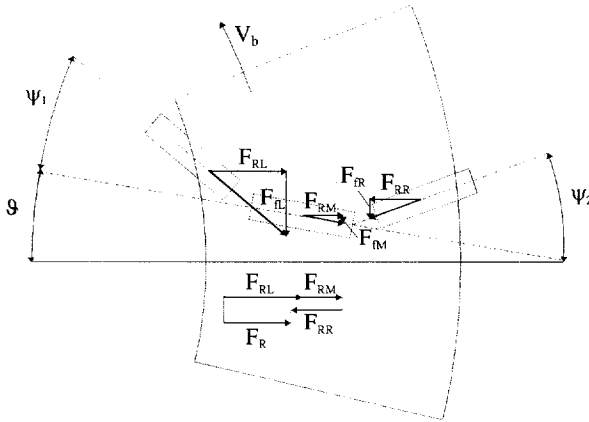
**Figure 5.8:** Lengths, angles and forces resulting from the belt weight within the range of a horizontal curve.

From Figure 5.8 it can be learned that the components of  $F_G$  are:

$$\begin{aligned} F_{G,beltL} &= (F_{NG,beltL} + F_{NG,bulkL}) \tan(\alpha_1 + \theta) \cos\alpha_1 \cos\delta_s \\ F_{G,beltM} &= (F_{NG,beltM} + F_{NG,bulkM}) \tan(\theta) \cos\delta_s \\ F_{G,beltR} &= -(F_{NG,beltR} + F_{NG,bulkR}) \tan(\alpha_2 - \theta) \cos\alpha_2 \cos\delta_s \end{aligned} \quad (5.40)$$

where  $F_{NG,beltL}$ ,  $F_{NG,beltM}$  and  $F_{NG,beltR}$  are forces normal to the three idler rolls due to the belt weight,  $F_{NG,bulkL}$ ,  $F_{NG,bulkM}$  and  $F_{NG,bulkR}$  are forces normal to the three idler rolls due to the bulk material weight, see Appendix A;  $\theta$  the super-elevation angle of the idler station;  $\alpha_1$  and  $\alpha_2$  the trough angles and  $\delta_s$  the inclination angle of the total belt conveyor system. The guide force  $F_R$  can also be divided into three parts corresponding to the idler rolls:

$$F_R = F_{RL} + F_{RM} + F_{RR} \quad (5.41)$$



**Figure 5.9:** Guide force resulting from friction forces between the idlers and the conveyor belt travelling through a horizontal curve.

Elevation only of an idler station does sometimes not result in guide forces that can counteract the traction force  $F_T$ . Therefore the idler station is also aligned. From Figure 5.9, which shows the alignment of the idler rolls, it can be learned that the (maximum) components of  $F_R$  are:

$$\begin{aligned} F_{RL} &= \mu_{br} \cos(\psi_1 + \vartheta) \cos \alpha_1 \cos \delta_s (F_{NG, belL} + F_{NG, bulkL}) \\ F_{RM} &= \mu_{br} \cos \vartheta \left[ \cos \delta_s (F_{NG, belM} + F_{NG, bulkM}) + (F_{G, belL} \tan \alpha_1 + F_{G, belR} \tan \alpha_2) \right] \\ F_{RR} &= -\mu_{br} \cos(\psi_2 - \vartheta) \cos \alpha_2 \cos \delta_s (F_{NG, belR} + F_{NG, bulkR}) \end{aligned} \quad (5.42)$$

where  $\mu_{br}$  is the friction coefficient between the belt and the rolls,  $\vartheta$  the super-tilt angle of the idler station and  $\psi_1$  and  $\psi_2$  are the two alignment angles. Due to the alignment of the idler station, a resistance force results. This resistance force  $F_{ar}$  can also be divided into three parts:

$$F_{ar} = F_{arL} + F_{arM} + F_{arR} \quad (5.43)$$

where the three components are equal to:

$$\begin{aligned}
 F_{arL} &= \tan(\psi_1 + \vartheta) F_{RL} \\
 F_{arM} &= \tan\vartheta F_{RM} \\
 F_{arR} &= \tan(\psi_2 - \vartheta) F_{RR}
 \end{aligned}
 \tag{5.44}$$

The horizontal curve resistance factor  $f_{ar}$ , which is the ratio between the resistance  $F_{ar}$  and the total vertical load,  $F_{TG}$ , is defined by:

$$f_{ar} = \frac{F_{ar}}{(m'_{belt} + m'_{bulk}) g L \cos\delta_s}
 \tag{5.45}$$

### 5.3 References.

- Greune, A. and Hager, F.R. (1990), "The Energysaving Design of Belt Conveyors", *Bulk Solids Handling* **10**, pp. 245-250.
- Grimmer, K.J. and Kessler, F. (1992), "The Design of Belt Conveyors with Horizontal Curves", *Bulk Solids Handling* **12**, pp. 557-563.
- Hager, M. and Hintz, A. (1993), "The Energysaving Design of Belts for Long Conveyor Systems", *Bulk Solids Handling* **13**, pp. 749-758.
- Hunter, S.C. (1961), "The Rolling Contact of a Rigid Cylinder with a Viscoelastic Half Space", *Applied Mechanics* **28**, pp. 611-617.
- Johnson, K.L. (1985), *Contact Mechanics*, Cambridge University Press, Cambridge.
- Jonkers, C.O. (1980), "The Indentation Rolling Resistance of Belt Conveyors", *Fördern und Heben* **30**, pp. 312-316.
- Lodewijks, G. (1995), "The Rolling Resistance of Conveyor Belts", *Bulk Solids Handling* **15**, pp. 15-22.
- May, W.D., Morris, E.L. and Atack, D. (1959), "Rolling Friction of a Hard Cylinder over a Viscoelastic Material", *Applied Physics* **30**, pp. 1713-1724.
- Morland, L.W. (1962), "A Plane Problem of Rolling Contact in Linear Viscoelasticity theory", *Applied Mechanics* **29**, pp. 345-352.
- Spaans, C. (1991), "The Calculation of the Main Resistance of Belt Conveyors", *Bulk Solids Handling* **11**, pp. 809-826.
- Watson, G.N. (1952), *A Treatise on the Theory of Bessel Functions (second edition)*, Cambridge University Press, Cambridge.
- Weigel, T. (1976), *Beitrag zur Kurvengängigkeit von Bandförderanlagen unter besonderer Berücksichtigung der normaler Fördergurte*, Doctorate thesis, University of Karlsruhe.



## Chapter 6

# The belt conveyor drive system

---

The drive system is one of the most important elements in a belt conveyor system, it affects the conveyor performance, capacity and economics. The integration of drive technology in belt conveyor design is therefore important. The drive system will significantly influence the belt tension during starting and stopping of large belt conveyor systems. A reduction in the transient loading will reduce the belt size. The reduction in belt size and weight will also reduce the size of all other conveyor components and the structure.

Despite the advantages of using an optimal drive system, the options available to the conveyor engineers are mostly only general purpose drives designed by their suppliers, to be satisfactory for a large number of industrial applications. Since most standard drive systems fall short of the specific requirements the system should meet, the conveyor engineer should be aware of these requirements to enable proper selection of the drive system components. Work based on finite element models of belt conveyors [Nordell and Ciozda, 1984], [Harrison, 1985], which is discussed in the next chapter, has accurately defined the conveyor drive system requirements. Some of these requirements for application in long belt conveyors are discussed in the following section.

## 6.1 Technical requirements of a drive system

The most important technical drive system requirements are the profile and length of the starting and stopping procedure, overload protection, proper load sharing among multiple drives and minimising load on the electrical components.

### 6.1.1 Starting and stopping procedures

A starting or stopping procedure of a belt conveyor can be velocity controlled or torque controlled. In this thesis only velocity-controlled starting and stopping procedures are considered. The velocity-controlled starting and stopping procedures of

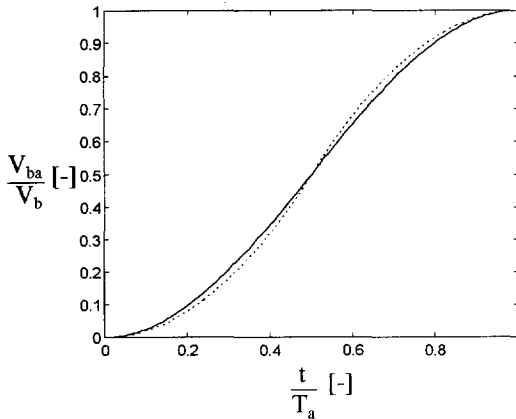
long belt conveyors, specified in velocity profile and length, are not standardised. In absence of standardisation, the drive system suppliers mostly try to design a start-up procedure with constant acceleration to minimise the acceleration force, or do not concern themselves with attaining any particular velocity profile of the start-up procedure. Based on simulation with finite element models of belt conveyor systems and experimental verification, Harrison (1983) and Nordell (1985) recommended profiles for the starting procedure in terms of the belt speed to minimise the transient belt tension. Harrison recommended for the belt speed during acceleration  $V_{ba}$ :

$$V_{ba}(t) = \frac{V_b}{2} \left( 1 - \cos\left(\frac{\pi t}{T_a}\right) \right), \quad 0 \leq t \leq T_a \quad (6.1)$$

where  $T_a$  is the length of the starting procedure, or the time it takes the belt to reach the design speed. Nordell recommended:

$$V_{ba}(t) = V_b \left( \frac{2t^2}{T_a^2} \right) \quad \text{for } 0 \leq t \leq \frac{T_a}{2} \quad (6.2)$$

$$V_{ba}(t) = V_b \left( -1 + \frac{4t}{T_a} - \frac{2t^2}{T_a^2} \right) \quad \text{for } \frac{T_a}{2} \leq t \leq T_a$$



**Figure 6.1:** Acceleration profile according to Harrison (solid line), equation (6.1), and Nordell (dotted line), equation (6.2).

With this velocity profile the so-called belt shock, which is the second derivative of  $V_b$  with respect to time, is not continuous. However, the maximum shock value is only 81% of the peak value obtained from equation (6.1). Although the velocity profiles of both of the above procedures, see Figure 6.1, will give very satisfactory results for minimising peak tension during transients, the results can further be improved by adding a rest period in the procedure. During this rest period, that takes place right after the start,

the belt speed is kept constant. During this rest period the initial belt slack can be pulled out, which permits all the conveyor elements to attain a running condition at very low torque and speed before the acceleration is continued to higher torque values [Nordell, 1991]. This eliminates over stressing of the belt that would otherwise be produced by the large initial error in the PID control loop. This method can reduce peak belt tension by about 15 %. Other velocity controlled start-up procedures will be discussed in Chapter 8.

An approximation of the start-up time which is often used, see for example [Singh, 1994], is that the length of the starting procedure, or start-up time, should at least be equal to five times the time it takes a longitudinal stress wave to travel through the return part of the belt from head to tail of the conveyor. Written in terms of the propagation speed,  $c_1$ , this is:

$$T_a \geq 5 \frac{L_{conv}}{c_1} \quad (6.3)$$

where  $L_{conv}$  is the length of the conveyor from head to tail. However, this start-up time is only valid if it is used for torque controlled start-ups and used as the time during which the drive torque is increased from zero to the required start-up torque, [Funke, 1973]. This start-up torque can for example be 1.4 times the nominal drive torque. If equation (6.3) is used as the length of a velocity controlled start-up then it will result in inadmissible belt tensions as will be shown in Chapter 8.

In practice the “one minute starting time per km of conveyor length” rule is often applied since application of equation (6.3) may result in very steep acceleration profiles and very high peak tensions during starting. Since the propagation speed of longitudinal waves varies from about 500 m.s<sup>-1</sup> till 2000 m.s<sup>-1</sup> depending on the reinforcement material of the belt, this implies that the factor which is 5 in equation (6.3), according to this rule, varies from 30 till 120. In case of conveyors with a length over 2-3 km this rule leads to unnecessary long starting procedures. In such a case the results of simulation of the dynamic behaviour of the conveyor belt should be used.

Using the belt speed variation given in equation (6.1) yields a maximum acceleration of:

$$\dot{V}_{b,a(max)} = \frac{V_b \pi}{2T_a} \quad (6.4)$$

If  $m^*$  is the effective mass of the belt contributing to the longitudinal vibrations then the acceleration force  $F_{ac}$  can be written as:

$$F_{ac} = m^* \dot{V}_{b,a(max)} \quad (6.5)$$

According to Harrison and Roberts (1984)  $m^*$  has a value of approximately one fourth of the belt system mass for the fundamental mode. However, taking only one fourth of the belt system mass into account leads to an underestimation of the total acceleration force as will be shown in Section 8.6.2. If  $F_1$  is the maximum belt tension during stationary operation then, according to Harrison and Roberts (1984), for steel cord belts the required safety factor with respect to the belt stress during stationary operation should be:

$$S_B \geq 3 \left( \frac{F_1 + F_{ac}}{F_1} \right) \quad (6.6)$$

Studies of Nordell (1989, 1993 and 1995) showed that for steelcord belts a reduction in safety factor from 6.7 to 5.5 or even lower is totally feasible by properly addressing the belt construction and belt dynamics considerations including the selection and use of the drive system. Similar conclusions can be reached for the safety factor of fabric belts.

A controlled stop can be achieved by applying a stopping procedure with a mirror characteristic of the start characteristic given in equations (6.1) or (6.2). Since the stopping of a conveyor belt is potentially more damaging and less controllable than its starting, the length of the stopping procedure may be more critical than the length of the starting procedure. Nordell and Ciozda (1984) found that the strain energy stored in the belt reacts with a higher specific impulse than can be generated by the drive system. Therefore the length of the stopping procedure may have to be extended by application of flywheels on the drive system input, moreover the inertia of the drive must stay connected to the conveyor belt. The start-up of a belt conveyor system equipped with a drive system with flywheels, however, requires a special motor. The simulation of the dynamic behaviour of a belt conveyor system during (emergency) stopping must be used to analyse the longitudinal waves and to ensure that the corresponding stresses remain within safe limits.

### 6.1.2 Overload protection

All belt conveyor components must be protected from mechanical or electrical overloading. The motor and the drive system may be sufficiently large to start an overloaded conveyor. However, when the drive system inputs excessive torque into the belt conveyor, a load surge going through the conveyor can overload the reducers and the mechanical components of the motors. Therefore the possibility of accidentally starting or running an overloaded conveyor must be eliminated, which

can be achieved by using a drive system with an adjustable maximum torque limit. The torque limiting device, which requires a control and feedback system, should be located just before the output shaft of the drive system. Also important is the dynamic responsiveness of the torque limiting device since it should eliminate the possibility of a momentary major load peak on the belt conveyor passing through the torque limiting section into the reducer and motor.

### 6.1.3 Drive requirements

Most long belt conveyor systems are driven by multiple drive systems. Proper load sharing among these drives during all phases of operation minimises the loads and stresses on the conveyor components. This requires cascaded PID control loops for the control of the drive speed and drive output torque.

Other requirements of belt conveyor systems have to do with limiting the load on the electrical system of the conveyor. The drive system should either allow the conveyor motors to be started unloaded or reduce the inrush currents to an acceptable level during acceleration. The drive system should also allow the conveyor to stop without stopping the motors. To avoid overloading of the power supply system resulting in excessive line voltage sags, the conveyor motor starts should be staggered. The drive system should also include self-monitoring and self-diagnostics to avoid drive system failures and thus minimising the down time of the conveyor and providing operational flexibility. For example, if one drive system of a multi-drive conveyor has to be taken off-line, the conveyor should still remain operating possibly at a lower loading level. Finally, the drive system should not lead to complications by generating unacceptable levels of line pollution and noise.

## 6.2 Components of a drive system

There are five major drive variants used for long belt conveyors [McCormick, 1985a], [Schulz, 1995]:

- 1) a combination of a squirrel cage motor and a fluid coupling with delayed filling chamber. The oil in the delaying chamber is circulated into the working chamber within approximately 25 s after acceleration of the motor. Especially for long distance belt conveyors with relatively high masses to be accelerated during start-up, the fluid coupling with delayed filling chamber may unacceptably be heated.
- 2) a combination of a squirrel cage motor and a drain-type fluid coupling which involves a constant circulation of oil. Control of the acceleration is achieved by simple torque control, i.e. by opening and closing the oil-delivery when 1.3-1.5 fold of the rated stationary torque is reached.

- 3) a combination of a squirrel cage motor and a control coupling. By adjusting the oil level or pressure in the working chamber of the coupling, the torque is made transmittable. Control of the coupling is made in such a way that the system accelerates to full speed via a prefixed torque ramp.
- 4) a combination of a squirrel cage motor with frequency control. The belt speed is adjusted in proportion to a prefixed ramp of the stator frequency of the motor. If the torque of the motor exceeds the prefixed limit value of for example 1.4 fold the rated stationary torque, the frequency ramp is stopped until the torque drops below this limit value. This drive variant has the advantage that it can be used to decelerate the system. In that case the ramp function decreases.
- 5) a slipping motor controlled through a number of, for example 12, resistance steps. The torque of the motor is controlled by switching between resistance steps. A torque limitation is realised by intermittently switching to the next resistance step as long as the torque generated by the slipping motor is smaller than the predetermined value of 1.4 fold the rated stationary torque.

Although the choice of a drive system should be based not only on the price but also on the technical requirements, the investment of a drive system has to be considered in the planning of the total conveyor system. An illustrative example [Schulz, 1995] shows that the share of all drives in the total investment amounts to approximately 4 % if drives with frequency control are used.

Compared to this drive variant, the investment cost of drive variants 1, 2, 3 and 5 are 43%, 60%, 94% and 62% respectively of the investment of drive variant 4.

In the next sections an overview of the components of a drive system for a belt conveyor system is given. Also the power equations and the equations of motion of each component of the drive system are derived in the following paragraphs. These equations are used in the simulation software system **TUDBELT**. The possible components of a drive system are summarised in Figure 6.2.

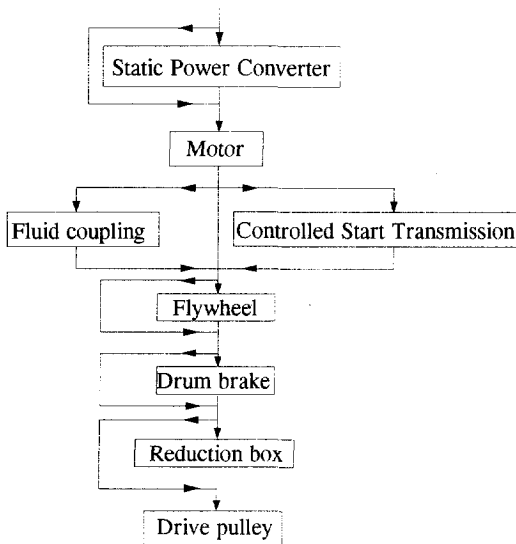


Figure 6.2: Possible components of a drive system.

### 6.3 Static power converter

If an induction motor is connected to a source with fixed supplied voltage or current and frequency, the motor torque and number of revolutions of the output shaft can not be controlled but are determined by the characteristics of the motor and the load. To control the voltage or current and the frequency supplied to a motor, a static power converter (SPC) can be used. An SPC is an electrical device which converts the fixed frequency to a variable frequency and either the fixed input voltage to a variable voltage, Voltage Source Inverter (VSI), or the fixed current, Current Source Inverter (CSI). Induction motors supplied with variable-voltage/current, variable-frequency sources are capable of meeting the requirement of control over a wide range of speed variations.

When ac motors are operated on variable voltage/frequency supplies, system instability may occur due to pulsation of the motor torque caused by the voltage and current harmonics applied to the machine [Lipo, Krause and Jordan, 1969]. In many cases these torque pulsations define the lower limit of the speed range which yields satisfactory system performance. The minimum frequency of these torque pulsations for a CSI is six times the supply frequency. Normally the supply frequency of belt conveyor drives is varied between 10 and 60 Hz which in this case results in torque pulsations of 60 to 360 Hz. The maximum first natural frequency of longitudinal vibrations of a belt conveyor system longer than 1 km is about 1 Hz whereas the maximum first natural frequency of transverse vibrations of the belt is about 20 Hz. The frequency of axial vibration caused by transverse vibration is twice the frequency of that vibration. Therefore the maximum significant frequency of axial vibration is 40 Hz. Since the frequency of torque pulsation is at least 60 Hz, no important interactions may be expected. Therefore no separate (mathematical) model of an SPC, as for example given in [Krause and Lipo, 1969] and [Lipo and Krause, 1969a & b], is included in **TUDBELT**. The SPC, which is assumed to be a symmetrically and ideally converter, is accounted for by directly changing the motor supply voltage and frequency.

### 6.4 Induction motor

Most belt conveyor systems are fitted with an induction motor of the squirrel-cage type or the slipring type. The mathematical analysis needed to determine the dynamic behaviour of an induction motor can be based on a circuit analysis approach and does not need a detailed description of the electromagnetic phenomena internal to the motor. This approach does not provide the same physical insight into the operation of a motor as a detailed electromagnetic approach, but can be used for the majority of motors.

### 6.4.1 The electromagnetic couple

The relation between the phase voltages and phase currents of a three phase induction motor is:

$$\mathbf{u} = \mathbf{R}\mathbf{i} + \frac{d}{dt}(\mathbf{L}\mathbf{i}) \tag{6.7}$$

where  $\mathbf{u}$  is the vector of phase voltages,  $\mathbf{i}$  the vector of phase currents,  $\mathbf{R}$  the matrix of phase resistances and  $\mathbf{L}$  the matrix of phase inductances. The components of vector  $\mathbf{u}$  are:

$$\mathbf{u}^T = [u_{sa} \quad u_{sb} \quad u_{sc} \quad u_{ra} \quad u_{rb} \quad u_{rc}] \tag{6.8a}$$

where the indices s and r refer to the stator and rotor respectively and the indices a, b and c refer to the three phases, see also Figure 6.3.

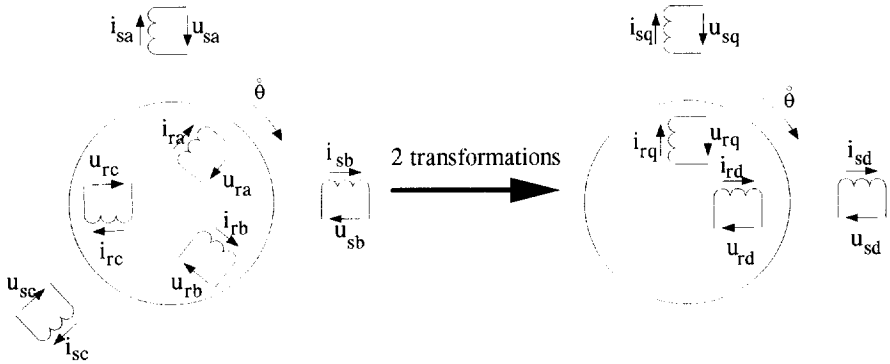


Figure 6.3: Transformation of the machine model.

If the stator windings are fed by a symmetrical three-phase supply and the rotor is star switched and short circuited then the phase voltages  $\mathbf{u}$  are:

$$\mathbf{u} = \begin{bmatrix} u_s \sqrt{2} \cos(\omega t + \phi) \\ u_s \sqrt{2} \cos(\omega t + \phi - \frac{2}{3} \pi) \\ u_s \sqrt{2} \cos(\omega t + \phi - \frac{4}{3} \pi) \\ 0 \\ 0 \\ 0 \end{bmatrix} \tag{6.8b}$$



where  $\omega$  is the supply frequency and  $u_s$  is the supply voltage. The components of  $\mathbf{i}$  are:

$$\mathbf{i}^T = [i_{sa} \quad i_{sb} \quad i_{sc} \quad i_{ra} \quad i_{rb} \quad i_{rc}] \quad (6.9)$$

The components of the matrix of phase resistances  $\mathbf{R}$  are:

$$\mathbf{R} = \begin{bmatrix} R_s & 0 & 0 & 0 & 0 & 0 \\ 0 & R_s & 0 & 0 & 0 & 0 \\ 0 & 0 & R_s & 0 & 0 & 0 \\ 0 & 0 & 0 & R_r & 0 & 0 \\ 0 & 0 & 0 & 0 & R_r & 0 \\ 0 & 0 & 0 & 0 & 0 & R_r \end{bmatrix} = \begin{bmatrix} \mathbf{R}_s & \mathbf{0} \\ \mathbf{0} & \mathbf{R}_r \end{bmatrix} \quad (6.10)$$

and the components of  $\mathbf{L}$  are:

$$\mathbf{L} = \begin{bmatrix} L_s & M_s & M_s & M_a & M_b & M_c \\ M_s & L_s & M_s & M_c & M_a & M_b \\ M_s & M_s & L_s & M_b & M_c & M_a \\ M_a & M_c & M_b & L_r & M_r & M_r \\ M_b & M_a & M_c & M_r & L_r & M_r \\ M_c & M_b & M_a & M_r & M_r & L_r \end{bmatrix} = \begin{bmatrix} \mathbf{L}_{ss} & \mathbf{L}_{sr} \\ \mathbf{L}_{rs} & \mathbf{L}_{rr} \end{bmatrix} \quad (6.11)$$

where  $L_s$  and  $L_r$  are the stator and the rotor inductances,  $M_s$  and  $M_r$  the mutual inductances between two phases of the stator and the rotor respectively, and

$$\begin{aligned} M_a &= M_{sr} \cos(p\theta) \\ M_b &= M_{sr} \cos\left(p\theta + \frac{2\pi}{3}\right) \\ M_c &= M_{sr} \cos\left(p\theta + \frac{4\pi}{3}\right) \end{aligned} \quad (6.12)$$

where  $M_{sr}$  is the maximum value of the mutual phase inductance in case the rotor coil and the stator coil are in opposite position,  $p$  is the number of pole pairs of the motor and  $\theta$  the rotor angle. The phase voltages can not be determined from the system of six equations (6.7) since this system contains seven unknowns: the six components of

the vector of phase currents and the rotor angle. The required seventh equation is the equation of motion of the motor:

$$T_e - T_l = J \frac{d^2\theta}{dt^2} + d_m \frac{d\theta}{dt} \quad (6.13)$$

where  $J$  is the equivalent moment of inertia of the rotating components of the drive,  $T_e$  the electromagnetic torque,  $T_l$  the external load torque and  $d_m$  the motor damping coefficient. The electromagnetic torque is equal to:

$$T_e = \frac{1}{2} \mathbf{i}^T \frac{d\mathbf{L}}{d\theta} \mathbf{i} \quad (6.14)$$

To simplify the system of equations (6.7), an orthogonal transformation of the phase voltages and phase currents may be performed, see also [White and Woodson, 1959], [Boldea and Nasar, 1986], [Deleroi, 1989a] and [Smith, 1990]. If a new vector of phase voltages  $\hat{\mathbf{u}}$  is introduced which is defined by:

$$\mathbf{u} = \mathbf{A}\hat{\mathbf{u}}; \hat{\mathbf{u}}^T = \begin{bmatrix} u_{s\alpha} & u_{s\beta} & u_{r\alpha} & u_{r\beta} \end{bmatrix} \quad (6.15)$$

and also a new vector of phase currents  $\hat{\mathbf{i}}$  which is defined by:

$$\mathbf{i} = \mathbf{A}\hat{\mathbf{i}}; \hat{\mathbf{i}}^T = \begin{bmatrix} i_{s\alpha} & i_{s\beta} & i_{r\alpha} & i_{r\beta} \end{bmatrix} \quad (6.16)$$

where:

$$\mathbf{A} = \sqrt{\frac{2}{3}} \begin{bmatrix} \frac{1}{2}\sqrt{2} & 1 & 0 & 0 & 0 & 0 \\ \frac{1}{2}\sqrt{2} & -\frac{1}{2} & \frac{1}{2}\sqrt{3} & 0 & 0 & 0 \\ \frac{1}{2}\sqrt{2} & -\frac{1}{2} & -\frac{1}{2}\sqrt{3} & 0 & 0 & 0 \\ 0 & 0 & 0 & \frac{1}{2}\sqrt{2} & 1 & 0 \\ 0 & 0 & 0 & \frac{1}{2}\sqrt{2} & -\frac{1}{2} & \frac{1}{2}\sqrt{3} \\ 0 & 0 & 0 & \frac{1}{2}\sqrt{2} & -\frac{1}{2} & -\frac{1}{2}\sqrt{3} \end{bmatrix} \quad (6.17)$$

then, after substitution of equation (6.15) and (6.16) in (6.7), the following system of equations can be obtained:

$$\hat{\mathbf{u}} = \hat{\mathbf{R}}\hat{\mathbf{i}} + \frac{d}{dt}(\hat{\mathbf{L}}\hat{\mathbf{i}}) = (\hat{\mathbf{R}} + \hat{\mathbf{G}})\hat{\mathbf{i}} + \hat{\mathbf{L}}\dot{\hat{\mathbf{i}}} \quad (6.18)$$

where:

$$\widehat{\mathbf{R}} = \mathbf{R} \quad (6.19)$$

$$\widehat{\mathbf{G}} = \frac{3}{2} p \mathbf{M}_{sr} \begin{bmatrix} 0 & 0 & 0 & 0 & 0 & 0 \\ & 0 & 0 & 0 & -\sin(p\theta) & -\cos(p\theta) \\ & & 0 & 0 & \cos(p\theta) & -\sin(p\theta) \\ & & & 0 & 0 & 0 \\ & & & & 0 & 0 \\ & & & & & 0 \\ & & & & & 0 \end{bmatrix} \quad (6.20)$$

(sym)

and

$$\widehat{\mathbf{L}} = \begin{bmatrix} L_s + 2M_s & 0 & 0 & 0 & 0 & 0 \\ & L_s - M_s & 0 & 0 & \frac{3}{2} M_{sr} \cos(p\theta) & -\frac{3}{2} M_{sr} \sin(p\theta) \\ & & L_s - M_s & 0 & \frac{3}{2} M_{sr} \sin(p\theta) & \frac{3}{2} M_{sr} \cos(p\theta) \\ & & & L_r + 2M_r & 0 & 0 \\ & & & & L_r - M_r & 0 \\ & & & & & L_r - M_r \end{bmatrix} \quad (6.21)$$

(sym)

Substitution of the equations (6.16) and (6.20) in equation (6.14) shows that the electromagnetic couple after transformation is equal to:

$$T_e = \frac{1}{2} \widehat{\mathbf{i}}^T \widehat{\mathbf{G}} \widehat{\mathbf{i}} \quad (6.22)$$

The phase voltages  $\widehat{\mathbf{u}}$  are:

$$\widehat{\mathbf{u}} = \begin{bmatrix} 0 \\ u_s \sqrt{3} \cos(\omega t + \phi) \\ u_s \sqrt{3} \sin(\omega t + \phi) \\ 0 \\ 0 \\ 0 \end{bmatrix} \quad (6.23)$$

From the equations (6.18) and (6.22) it can be learned that the zero sequence variables  $i_{s0}$  and  $i_{r0}$  do neither determine the  $\alpha$  and  $\beta$  components of the voltages nor the electromagnetic torque. Therefore, they are suppressed in what follows.

To further simplify the system of equations (6.18), a second orthogonal transformation is performed such that the resulting equations have matrices independent of  $\theta$ . New vectors of phase voltages  $\hat{\mathbf{u}}$  and phase currents  $\hat{\mathbf{i}}$  are introduced, see also Figure 6.3, which are defined by:

$$\hat{\mathbf{u}} = \mathbf{B}\hat{\mathbf{u}} ; \hat{\mathbf{u}}^T = [u_{sd} \quad u_{sq} \quad u_{rd} \quad u_{rq}] \quad (6.24)$$

and

$$\hat{\mathbf{i}} = \mathbf{B}\hat{\mathbf{i}} ; \hat{\mathbf{i}}^T = [i_{sd} \quad i_{sq} \quad i_{rd} \quad i_{rq}] \quad (6.25)$$

where the transformation matrix  $\mathbf{B}$  is equal to:

$$\mathbf{B} = \begin{bmatrix} \cos(p\theta_s) & \sin(p\theta_s) & 0 & 0 \\ -\sin(p\theta_s) & \cos(p\theta_s) & 0 & 0 \\ 0 & 0 & \cos(p\theta_r) & \sin(p\theta_r) \\ 0 & 0 & -\sin(p\theta_r) & \cos(p\theta_r) \end{bmatrix} \quad (6.26)$$

where the angles  $\theta_s$  and  $\theta_r$  are not determined yet. Substitution of the equations (6.24) and (6.25) in (6.18) yields the following system of equations:

$$\hat{\mathbf{u}} = (\hat{\mathbf{R}} + \hat{\theta}\hat{\mathbf{G}})\hat{\mathbf{i}} + \hat{\mathbf{L}}\dot{\hat{\mathbf{i}}} \quad (6.27)$$

where:

$$\hat{\mathbf{R}} = \begin{bmatrix} R_s & 0 & 0 & 0 \\ 0 & R_s & 0 & 0 \\ 0 & 0 & R_r & 0 \\ 0 & 0 & 0 & R_r \end{bmatrix} \quad (6.28)$$

$$\dot{\theta} \hat{\mathbf{G}} = \begin{bmatrix} p \frac{d\theta_s}{dt} \begin{bmatrix} 0 & \hat{L}_s \\ -\hat{L}_s & 0 \end{bmatrix} & p \frac{d(\theta - \theta_r)}{dt} \begin{bmatrix} -\hat{M}_s & -\hat{M}_c \\ \hat{M}_c & -\hat{M}_s \end{bmatrix} \\ p \frac{d(\theta + \theta_s)}{dt} \begin{bmatrix} -\hat{M}_s & \hat{M}_c \\ -\hat{M}_c & -\hat{M}_s \end{bmatrix} & p \frac{d\theta_r}{dt} \begin{bmatrix} 0 & \hat{L}_r \\ -\hat{L}_r & 0 \end{bmatrix} \end{bmatrix} \quad (6.29)$$

and

$$\hat{\mathbf{L}} = \begin{bmatrix} \hat{L}_s & 0 & \hat{M}_c & -\hat{M}_s \\ 0 & \hat{L}_s & \hat{M}_s & \hat{M}_c \\ \hat{M}_c & \hat{M}_s & \hat{L}_r & 0 \\ -\hat{M}_s & \hat{M}_c & 0 & \hat{L}_r \end{bmatrix} \quad (6.30)$$

The constants  $\hat{L}_s$ ,  $\hat{L}_r$ ,  $\hat{M}_s$ , and  $\hat{M}_c$  are equal to:

$$\begin{aligned} \hat{L}_s &= L_s - M_s; \quad \hat{L}_r = L_r - M_r \\ \hat{M}_s &= \hat{M} \sin p(\theta_s - \theta_r + \theta); \quad \hat{M}_c = \hat{M} \cos p(\theta_s - \theta_r + \theta) \end{aligned} \quad (6.31a)$$

where

$$\hat{M} = \frac{3}{2} M_{sr} \quad (6.31b)$$

The simplest form of the system of equations (6.27) is obtained when:

$$\theta_s - \theta_r + \theta = 0 \quad (6.32)$$

For a short-circuited rotor, the phase voltages  $\hat{\mathbf{u}}$  are:

$$\hat{\mathbf{u}} = \begin{bmatrix} \sqrt{3} u_s \cos(\omega t + \phi + p\theta_s) \\ \sqrt{3} u_s \sin(\omega t + \phi + p\theta_s) \\ 0 \\ 0 \end{bmatrix} \quad (6.33)$$

The simplest form of the phase voltages is obtained by choosing  $\theta_s$  such that:

$$\omega t + \phi + p\theta_s = 0 \quad (6.34)$$

In that case the phase voltages (6.33) reduce to direct phase voltages:

$$\hat{\mathbf{u}}^T = [u_s \sqrt{3} \quad 0 \quad 0 \quad 0] \quad (6.35)$$

With equation (6.32) the matrix  $\hat{\mathbf{G}}$  can be rewritten to:

$$\hat{\theta} \hat{\mathbf{G}} = \begin{bmatrix} \omega \hat{L}_s \begin{bmatrix} 0 & -1 \\ 1 & 0 \end{bmatrix} & \omega \hat{M} \begin{bmatrix} 0 & -1 \\ 1 & 0 \end{bmatrix} \\ \left( \omega - p \frac{d\theta}{dt} \right) \hat{M} \begin{bmatrix} 0 & -1 \\ 1 & 0 \end{bmatrix} & \left( \omega - p \frac{d\theta}{dt} \right) \hat{L}_r \begin{bmatrix} 0 & -1 \\ 1 & 0 \end{bmatrix} \end{bmatrix} \quad (6.36)$$

where

$$\omega - p\dot{\theta} = s\omega \quad (6.37)$$

which defines the slip  $s$ . The matrix  $\hat{\mathbf{G}}$  can also be written in terms of the slip. Substitution of the equations (6.25) and (6.26) in equation (6.22) shows that the electromagnetic couple after transformation is equal to:

$$T_e = \frac{1}{2} \hat{\mathbf{i}}^T (\mathbf{B}^T \hat{\mathbf{G}} \mathbf{B}) \hat{\mathbf{i}} = p \hat{M} (i_{sq} i_{rd} - i_{sd} i_{rq}) \quad (6.38)$$

Figure (6.3) schematically shows the transformations.

The different machine parameters can be given in the per unit form. The real motor parameters are obtained from the per unit values by multiplying them with the corresponding nominal impedances. The nominal phase impedance of the stator parameters  $Z_{ns}$  and the rotor parameters  $Z_{nr}$  are defined as follows:

$$Z_{ns} = \frac{U_{ns}}{I_{ns}}, \quad Z_{nr} = \frac{U_{nr}}{I_{nr}} = c_{sr}^2 Z_{ns} \quad (6.39)$$

where  $U_{ns}$  and  $U_{nr}$  are the amplitudes of the nominal stator and rotor supply phase voltages respectively and  $I_{ns}$  and  $I_{nr}$  the amplitudes of respectively the nominal stator and rotor phase current of a specific motor (catalogue values). With the per unit values, denoted by non-capitals, the values of real motor parameters can be calculated. For example the rotor and stator resistances can be obtained from their per unit values by:

$$R_s = Z_{ns} r_s = Z_n r_s ; R_r = Z_n (c_{sr}^2 r_r) = Z_n r_r^* \quad (6.40)$$

In most catalogues the per unit values of the rotor parameters include the transformation factor  $c_{sr}^2$ . In that case the nominal impedance of the stator is used to calculate both the stator and the rotor parameters. The per unit values of different motor parameters can be found in [Deleroi, 1989b].

### 6.4.2 Induction motor parameters

When selecting an induction motor from a catalogue, the following data are given or can be determined from the given data:

- $P_n$  the nominal power [kW]
- $n_n$  the nominal number of revolutions per minute [rpm] ;  $\dot{\theta} = \pi/30 n_n$  [ $s^{-1}$ ].
- $n_s$  the synchronous number of revolutions [rpm] ;  $\omega = \pi/30 p n_s$  [ $s^{-1}$ ].
- $U_n$  the nominal supply phase voltage [V]
- $I_n$  the nominal supply phase current [A]
- $f_n$  the nominal frequency of the (supply) alternating current (normally 50) [Hz]
- $\eta$  the efficiency [-]
- $p$  number of pole pairs

In **TUBBELT** the real motor parameters are determined with use of these catalogue data which should be provided by the user. The procedure to determine the real motor parameters is as follows. The (nominal) motor slip is equal to:

$$s = \frac{n_s - n_n}{n_s} = 1 - \frac{p\dot{\theta}}{\omega} \quad (6.41)$$

This slip approximates the per unit rotor resistance as can be noticed in practice:

$$r_r \approx s \quad (6.42)$$

The stator resistance can for example be found in the figures in [Deleroi, 1989b]. For normal induction motors used in drive systems of belt conveyors the per unit stator resistance

$$r_s \approx 0.02 \quad (6.43)$$

In practice, the efficiency of the motor without iron losses, is approximately equal to:

$$\eta = 1 - 2(r_r + r_s) \quad (6.44)$$

which can be found in the catalogue and can be used as a check. The induction coefficients of the induction motor can be approximated by

$$\frac{R_s}{\omega \hat{L}_s} \approx 0.005; \quad \frac{R_r}{\omega \hat{L}_r} \approx 0.006 \quad (6.45)$$

Finally the mutual inductance can be derived from:

$$\frac{\hat{M}}{\sqrt{\hat{L}_s \hat{L}_r}} = \sqrt{1 - \sigma} \quad (6.46)$$

where the coefficient of Blondel  $\sigma \approx 0.04$ .

### 6.4.3 Steady state torque of an induction motor

Under (electrical) steady state,  $\hat{\dot{\mathbf{i}}} = \mathbf{0}$ , and assumption (6.34), the system of equations (6.27) reduces to:

$$\hat{\mathbf{u}} = (\hat{\mathbf{R}} + \hat{\theta} \hat{\mathbf{G}}) \hat{\mathbf{i}} \quad (6.47)$$

From this system of equations and equation (6.13) the steady state drive power of an induction motor will be determined. Similar to equation (6.33) the stator phase currents are:

$$\hat{i}_{sd} = \sqrt{3} i_s \cos(\omega t + p\theta_s); \quad \hat{i}_{sq} = \sqrt{3} i_s \sin(\omega t + p\theta_s) \quad (6.48)$$

If the angle  $\theta_s$  is chosen such that  $\omega t + p\theta_s = 0$  then substitution of this angle in the equations (6.33) and (6.48) yields:

$$\hat{\mathbf{u}}^T = [\sqrt{3} u_s \cos(\phi) \quad \sqrt{3} u_s \sin(\phi) \quad 0 \quad 0] \quad (6.49)$$

and



$$\hat{i}_{sd} = \sqrt{3} i_s ; \hat{i}_{sq} = 0 \quad (6.50)$$

Substitution of the equations (6.28), (6.36), (6.49) and (6.50) in equation (6.47) leads to:

$$i_{rd} = \frac{\omega_{sr} \hat{L}_r}{R_r} i_{rq} ; i_{rq} = \frac{-\omega_{sr} \hat{M} R_r}{(\omega_{sr} \hat{L}_r)^2 + R_r^2} i_{sd} \quad (6.51)$$

where

$$\omega_{sr} = s\omega \quad (6.52)$$

The first and the second equation of (6.47) can be written as follows:

$$\begin{aligned} u_{sd} &= \sqrt{3} u_s \cos(\phi) = R_s i_{sd} - \omega \hat{M} i_{rq} \\ u_{sq} &= \sqrt{3} u_s \sin(\phi) = \omega \hat{L}_s i_{sd} + \omega \hat{M} i_{rd} \end{aligned} \quad (6.53)$$

and combining the equations (6.51) and (6.53) yields:

$$u_s^2 = i_s^2 \left[ \left( R_s + \frac{\omega \omega_{sr} \hat{M}^2 R_r}{(\omega_{sr} \hat{L}_r)^2 + R_r^2} \right)^2 + \omega^2 \left( \hat{L}_s - \frac{\omega_{sr}^2 \hat{M}^2 \hat{L}_r}{(\omega_{sr} \hat{L}_r)^2 + R_r^2} \right)^2 \right] \quad (6.54)$$

The electromagnetic torque can be obtained by combining the equations (6.38) and (6.51):

$$T_c = -p \hat{M} i_{sd} i_{rq} = 3 p \hat{M} i_s^2 \frac{\omega_{sr} \hat{M} R_r}{(\omega_{sr} \hat{L}_r)^2 + R_r^2} \quad (6.55)$$

Substituting  $i_s^2$  from equation (6.54) in terms of  $u_s^2$  yields the expression for the torque when the machine is voltage-excited, whereas equation (6.55) corresponds to a current-excited machine.

Since electric-magnetic transient phenomena in the induction motor vanish within about two periods of the supply frequency, the steady-state equation of the torque can be used in the equations of motion of a belt conveyor system. Therefore equation (6.55) is used in **TUDBELT** to calculate the torque of an induction motor.

### 6.4.4 Simulation of a start of an induction motor

TUDBELT has been used to determine the dynamic behaviour of a 200 kW induction motor with the following catalogue (phase) parameters:

$$U_n = 220 \text{ V} ; I_n = 340 \text{ A} ; f_n = 50 \text{ Hz} ; p = 2 ; J = 5.8 \text{ kgm}^2 ; d_m = 0 \text{ Nms}$$

$$\eta = 0.95 ; n_n = 1489 \text{ rpm} ; n_s = \frac{60f_n}{p} = 1500 \text{ rpm}$$

and loaded by an external load  $T_l=1000 \text{ N.m}$ . Figure 6.4 shows the torque-speed characteristics of the motor fed by different supply frequencies  $f=\omega/2\pi$ .

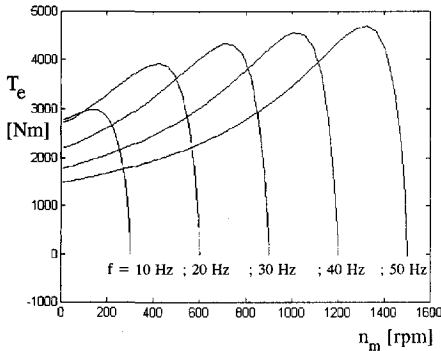


Figure 6.4: Torque-speed characteristics of an induction motor for different supply frequencies.

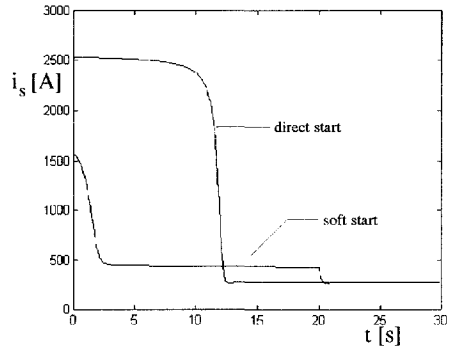


Figure 6.5: Supply current versus time.

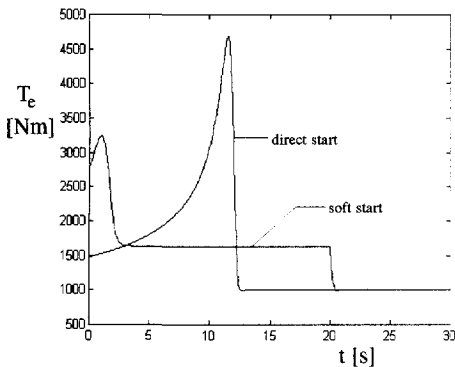


Figure 6.6: Motor torque versus time.

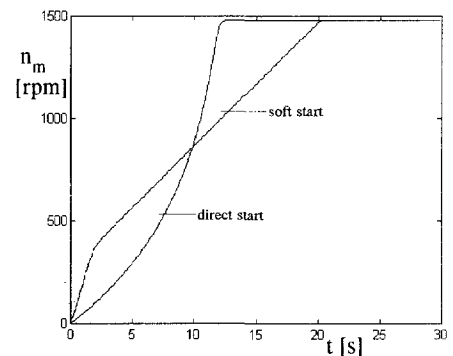


Figure 6.7: Number of revolutions of the motor shaft versus time.

Two start-up-procedures have been simulated. During the first start-up the motor is switched on directly (direct start) with a supply frequency of 50 Hz. During the second start-up the motor is switched-on at 10 Hz while the supply frequency is increased linearly to 50 Hz in 20 s (frequency controlled or soft start). During the interval the ratio voltage/frequency is kept constant by application of an SPC. The Figures 6.5-6.7 show the source current, the motor torque and the number of revolutions pro minute of the motor shaft during the start-ups. These figures clearly show three advantages of an SPC-regulated start-procedure:

- lower source current during soft start, see Figure 6.5.
- lower peak torque during soft-start, see Figure 6.6
- smaller energy losses

## 6.5 Fluid coupling

A fluid coupling is a hydrodynamic transmission comprising a motor driven centrifugal pump (the impeller) supplying liquid to a load connected turbine (the runner). The impeller, connected to the motor shaft, and the runner, connected to the reducer shaft, can be both similar in construction, each consisting of a series of blades or vanes mounted into convex shaped housings. When the elements are put together, a hydraulic circuit in the form of a vortex can be established. In action, rotation of the impeller creates centrifugal forces and these result in the liquid flowing outwards from the impeller into the runner, whose shape directs the liquid back into the impeller.

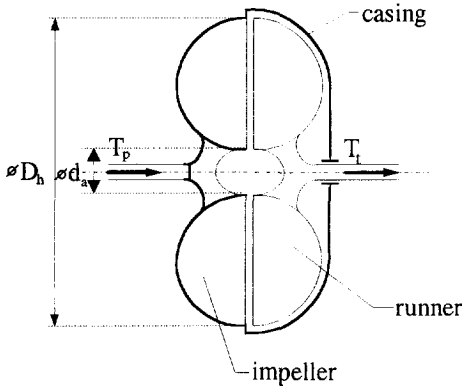
To change the power transmitted, a change of flowrate is necessary. If the runner is free to rotate, then both input and output speed are equal. If a load is applied to the runner, a slight speed difference between impeller and runner indicates the development of torque. The torque developed by the coupling varies with the degree of speed difference (the slip). The slip is defined by:

$$s = \frac{n_p - n_t}{n_p} \quad (6.56)$$

where  $n_p$  is the number of revolutions of the impeller or pump and  $n_t$  the number of revolutions of the runner or turbine. Since input and output torques,  $T_p$  and  $T_t$ , are equal it follows that the fluid coupling efficiency  $\eta$  is equal to:

$$\eta = \frac{P_t}{P_p} = \frac{T_t n_t}{T_p n_p} = \frac{n_t}{n_p} = 1 - s \quad (6.57)$$

where  $P_t$  and  $P_p$  are the turbine and pump power respectively. While the efficiency is high at the design point, sustained operation at other conditions can lead to overheating unless adequate cooling is provided.



The torque that can be transmitted from the pump to the turbine can be approximated by [Middelmann, 1992]:

$$T_{hc} = \lambda \rho_f D_h^5 \dot{\phi}_p^2 \quad (6.58)$$

where  $\rho_f$  is the fluid density,  $\dot{\phi}_p$  the angular speed of the pump and  $\lambda$  a constant which depends on the slip and on specific fluid and coupling parameters. This equation is used in **TUDBELT**. The factor  $\lambda$  can be approximated by:

**Figure 6.8:** Basic sizes of a hydrodynamic coupling.  $\lambda(s) = \lambda^* s^n \quad (6.59)$

assuming a constant filling degree, see also [Höller, 1996]. According to Thoma (1964) the power  $n$  is 1 and  $\lambda^* \approx 75 \cdot 10^{-3}$  for couplings containing a low viscosity fluid, a low number of blades and a small diameter-ratio  $d_a/D_b$ , also see Figure 6.8, and  $\lambda^* \approx 50 \cdot 10^{-3}$  for couplings containing a high viscosity fluid, a high number of blades and a large diameter-ratio. However,  $n=1/2$  results in a torque/slip characteristic that is closer to characteristics found in experiments performed by Middelmann (1992). More detailed torque equations based on experiments are given by Timm (1958) and Middelmann (1992).

It is clear that for a given (standard) fluid coupling the relationship between moment (or power) and speed is fixed, and in this sense the fluid coupling does not need a control system. However, the drive system requires the addition of a gearbox for torque multiplication and angular speed reduction. Thus the fluid coupling acts as an automatic clutch between gearbox and motor, and a control system can be required to match the motor output to the load (that is the gearbox output). Since the fluid coupling of given dimensions has its own torque-speed curve it is essential to match coupling and motor characteristics to obtain good acceleration of the load with acceptable efficiency. Especially in systems with a high inertia, like long overland belt conveyors [McCormick, 1985b], it is important that the motor can run-up under no-load/low-load conditions to prevent the motor, drive train and the belt from overloading and to limit the period of high starting currents. Two special types of

fluid couplings have been developed for this purpose: the delay-chamber fluid coupling and the drainable or pump-filled fluid coupling [Annon, 1989]. The use of a delay-chamber fluid coupling, with emptying of the delay-chamber by use of centrifugal forces, ensures that the motor will always start, regardless of the voltage ( $>0$ ) available and will transmit the maximum pull-out torque available to start an overloaded conveyor. On the average, the torque of a fluid coupling with delay chamber is limited to approximately 1.3 times full load torque. The use of a drainable fluid coupling enables a run-up under no-load condition. At motor start-up, the coupling is empty and acts like a clutch completely disengaging the motor from the conveyor. Once the motor has run-up to speed, fluid (water or oil) is fed into the coupling so that torque is transmitted. This increases the motor current which is constantly monitored. As soon as the current reaches a pre-set limit the fluid supply to the coupling is switched off and, since the fluid is continuously escaping from the coupling through the discharge nozzles, the amount of fluid in the coupling drops, reducing the torque transmission and the motor current.

A typical belt conveyor start-up procedure with use of a drainable fluid coupling is as follows. The conveyor starting is split into three phases.

1. pre-tensioning of the belt
2. acceleration of the belt conveyor to 10 % of full speed
3. acceleration of the belt conveyor to full speed

The third phase begins only when the whole conveyor is running at 10 % of full speed. As an example, for a long belt conveyor system of 10.5 km the time taken from rest to full belt speed is approximately 320 seconds [Annon, 1989].

## 6.6 Drum brake

To ensure a proper deceleration of a belt conveyor system a drum brake is added to the drive train of large conveyor systems. Especially in case of (regenerative) downhill conveyors the brakes play an important role in the reliability of the system. The brake torque  $T_{br}$  is given by:

$$T_{br} = F_{br} R_{br} \quad (6.60)$$

where  $F_{br}$  is the brake force and  $R_{br}$  is the radius of the drum brake.

Apart from the ordinary brakes, it is important to take certain safety measures for inclined conveyors. In case of drive failure of an inclined belt conveyor, a reversal

of the conveyor, caused by the weight of the conveyed material, must be prevented. This is the function of backstops. Depending on the size of the belt conveyor, the backstop units are located in various positions. In small and medium size conveyor systems, it is common practice to place backstops directly at the motor or the reducer. In large belt conveyor systems, backstops are often placed directly on the drive pulley shaft between the bearings and the output shaft of the gear box. In case of a multiple drive system, each drive pulley input shaft is fitted with a backstop. Because of the high cost of these kind of (low-speed) backstops, they are nowadays replaced by (high-speed) backstops installed on the input or intermediate gear shaft.

During braking the torque in the backstop can be 4 to 10 times the normal input or motor torque. The wind-up characteristic of a backstop, required to find out whether or not the backstop is strong enough to resist this brake torque and to determine the influence of the backstop wind-up characteristics on the dynamic behaviour of the belt conveyor, is given by [Timtner, 1994]:

$$T_{bs} = C_1 \varphi_{bs} + C_2 \varphi_{bs}^n \quad (6.61)$$

where  $T_{bs}$  is the wind-up torque in the backstop,  $C_1$ ,  $C_2$  and  $n$  are backstop parameters and  $\varphi_{bs}$  is the wind-up angle. The constants of a typical wind-up characteristic of a backstop with load-sharing and clearance are [Timtner, 1994]:

$$C_1 = 7.31 \cdot 10^5 \text{ [Nm]}, C_2 = 6.92 \cdot 10^{10} \text{ [Nm]}, n = 5.$$

Both the normal drum brake and the backstop equations are included in **TUDBELT**.

## 6.7 Reduction box

Since the angular speed of the induction motor shaft is much higher than required for the drive pulley shaft, a reduction box is applied to obtain the required speed at the drive pulley. If the losses in the reduction box are neglected then the input power  $P_{rb,in}$  and output power  $P_{rb,out}$  are equal. With the required reduction factor  $i$ , the input and output torque,  $T_{rb,in}$  and  $T_{rb,out}$ , and the radii of the two gear wheels,  $R_{rb1}$  and  $R_{rb2}$ , can be obtained from:

$$\left. \begin{aligned} P_{rb} = T_{rb,in} \dot{\varphi}_{rb,in} = T_{rb,out} \dot{\varphi}_{rb,out} \\ \dot{\varphi}_{rb,in} = i \dot{\varphi}_{rb,out} \end{aligned} \right\} \Rightarrow T_{rb,out} = i T_{rb,in} ; R_{rb1} = \frac{1}{i} R_{rb2}, i \geq 1 \quad (6.62)$$

In **TUDBELT** a model of the reduction box is included which also accounts for the reduced moments of inertia of the gear wheels. The effect of clearance between the teeth of the gear wheels has been neglected.

## 6.8 Disc pack

Apart from the fluid coupling, several soft start units exist using wet (oil) disc packs to transmit the drive power from the induction motor to the drive pulley [McCormick, 1985b]. These units offer two advantages. Firstly, they lock up at running speed and therefore they do not have slip associated with fluid couplings. Secondly, they enable the motor to reach full speed before application of the load. Some units are either mounted directly on the motor shaft or coupled to the motor shaft and then attached to

a separate reducer by means of a coupling. Other units are build directly into the reducer.

A wet disc pack unit, which controls the output torque, is a torque controlled system instead of the usually applied velocity controlled system, see Figure 6.9. Some units are open loop control systems to control the torque of the drive system by the amount of fluid in the unit or by changing the orifices which control the rate of flow between a prefill chamber and a piston chamber. If, in case of a torque controlled system with constant acceleration, a load change occurs, the acceleration remains constant. Due to the temporary disturbance of the acceleration, however, the length of time to reach full running speed increases. Conversely, with a velocity controlled system, torque has to be increased in order to keep the time to reach full running speed constant, see Figure 6.9.

Two types of wet disc pack units exist that differ in principle. Both types have plates that interact to transmit the drive power. The gap between the plates is closed by increasing the pressure of the fluid through a hydraulic actuator. The plates of units of the first type are mounted directly on the incoming and outgoing shafts, units of the second type use a reaction clutch grounded system utilising a planetary gear

Figure 6.9 consists of four line graphs arranged in a 2x2 grid. The top row shows 'belt speed' vs 'time' for 'torque controlled system' and 'velocity controlled system'. The bottom row shows 'full load torque' vs 'time' for the same two systems. In the torque controlled system graphs, belt speed shows a dip during a load change but continues to rise linearly, while full load torque shows a step increase. In the velocity controlled system graphs, belt speed remains constant during a load change, but the acceleration phase is longer, and full load torque shows a sharp spike during the load change.

**Figure 6.9:** Load change during acceleration of a fully closed loop system.

output. This latter unit, the controlled start transmission (CST), has been applied successfully in many large belt conveyor systems [Spear, 1986], [Singh, 1994].

The CST internals consist of three distinct parts: an input section, an output section and a disk pack, see Figure 6.10 [Singh, 1994]. The other major parts of the CST are a cooling system, a hydraulic actuator and electronic controls. The input section consists of either a one- or two-stage helical

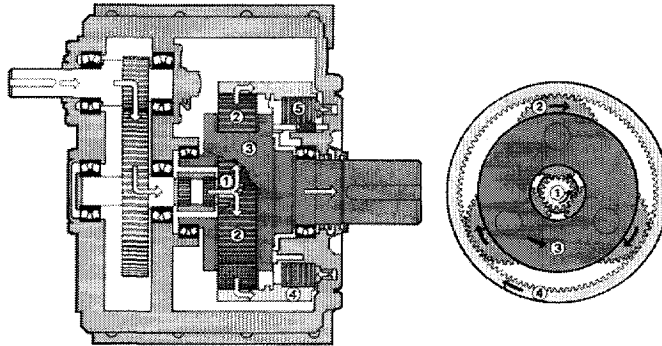


Figure 6.10: The CST [Singh, 1994].

reduction gear for parallel units, or a spiral bevel stage followed by a helical stage for right angle units. The output section consists of a sun gear (1), planet gears (2) which are connected to a planet carrier (3), and a ring gear (4). The disc pack, see Figure 6.11, consists of two sets of meshed plates. The stationary plates are connected to the housing, and the rotating plates are connected to the ring gear. When no hydraulic pressure is applied to the disc pack, the rotating plates (and ring gear) are free to rotate. As hydraulic pressure is applied to the disc pack, the motion

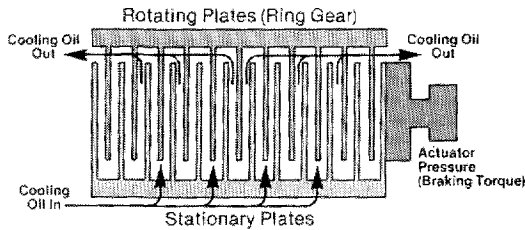


Figure 6.11: The disc pack [Singh, 1994].

of rotating plates (and ring gear) is retarded. Finally, if there is sufficient pressure, the rotating plates (and ring gear) will lock up with the stationary plates. The motor rotation is transmitted through the input section to the sun gear (1) in the output section. The sun gear rotates the three planet gears (2). When the ring gear (4) is free to rotate, i.e. when there is no hydraulic pressure in the disc pack, the planet gears



rotate the free-floating ring gear. The planet carrier (3) does not turn. The output shaft, which is part of the planet carrier, remains stationary. As the pressure is applied to the disc pack, the ring gear motion is impeded, and the planet gears start revolving on the ring gear to compensate for this impeded motion. As a result, the planet carrier and the output shaft start turning. By controlling the hydraulic pressure in the disc pack, the transmission of motion and torque from the motor to the CST output shaft can be precisely controlled.

In **TUDBELT** the influence of a CST on the dynamics of a belt conveyor system can be simulated through prescription of the reducer input torque.

## 6.9 References

- Annon, L. (1989), "Modern drive technology in mines and quarries: conveyor drives today", *Mine & Quarry* 18, nr. 4 pp. 27-28.
- Boldea, I. and Nasar, S.A. (1986), *Electrical Machine Dynamics*, Macmillian Publishing Company, New York.
- McCormick, W.J. (1985a), "Controlled starting of belt conveyors, part I", *Pit & Quarry* 77, nr. 8, pp. 33-37.
- McCormick, W.J. (1985b), "Controlled starting of belt conveyors, part II", *Pit & Quarry* 77, nr. 9, pp. 34-36.
- Deleroi, W. (1989a), *Elektrische Machines IB*, Lecture book, Delft University of Technology, Delft.
- Deleroi, W. (1989b), *Elektrische Machines II*, Lecture book, Delft University of Technology, Delft, 1989.
- Funke, H. (1973), *Zum dynamischen Verhalten von Förderbandanlagen beim Anfahren und Stillsetzen unter Berücksichtigung der Bewegungswiderstände*, Doctorate thesis, Universität Hannover.
- Harrison, A. (1983), "Criteria for minimizing transient stress in conveyor belts", *Proceedings of the International Material Handling Conference Johannesburg South Africa*, May 1983.
- Harrison, A. and Roberts, A.W. (1984), "Technical requirements for operating conveyor belts at high speed", *Bulk Solids Handling* 4, pp. 99-104.
- Harrison, A. (1985), "Modern concepts in belt conveyor engineering: propagation of dynamic stress in high modulus belts", *Proceedings of the International Material Handling Conference Johannesburg South Africa*, September 1985.
- Höller, H. (1996), "Hydrodynamische Kupplungen im Antrieb von Gurtförderern-Teil I", *Fördern und Heben* 46, pp. 396-399.
- Krause, P.C. and Lipo, T.A. (1969), "Analysis and Simplified Representations of a Rectifier-Inverter Induction Motor Drive", *IEEE Transaction of Power Apparatus and Systems* 88, pp. 588-596.
- Lipo, T.A. and Krause, P.C. (1969), "Stability Analysis of a Rectifier-Inverter Induction Motor Drive", *IEEE Transaction of Power Apparatus and Systems* 88, pp. 55-66.

- Lipo, T.A. and Krause, P.C. (1969), "Stability Analysis of a Symmetrical Induction Machine", *IEEE Transaction of Power Apparatus and Systems* **88**, pp. 1710-1717.
- Lipo, T.A., Krause, P.C. and Jordan, H.E. (1969), "Harmonic Torque and Speed Pulsations in a Rectifier-Inverter Induction Motor Drive", *IEEE Transaction of Power Apparatus and Systems* **88**, pp. 579-587.
- Middelmann, V. (1992), *Analyse des Systemverhaltens hydrodynamischer Kupplungen bei Variation der Kreislaufgeometrie*, Ph.D. Dissertation, Universität Bochum.
- Nordell, L.K. and Ciozda, Z.P. (1984), "Transient belt stresses during starting and stopping: elastic response simulated by finite element methods", *Bulk Solids Handling* **4**, pp. 93-98.
- Nordell, L.K. (1985), "The theory and practice of belt conveyors dynamics analysis", *Proceedings of the International Material Handling Conference Johannesburg South Africa*.
- Nordell, L.K. (1989), "Improved high capacity conveyor designs", *Proceedings of the American Mining Congress, San Francisco, USA*.
- Nordell, L.K. (1991), "The channar 20 km overland - a flagship of modern belt conveyor technology", *Bulk Solids Handling* **11**, pp. 781-792.
- Nordell, L.K. (1993), "Steelcord belt and splice construction: modernising their specifications, improving their economics", *Bulk Solids Handling* **13**, pp. 685-693.
- Nordell, L.K. (1995), "Steel cord splice design and fabrication techniques", *Proceedings of the SMME Annual Meeting Reno, Nevada, USA*.
- Schulz, G. (1995), "Comparison of drives for long belt conveyors", *Bulk Solids Handling* **15**, pp. 247-251.
- Singh, M.P. (1994), "The role of drive system technology in maximizing the performance and economics of long belt conveyors", *Bulk Solids Handling* **14**, pp. 695-702.
- Smith, J.R. (1990), *Response Analysis of A.C. Electrical Machines: Computer Models and Simulation*, Research Studies Press Ltd, Taunton, England.
- Spear, D. (1986), "Smart drives power large conveyors", *Power Transmission Design* **28**, nr. 2 pp. 17-19.
- Thoma, J.K. (1964), *Hydrostatic power transmission*, Trade and Technical Press, Morden, Surrey, England.
- Timm, K. (1958), *Untersuchungen an Föttinger Kupplungen*, Ph.D. Dissertation, Technischen Hochschule Hannover.
- Timtner, K. (1994), "Peak torque calculations for backstops in conveyors", *Bulk Solids Handling* **14**, pp. 711-721.
- White, D.C. and Woodson, H.H. (1959), *Electromechanical Energy Conversion*, John Wiley & Sons, New York.

## Chapter 7

# Discrete modelling of belt systems

---

Since powerful computer systems are available, discrete models and techniques based on the finite element method (FEM) and the finite difference method (FDM) are applied in all branches of engineering. In the field of belt systems, discrete models are used in two specific classes of applications. Firstly to analyse the global dynamic response of the belt during starting and stopping. Secondly, they are used to model the belt splice to determine the local stress distribution due to the global response of the belt and the corresponding safety factor with respect to failure, see for example [Hager and Von der Wroge, 1991], [Nordell, Qiu and Sethi, 1991] and [Shi, 1993a-c]. The discrete analysis focusing on the dynamics of belt conveyor systems will be discussed in this chapter. In the first section the state of the art in the development of discrete models of belt conveyor systems will be described. The second section describes the finite elements which can be used to model the belt and other components of the belt conveyor system.

### 7.1 Introduction

Due to the development of the rubber technology, conveyor belts improved significantly after the Second World War and the application of belt conveyor systems for the transportation of bulk materials became widespread. Besides the application for in-plant transportation of bulk materials, the improved belt types enabled application in long overland systems as well. Therefore the capacity as well as the length of belt conveyor systems increased significantly.

To calculate the total power supply needed to drive a belt conveyor system, design standards like DIN 22101 are used. In these standards the belt is assumed to be inextensible. This implies that the axial forces exerted on the belt during starting and stopping can be approximated by Newtonian rigid body dynamics and the forces yield the belt stresses. With these stresses and dropping the assumption of inextensibility, the maximum extension of the belt can be calculated. This way of determining the elastic

response of the belt is called the quasi-static (design) approach. For low capacity and small belt-conveyor systems this led to an acceptable design and acceptable operational behaviour of the belt. However, the upscaling of belt conveyor systems to high capacity or long distance systems introduced operational problems including:

- excessive displacement of the weight of the gravity take-up device
- premature rupture of the belt, mostly due to failure of a splice
- destruction of the pulleys and major damage of the idlers
- lifting of the belt off the idlers which can result in spillage of bulk material
- damage and malfunctioning of drive systems

To detect the cause of these operational problems, the behaviour of the belt and drive system during nonstationary operation were experimentally investigated. Relevant studies include Coeuillet (1955), Vierling and Oehmen (1958), Bahr (1960) and Vierling (1961). The first objective of the experiments was to determine the development of axial stress waves in the belt and their influence on the belt tension and the drive force. Also the delay effect, caused by the finite propagation speed of the stress waves, which appears during non-stationary operation of the belt, was of interest. Oehmen (1959) experimentally studied the start-up of a belt conveyor system in detail, accounting for the characteristics of the drive system, the tensioning system and the belt. He distinguished three phases during the start-up of a conveyor: the break-away phase, during which the belt tension is increased until the belt starts to move, the acceleration phase and the stationary phase. The results of Oehmen's study were supplemented by Vierling (1961) and confirmed by experiments of Rottky (1961), Matting and Vierling (1962), and Funke and Winterberg (1964). With the knowledge gained from these experiments the starting sequence of multiple-engine drives and the design of automatic tensioning systems, like for example a winch tensioner, could be improved, as has been described by a number of authors including Brade (1965), Zur (1966), Havelka (1967), Brade and Menning (1969) and Bierhof (1973).

Field experiments during start-up of a conveyor were not always possible and the number of start-up variations that could be tested was limited. Therefore the need for a mathematical model, which could be used to obtain detailed insight in the behaviour of the belt during nonstationary operation, increased. Because of the complexity of the equations of motion that describe the behaviour of a conveyor belt during nonstationary operation, the first mathematical models that have been implemented for this purpose were the electrical analogue models, see for example Vasilev and Tipilin (1962), Bacholdin and Rychalskij (1963), Segal (1969), Masin (1972) and Karolewski (1983&1986). However, parallel to the development of these models, also an analytical solution of the equations of motion was developed by Havelka (1963) and Sobolski (1963). They simplified the equations of motion by assuming a constant belt acceleration and neglecting the motion

resistances, the inertia effect of the rotating conveyor components and the drive characteristics. His model is comparable to that of Karbasov (1962) except that Karbasov did not assume the belt acceleration to be constant. Pankratov (1964) considered the influence of the inertia but he also neglected the motion resistances and drive characteristics. Besides the inertia, Bacholding and Leskevic (1965) also considered the mass of the bulk material on the belt and studied the influence of the loading degree on the propagation speed of the stress waves. Dumonteil (1967) included the motion resistances in his model but assumed them to be independent of the belt speed and the direction of motion. Besides that Richolm (1969&1970) accounted for speed independent motion resistances, he included a time-dependent drive force. As a result the break-away phase was neglected in the models of Dumonteil (1967) and Richolm (1969). In the study of Funke (1973) the motion resistances are velocity-dependent. He also considered the visco-elastic character of the belt material, and discretised the belt into two homogenous and continuous elements that model the carrying and the non-carrying or return part of the belt. The motion of the two parts is coupled through the motion of the pulleys. With the results obtained from this model, the insight into the behaviour of the belt during nonstationary operation increased considerably. This enabled the improvement of the design of high capacity or long distance belt conveyor systems. The application of simulation tools in the design process of belt conveyor systems is called the dynamic (design) approach. It was recognised that discretisation of the belt in more than two belt parts would increase the accuracy of the calculations. Instead of using one or two elastic elements with homogenous mass distribution, the belt should be modelled by a number of finite elements to account for the distribution of the resistances and forces exerted on the belt. However, the application of this kind of models requires advanced computational equipment that was not available at the end of the sixties, Tol (1974). Besides Funke (1973) also Rao (1973) and Harrison (1981) used computers to study the transient stresses during starting and stopping of the belt.

The first finite element model of a belt conveyor system was developed by Nordell and Ciozda (1984). Their model includes the time dependent drive force, motion resistances and visco-elastic behaviour of the belt material. Schulz (1985) included a random factor generator to represent the belt loading degree as a stationary Gaussian process to account for the stochastic character of the mass flow. Ellis and Miller (1987) used a moving finite element model to determine the development of stress waves with a steep front. Morrison (1988) illustrated the power of applying computer graphics to visualise the simulation results. Verification of the results of simulations has shown that software based on this kind of belt conveyor models are quite successful in predicting the elastic response of the belt during starting and stopping, see for example Nordell and Ciozda (1984), Surtees (1986), Funke and Könneker (1988), Harrison (1988) and Schulz (1995). Nowadays, these models are still being developed to improve the description of the motion resistances. For example, in the model of Lieberwirth (1994) the motion resistance met by the belt in a horizontal curve is included.

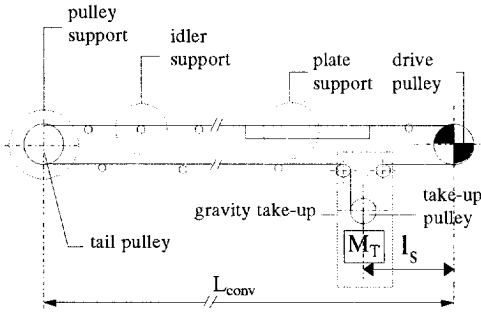
Although it is possible to include the effect of belt sag on the propagation of axial stress waves, as will be shown in Section 7.2.1.2, most finite element models as mentioned above determine only the longitudinal elastic response of the belt. Therefore they fail in the accurate determination of:

- the motion of the belt over the idlers and the pulleys
- the dynamic stresses in the belt during passage of the belt over a (driven) pulley
- the dynamic drive phenomena
- the motion resistance due to bending stiffness of the belt
- the development of stress waves with steep gradients
- the interaction between the belt sag and the propagation of longitudinal stress waves
- the influence of the belt speed on the stability of motion of the belt
- the influence of parametric resonance of the belt due to the interaction between vibrations of the take up mass and the transverse displacements of the belt
- the influence of direct excitation of the belt due to eccentricities of the idlers on transverse vibrations
- the development of transverse vibrations
- the influence of the damping caused by bulk material and by the deformation of the cross-sectional area of the belt and bulk material during passage of an idler
- the lifting of the belt off the idlers in vertical curves

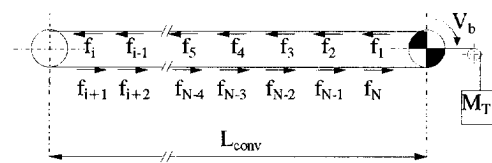
The transverse elastic response of the belt is also often the cause of breakdowns in long belt-conveyor systems and should therefore be taken into account. The transverse response of a belt can be determined with special models as proposed in [Harrison, 1984] and [Lodewijks, 1994b], but it is more convenient to extend the present finite element models with special elements which take this response into account, [Lodewijks, 1994a, 1995a-d].

## 7.2 Finite element models of belt conveyors

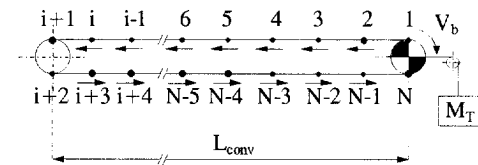
To illustrate the transition of a belt conveyor system to a finite element model, consider the typical long belt-conveyor geometry shown in Figure 7.1, [Lodewijks, 1994a&c, 1995e]. This conveyor consists of the belt, a drive pulley, a tail pulley, a vertical gravity take-up, a number of idlers and a plate support. Since the length of the belt part between the drive pulley and the take-up pulley,  $l_s$ , is normally negligible compared to the length of the total belt,  $2L_{conv}$ , these pulleys can mathematically be combined to one pulley as long as the inertias of the pulleys of the take-up system are accounted for. The mass of the gravity take-up system is  $M_T$ , see Figure 7.2. The position of the drive pulley in Figure 7.1 is fixed whereas the position of the combined drive/take-up pulley in Figure 7.2 is not fixed.



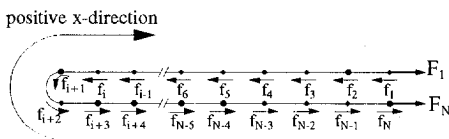
**Figure 7.1:** Typical belt-conveyor geometry indicating three support sections.



**Figure 7.2:** Combination of the take-up pulley and the drive pulley. The distribution of the motion resistance forces is shown.



**Figure 7.3:** Belt divided into finite elements.



**Figure 7.4:** Replacing the interaction of the belt and its supporting structure by forces.

If the main interest is in the longitudinal elastic response of the belt then the influence of the belt support on the longitudinal behaviour of the belt can be represented by forces that account for the motion resistance forces such as the resistance of the idlers to rotation on their bearings, the indentation rolling resistance etc. These forces vary from place to place depending on the exact local (maintenance) conditions and geometry of the belt conveyor and are therefore distributed along the length of the belt (Figure 7.2). To determine accurately the influence of these distributed forces on the motion of the belt, the belt is divided into a number of finite elements and the forces which act on a specific part of the belt are allocated to the corresponding element, see Figure 7.3. If the interest is in the longitudinal elastic response of the belt only, then the belt is not discretised on those places where it is supported by a pulley which does enforce its motion, for example the drive pulley. The belt is discretised on those places where it is supported by a pulley that does not enforce its motion for example the tail pulley. This is shown in Figure 7.4. The last step in building the model is to replace the belt's drive and tensioning system by two forces which represent the drive characteristic and the tension forces. See the forces  $F_1$  and  $F_N$  in Figure 7.4 which account for the coupling between the two nodal points 1 and N. Forces allocated to the nodal points around a pulley account for the

resistances in the bearings of the pulley and its inertia, see  $f_{i+1}$  and  $f_{i+2}$  in Figure 7.4. The maximum belt speed is about 10 m/s whereas the propagation speed of the longitudinal stress waves, as mentioned in section 3.1.4, varies from about 1,000 m/s for fabric belts to 2,500 m/s for steelcord belts. Hence the influence of the belt speed on the axial elastic response of the belt is negligible which was also mentioned in Section 4.2.3.1. This implies that all the elements and forces that account for the interaction between the belt and its supporting structure remain in their position relative to the supporting structure. The

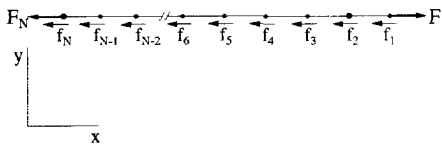


Figure 7.5: Belt laid in x-direction.

magnitude of these forces, however, may vary from time to time. This depends on the temporary local belt speed and belt load that results from the distributed bulk material load which travels through the fixed element grid with the belt speed. In Figure 7.4 the orientation of the elements is given which results in the configuration of Figure 7.5 when the belt is laid in the x-direction. The exact interpretation of the finite elements depends on which resistances and influences of the interaction between the belt and its supporting structure are taken into account and the mathematical description of the constitutive behaviour of the belt material. Depending on this interpretation, the elements can be represented by a system of masses, springs and dashpots as is shown in Figure 7.6, [Nordell and Ciozda, 1984], where such a system is given for one finite element with nodal points  $c$  and  $c+1$ . The springs  $K_1$  and  $K_2$  and dashpot  $H$  model the visco-elastic behaviour of the tensile member,  $G$  models the belt's variable longitudinal geometric stiffness produced by the vertical acting forces on the belt section between two idlers,  $C$  represents a Coulomb friction with a friction coefficient varying between the static and dynamic coefficient and  $V$  indicates the velocity dependent resistances. The belt length represented by one element lies in the range of 10 to 250 m

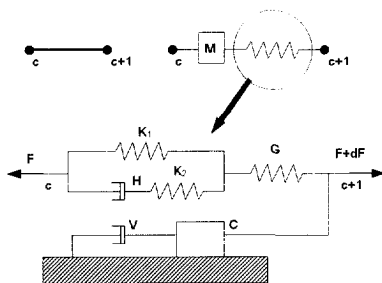


Figure 7.6: Five element composite model [Nordell and Ciozda, 1984].

depending on the total belt length and the desired accuracy. If, besides the axial elastic response, also the transverse response is of interest (total elastic response), then the belt has to be discretised at such a scale that the motion of the belt over the supports, as for example an idler or pulley, can be determined. This implies that the belt length represented by one element in this case lies in the range of 0.1 to 0.25 m. Apart from the difference in belt length, the most important difference between models used to determine only the axial elastic response and models used to determine the total elastic respon-



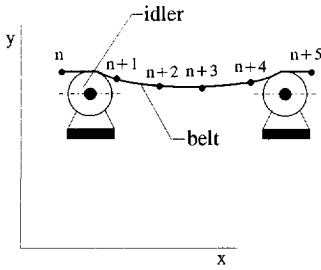


Figure 7.7: Belt supported by idlers.

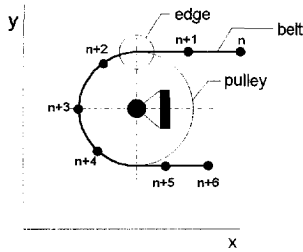


Figure 7.8: Belt supported by a pulley.

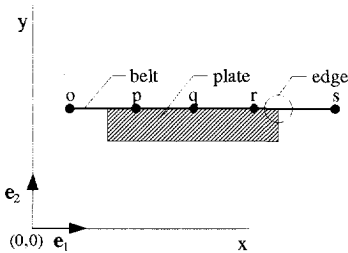


Figure 7.9: Belt supported by a plate.

se is that the position of the elements relative to the conveyor is not fixed for the latter. This is caused by the relative low axial propagation speed of transverse belt waves which is about 25 to 100 m/s, see Section 3.1.4. Compared to this speed the belt speed can not be neglected. Therefore the belt elements move relative to the conveyor as does the real belt. This also implies that the bulk solid material does not move through the element grid but is fixed to an element as long as it is not discharged from the belt (head pulley). The motion of the elements through the conveyor also affects the handling of the boundary conditions. For determination of the total elastic response of the belt, it is not sufficient just to allocate forces to the relevant nodal points of the elements which account for the interaction between the belt and a support. Also the exact position of the element on the support has to be determined to check whether this position is geometrically possible. This procedure has to be repeated every time step and is different for each type of support. Therefore three types of supports have to be distinguished, the idler support, the pulley support and the plate support, see the Figures 7.7, 7.8 and 7.9. The nodal points of elements representing a belt part supported by an idler, the nodal points  $n$ ,  $n+1$ ,  $n+4$  and  $n+5$  in Figure 7.7, are subject to constraint conditions that constrain their motion relative to the idler. The motion of nodal points  $n+2$  and  $n+3$  is not constrained. The motion of nodal points of elements representing a belt part on a pulley is described by the motion of that pulley if the belt does not slip. In case of belt slip the radius of the motion of the

nodal points to the pulley centre is fixed but the elements are free to move on the surface of the pulley. Special attention is drawn to the nodal points of pulley supported elements which are not located on a pulley, nodal point  $n+1$  and  $n+5$  of Figure 7.8. The motion of those (edge) nodal points is constrained to prevent the belt from taking geometrically impossible positions. Finally, if elements represent a belt part supported by plates or bars, for example on the loading section, then the motion of the belt supported by the plate support is constrained which normally implies that there remains only one direction of motion. Also in this case special attention should be given to the edge elements.

### 7.2.1 Belt elements

In this section the mathematical description of three finite elements is given that can be used to model the belt. In the section 7.2.2 the relevant mass matrices and constitutive relations are given.

#### 7.2.1.1 Truss

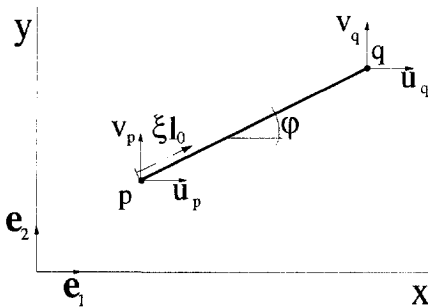


Figure 7.10: Definition of the displacements of a truss element

If only the longitudinal deformation of the belt, and not its bending, has to be taken into account then a truss element can be used to model the response of the belt, [Lodewijks, 1991]. The two-dimensional truss element shown in Figure 7.10 has four degrees of freedom. Each nodal point has two displacement components which define the component vector  $u$  :

$$u^T = [u_p \quad v_p \quad u_q \quad v_q] \quad (7.1)$$

Four vectors fix the position of the nodal points with respect to the global Cartesian coordinate system :

$$\begin{aligned} x_p &= x_p e_1 + y_p e_2 \\ u_p &= u_p e_1 + v_p e_2 \\ x_q &= x_q e_1 + y_q e_2 \\ u_q &= u_q e_1 + v_q e_2 \end{aligned} \quad (7.2)$$

The vector which connects the two nodal points of the deformed element is :

$$\mathbf{l}_{pq} = \mathbf{x}_q + \mathbf{u}_q - \mathbf{x}_p - \mathbf{u}_p \quad (7.3)$$

To describe the position of any point on the element, a linear shape function is used. The vector which fixes this position is, in the undeformed state :

$$\mathbf{x}_\xi = \mathbf{x}_p + (\mathbf{x}_q - \mathbf{x}_p)\xi \quad (7.4)$$

and in the deformed state :

$$\mathbf{x}_\xi + \mathbf{u}_\xi = \mathbf{x}_p + \mathbf{u}_p + (\mathbf{x}_q + \mathbf{u}_q - \mathbf{x}_p - \mathbf{u}_p)\xi \quad (7.5)$$

where  $\xi$  is a dimensionless co-ordinate along the axis of the element which varies from 0, in nodal point p, to 1 in nodal point q, see Figure 7.10. For the in-plane motion of the truss element there are three independent rigid body modes. Therefore one deformation mode remains which describes the change of length of the axis of the truss element. The axial deformation of the truss element is defined by :

$$\begin{aligned} \varepsilon_1 = \mathbf{D}_1(\mathbf{x}) &= \frac{1}{2l_0^2} (\mathbf{l}_{pq} \cdot \mathbf{l}_{pq} - l_0^2) = \\ &= \frac{1}{2l_0^2} \left[ 2(x_q - x_p)(u_q - u_p) + 2(y_q - y_p)(v_q - v_p) + (u_q - u_p)^2 + (v_q - v_p)^2 \right] \end{aligned} \quad (7.6)$$

where the length of the undeformed element,  $l_0$ , is equal to :

$$l_0 = \sqrt{(x_q - x_p)^2 + (y_q - y_p)^2} \quad (7.7)$$

In equation (7.6) the quadratic length of the material line element is used which is in agreement with the continuum definition of the strain component. The virtual power corresponding to the virtual rate of deformation  $\delta \dot{\varepsilon}_1$  of axial deformation of the truss element defines the dual of the generalised strain rate  $\dot{\varepsilon}_1$ : the generalised stress  $\sigma_1$ . From this definition it follows that  $\sigma_1/l_0^2$  is equal to the normal force in the truss element.

### 7.2.1.2 Truss with belt sag

If it is to be expected that there are belt sections in the conveyor where  $v_x^2$  is of the order  $u_x$  then it is necessary to take the influence of the belt sag on the axial deformation into account, [Lodewijks, 1991&1992]. This situation can for example occur in long belt-

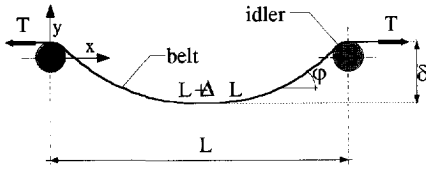


Figure 7.11: Static sag of a tensioned belt.

from the equilibrium equations of a tensioned string which is simply supported at both ends, is equal to:

$$\delta = \frac{qL^2}{8T} = K_s L \tag{7.8}$$

where  $q$  is the distributed load due to the belt and bulk material,  $L$  the length of the belt span between two idlers,  $T$  the belt tension and  $K_s$  the static belt sag ratio, see Figure 7.11. The angle between the horizontal and the tangent to the belt is:

$$\varphi(x) = v_{,x} = \frac{qx}{T} - \frac{qL}{2T} \tag{7.9}$$

where  $v$  is the transverse displacement of the belt. With this angle, the length of sagged belt can be calculated:

$$L^* = L + \Delta L \approx \int_0^L \left( 1 + \frac{1}{2} v_{,x}^2 \right) dx = L \left( 1 + \frac{1}{24} \left( \frac{qL}{T} \right)^2 \right) \tag{7.10}$$

This yields the additional axial strain due to the vertical belt load:

$$\varepsilon_s = \frac{\Delta L}{L} = \frac{1}{24} \left( \frac{qL}{T} \right)^2 = \frac{8}{3} K_s^2 \tag{7.11}$$

With this equation the total axial strain can be written as follows:

$$\varepsilon_1^* = \varepsilon_1 + \varepsilon_s \tag{7.12}$$

Substituting (7.11) in (7.12) and writing the total axial strain in terms of the belt tension  $T$ , assuming linear elastic material, yields the axial deformation  $\varepsilon_1$ :

conveyor systems with up-hill and down-hill sections, heavily loaded conveyors or after an emergency stop, [Ellis and Miller, 1987]. Although bending deformations are not included in the truss element, it is possible to take the static influence of small values of the belt sag approximately into account. The belt sag  $\delta$ , which is determined

$$\varepsilon_1 = \frac{T}{E_b A} - \frac{1}{24} \frac{(qL)^2}{T^2} \quad (7.13)$$

where  $E_b$  is the average Young's modulus of the belt and  $A$  the cross sectional area:

$$A = Bd_b \quad (7.14)$$

The effective Young's modulus of a sagged belt can be obtained from equation (7.13) by differentiation of the axial deformation  $\varepsilon_1$  with respect to the belt tension  $T$ :

$$\frac{1}{E_{b,\text{eff}}} = A \frac{d\varepsilon_1}{dT} = \frac{1}{E_b} + \frac{A}{12} \frac{(qL)^2}{T^3} = \frac{1}{E_b} \left( 1 + \frac{16}{3} \frac{E_b A}{T} K_s^2 \right) \quad (7.15)$$

which can be rewritten to:

$$E_{b,\text{eff}} = \frac{E_b}{1 + \frac{E_b}{E_s}} \quad (7.16)$$

where

$$E_s = 12 \frac{T^3}{(qL)^2 A} = \frac{3}{16} \frac{T}{AK_s^2} \quad (7.17)$$

The effective Young's modulus of equation (7.16) was also used by Funke (1973), and Ellis and Miller (1987).

### 7.2.1.3 Beam

If the bending deformation has to be taken accurately into account then beam elements can be used to model the belt, [Lodewijks, 1993]. Parts of the belt can have considerable transverse displacements and rotations. The local deformations, however, should still be small if only elastic deformations are considered. Therefore, the relative displacements of all material points of a beam element between two nodal points should be small compared to the distance between these nodal points.

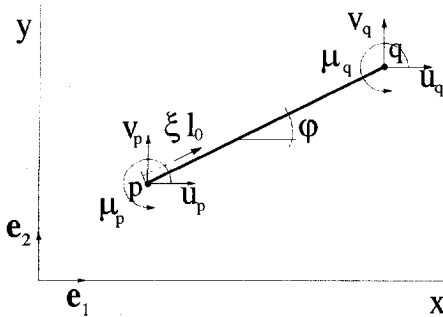


Figure 7.12: Definition of the nodal point displacements and rotations of a beam element.

The beam element in two-dimensional space shown in Figure 7.12 has six degrees of freedom. Each nodal point has two displacement components and one angle of rotation which define the component vector  $u$  :

$$u^T = [u_p \quad v_p \quad \mu_p \quad u_q \quad v_q \quad \mu_q] \tag{7.18}$$

For the motion of the beam element there are three independent rigid body modes, therefore three independent deformation modes remain. The beam element has, besides a longitudinal

deformation parameter, two bending deformation parameters, see Figure 7.13. These bending deformations,  $\epsilon_2$  and  $\epsilon_3$ , can be specified by the inner product of the vector  $l_{pq}$  and the vectors  $e_2^p$  and  $e_2^q$ , respectively, also see [Jonker, 1988]:

$$\epsilon_2 = D_2(u) = \frac{e_2^p \cdot l_{pq}}{l_0} \tag{7.19}$$

$$\epsilon_3 = D_3(u) = -\frac{e_2^q \cdot l_{pq}}{l_0} \tag{7.20}$$

The relationship between the local and the global unit vectors is:

$$e_i^p = R_{ij}^* R_{jk}^p e_k \tag{7.21a}$$

where the matrix  $R^*$  describes the transformation of the global base vectors to the local base vectors of the undeformed state and  $R^p$  the transformation due to nodal point rotation at node p. In case of Figure 7.12 it can be seen that (7.21a) becomes:

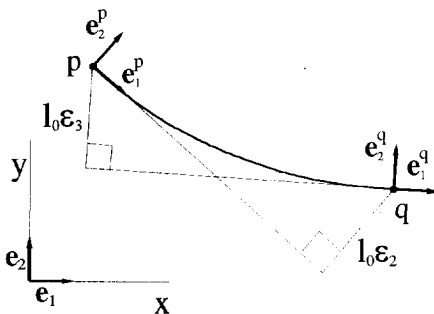


Figure 7.13: The bending deformations of a beam element.

$$\begin{bmatrix} \mathbf{e}_1^k \\ \mathbf{e}_2^k \end{bmatrix} = \begin{bmatrix} \cos\varphi & \sin\varphi \\ -\sin\varphi & \cos\varphi \end{bmatrix} \begin{bmatrix} \cos\mu_k & \sin\mu_k \\ -\sin\mu_k & \cos\mu_k \end{bmatrix} \begin{bmatrix} \mathbf{e}_1 \\ \mathbf{e}_2 \end{bmatrix} = \begin{bmatrix} \cos(\varphi + \mu_k) & \sin(\varphi + \mu_k) \\ -\sin(\varphi + \mu_k) & \cos(\varphi + \mu_k) \end{bmatrix} \begin{bmatrix} \mathbf{e}_1 \\ \mathbf{e}_2 \end{bmatrix} \quad (7.21b)$$

where  $k$  is  $p$  or  $q$ . To account for the influence of the bending deformations on the stretching of the centroidal axis of the beam element, the bending displacements are superimposed on the linearly varying displacements between the two nodal points. In the deformed state the position of any point on the axis of the beam element is approximated by :

$$\mathbf{x}_\xi + \mathbf{u}_\xi = \mathbf{x}_p + \mathbf{u}_p + (\mathbf{x}_q + \mathbf{u}_q - \mathbf{x}_p - \mathbf{u}_p) \xi - l_0 \left[ \varepsilon_2 \mathbf{e}_2^p (\xi^3 - 2\xi^2 + \xi) + \varepsilon_3 \mathbf{e}_3^p (-\xi^3 + \xi^2) \right] \quad (7.22)$$

This yields for small bending deformations the axial deformation of the beam element:

$$\varepsilon_1 = \mathbf{D}_1(\mathbf{u}) = \frac{1}{2l_0^2} (\mathbf{l}_{pq} \cdot \mathbf{l}_{pq} - l_0^2) + \frac{1}{30} (2\varepsilon_2^2 + \varepsilon_2\varepsilon_3 + 2\varepsilon_3^2) \quad (7.23)$$

The virtual power of deformation of the beam element defines the duals of the generalised virtual strain rates  $\delta\dot{\varepsilon}_i$  : the generalised stresses  $\sigma_i$ . In case of small strains the generalised stress  $\sigma_1$  is the normal force multiplies by the length of the element. The other two generalised stresses are the resultant moments of the normal stress distributions in the end cross sections.

#### 7.2.1.4 Idler supported beam

If a belt moves over an idler then the length co-ordinate  $\xi$ , which determines the position of the idler, see Figure 7.14, is added to the component vector of the beam-idler system, see Figure 7.15, thus resulting in a vector of seven displacement parameters, also see [Van Oostveen, 1987]:

$$\mathbf{u}^T = [u_p \quad v_p \quad \mu_p \quad u_q \quad v_q \quad \mu_q \quad \xi] \quad (7.24)$$

There are two independent rigid body motions for an in-plane beam element with sliding support at one point, therefore five deformation parameters remain. Three of them,  $\varepsilon_1$ ,  $\varepsilon_2$  and  $\varepsilon_3$ , determine the deformation of the belt and are already given in 7.2.1.3. The remaining two,  $\varepsilon_4$  and  $\varepsilon_5$ , determine the relative displacement between idler and support, see Figure 7.15. These deformation parameters are zero for a rigid support.

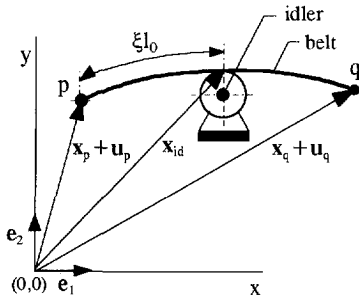


Figure 7.14: Belt supported by an idler.

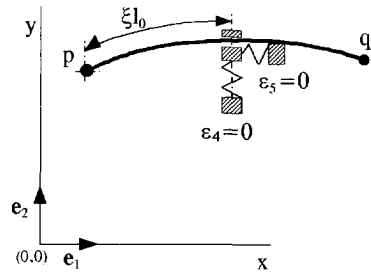


Figure 7.15: Idler supported beam element with two constraint conditions.

If the radius vector to the top surface of the idler is given by (see also Figure 7.14)

$$\mathbf{x}_{id} = x_{id}\mathbf{e}_1 + y_{id}\mathbf{e}_2 \quad (7.25)$$

then the strain component  $\epsilon_4$  can be defined by:

$$\epsilon_4 = \mathbf{D}_4(\mathbf{u}) = (\mathbf{x}_\xi + \mathbf{u}_\xi) \cdot \mathbf{e}_2 - \mathbf{x}_{id} \cdot \mathbf{e}_2 = 0 \quad (7.26)$$

and  $\epsilon_5$  by:

$$\epsilon_5 = \mathbf{D}_5(\mathbf{u}) = (\mathbf{x}_\xi + \mathbf{u}_\xi) \cdot \mathbf{e}_1 - \mathbf{x}_{id} \cdot \mathbf{e}_1 = 0 \quad (7.27)$$

If during simulation  $\epsilon_4 > 0$  then the belt is lifted off the idler and the constraint conditions have to be removed from the finite element description of the belt.

### 7.2.1.5 Pulley supported beam

When the belt moves over a pulley it depends on the position of the element whether the whole element or a part of the element is supported. Elements with only one node on the pulley are partly supported, see Figure 7.17. The distance between a nodal point on a pulley and the shaft of the pulley is equal to the radius of that pulley. The angle between the orientation at the nodal point and the horizontal is equal to the angle between the tangent to the pulley and the horizontal. These constraints are forced by a rigid truss element which is placed between the shaft of the pulley and the supported nodal point of the element, and by a deformation parameter  $\epsilon_6$  which can be considered as a torsion spring of infinite stiffness, see Figure 7.17.



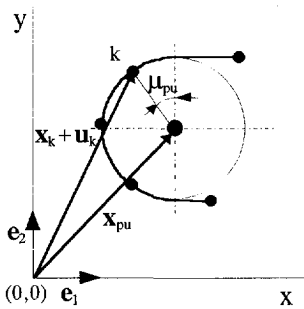


Figure 7.16: Belt supported by a pulley.

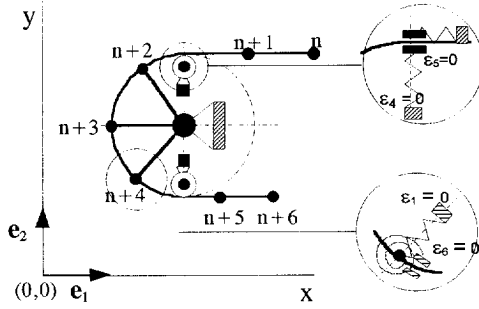


Figure 7.17: Pulley supported beam elements.

If the radius vector to the pulley shaft is given by, see also Figure 7.16:

$$\mathbf{x}_{pu} = x_{pu}\mathbf{e}_1 + y_{pu}\mathbf{e}_2 \tag{7.28}$$

then the strain component  $\epsilon_6$  of nodal point  $k$  can be defined by:

$$\epsilon_6 = D_6(\mathbf{x}) = \mu_k - \mu_{pu} = \mu_k - \text{atan}\left(\frac{-(\mathbf{x}_k + \mathbf{u}_k - \mathbf{x}_{pu}) \cdot \mathbf{e}_1}{(\mathbf{x}_k + \mathbf{u}_k - \mathbf{x}_{pu}) \cdot \mathbf{e}_2}\right) = 0 \tag{7.29}$$

Nodal points of partly supported elements which are not located on the pulley are coupled with the supported nodal point by an idler support which is located on the edge of the pulley. This prevents the edge elements from geometrically impossible positions.

The shaft of a pulley is modelled as a hinge element which enables the connection rods to rotate. Two types are distinguished: the single and the plural hinge element, see Figure 7.18. A single hinge element has only one angle of rotation whereas a plural hinge element has a number of angles of rotation. A single hinge element is used for non-driven pulleys where the belt does not slip over the pulley surface. In case of a driven pulley, a part of the belt can slip and a plural hinge element should be used. To determine slip between the belt and the pulley surface, a detailed description of the contact phenomena between the belt and a driven pulley is required. Since this has not been considered, up to now only single hinge elements have been used in the belt system models.

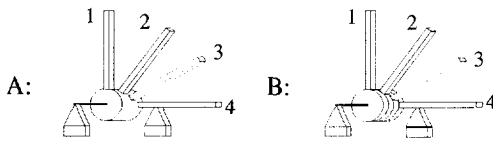


Figure 7.18: The shaft of the pulley as single (A) and plural (B) hinge element.

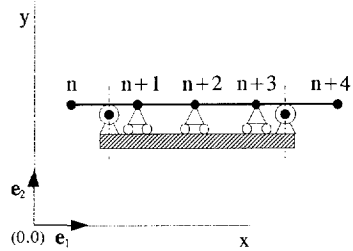


Figure 7.19: Plate supported beam elements.

### 7.2.1.6 Plate supported beam

The transverse displacement of a belt is zero when the belt moves over a plate, see Figure 7.19. In that case the transverse displacement parameters of the beam elements are constrained. To allow the belt to enter and to leave the plate supported section smoothly, two idler supports are used on the edges of the plate.

## 7.2.2 Dynamic characteristics

The stiffness and inertia properties determine the dynamic characteristics of the (finite) belt elements. The stiffness properties are described by stiffness matrices relating stresses and deformations in a similar way as in the continuum description. Linear visco-elastic behaviour of the belt elements is characterised by the linear constitutive equation (Kelvin-Voigt model):

$$\begin{bmatrix} \sigma_1 \\ \sigma_2 \\ \sigma_3 \end{bmatrix} = \mathbf{S} \begin{bmatrix} \varepsilon_1 \\ \varepsilon_2 \\ \varepsilon_3 \end{bmatrix} + \mathbf{S}_d \begin{bmatrix} \dot{\varepsilon}_1 \\ \dot{\varepsilon}_2 \\ \dot{\varepsilon}_3 \end{bmatrix} \quad (7.30)$$

where  $\mathbf{S}$  and  $\mathbf{S}_d$  are symmetric matrices containing the elastic constants and the viscous damping coefficients respectively. The displacements of any point on a one-dimensional finite element can be written in terms of the nodal point displacements and rotations:

$$\mathbf{u}(\xi, t) = \mathbf{N}(\xi) \mathbf{u}(t) \quad (7.31)$$

where  $\mathbf{u}(t)$  is the component vector of the local displacements and  $\mathbf{N}$  the matrix of shape functions, prescribing the shape functions in terms of the independent variable  $\xi$ . In case of a truss element as discussed in Section 7.2.1.1, the shape functions are described by:

$$\mathbf{N}(\xi) = \begin{bmatrix} 1 - \xi & 0 & \xi & 0 \\ 0 & 1 - \xi & 0 & \xi \end{bmatrix} \quad (7.32)$$

For the transverse displacement of a beam element in a two-dimensional space the shape function is a third-order polynomial. For a prismatic homogeneous beam, the elasticity matrix  $\mathbf{S}$  is [Besseling, 1977]:

$$\mathbf{S} = E_b A l_0 \begin{bmatrix} 1 & 0 & 0 \\ 0 & 4 \frac{i_y^2}{l_0^2} & -2 \frac{i_y^2}{l_0^2} \\ 0 & -2 \frac{i_y^2}{l_0^2} & 4 \frac{i_y^2}{l_0^2} \end{bmatrix} \quad (7.33)$$

where  $i_y$  is the radius of gyration of the cross sectional area of the element. For the truss element  $\mathbf{S}$  is a scalar:  $S = E_b A l_0$ . The matrix of viscous damping coefficients  $\mathbf{S}_d$  is determined by the chosen linear visco-elastic model [Zur, 1986a&b].

The inertia properties of the concentrated or distributed mass of the elements are described by mass matrices. The components of the mass matrices can be calculated by evaluating the virtual power of the inertia forces:

$$-l_0 \int_0^1 \left\langle \delta \dot{\mathbf{u}}(\xi, t), \frac{d}{dt} (\mathbf{M}(\xi) \dot{\mathbf{u}}(\xi, t)) \right\rangle d\xi = -l_0 m'_{\text{const}} \int_0^1 \left\langle \delta \dot{\mathbf{u}}(\xi, t), \ddot{\mathbf{u}}(\xi, t) \right\rangle d\xi \quad (7.34)$$

assuming that the mass per unit length is constant and given by  $m'_{\text{const}}$ . The mass matrix which can be obtained from equation (7.34) is called a consistent mass matrix if the linear shape functions, given in equation (7.31), are used. For a truss element with the mass per unit length

$$m'_{\text{const}} = \rho A \quad (7.35)$$

the consistent mass matrix is obtained by:

$$-l_0 \rho A \int_0^1 \left\langle \delta \dot{\mathbf{u}}(\xi, t), \ddot{\mathbf{u}}(\xi, t) \right\rangle d\xi = -l_0 \rho A \delta \dot{\mathbf{u}}^T \int_0^1 \mathbf{N}^T \mathbf{N} d\xi \ddot{\mathbf{u}} = -\delta \dot{\mathbf{u}}^T \mathbf{M} \ddot{\mathbf{u}} \quad (7.36)$$

where

$$\mathbf{M} = \frac{\rho A l_0}{6} \begin{bmatrix} 2 & 0 & 1 & 0 \\ 0 & 2 & 0 & 1 \\ 1 & 0 & 2 & 0 \\ 0 & 1 & 0 & 2 \end{bmatrix} \quad (7.37)$$

The displacements of any point on a beam element as function of the length parameter  $\xi$  are given in equation (7.22). From this equation the velocity and acceleration of any point on a beam element can be obtained:

$$\dot{\mathbf{u}}_\xi = (1 - \xi)\dot{\mathbf{u}}_p + \xi\dot{\mathbf{u}}_q - l_0 \left[ (\dot{\varepsilon}_2 \mathbf{e}_2^p + \varepsilon_2 \dot{\mathbf{e}}_2^p)(\xi^3 - 2\xi^2 + \xi) + (\dot{\varepsilon}_3 \mathbf{e}_3^q + \varepsilon_3 \dot{\mathbf{e}}_3^q)(-\xi^3 + \xi^2) \right] \quad (7.38a)$$

$$\begin{aligned} \ddot{\mathbf{u}}_\xi = & (1 - \xi)\ddot{\mathbf{u}}_p + \xi\ddot{\mathbf{u}}_q - l_0 \left[ (\ddot{\varepsilon}_2 \mathbf{e}_2^p + 2\dot{\varepsilon}_2 \dot{\mathbf{e}}_2^p + \varepsilon_2 \ddot{\mathbf{e}}_2^p)(\xi^3 - 2\xi^2 + \xi) \right. \\ & \left. + (\ddot{\varepsilon}_3 \mathbf{e}_3^q + 2\dot{\varepsilon}_3 \dot{\mathbf{e}}_3^q + \varepsilon_3 \ddot{\mathbf{e}}_3^q)(-\xi^3 + \xi^2) \right] \end{aligned} \quad (7.38b)$$

In these equations the deformation parameters  $\varepsilon_2$  and  $\varepsilon_3$  and their derivatives with respect to time are used. From  $\mathbf{e}_2^k$ ,  $\varepsilon_2$  and  $\varepsilon_3$  given in the equations (7.21b), (7.19) and (7.20) respectively, the following time derivatives can be obtained:

$$\dot{\mathbf{e}}_2^k = -\cos(\varphi + \mu_k)\dot{\mu}_k \mathbf{e}_1 - \sin(\varphi + \mu_k)\dot{\mu}_k \mathbf{e}_2 \quad (7.39a)$$

$$\ddot{\mathbf{e}}_2^k = \left( -\cos(\varphi + \mu_k)\ddot{\mu}_k + \sin(\varphi + \mu_k)\dot{\mu}_k^2 \right) \mathbf{e}_1 + \left( -\sin(\varphi + \mu_k)\ddot{\mu}_k - \cos(\varphi + \mu_k)\dot{\mu}_k^2 \right) \mathbf{e}_2 \quad (7.39b)$$

$$\begin{aligned} \dot{\varepsilon}_2 = & \frac{1}{l_0} \left[ -(\dot{u}_q - \dot{u}_p)\sin(\varphi + \mu_p) + (\dot{v}_q - \dot{v}_p)\cos(\varphi + \mu_p) \right] - \\ & \frac{1}{l_0} \left[ (x_q + u_q - x_p - u_p)\cos(\varphi + \mu_p) + (y_q + v_q - y_p - v_p)\sin(\varphi + \mu_p) \right] \dot{\mu}_p \end{aligned} \quad (7.39c)$$

$$\begin{aligned} \dot{\varepsilon}_3 = & \frac{1}{l_0} \left[ (\dot{u}_q - \dot{u}_p)\sin(\varphi + \mu_q) - (\dot{v}_q - \dot{v}_p)\cos(\varphi + \mu_q) \right] + \\ & \frac{1}{l_0} \left[ (x_q + u_q - x_p - u_p)\cos(\varphi + \mu_q) + (y_q + v_q - y_p - v_p)\sin(\varphi + \mu_q) \right] \dot{\mu}_q \end{aligned} \quad (7.39d)$$

$$\begin{aligned}
 \ddot{\varepsilon}_2 = & \frac{1}{l_0} \left[ -(\ddot{u}_q - \ddot{u}_p) \sin(\varphi + \mu_p) + (\ddot{v}_q - \ddot{v}_p) \cos(\varphi + \mu_p) \right] - \\
 & \frac{2}{l_0} \left[ (\dot{u}_q - \dot{u}_p) \cos(\varphi + \mu_p) + (\dot{v}_q - \dot{v}_p) \sin(\varphi + \mu_p) \right] \dot{\mu}_p + \\
 & \frac{1}{l_0} \left[ (x_q + u_q - x_p - u_p) (\dot{\mu}_p^2 \sin(\varphi + \mu_p) - \ddot{\mu}_p \cos(\varphi + \mu_p)) \right] - \\
 & \frac{1}{l_0} \left[ (y_q + v_q - y_p - v_p) (\dot{\mu}_p^2 \cos(\varphi + \mu_p) + \ddot{\mu}_p \sin(\varphi + \mu_p)) \right]
 \end{aligned} \tag{7.39e}$$

$$\begin{aligned}
 \ddot{\varepsilon}_3 = & \frac{1}{l_0} \left[ (\ddot{u}_q - \ddot{u}_p) \sin(\varphi + \mu_q) - (\ddot{v}_q - \ddot{v}_p) \cos(\varphi + \mu_q) \right] + \\
 & \frac{2}{l_0} \left[ (\dot{u}_q - \dot{u}_p) \cos(\varphi + \mu_q) + (\dot{v}_q - \dot{v}_p) \sin(\varphi + \mu_q) \right] \dot{\mu}_q - \\
 & \frac{1}{l_0} \left[ (x_q + u_q - x_p - u_p) (\dot{\mu}_q^2 \sin(\varphi + \mu_q) - \ddot{\mu}_q \cos(\varphi + \mu_q)) \right] + \\
 & \frac{1}{l_0} \left[ (y_q + v_q - y_p - v_p) (\dot{\mu}_q^2 \cos(\varphi + \mu_q) + \ddot{\mu}_q \sin(\varphi + \mu_q)) \right]
 \end{aligned} \tag{7.39f}$$

where  $k$  is  $p$  or  $q$ . Substitution of the equations (7.39) in the equations (7.38) yields complicated expressions for the velocities and accelerations. To simplify the equations (7.39), it is assumed that the relative rotations of the nodal points of a beam element are small compared to the absolute rotation of the beam element. In that case the following approximations are allowed:

$$\begin{aligned}
 \sin(\varphi + \mu_p) & \approx \sin(\varphi + \mu_q) \approx \sin(\varphi) \approx \Delta y / l_0 \\
 \cos(\varphi + \mu_p) & \approx \cos(\varphi + \mu_q) \approx \cos(\varphi) \approx \Delta x / l_0
 \end{aligned} \tag{7.40}$$

where

$$\begin{aligned}
 \Delta x & = x_q + u_q - x_p - u_p \\
 \Delta y & = y_q + v_q - y_p - v_p
 \end{aligned} \tag{7.41}$$

Substitution of (7.40) in the equations (7.39) yields:

$$\dot{\varepsilon}_2^k = -\frac{\Delta x \dot{\mu}_k}{l_0} \mathbf{e}_1 - \frac{\Delta y \dot{\mu}_k}{l_0} \mathbf{e}_2 \tag{7.42a}$$

$$\ddot{\mathbf{e}}_2^k = \frac{1}{l_0} (-\Delta x \ddot{\mu}_k + \Delta y \dot{\mu}_k^2) \mathbf{e}_1 + \frac{1}{l_0} (-\Delta y \ddot{\mu}_k - \Delta x \dot{\mu}_k^2) \mathbf{e}_2 \quad (7.42b)$$

$$\dot{\mathbf{e}}_2 = \frac{1}{l_0^2} [-(\dot{u}_q - \dot{u}_p) \Delta x + (\dot{v}_q - \dot{v}_p) \Delta y - 2 \Delta x \Delta y \dot{\mu}_p] \quad (7.42c)$$

$$\dot{\mathbf{e}}_3 = \frac{1}{l_0^2} [(\dot{u}_q - \dot{u}_p) \Delta x - (\dot{v}_q - \dot{v}_p) \Delta y + 2 \Delta x \Delta y \dot{\mu}_q] \quad (7.42d)$$

$$\begin{aligned} \ddot{\mathbf{e}}_2 = \frac{1}{l_0^2} [-(\ddot{u}_q - \ddot{u}_p) \Delta x + (\ddot{v}_q - \ddot{v}_p) \Delta y] - \frac{2}{l_0^2} [(\dot{u}_q - \dot{u}_p) \Delta y + (\dot{v}_q - \dot{v}_p) \Delta x] \dot{\mu}_p + \\ \frac{1}{l_0^2} [(\Delta x^2 - \Delta y^2) \dot{\mu}_p^2 - 2 \Delta x \Delta y \ddot{\mu}_p] \end{aligned} \quad (7.42e)$$

$$\begin{aligned} \ddot{\mathbf{e}}_3 = \frac{1}{l_0^2} [(\ddot{u}_q - \ddot{u}_p) \Delta x - (\ddot{v}_q - \ddot{v}_p) \Delta y] + \frac{2}{l_0^2} [(\dot{u}_q - \dot{u}_p) \Delta y + (\dot{v}_q - \dot{v}_p) \Delta x] \dot{\mu}_q - \\ \frac{1}{l_0^2} [(\Delta x^2 - \Delta y^2) \dot{\mu}_q^2 - 2 \Delta x \Delta y \ddot{\mu}_q] \end{aligned} \quad (7.42f)$$

where k is p or q. After substitution of (7.38) in (7.34) using (7.42), the following equation can be obtained:

$$-l_0 \rho A \int_0^l \langle \delta \dot{\mathbf{u}}(\xi, t), \ddot{\mathbf{u}}(\xi, t) \rangle d\xi = -\delta \dot{\mathbf{u}}^T (\mathbf{M} \ddot{\mathbf{u}} + \mathbf{M}, \mathbf{q}) \quad (7.43)$$

where:

$$\mathbf{M} = \frac{\rho A l_0}{420} \begin{bmatrix} 140 + 16 \frac{\Delta y^2}{l_0^2} & -16 \frac{\Delta x \Delta y}{l_0^2} & -22 \Delta y & 70 - 16 \frac{\Delta y^2}{l_0^2} & 16 \frac{\Delta x \Delta y}{l_0^2} & 13 \Delta y \\ & 140 + 16 \frac{\Delta x^2}{l_0^2} & 22 \Delta x & 16 \frac{\Delta x \Delta y}{l_0^2} & 70 - 16 \frac{\Delta x^2}{l_0^2} & -13 \Delta x \\ & & 4l_0^2 & -13 \Delta y & 13 \Delta x & -3l_0^2 \\ & & & & & & & 140 + 16 \frac{\Delta y^2}{l_0^2} & -16 \frac{\Delta x \Delta y}{l_0^2} & 22 \Delta y \\ & & & & & & & & & & & 140 + 16 \frac{\Delta x^2}{l_0^2} & -22 \Delta x \\ & & & & & & & & & & & & & & & & 4l_0^2 \end{bmatrix} \quad (7.44)$$

and

$$\mathbf{M}_v = \frac{\rho A l_0}{420} \begin{bmatrix}
 86 \frac{\Delta x \Delta y}{l_0^2} & 44 \frac{\Delta y^2}{l_0^2} - 42 \frac{\Delta x^2}{l_0^2} & -42 \Delta x & -86 \frac{\Delta x \Delta y}{l_0^2} & -44 \frac{\Delta y^2}{l_0^2} + 42 \frac{\Delta x^2}{l_0^2} \\
 42 \frac{\Delta y^2}{l_0^2} - 44 \frac{\Delta x^2}{l_0^2} & -86 \frac{\Delta x \Delta y}{l_0^2} & -42 \Delta y & -42 \frac{\Delta y^2}{l_0^2} + 44 \frac{\Delta x^2}{l_0^2} & 86 \frac{\Delta x \Delta y}{l_0^2} \\
 -8 \Delta x & -8 \Delta y & 0 & 8 \Delta x & 8 \Delta y \\
 54 \frac{\Delta x \Delta y}{l_0^2} & 26 \frac{\Delta y^2}{l_0^2} - 28 \frac{\Delta x^2}{l_0^2} & -28 \Delta x & -54 \frac{\Delta x \Delta y}{l_0^2} & -26 \frac{\Delta y^2}{l_0^2} + 28 \frac{\Delta x^2}{l_0^2} \\
 28 \frac{\Delta y^2}{l_0^2} - 26 \frac{\Delta x^2}{l_0^2} & -54 \frac{\Delta x \Delta y}{l_0^2} & -28 \Delta y & -28 \frac{\Delta y^2}{l_0^2} + 26 \frac{\Delta x^2}{l_0^2} & 54 \frac{\Delta x \Delta y}{l_0^2} \\
 6 \Delta x & 6 \Delta y & 0 & -6 \Delta x & -6 \Delta y \\
 \\
 -54 \frac{\Delta x \Delta y}{l_0^2} & -26 \frac{\Delta y^2}{l_0^2} + 28 \frac{\Delta x^2}{l_0^2} & 54 \frac{\Delta x \Delta y}{l_0^2} & 26 \frac{\Delta y^2}{l_0^2} - 28 \frac{\Delta x^2}{l_0^2} & 28 \Delta x \\
 -28 \frac{\Delta y^2}{l_0^2} + 26 \frac{\Delta x^2}{l_0^2} & 54 \frac{\Delta x \Delta y}{l_0^2} & 28 \frac{\Delta y^2}{l_0^2} - 26 \frac{\Delta x^2}{l_0^2} & -54 \frac{\Delta x \Delta y}{l_0^2} & 28 \Delta y \\
 6 \Delta x & 6 \Delta y & -6 \Delta x & -6 \Delta y & 0 \\
 -86 \frac{\Delta x \Delta y}{l_0^2} & -44 \frac{\Delta y^2}{l_0^2} + 42 \frac{\Delta x^2}{l_0^2} & 86 \frac{\Delta x \Delta y}{l_0^2} & 44 \frac{\Delta y^2}{l_0^2} - 42 \frac{\Delta x^2}{l_0^2} & 42 \Delta x \\
 -42 \frac{\Delta y^2}{l_0^2} + 44 \frac{\Delta x^2}{l_0^2} & 86 \frac{\Delta x \Delta y}{l_0^2} & 42 \frac{\Delta y^2}{l_0^2} - 44 \frac{\Delta x^2}{l_0^2} & -86 \frac{\Delta x \Delta y}{l_0^2} & 42 \Delta y \\
 -8 \Delta x & -8 \Delta y & 8 \Delta x & 8 \Delta y & 0
 \end{bmatrix} \quad (7.45)$$

The vectors  $\ddot{\mathbf{u}}$  and  $\mathbf{q}$  in equation (7.43) are

$$\ddot{\mathbf{u}}^T = [\ddot{u}_p \quad \ddot{v}_p \quad \ddot{\mu}_p \quad \ddot{u}_q \quad \ddot{v}_q \quad \ddot{\mu}_q] \quad (7.46)$$

and

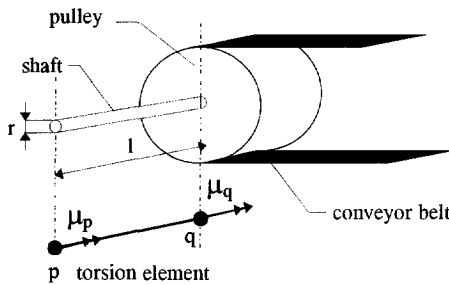
$$\mathbf{q}^T = [\dot{u}_p \dot{\mu}_p \quad \dot{v}_p \dot{\mu}_p \quad \dot{\mu}_p^2 \quad \dot{u}_q \dot{\mu}_p \quad \dot{v}_q \dot{\mu}_p \quad \dot{u}_p \dot{\mu}_q \quad \dot{v}_p \dot{\mu}_q \quad \dot{u}_q \dot{\mu}_q \quad \dot{v}_q \dot{\mu}_q \quad \dot{\mu}_q^2] \quad (7.47)$$

As can be seen in the matrices  $\mathbf{M}$  and  $\mathbf{M}_v$ , the non-linear effect of large rotations cause the configuration dependency of the consistent mass formulation for a beam element.

### 7.2.3 Electrical and mechanical elements of belt conveyor systems

In this section the discrete models of the electrical and mechanical components of belt conveyor systems are presented. Not all the components are discretised to elements, some are only modelled by one nodal point.

#### 7.2.3.1 Torsion



The linear torsion element has two degrees of freedom,  $\mu_p$  and  $\mu_q$ , and one rigid body mode, the rigid rotation of the shaft. Therefore one deformation mode, which indicates the angle of twist of the shaft, remains. It is defined by:

$$\varepsilon_7 = \mathbf{D}_7(\mathbf{u}) = \mu_q - \mu_p \quad (7.48)$$

Assuming a linear interpolation function, the inertia properties are summarised in the following mass matrix :

$$\mathbf{M} = \frac{\rho I_p l_0}{6} \begin{bmatrix} 2 & 1 \\ 1 & 2 \end{bmatrix} \quad (7.49)$$

where  $I_p$  is the polar moment of inertia of the element. One stiffness property relates the stress to the deformation of the torsion element:

$$\sigma_7 = S_7 \varepsilon_7 = \frac{GI_p}{l_0} \varepsilon_7 \quad (7.50)$$

where  $G$  is the shear modulus.

#### 7.2.3.2 Induction motor

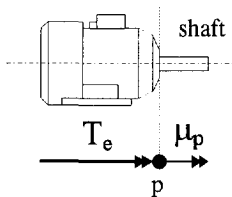


Figure 7.21: Induction motor.

The shaft of an induction motor is modelled by a torsion element. The electric torque of the motor, which is given in equation (6.55), is attached to the drive shaft. The moments of inertia of the rotating parts of the motor are added to the mass matrix of the torsion element.



### 7.2.3.3 Fluid coupling

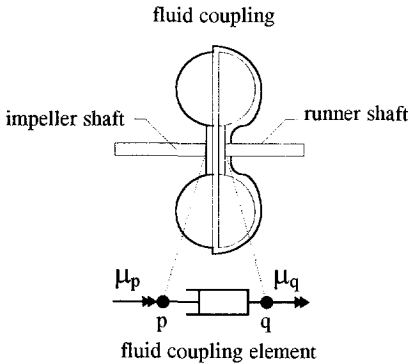


Figure 7.22: Fluid coupling element.

The fluid coupling, which connects the impeller shaft and the runner shaft, is modelled by a fluid coupling element. This element has two rotations,  $\mu_p$  and  $\mu_q$ . The virtual power of deformation of the fluid coupling element defines the dual of the generalised virtual strain rate  $\delta \dot{\epsilon}_8 = D_8(\dot{\mathbf{u}})$ : the generalised stress  $\sigma_8$  which is the torque acting on the impeller and the runner. From the approximation of equation (6.58) it follows that:

$$\sigma_8 = S_8 \dot{\epsilon}_8 = \lambda^* \rho_f D_h^5 (\dot{\mu}_p - \dot{\mu}_q)^n \dot{\mu}_p^{2-n} \quad (7.51)$$

The moments of inertia of the impeller and the runner are added to the masses of the corresponding nodal points of the two shafts. In Figure 6.2 the fluid coupling was placed before the reduction box. This reduces the torque by a factor equal to the reduction factor when compared to the coupling placed after the reduction box which directly influences the size of the coupling.

### 7.2.3.4 Drum brake and back stop

The brake couple caused by the brake force is an external moment connected to a nodal point. The mass of the (rotating) brake drum, see Figure 7.23, is added to the mass of the corresponding nodal point. The required couple of a drum brake placed before the reduction box is a factor equal to the reduction factor smaller than for a drum brake placed after the reduction box. For this reason the drum brake in Figure 6.2 was placed before the reduction box.

### 7.2.3.5 Reduction box

The transition elements of the drive system, as for example the reduction box, are modelled with constraint conditions as described in Section 7.1.2.4. A reduction box with rigid wheels and shafts and a reduction ratio  $i$  can be modelled by a reduction box element with two rotations,  $\mu_p$  and  $\mu_q$ , one rigid body motion (rotation) and therefore one deformation parameter :

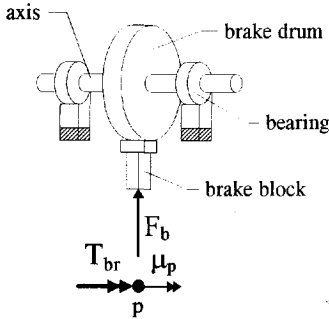


Figure 7.23: Drum brake.

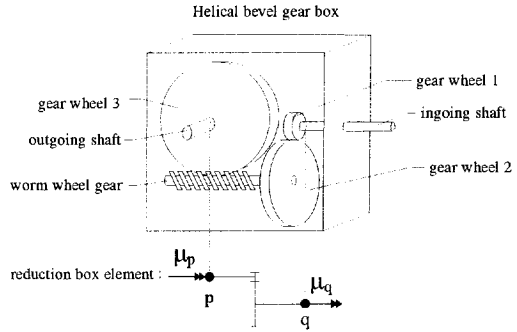


Figure 7.24: Reduction box element.

$$\epsilon_9 = \mathbf{D}_9(\mathbf{u}) = \mu_p + i\mu_q = 0 \tag{7.52}$$

The inertia properties of the reduction box element are important. The inertias of the gear wheels are added as equivalent inertias to the nodal points.

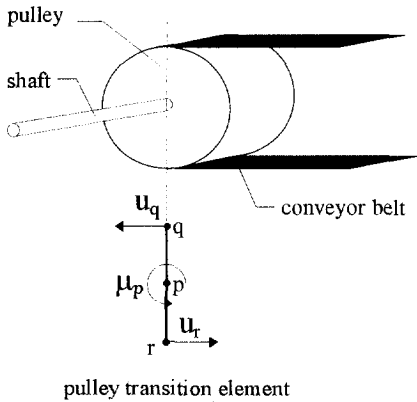
### 7.2.3.6 Pulley transition

The pulley transition element is used to connect torsion elements, via a pulley, with truss elements of the belt. This element has three nodal points, p, q and r. The nodal points q and r are shared with two truss elements, the nodal point p is shared with a torsion element. If the drive shaft is fixed to the conveyor structure then the element has three displacement parameters  $\mu_p$ ,  $u_q$  and  $u_r$ . The element has one rigid body mode, a rotation, and therefore two deformation parameters remain. The first describes the relative rotation between the pulley shaft and the pulley surface and is defined by:

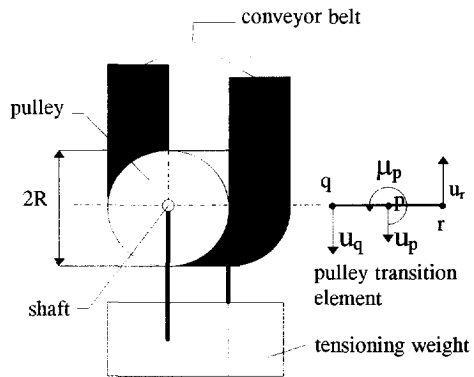
$$\epsilon_{10} = \mathbf{D}_{10}(\mathbf{u}) = \mu_p - \frac{u_q + u_r}{2R} = 0 \tag{7.53}$$

where R is the radius of the pulley. Since the pulley shaft is assumed to be rigidly connected to the pulley wall this deformation parameter is zero. The second deformation parameter describes the relative motion (slip) between the upper and the lower part of the belt and is defined by:

$$\epsilon_{11} = \mathbf{D}_{11}(\mathbf{u}) = \frac{u_q - u_r}{2} \tag{7.54}$$



**Figure 7.25:** Definition of the displacements parameters of the pulley transition element.



**Figure 7.26:** Definition of the generalised displacements of a pulley transition element for the take-up pulley.

Since the lateral motion of the belt is governed by the rotation of the pulley, no slip is possible between the belt and the pulley surface. Therefore also this deformation parameter is zero. If the drive pulley can move laterally, then the pulley transition element has four displacement parameters. Since the element in this case has two rigid body modes, one rotation and one translation, two deformation parameters can be defined. One describes the coupling between the pulley shaft and the pulley surface and is already given in equation (7.53). The other describes the coupling between the lateral motion of the pulley centre and the belt ends and is defined by:

$$\varepsilon_{12} = \mathbf{D}_{12}(\mathbf{u}) = u_p - \frac{u_q - u_r}{2} = 0 \quad (7.55)$$

## 7.3 References

- Bacholdin, B.A. and Leskevic, V.I. (1965), *Zur Frage der Dynamik von Gurtförderern*, Voprosy rudnicogo transporta band 8, Moskou.
- Bacholdin, B.A. and Rychalskij, J.A. (1963), "Die Modellierung des Anfahrens von Bandförderern mit Eintrommelantrieb", *Izvestija VUZ, Gronjz jurnal* 6/9, pp. 39-44.
- Bahr, J. (1960), "Ergebnisse der Untersuchungen an der Bandanlage Mueheln", *Freiberger Forschungshefte A 152*, pp. 78-97.
- Besseling, J.F. (1977), "Derivatives of deformation parameters for bar elements and their use in buckling and post-buckling analysis", *Computational Methods in Applied Mechanics* 12, pp. 97-124.

- Bierhof, A. (1973), *Spanningen bij bandtransporteurs*, report 456, Delft University of Technology, Section of Transporttechnology.
- Brade, K. (1965), "Untersuchung automatischer Gurtspannvorrichtungen an langen Gurtförderern im Tagebau", *Bergbautechnik* **15**, pp. 413-419.
- Brade, K. and Menning, G. (1969), "Rationalisierung an Grossbandanlagen durch zweckmässige Gurtspannungsregelung", *Bergbautechnik* **19**, pp.535-540.
- Coeuillet, R. (1955), "Étude pratique d'un convoyeur en démarrage", *Revue de l'Industrie Minérale* **36**, pp. 635-686.
- Dumonteil, P. (1967), "Ebauche d'une theorie du démarrage des transporteur à courroie", *Revue de l'Industrie Minérale* **49**, pp. 185-193.
- Ellis, D. and Miller, K. (1987), "A mathematical analysis of tension shocks in long belt conveyors", *Mathematical Modelling* **9**, pp., 613-623.
- Funke, H. and Winterberg, H. (1964), "Betriebsverhalten einer langen Förderbandanlage mit Kopf-, Heck- und Mittelantrieb", *Braunkohle, Wärme und Energie* **16**, page 409-422.
- Funke, H. (1973), *Zum dynamischen Verhalten von Förderanlagen beim Anfahren und Stillsetzen unter Berücksichtigung der Bewegungswiderstände*, Doctorate dissertation, Universität Hannover.
- Funke, H. and Kömneker, F.K. (1988), "Experimental investigations and theory for the design of a long-distance belt-conveyor system". *Bulk Solids Handling* **8**, pp. 567-579.
- Hager, M. and von der Wroge, H. (1991), "Design of steelcord conveyor belt splices". *Bulk Solids Handling* **11**, pp. 849-860.
- Harrison, A. (1981), *Transient stresses in long conveyor belts*, CSIRO Division of Applied Physics, Sydney.
- Harrison, A. (1984), "Flexural behaviour of tensioned conveyor belts", *Bulk Solids Handling* **4**, pp. 67-71.
- Harrison, A (1988). "On the appropriate use of dynamic stress models for conveyor design", *Bulk Solids Handling* **8**, pp. 677-680.
- Havelka, Z. (1963), "Zur Theorie des Gurtbandförderers", *Hebezeuge und Fördermittel* **3/2**, pp. 47-51.
- Havelka, Z. (1967), "Möglichkeiten der Steigerung der Betriebszuverlässigkeit und der Arbeitsproduktivität von Grossbandanlagen", *Bergbautechnik* **17**, pp. 630-635.
- Jonker, B. (1988), *A Finite Element Dynamic Analysis of Flexible Spatial Mechanisms and Manipulators*, Ph.D. thesis, Delft University of Technology, Delft.
- Karbosov, O.G. (1962), "Bestimmung der dynamischen Kräfte im Fördergurt beim Anfahren von Gurtförderers", *Izvestija VUZ, Gronyj zurnal* **5/9**, pp. 80-86.
- Karolewski, B. (1983), "Elektrische Modellierung des Bandförderers", *Stetigförderer für Schüttgut* **13**, pp. 309-315.
- Karolewski, B. (1986), "An investigation of various conveyor belt drive systems using a mathematical model", *Bulk Solids Handling* **6**, pp. 61-66.
- Lieberwirth, H. (1994), "Design of belt conveyors with horizontal curves", *Bulk Solids Handling* **14**, pp. 283-285.
- Lodewijks, G. (1991), *Het modelleren van een bandtransporteur* (in Dutch), Reportno. 91.3.TT.2830, Department of Transporttechnology, Delft University of Technology.

- Lodewijks, G. (1992), *Het schrijven van een computerprogramma waarmee het ontstaan van schokgolven gesimuleerd kan worden* (in Dutch), M.Sc. thesis, Reportno. 92.3.TT.2984, Department of Transporttechnology, Delft University of Technology.
- Lodewijks, G. (1993), *A Finite Element Approach to Calculate the Dynamic Behaviour of a Discontinuously Supported Conveyor Belt*, Reportno. 93.3.TT.4051, Department of Transporttechnology, Delft University of Technology.
- Lodewijks, G. (1994a), "On the application of beam elements in finite element models of belt conveyors: part I", *Bulk Solids Handling* **14**, pp. 729-737.
- Lodewijks, G. (1994b), *Transverse vibrations in flexible belt systems*. Delft University of Technology, report no. 94.3.TT.4270.
- Lodewijks, G. (1994c), "Het ontwerp van lange bandtransporteurs", *BULK* **2(4)**, pp. 58-60.
- Lodewijks, G. (1995a), "The Rolling Resistance of Belt Conveyors", *Bulk Solids Handling* **15**, pp. 15-22.
- Lodewijks, G. (1995b), "Present Research at Delft University of Technology, The Netherlands", *1995 5th International Conference on Bulk Material Storage, Handling and Transportation*, Newcastle, Australia, 10-12 July 1995, The Institution of Engineers, Australia Preprints pp. 381-394.
- Lodewijks, G. (1995c), "The two-dimensional behaviour of belt conveyors", *Proceedings of the Beltcon 8 Conference*, 24-26 October 1995, Pretoria, South Africa.
- Lodewijks, G. (1995d), "Dynamics of Belt Conveyor Systems", *Proceedings of the International Powder & Bulk Solids Conference Europe: BULK '95*, Utrecht, The Netherlands, 30 October - 3 November 1995.
- Lodewijks, G. (1995e), "On the application of beam elements in finite element models of belt conveyors: part II", *Bulk Solids Handling* **15**, pp. 587-591.
- Mašin, O. (1972), "Die Lösung des Anlaufes von Gurtbandförderern mit Zweitrommelantrieb und hydrodynamischen Anlaufkupplungen", *Bergbautechnik* **22**, pp. 703-710.
- Matting, A. and Vierling, P. (1962), "Zum dynamischen Verhalten von Gummifördergurten mit Gewebereinlagen", *Fördern und Heben* **11**, page 355 and 414.
- Morrison, W.R.B. (1988), "Computer graphics techniques for visualising belt stress waves", *Bulk Solid Handling* **8**, pp. 221-227.
- Nordell, L.K. and Ciozda, Z.P. (1984), "Transient belt stresses during starting and stopping: Elastic response simulated by finite element methods", *Bulk Solids Handling* **4**, pp. 99-104.
- Nordell, L.K., Qui, X. and Sethi, V. (1991), "Belt conveyor steel cord splice analysis", *Bulk Solids Handling* **11**, pp. 863-868.
- Oehmen, H. (1959), *Das Anlaufverhalten von Förderbandanlagen*. Doctorate thesis, Hannover University of Technology.
- Oostveen, H.J. van (1987), *Simulatie van de beweging van een dynamische bandbuffer*, Delft University of Technology, Lab. Eng. Mech., report TM 866.
- Pankratov, S. A. (1963), "Näherungslösungen einiger Fragen der Dynamik von Bandförderern", *Wissenschaftliche Zeitschrift der Technischen Universität Dresden* **12**, pp. 1275-1282.
- Rao, K.R.M. (1973), "Computer study of starting phenomenon of a conveyor", *J. Inst. Eng. Mining Metal Division* **53 part MM**, pp. 109-113.

- Richolm, I. (1969), *Untersuchungen zur Entwicklung von automatischen Spannvorrichtungen mit besonderer Rücksicht auf das dynamische Verhalten der Gurtbandförderer*, Doctorate thesis, Bergakademie Freiberg.
- Richolm, I. (1970), "Über das dynamische Verhalten der Gurtförderer während des Anlaufs", *Bergbautechnik* **20**, pp. 138-144.
- Rottky, O. (1961), "Das Anfahren und Stillsetzen von langen Förderbändern", *Bergbautechnik* **11**, pp. 585-592.
- Schulz, G., (1985), *Beitrag zur Untersuchung des dynamischen Verhaltens von Gurtbandförderern unter besonderer Berücksichtigung mittels untersynchroner Stromrichter-kaskade stellbarer Antriebe*, Doctorate thesis, University of Freiberg.
- Schultz, G. (1995), "Comparison of drives for long belt conveyors", *Bulk Solids Handling* **15**, pp. 247-251.
- Segal, H. (1969), "Anwendung der elektrischen Analogie zur Bestimmung der dynamischen Kräfte beim Anlauf eines Fördergurtes", *Buletinul Institutului Politehnic Gheorghe gheorghin-dej Bucuresti* **31/6**, pp. 83-99.
- Shi, W.D. (1993a), *Stress analysis of the double overlap belt splice under longitudinal loads*, report 93.3.TT.4204, Delft University of Technology, Section of Transporttechnology.
- Shi, W.D. (1993b), *Stress analysis of the double overlap splice for aramid belt via ANSYS FEM program*, report 93.3.TT.4215, Delft University of Technology, Section of Transporttechnology.
- Shi, W.D. (1993c), *Stress analysis of Dunloflex belt splice via the DIANA FEM program*, report 93.3.TT.4221, Delft University of Technology, Section of Transporttechnology.
- Sobolski, R. (1963), "Anlaufbedingungen bei Gurtbandförderern", *Hebezeuge und Fördermittel* **3/9**, pp. 271-274.
- Surtees, A.J. (1986), "Longitudinal stresses occurring in long conveyor belts during starting and stopping", *Bulk Solids Handling* **6**, pp. 93-97.
- Tol, L.A.J. (1974), *Dynamische aanloopverschijnselen van bandtransporteurs*, report 499, Delft University of Technology, Section of Transporttechnology.
- Vasilev, V.G. and Tipikin, A.P. (1962), "Elektronisches Modell für einen langen vorgespannten Bandförderer", *Izvestija VUZ, Gronyj zurnal* **5/12**, pp. 154-161.
- Vierling, A. and Oehmen, H. (1958), "Messungen an Förderbandanlagen", *Braunkohle, Wärme und Energie* **9**, page 313.
- Vierling, A. (1961), "Ergebnisse weiterer Messungen an Förderbandanlagen", *Braunkohle, Wärme und Energie* **9**, pp. 41-52.
- Vierling, P. (1961), *Zum dynamischen Verhalten von Gummifördergurte mit Gewebeeinlagen*, Doctorate thesis, University of Hannover.
- Zur, T.W. (1966), "Verfahren zur Berechnung der Bandspanngeschwindigkeit bei Bandförderern", *Wegiel Brunatny* **8/2**, pp. 212-126.
- Zur, T.W. (1986a), "Visco-elastic properties of conveyor belts, modelling of vibration phenomena in belt conveyors during starting and stopping", *Bulk Solids Handling* **6**, pp. 85-91.
- Zur, T.W. (1986b), "Viscoelastic properties of conveyor belts, properties of aramid belts", *Bulk Solids Handling* **6**, pp.1163-1168.

## Chapter 8

# Numerical results of belt conveyor simulations

---

In this chapter results of simulations of the dynamic behaviour of a long belt conveyor system during non-stationary operation are given. The lay-out of the system is given in the first paragraph. In paragraph 8.2 the drive force and power, the required belt strength and type, and the masses of the conveyor components, which are required for the finite element models described in paragraph 8.3, are calculated according to DIN 22101. In paragraph 8.4 the results of a number of simulations are given which show the influence of model parameters on the simulated dynamic behaviour of the belt. In the fifth paragraph, the results of an approximate dynamic analysis of the start-up of the belt conveyor are given. In paragraph 8.6 these results are compared with the results obtained from finite element simulations, using the discrete model described in Chapter 7.

### 8.1 Problem description

Figure 8.1 depicts a typical horizontal belt conveyor lay-out. For reason of simplicity no horizontal or vertical curves, no trippers or booster drives etc. are considered. In Table 8.1 the relevant belt conveyor and bulk solid material data are given, where

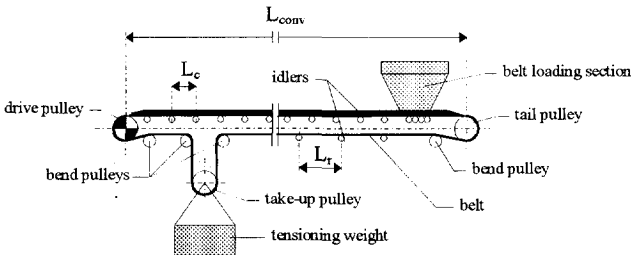


Figure 8.1: Horizontal belt conveyor lay-out.

$C_{des}$  is the design capacity and  $\varphi_0$  the angle of surcharge of the bulk solid material, see also Appendix A. In the design stage of the conveyor system, the most important consideration from the engineers point of

$C_{des} = 694.44 \text{ kg}\cdot\text{s}^{-1} (=2500 \text{ t/h})$	bulk solid = coal
$L_{conv} = 1000 \text{ m}$	$\rho_{bulk} = 850 \text{ kg}\cdot\text{m}^{-3}$
	$\phi_0 = 20^\circ$

Table 8.1: Conveyor belt data.

view is the calculation of the required belt type and size and drive power since they govern the size of all the other conveyor components. The drive power and belt type, although mainly determined by the forces that act on the belt during stationary operation of the belt system, are significantly influenced by the forces that act on the belt during non-stationary operation. Therefore, besides the calculation of the drive power and the belt strength, also a drive system and a start and stop procedure have to be selected. In the next paragraph a calculation of the drive power and the belt type according to DIN 22101 is given. The data obtained from this calculation are used to make a finite element model. With this model the dynamic behaviour of the belt during non-stationary operation of the conveyor is simulated to check the selection of the drive system, starting procedure and belt type.

## 8.2 Calculation according to DIN 22101

The design capacity of the conveyor can be calculated by:

$$C_{des} = \rho_{bulk} A_{bulk,des} V_b \tag{8.1}$$

where the subscript *des* refers to the design stage of the conveyor. Based on the data provided in Table 8.1, the belt width and trough shape, which determine the cross-sectional area of the bulk solid material, and the belt speed have to be chosen. From literature [Roberts et al., 1981] it is known that from the economical point of view the belt width *B* is limited to 1200 mm. If three-roll idlers are used with a trough angle of 35° and *B*=1200 mm then the maximum cross-sectional area of the bulk solid material on the belt can be obtained from equation (A.5):  $A_{bulk,max} = 0.1911 \text{ m}^2$ . With this area the required belt speed is  $4.3 \text{ m}\cdot\text{s}^{-1}$ . However, to include a safety margin for the belt capacity and to choose a DIN prescribed belt speed, the belt speed is chosen  $5.2 \text{ m}\cdot\text{s}^{-1}$ . The corresponding cross-sectional area of the bulk solid material on the belt obtained from equation (8.1):  $A_{bulk,des} = 0.1571 \text{ m}^2$ . The specific mass of the bulk solid material on the belt,  $m'_{bulk}$ , and the total mass of the bulk material,  $m_{bulk}$ , are:

$$m'_{bulk} = \rho_{bulk} A_{bulk,des} = 133.54 \text{ kg}\cdot\text{m}^{-1}; m_{bulk} = m'_{bulk} L_{conv} = 133,547 \text{ kg} \tag{8.2}$$



A five layer fabric belt EP 500/5, with a fabric thickness of 4.3 mm and rubber belt cover thicknesses of 2 and 4 mm, is selected<sup>1</sup>. The density of the rubber and the fabric material are  $1150 \text{ kg.m}^{-3}$  and  $1163 \text{ kg.m}^{-3}$  respectively. The average Young's modulus of the belt is 340.917 MPa. The specific mass of the belt,  $m'_{\text{belt}}$ , and the total belt mass,  $m_{\text{belt}}$ , are:

$$m'_{\text{belt}} = B (\rho_{\text{rubber}} d_{\text{covers}} + \rho_{\text{fabric}} d_{\text{fabric}}) = 14.28 \text{ kg.m}^{-1} \quad (8.3)$$

$$m_{\text{belt}} = 2 m'_{\text{belt}} L_{\text{conv}} = 28,560 \text{ kg}$$

The carrying part of the belt is supported by three-roll idler stations. The return part is supported by one-roll idlers. The idler spacing<sup>2</sup> for the carrying idlers,  $L_c$ , is chosen to be 1.5 m and the idler spacing for the return idlers,  $L_r$ , is 2.5 m. The rolls all have a diameter<sup>3</sup> of 0.133 m. The masses of a carrying roll,  $m_{\text{roll},c}$ , and a return roll,  $m_{\text{roll},r}$ , are 7.43 kg and 19.3 kg respectively. The average mass per unit length due to the idlers,  $m'_{\text{roll}}$ , is given by:

$$m'_{\text{roll},c} = \frac{n_c m_{\text{roll},c}}{L_c} = 14.87 \text{ kg.m}^{-1}; m'_{\text{roll},r} = \frac{n_r m_{\text{roll},r}}{L_r} = 7.72 \text{ kg.m}^{-1} \quad (8.4)$$

$$m'_{\text{roll}} = m'_{\text{roll},c} + m'_{\text{roll},r} = 22.59 \text{ kg.m}^{-1}$$

where the indices c and r indicate the carrying and return part respectively;  $n_c$  and  $n_r$  are the number of rolls in the carrying and return idler stations. According to Simonsen (1987) the reduced mass of the idler rolls, which is the mass to be added to the belt to take into account the inertia effect of the rolls, is about 90 % of the mass of the roll:

$$m'_{\text{red},rc} = 0.9 m'_{\text{roll},c} = 13.38 \text{ kg.m}^{-1}; m'_{\text{red},rr} = 0.9 m'_{\text{roll},r} = 6.95 \text{ kg.m}^{-1} \quad (8.5)$$

$$m'_{\text{red},r} = m'_{\text{red},rc} + m'_{\text{red},rr} = 20.33 \text{ kg.m}^{-1}; m_{\text{red},r} = m'_{\text{red},r} L_{\text{conv}} = 20,328 \text{ kg}$$

The total stationary drive force can be calculated in approach of DIN 22101:

<sup>1</sup> This choice has to be checked at the end of the calculations. The parameters of the rubber material of the belt covers are already given in Section 5.2.1.

<sup>2</sup> At the end of the calculations the belt sag has to be calculated to check this choice.

<sup>3</sup> This choice depends on the belt width and belt speed. The roll parameters are already given in Section 5.2.2.

$$F_{dc} = C f L_{conv} (m'_{roll,c} + m'_{belt} + m'_{bulk})g ; F_{dr} = C f L_{conv} (m'_{roll,r} + m'_{belt})g \quad (8.6)$$

$$F_d = F_{dc} + F_{dr} = C f L_{conv} (m'_{roll} + 2 m'_{belt} + m'_{bulk})g$$

where  $C$  is the ratio between the total resistance force including the effects of accessories like side skirts and the main resistance force calculated above, and  $f$  the effective friction coefficient which is the average friction coefficient for the carrying and the return part of the belt. For a belt conveyor length of 1000 m the DIN standard prescribes a  $C$  factor of 1.09. The effective friction factor  $f$  is chosen to be 0.018 in accordance with the results of a calculation of the rolling resistance with the model as described in Section 5.2. The drive forces for an unloaded and a loaded belt are, with equation (8.6):

$$F_{dc(empty)} = 5.61 \text{ kN} \quad F_{dr(empty)} = 4.23 \text{ kN} \quad F_{d(empty)} = 9.85 \text{ kN}$$

$$F_{dc(loaded)} = 31.32 \text{ kN} \quad F_{dr(loaded)} = 4.23 \text{ kN} \quad F_{d(loaded)} = 35.55 \text{ kN}$$

The maximum drive force during start-up of a belt conveyor is:

$$F_{dA} = \frac{P_{dn} \eta_d}{V_b} K_A \quad (8.7a)$$

where the subscript  $A$  denotes acceleration,  $P_{dn}$  is the nominal drive power,  $\eta_d$  the drive efficiency and  $K_A$  is a drive-system dependent start-up factor, see Table 8.2. The start-up factor is considerably influenced by the inertia of the drive system. The start-up factor of high inertia drive systems is lower than given in Table 8.2. If the nominal drive power, accounting for the drive efficiency, is equal to the required stationary drive power then equation (8.7a) can be simplified to:

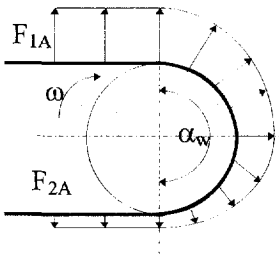
$$F_{dA} = F_d K_A \quad (8.7b)$$

Drive system	Start-up factor $K_A$
induction motor, drain-type fluid coupling controlled start-up	1.2
induction motor, resistance stepped start-up	1.4
induction motor, normal fluid coupling controlled start-up	1.5
induction motor, star delta switched start-up	1.6
induction motor, direct start-up	2-3

Table 8.2: Start-up factors, [Simonsen, 1987].

In case of a drain-type fluid coupling controlled start-up, assuming that the nominal drive power is equal to the required stationary drive power, the maximum drive forces for an unloaded and a loaded belt are, with equation (8.7b):

$$F_{dA(\text{empty})} = 11.82 \text{ kN} ; F_{dA(\text{loaded})} = 42.66 \text{ kN}$$



To enable transmission of the drive power from the drive pulley to the belt a minimum belt tension is necessary to prevent slip. The maximum ratio between the belt tension before the drive pulley,  $F_{1A}$ , and after the drive pulley,  $F_{2A}$ , during start-up can be calculated with the Euler-Eytelwein equation [Kuhnert and Schulz, 1995]:

**Figure 8.2:** Belt tension distribution over a driven pulley.

$$\frac{F_{1A}}{F_{2A}} \leq \exp(\mu_{bp} \alpha_w) \quad (8.8)$$

where  $\alpha_w$  is the wrap angle and  $\mu_{bp}$  the friction coefficient between the belt and the pulley. In the considered belt conveyor the wrap angle is  $\alpha_w = \pi$  and an approximate friction coefficient is  $\mu_{bp} = 0.35$  [DIN 22101]. The maximum difference in belt tension before and after the drive pulley is equal to the drive force during start-up:

$$F_{1A} - F_{2A} = F_{dA} \quad (8.9)$$

With the equations (8.8) and (8.9), the minimum belt tension for an accelerating loaded belt  $F_{2A} = 21.33 \text{ kN}$  and for a stationary moving loaded belt  $F_2 = 17.78 \text{ kN}$ . The minimum tensioning force<sup>4</sup> required to enable transmission of the drive power of an accelerating belt is twice the force  $F_{2A}$ :  $F_v = 42.66 \text{ kN}$ . Therefore, also in case of a stationary moving belt the minimum belt tension is  $21.33 \text{ kN}$ . The maximum belt tension for an accelerating belt  $F_{1A} = F_{2A} + F_{dA} = 63.99 \text{ kN}$  and for a stationary moving belt  $F_1 = F_{2A} + F_d = 56.88 \text{ kN}$ . The belt safety factor on the tension of a stationary moving belt, see also Section 3.1.4, is  $S_B = 8$ . Therefore the required strength capacity per unit width is:

$$k = \frac{S_B F_1}{B \eta_{\text{splice}}} = 474 \text{ N} \cdot \text{mm}^{-1} \quad (8.10)$$

<sup>4</sup> With this force and the selected idler spacings, the belt sag is below 1.5 %.

where the belt splice efficiency taken to be  $\eta_{\text{splice}}=0.80^5$ . This shows that the strength of the selected belt type of  $500 \text{ N}\cdot\text{mm}^{-1}$  is sufficient for this application. The required drive power  $P_d$  for a stationary moving fully loaded belt is:

$$P_d = \frac{V_b F_d}{\eta_d} = 205.4 \text{ kW} \quad (8.11)$$

The efficiency of the drive system is assumed to be  $\eta_d=0.90$ . A drive power of  $P_d=250 \text{ kW}$  is selected. The angular speed of the drive pulley  $\omega_d$  with radius  $R_d=0.6 \text{ m}$  is<sup>6</sup>:

$$\omega_d = \frac{V_b}{R_d} = 8.67 \text{ s}^{-1} \quad (8.12)$$

The motor has a nominal angular speed  $\omega_m=155.93 \text{ s}^{-1}$  which yields the necessary reduction factor of the gearbox:

$$i = \frac{\omega_d}{\omega_m} = 17.99 \quad (8.13)$$

The inertia of the selected motor<sup>7</sup> reduced to a mass on the drive pulley radius is:

$$m_{\text{red,m}} = \frac{i^2 J_m}{R_d^2} \approx 6,654 \text{ kg} \quad (8.14)$$

where the moment of inertia of the motor is  $J_m=7.4 \text{ kg}\cdot\text{m}^2$ . The inertia of the gearbox reduced to a mass on the drive pulley radius is:

$$m_{\text{red,g}} = \frac{J_g}{R_d^2} \approx 37 \text{ kg} \quad (8.15)$$

where the moment of inertia of the gearbox reduced on the motor axis is  $J_g=13.3 \text{ kg}\cdot\text{m}^2$ . The reduced mass of the steel drive pulley, neglecting the pulley ends, is:

---

<sup>5</sup> The belt splice efficiency of a multi-layer fabric belt can be estimated by dividing the number of fabric layers minus one by the number of fabric layers. This results in a splice efficiency of 4/5 for the five layer fabric belt in the considered belt conveyor.

<sup>6</sup> The minimum diameter of the pulleys is prescribed by the conveyor belt manufacturer.

<sup>7</sup> For example type DKR 355 M-4, see the Vector brochure on Squirrel cage induction motors.

$$m_{\text{red,dp}} = \frac{J_{\text{dp}}}{R_d^2} \approx \frac{\frac{1}{2} \pi \rho_{\text{pulley}} b_{\text{pulley}} (R_d^4 - R_{d,\text{in}}^4)}{R_d^2} = 1606 \text{ kg} \quad (8.16)$$

where the density of the pulley material  $\rho_{\text{pulley}}=7850 \text{ kg.m}^{-3}$ , the width of the drive pulley  $b_{\text{pulley}}=1.5 \text{ m}$  and the inner radius of the pulley  $R_{d,\text{in}}=0.56 \text{ m}$ . The drive pulley, the tension pulley and the tail pulley are equal. The steel bend pulleys have a radius of 0.2 m, an inner radius of 0.17 m and a width of 1.5 m. The reduced mass of the bend pulleys is equal to:

$$m_{\text{red,bp}} = \frac{J_{\text{bp}}}{R_s^2} \approx \frac{\frac{1}{2} \pi \rho_{\text{pulley}} b_{\text{pulley}} (R_s^4 - R_{s,\text{in}}^4)}{R_s^2} = 354 \text{ kg} \quad (8.17)$$

The drive torque  $T_d$  for a stationary moving belt is:

$$T_d = F_d R_d = 21.33 \text{ kNm} \quad (8.18)$$

The combination of the drive power/torque and reduction factor is used to select the gearbox<sup>8</sup>.

### 8.3 Finite element models

In this chapter three finite element models are used which are shown in Figure 8.3. Model 1 consists of 20 truss elements with bending deformation and has 21 degrees of freedom; only the conveyor belt is discretised. Each element models a belt segment of 100 m. In model 2 the induction motor and the gear box are included in the model. Therefore two torsion elements, one reduction box element and a pulley transition element are added to the truss elements. Taking all constraints into account this yields two extra degrees of freedom. Model 3 is almost equal to model 2 but it includes a detailed analysis of one idler supported belt section 25 m from the drive pulley, see Figure 8.3. The idler spacing is 1.5 m. This demands additional beam elements (nodes 5-12). Each beam element models a belt segment of about 0.5 m. Model 3 has 43 degrees of freedom. The belt is tensioned by either a weight tensioner or a winch tensioner. The weight tensioner is shown in Figure 8.3. In case of a controlled (ideal) winch tensioner the weight is replaced by a constant tension force. The element types of the three models are listed in Table 8.3, more information on specific elements can be found in Chapter 7.

<sup>8</sup> For example type KH 186, see the brochure Vector squirrel cage induction motors.

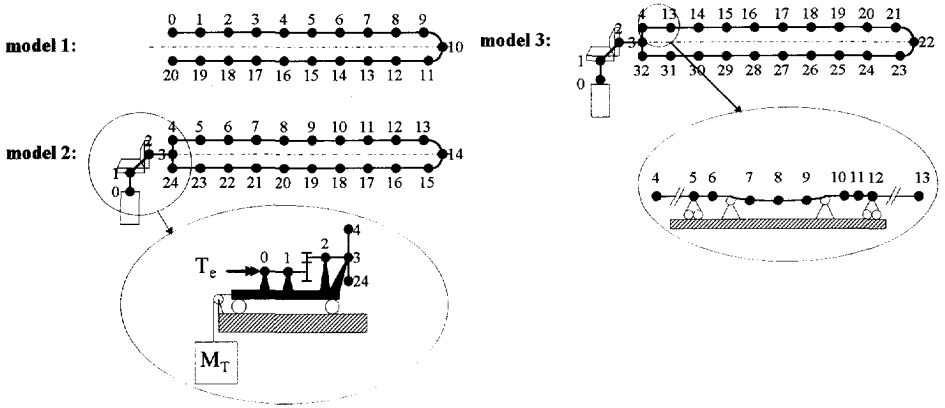


Figure 8.3: Model 1, 2 & 3.

elementnr.	model 1	model 2	model 3	p node	q node
0	truss	torsion	torsion	0	1
1	truss	reduction box	reduction box	1	2
2	truss	torsion	torsion	2	3
3	truss	pulley transition	pulley transition	3	4
4	truss	truss	truss	4	5
5	truss	truss	beam	5	6
6	truss	truss	supported beam	6	7
7	truss	truss	beam	7	8
8	truss	truss	beam	8	9
9	truss	truss	supported beam	9	10
10	truss	truss	beam	10	11
11	truss	truss	beam	11	12
12	truss	truss	truss	12	13
13	truss	truss	truss	13	14
14	truss	truss	truss	14	15
15	truss	truss	truss	15	16
16	truss	truss	truss	16	17
17	truss	truss	truss	17	18
18	truss	truss	truss	18	19
19	truss	truss	truss	19	20
20	-	truss	truss	20	21
21	-	truss	truss	21	22
22	-	truss	truss	22	23
23	-	truss	truss	23	24
24	-	-	truss	24	25
25	-	-	truss	25	26
26	-	-	truss	26	27
27	-	-	truss	27	28
28	-	-	truss	28	29
29	-	-	truss	29	30
30	-	-	truss	30	31
31	-	-	truss	31	32

Table 8.3: Element types in model 1, 2 & 3.

## 8.4 Model implications

In this section the results of a number of simulations are given which show the influence of the model parameters on the dynamic behaviour of the belt. The considered subjects are the axial and transverse vibration of a belt segment, the propagation of longitudinal waves and the motion of bulk material on the belt.

### 8.4.1 Frequency of axial vibration

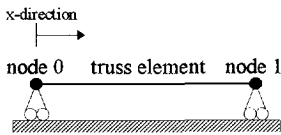


Figure 8.4: Truss element.

Figure 8.4 shows a belt segment modelled by one truss element. It is known from Chapter 4 that the first natural frequency of axial vibration of a belt segment with length  $L$  is given by:

$$\omega = \frac{\pi}{L} c_1 \quad (8.19)$$

Hence the period of axial vibration is:

$$\tau = \frac{2\pi}{\omega} = \frac{2L}{c_1} \quad (8.20)$$

The first natural frequency and corresponding period of axial vibration of a linear truss element, using a consistent mass matrix, are:

$$\omega = \frac{2\sqrt{3}}{L} c_1, \quad \tau = \frac{\pi L}{\sqrt{3} c_1} \quad (8.21)$$

The influence of the belt tension dependent sag may approximately be taken into account by using the effective Young's modulus (7.16). In that case the wave speed  $c_1$  in the equations (8.20) and (8.21) is replaced by  $c_1^*$  which is defined by:

$$c_1^* = \sqrt{\frac{E_{b,\text{eff}}}{\rho_{\text{belt}}}} = c_1 \sqrt{\frac{1}{1 + \frac{(qL)^2 E_b A}{12T^3}}} \quad (8.22)$$

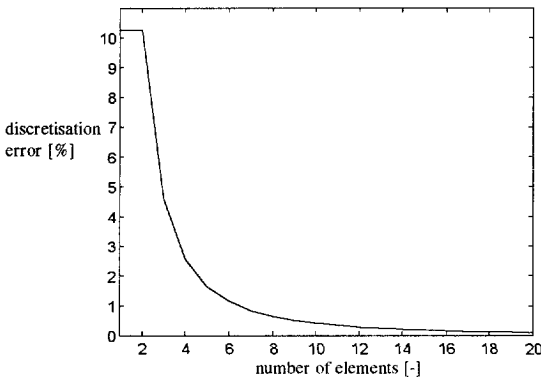
With Young's modulus of the belt  $E_b = 340.917$  MPa and the belt density  $\rho_b = 1155.34$  kg.m<sup>-3</sup>, the propagation speed of the axial waves is equal to 543.21 m/s. If the length of the element is the total belt length of 2000 m, then the approximate lowest

frequency and corresponding period of axial vibration of the truss element are given in Table 8.4. The differences between the periods of axial vibration imply that the (apparent) axial wave speed in a finite element model which consists of one truss element, using a consistent mass matrix, will be about 10.3 % higher than in the real belt. This is caused by the assumption that the axial displacement of the belt can be approximated by a linear displacement function (7.32). However, from equation (4.97) it can be seen that axial displacement function is not linear. Applying more truss elements will result in a better approximation of the real displacement field. The discretization error will therefore decrease with increasing number of truss elements, see Figure 8.5. In the finite element models 1-3 20 truss elements have been used. The discretization error on the lowest natural frequency is in that case 0.103 %.

	frequency [rad.s <sup>-1</sup> ]	period [s]
Analytic	0.853	7.364
Consistent mass	0.941	6.678

**Table 8.4:** Lowest frequency and period of axial vibration. Analytical solution and solution using a truss element.

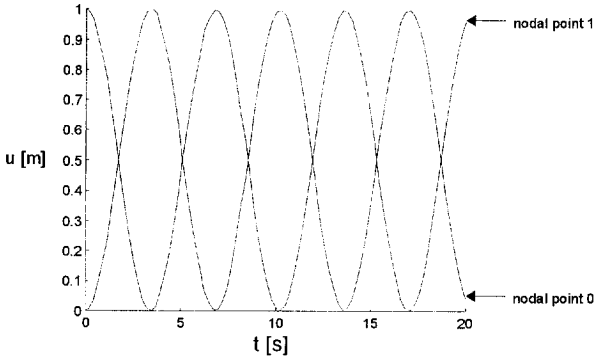
To check the integration procedure of **TUDBELT**, the free vibration of a 2000 m long truss element with an initial displacement of nodal point 1 of 1 m has been simulated. Figure 8.6 shows the axial displacements  $u$  of the two nodal points. The period of vibration is exactly as given in Table 8.4. The maximum relative error



**Figure 8.5:** Relative error between the analytical solution and the solution using truss elements for the lowest natural frequency of axial vibration (symmetric vibration).

between the frequencies given in Table 8.4 and those obtained from the simulations is 0.04 % which confirms the accuracy of the used integration procedure. Accounting for the discretization error of 20 elements, the maximum relative error between the analytical solution and the solution found by **TUDBELT** for the lowest frequency of the natural axial vibration using 20 truss elements is 0.15 %.





**Figure 8.6:** Nodal point displacement for a linear truss element with consistent mass matrix (symmetric vibrations).

## 8.4.2 Frequency of transverse vibration

In Section 8.4.1 the frequency of axial vibration of a belt segment modelled by a truss element has been considered. In this section the lowest frequency of free transverse vibrations is considered. To determine whether or not the beam elements can be used to accurately model the belt, nine test cases are considered as depicted in Table 8.5. In the first three cases a belt segment of 1.5 m is clamped at one side whereas it is free to move at the other end (clamped-free belt). The analytical result for the first natural frequency of small amplitude transverse vibration of the clamped-free belt in the cases 1-3 is [Den Hartog, 1956]:

$$f = \frac{3.516}{2\pi} \sqrt{\frac{E_b I_y}{\rho A L^4}} \quad (8.23)$$

In case 4 an end load of 12.5 N is applied at  $t=0$  to a beam element at rest. Due to the low bending stiffness, the amplitudes of vibration are large. In case 5 a belt segment of 3 m is clamped at both sides. The analytical result for the first natural frequency of small amplitude transverse vibration of a clamped-clamped beam is [Den Hartog, 1956]:

$$f = \frac{22.0}{2\pi} \sqrt{\frac{E_b I_y}{\rho A L^4}} \quad (8.24)$$

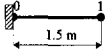
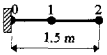
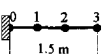

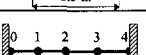
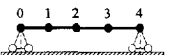
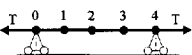
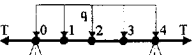
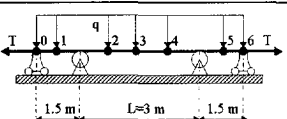
case		Analytical solution [Hz]	TUDBELT solution [Hz]	relative error [%]
1		0.402	0.409	1.8
2		0.402	0.405	0.8
3		0.402	0.403	0.4
4		-	0.382	-
5		.628	0.630	0.4
6		0.282	0.284	0.7
7		2.625	2.636	0.4
8		2.625	2.636	0.4
9		-	2.842	-

Table 8.5: Results for the first natural frequency of transverse vibration.

In case 6 both ends of the belt are free to translate and rotate. The analytical result for the first natural frequency of small amplitude transverse vibration of a simply supported belt is [Den Hartog, 1956]:

$$f = \frac{\pi}{2} \sqrt{\frac{E_b I_y}{\rho A L^4}} \quad (8.25)$$

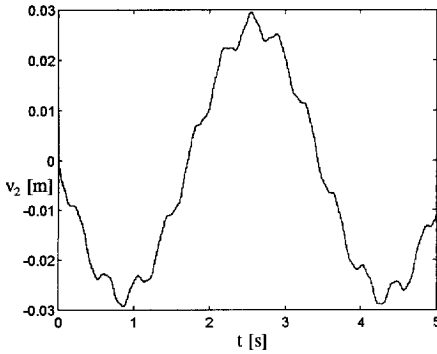
In case 7, which has already been considered in Chapter 4, the belt is pre-tensioned ( $T=3500$  N). In the cases 8 and 9 the gravity load is applied. In case 8 the belt is simply supported and in case 9 the belt is also supported by two idler supports, see also Section 7.2.1.4. Due to the high pre-tension, the deflection of the belt in case 8 is very small and therefore the non-linear effects in this case are negligible. The effect of bending of the belt (on the idler supports) can be determined by consideration of the differences between the results of the cases 8 and 9. The relevant belt parameters used in the examples are:

$$\rho = 1155.34 \text{ kg.m}^{-3} ; A = 0.01236 \text{ m}^2 ; E_b = 340.917 \cdot 10^6 \text{ N.m}^{-2}$$

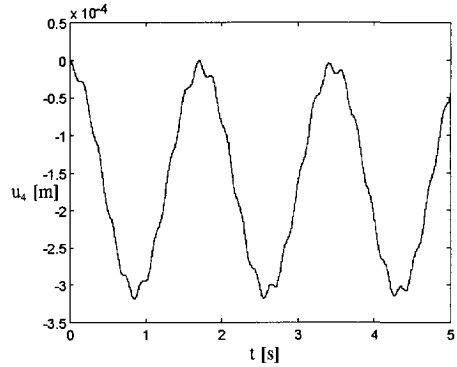
$$I_y = 1.093 \cdot 10^{-7} \text{ m}^4 ; L = 1.5 - 3 \text{ m} ; T = 3500 \text{ N}$$

The first transverse vibration mode of the belt can in good approximation be described by the finite element model made of beam elements since the shape functions of the beam element are of the third order. The accuracy can be improved by increasing the number of elements as can be learned from the results of the cases 1-3. The vibration was initiated by giving the nodal points 1, 2 and 3 of respectively case 1, 2 and 3 an initial transverse velocity of  $-0.1 \text{ m.s}^{-1}$ . In case 4 nodal point 1 and in the cases 5-8 nodal point 2 was given an initial transverse velocity of  $-0.1 \text{ m.s}^{-1}$ . In case 9 the initial transverse velocity of nodal point 3 was  $-0.1 \text{ m.s}^{-1}$ . The amplitude of vibration varies from 0.05 m in case 1 to 0.025 m in case 3. In case 4 the displacements are large, with a maximum of about 0.8 m. Since only one element is used the solution for the first natural frequency of the large amplitude vibration is not very accurate. However, the solution indicates that the belt load may cause large displacements and hence requires a non-linear solution for a not pre-tensioned low stiffness beam. Comparison of the frequencies of the cases 7 and 8 show that in case 8 the influence of the gravity load is almost negligible due to the pre-tension of 3500 N.

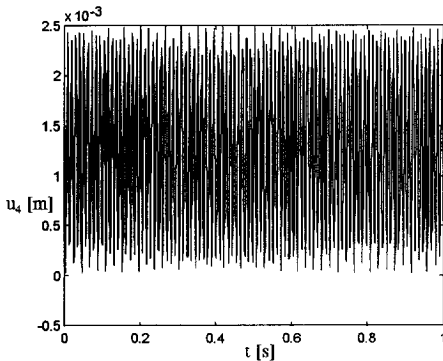
Figure 8.7 shows the transverse displacement of the middle of the belt segment, nodal point 2, of case 6. The frequency of transverse vibration is 0.284 Hz. The frequency of forced longitudinal vibration, due to the transverse vibration, is 0.568 Hz which is twice this frequency. The longitudinal displacement of one end of the belt, nodal point 4, is shown in Figure 8.8.



**Figure 8.7:** Transverse displacement of nodal point 2 of the simply supported beam (case 6).



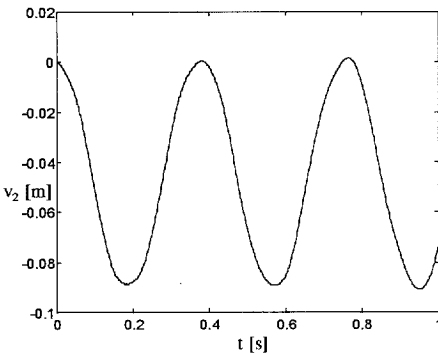
**Figure 8.8:** Axial displacement of nodal point 4 of the simply supported beam (case 6).



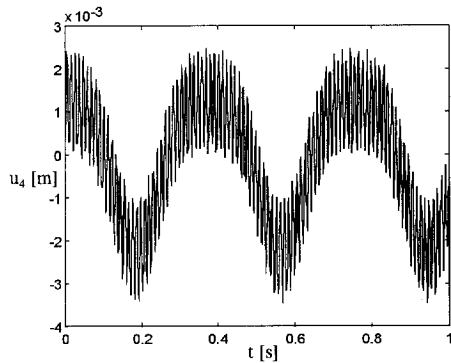
**Figure 8.9:** Axial displacement of nodal point 4 of the simply supported beam (case 7).

Figure 8.9 shows the axial displacement of nodal point 4 of case 7 which in that case is governed by the free longitudinal vibration. The frequency of longitudinal vibration which is obtained from Figure 8.9 is 93.284 Hz which is about 3.0 % higher than the first natural frequency obtained from equation (8.18). The influence of the transverse vibration on the longitudinal vibration of the belt can not be seen in Figure 8.9. This is caused by the differences in amplitude of both longitudinal vibrations. The amplitude is about  $3 \cdot 10^{-4}$  for the forced

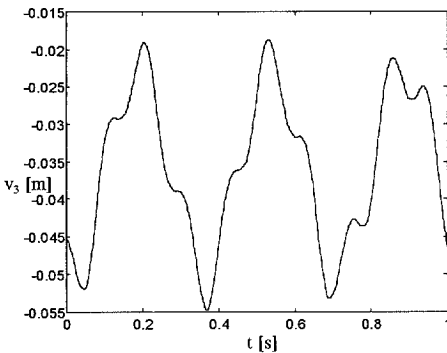
longitudinal vibration due to the transverse vibration and about  $2.5 \cdot 10^{-3}$  for the natural longitudinal vibration. The amplitude of the forced longitudinal vibration increases considerably when the belt load due to the weight of the belt is considered (case 8&9). In that case both frequencies of longitudinal vibration can be determined. Figure 8.10 shows the transverse displacement of the middle of the belt, nodal point 2, of case 8. The frequency of transverse vibration is 2.632 Hz. From Figure 8.11, which shows the longitudinal displacement of one belt end, two frequencies, 2.632 Hz and 93.400 Hz, are obtained. In this case the dominant frequency of forced longitudinal vibration is equal to, and not twice, the frequency of transverse vibration, because of the belt sag.



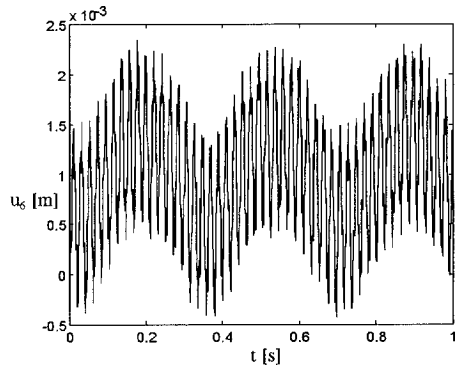
**Figure 8.10:** Transverse displacement of nodal point 2 of the simply supported beam (case 8).



**Figure 8.11:** Axial displacement of nodal point 4 of the simply supported beam (case 8).



**Figure 8.12:** Transverse displacement of nodal point 3 of the idler supported beam (case 9).



**Figure 8.13:** Axial displacement of nodal point 6 of the idler supported beam (case 9).

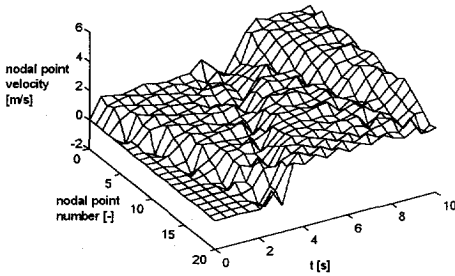
The belt sag, which is the mean transverse displacement of the belt, is 1.5 % of the idler spacing as was intended. If two idler supports are used and in addition two pin supports, then extra stiffness is introduced in the model. The frequency of transverse vibration, which can be obtained from Figure 8.12, is 2.842 Hz which is 7.8 % higher than in case of pin supports (case 7). The frequencies of longitudinal vibration, which are obtained from Figure 8.13, are 2.842 Hz and 47.441 Hz. The natural frequency of longitudinal vibration is in this case 4.8 % higher than the analytical result. In case 7, this frequency was 1.5 % higher than the analytical result.

In model 3 four beam elements are used to model the belt segment between the two idlers. From Table 8.5 it follows that the maximum relative error between the **TUDBELT** solution and the analytic solution for the lowest frequency of transverse vibration in that case is 0.7 %.

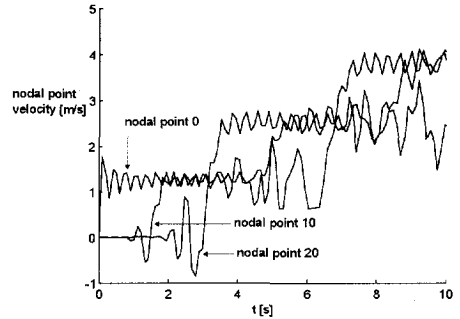
### 8.4.3 Wave propagation

In Section 3.1.4 formulations were given for the velocity of longitudinal waves,  $c_1$ . To illustrate the difference in velocity of longitudinal waves travelling through an unloaded and waves travelling through a loaded belt, two simulations have been made. For these simulations finite element model 1 has been used. In both simulations the belt was started by a constant drive force and the reduced masses of the idlers and pulleys were neglected.

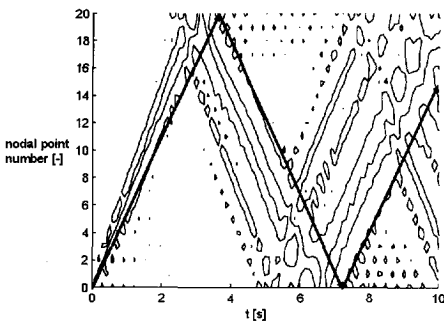
In the first simulation the whole belt was unloaded and therefore the mass of the nonlinear truss elements was only determined by the specific mass of the belt. Since all elements model a belt segment of the same length, the mass of all elements was equal. Figure 8.14 shows the first 10 seconds of the start-up of the unloaded belt



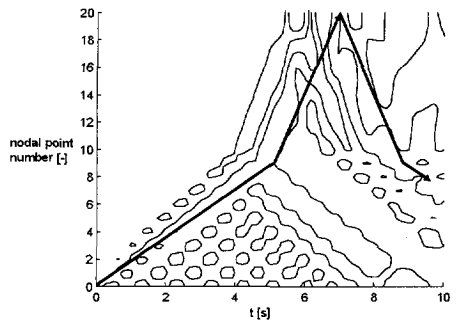
**Figure 8.14:** Longitudinal nodal point velocity during start-up of the unloaded belt conveyor.



**Figure 8.15:** Longitudinal velocity of nodal points 0, 10 and 20 during start-up of the unloaded belt conveyor.



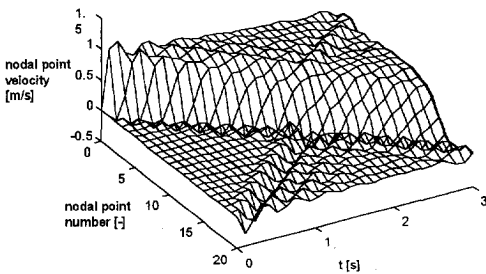
**Figure 8.16:** Contour plot of the longitudinal velocity of the nodal points during start-up of the unloaded belt conveyor.



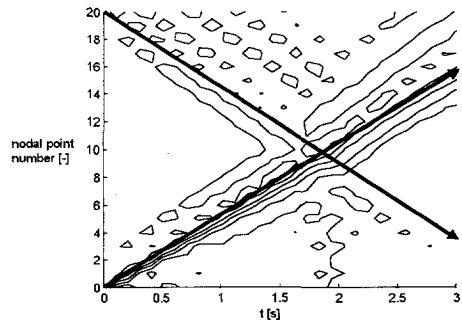
**Figure 8.17:** Contour plot of the longitudinal velocity of the nodal points during start-up of a loaded belt conveyor.

conveyor. On  $t=0$  s a velocity wave departs from the head of the belt (node 0) with a constant wave velocity  $c_1=543.21$  m/s. It passes the tail pulley (node 10) at  $t=1.9$  s and arrives at the end of the belt (node 20) on  $t=3.7$  s. Then it reflects against the tensioning pulley (node 20) and returns to the head of the belt where it arrives at  $t=7.4$  s. Figure 8.15 shows the belt velocity versus time at the head (node 0), the tail (node 10) and tensioning pulley (node 20). Note that the speed jump, and not the preceding speed variation, represents the head of the velocity wave. Figure 8.16 is a contour plot of Figure 8.14 which shows the stationary propagation of the stress wave through the belt. The wave speed  $c_1$  is constant through the whole belt.

In the second simulation the carrying part of the belt was loaded. In that case the mass of the elements was determined by the sum of the specific mass of the belt and that of the bulk solid material. Therefore the mass of the elements modelling a segment of the (loaded) carrying part was higher than the mass of elements modelling a segment of the return part. As a result, longitudinal waves propagate slower through elements modelling a segment of the carrying part than they do through elements modelling a segment of the return part of the belt. In model 1 the elements 0 through 9 (nodal points 0 through 10) model a loaded belt segment. Figure 8.17 shows a contour plot of the start-up of the loaded conveyor. With a specific bulk mass,  $m'_{\text{bulk}}=133.54$  kg.m<sup>-1</sup>, and a specific belt mass,  $m'_{\text{belt}}=14.28$  kg.m<sup>-1</sup>, the factor  $C_1=0.31$ , see also Section 3.1.4. Therefore the wave speed in the loaded belt part is  $c_1=168.8$  m/s. The different velocities of longitudinal waves in the load carrying part and the unloaded return part are visible in Figure 8.17. Figure 8.18 shows a start-up of the unloaded belt conveyor with the reduced mass of the tensioning pulley. This reduced mass is equally distributed over the nodal points 0 and 20. Besides the longitudinal wave departing from the drive pulley (node 0), also a longitudinal wave with a small negative velocity departs from the tensioning pulley due to the inertia of that pulley. This can also be seen in the contour plot Figure 8.19.



**Figure 8.18:** Longitudinal velocity of the nodal points during start-up of an unloaded belt conveyor with tension pulley inertia.



**Figure 8.19:** Contour plot of the longitudinal velocity of the nodal points during start-up of an unloaded belt conveyor with tension pulley inertia.

### 8.4.4 Bulk solid material stream

As introduced in Chapter 7, models made of beam elements require a different description of the transported bulk material than models made of truss elements.

In case of a belt conveyor system modelled by beam elements, where the elements actually move through the conveyor, the mass of the elements modelling a loaded belt segment is increased by the mass of the bulk solid material on that segment. This mass is constant as long as the belt segment is loaded and no further action has to be taken to control the mass flow of the bulk solid material.

In case of a belt conveyor system modelled by truss elements, the elements remain in their place relative to the conveyor and the bulk solid material stream moves through the element grid. This is illustrated in Figure 8.20 for a truss element representing three belt sections. The belt loading degree ratio  $k_{LD}$ , shown in Figure 8.20, indicates the ratio between the actual and the maximum mass of the bulk solid material on the belt. The maximum or design mass of the bulk solid material on the belt is prescribed by the design capacity of the conveyor. The belt can to a certain extent be overloaded, the maximum load being described by design standards. In that case the actual production exceeds the design capacity. Since the maximum value of the belt loading degree ratio is one, overloading can be realised by increasing the area of the cross section of the bulk solid material in the model and thus increasing the capacity of the belt.

In Figure 8.20 the length of a segment of the bulk solid body, which is the product of the belt loading time and the belt speed, is chosen to be equal to the element length. If the length of one element is longer than the length of the bulk solid material body then the length of the elements must be decreased to represent accurately the actual bulk solid material stream.

To calculate the correct mass of an element during a simulation, the mass balance of bulk solid material on the belt is determined every time step for the belt elements. The maximum mass of the bulk solid material on a belt part modelled by a belt element is:

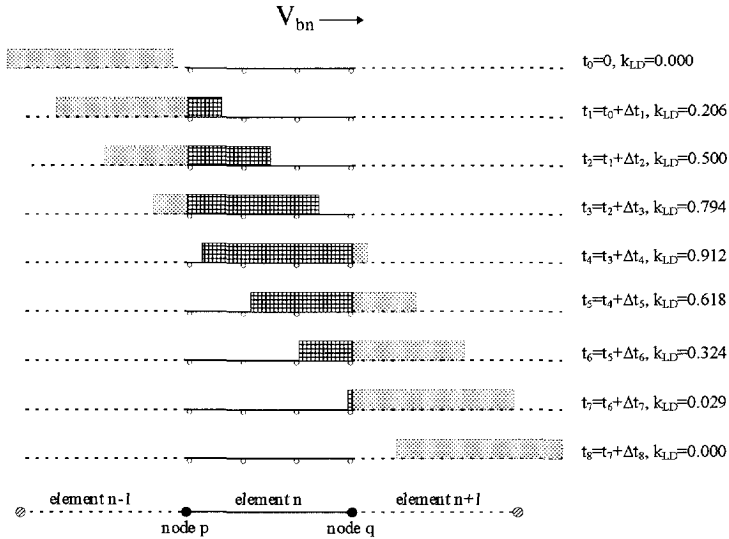
$$M_{\max}^n = \rho_{\text{bulk}} A_{\text{bulk,des}} L_n \quad (8.26)$$

where  $n$  indicates the element number and  $L_n$  is the element length. At time  $t$  the actual mass of the bulk solid material in the belt element is:

$$M^n(t) = M_{\max}^n k_{LD}^n(t) \quad (8.27)$$

where  $k_{LD}^n(t)$  is the loading degree ratio.





**Figure 8.20:** Flow of bulk material through a truss element.

The mass which enters the belt element is equal to the mass which leaves the foregoing element:

$$M_{in}^n(t) = M_{out}^{n-1}(t) \quad (8.28)$$

The mass which leaves the element is:

$$\begin{aligned}
 k_{LD}^n(t) = 0 &\Rightarrow M_{out}^n(t) = 0 && ; V_{bn}(t)\Delta t < L_n \\
 k_{LD}^n(t) = 1 &\Rightarrow M_{out}^n(t) = \rho_{bulk} A_{bulk,des} V_{bn}(t)\Delta t
 \end{aligned} \quad (8.29a)$$

If  $0 < k_{LD}^n(t) < 1$  then two cases can occur. In the first case bulk material is present at node p and the bulk material body has not yet reached node q of the element, see  $t_1-t_3$  of Figure 8.20. In that case the mass which leaves the element is:

$$\begin{aligned}
 (1 - k_{LD}^n(t)) L_n \geq V_{bn}(t)\Delta t &\Rightarrow M_{out}^n(t) = 0 \\
 (1 - k_{LD}^n(t)) L_n < V_{bn}(t)\Delta t &\Rightarrow M_{out}^n(t) = \rho_{bulk} A_{bulk,des} (V_{bn}(t)\Delta t - (1 - k_{LD}^n(t)) L_n)
 \end{aligned} \quad (8.29b)$$

In the second case no bulk material is present at node p and the bulk material body has not yet left the element, see  $t_4$ - $t_7$  of Figure 8.20 and the mass which leaves the element is:

$$\begin{aligned}
 k_{LD}^n(t) L_n \geq V_{bn}(t)\Delta t &\Rightarrow M_{out}^n(t) = \rho_{bulk} A_{bulk,des} V_{bn}(t)\Delta t \\
 k_{LD}^n(t) L_n < V_{bn}(t)\Delta t &\Rightarrow M_{out}^n(t) = \rho_{bulk} A_{bulk,des} k_{LD}^n(t) L_n
 \end{aligned}
 \tag{8.29c}$$

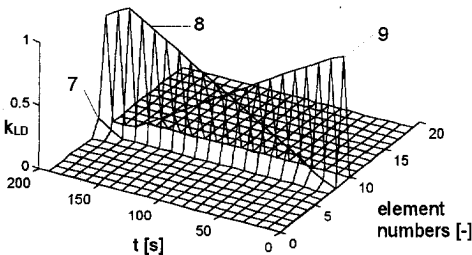
At time  $t + \Delta t$  the actual mass of the bulk solid material in the element is:

$$M^n(t + \Delta t) = M^n(t) + M_{in}^n(t) - M_{out}^n(t)
 \tag{8.30}$$

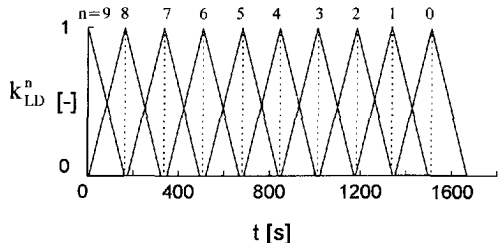
Substitution of the equations (8.26) till (8.29) in (8.30) yields the loading degree ratio  $k_{LD}^n(t + \Delta t)$ :

$$k_{LD}^n(t + \Delta t) = \frac{M^n(t + \Delta t)}{M_{max}^n}
 \tag{8.31}$$

To check this procedure, a simulation, using finite element model 1, has been made of the movement of the bulk solid material through the elements for a stationary moving belt. The simulation starts with a fully loaded belt element 9 and a stationary belt speed of 0.60 m/s. Element 9 is not being reloaded during simulation. The figure 8.21 and 8.22 show the loading degree ratio of the elements. As can be seen the belt loading ratio of element 9 decreases linearly, whereas the belt loading degree of element 8 increases linearly. With a belt speed of 0.60 m/s and a belt element length of 100 m, element 9 should be unloaded and element 8 should be fully loaded after 167 seconds. This is confirmed by the results of the simulation. As may be expected, the total carrying part of the belt, which has a length of 1000 m, is unloaded after 1667 seconds.



**Figure 8.21:** Surface plot of the loading degree ratio  $k_{LD}$  during the first 200 seconds of belt motion.



**Figure 8.22:** Side view of surface plot of the loading degree ratio of the elements during movement of bulk solid material body through the elements.

## 8.5 Start-up of an inextensible conveyor belt

The analysis of a start-up of a belt conveyor system focuses on the question whether or not the transient belt tension is admissible and whether or not the performance of the system is acceptable. The belt tension during start-up is admissible if the nominal belt strength  $kN$ , taking into account the splice efficiency, multiplied by the belt width  $B$  and divided by the maximum transient belt force is larger than the required safety factor  $S_A$  on that tension. The performance of a belt system is acceptable if the belt is always in tension, the belt remains on the supports and the bulk solid material remains on the belt. It is desirable that the amplitudes of transverse vibration of belt segments are small to reduce the energy consumption of the system and that the displacements of the belt tensioner are small to reduce its size.

The maximum belt tension during start-up can easily be approximated by assuming that the belt is inextensible and that the drive force during start-up is constant. As a result the acceleration of the belt during start-up is constant. The transient drive force  $F_{dA}$  can be calculated by multiplying the required drive force during stationary operation  $F_d$ , see equation (8.6), and a drive-system dependent start-up factor  $K_A$ , see Table 8.2<sup>9</sup>. From Section 8.2 it follows that for the design under consideration the drive force during stationary operation,  $F_d$ , for the unloaded belt is 9.85 kN and for the loaded belt is 35.55 kN. The start-up factor  $K_A$  for a direct start-up is about 2.5 for a drive system without slip coupling. Therefore the maximum drive force during start-up is 24.63 kN for the unloaded belt and 88.89 kN for the loaded belt. Remember that the drive force  $F_d$  was equal to the motion resistance force met by the belt, which in this case is assumed to be independent of the belt speed. Therefore the acceleration of the belt during start-up can be obtained from:

$$a_A = \frac{F_{dA} - F_d}{\sum m} \quad (8.32)$$

The total mass of the moving parts of the considered belt conveyor system is equal to the sum of the total reduced masses of the idlers, the total mass of the carrying and the return belt parts, the total mass of the bulk material on the belt (only for the loaded belt), the reduced masses of the four bend pulleys, the reduced mass of the drive pulley, the tail pulley and the tension pulley, the reduced mass of the induction motor and the reduced mass of the gear box:

<sup>9</sup> Normally the start-up factors of an unloaded and a loaded belt conveyor differ. Here they are assumed to be equal.

$$\sum m = m_{red,r} + 2 m_{belt} + m_{bulk} + 4m_{red,bp} + 3m_{red,dp} + m_{red,m} + m_{red,g} \quad (8.33)$$

Substituting the masses given in (8.2), (8.3), (8.5) and in (8.14)-(8.17) in equation (8.33) results in a total mass of 61,813 kg for the unloaded belt and 195,360 kg for the loaded belt. Substituting these masses and the drive forces given in (8.6) and (8.7b) in equation (8.32), yields an acceleration of 0.24 m.s<sup>-2</sup> for an unloaded belt and 0.27 m.s<sup>-2</sup> for a loaded belt. Since the final belt speed is about 5.2 m.s<sup>-1</sup>, this constant acceleration results in a start-up time of 21.8 s for the unloaded belt and 19.2 s for the loaded belt<sup>10</sup>. These start-up times are not equal as may be expected which is caused by the difference in mass terms in the equation of the motion resistance force, equation (8.6), and the total mass of the moving parts, equation (8.33). With the drive force during start-up, F<sub>dA</sub>, also the actual safety factor of the belt during start-up can be calculated:

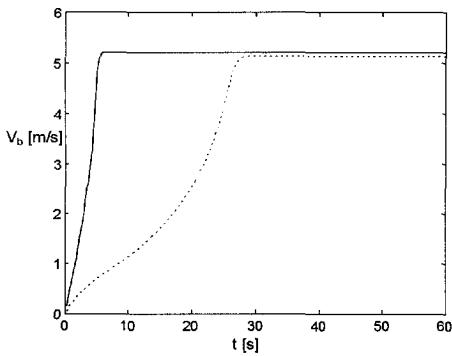
$$S_{act} = \frac{k_N B \eta_{splice}}{T_{1A}} = \frac{k_N B \eta_{splice}}{\left( \frac{e^{\mu\alpha}}{e^{\mu\alpha} - 1} \right) F_{dA}} \quad (8.34)$$

With the selected EP 500/5 belt with width B=1.2 m, a wrap angle  $\alpha=\pi$ <sup>11</sup>, a friction factor between belt and pulley  $\mu=0.35$  and the drive force F<sub>dA</sub>=88.89 kN, the actual safety factor is S<sub>act</sub>=12.2 for the unloaded belt and 3.4 for the loaded belt. According to the DIN standard the safety factor during non stationary operation should be at least 5.4, see also Section 3.1.4. Therefore, based on this calculation, it can be concluded that the maximum drive force during start-up of the loaded belt should be limited to 55.55 kN. This implies that the maximum start-up factor is 1.5 which can for example be achieved by application of a fluid coupling, see Table 8.2. In that case the average acceleration of the belt is 0.10 m.s<sup>-2</sup> which results in a start-up time for the loaded belt of 50.8 s. In the following, the calculation of the start-up time and safety factor of the unloaded belt is referred to as calculation I, whereas the calculation of the start-up time and safety factor of the loaded belt is referred to as calculation II.

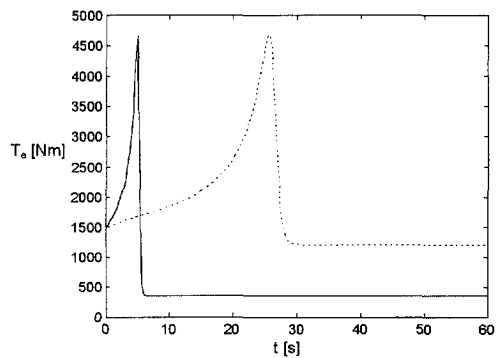
The constant start-up drive force used in the above calculation is an approximation. To determine the influence of the relation between the motor torque and the angular speed of the motor shaft, and thus determine the start-up torque or force based on the motor characteristics as has been discussed in Section 6.4.3, **TUBELT** is used.

<sup>10</sup> The start-up time for the unloaded belt is 6.03 s in case the drive force F<sub>dA</sub> of the loaded belt is used to start the unloaded belt.

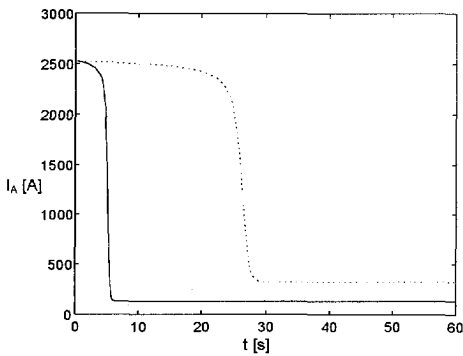
<sup>11</sup> The wrap angle  $\alpha$  is only equal to  $\pi$  in case of the start-up of a loaded belt conveyor. In all other cases it is smaller than  $\pi$ .



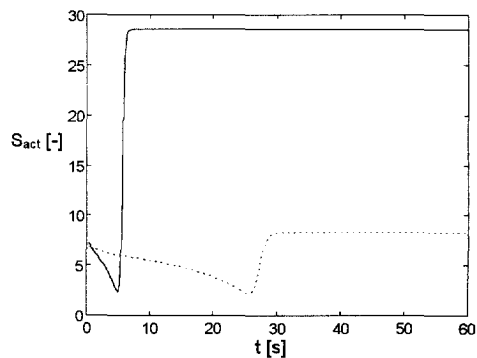
**Figure 8.23:** Belt speed of the unloaded belt (solid line) and the loaded belt (dotted line).



**Figure 8.24:** Motor torque during the direct start-up of the unloaded belt (solid line) and the loaded belt (dotted line).



**Figure 8.25:** Motor current during the direct start-up of an unloaded belt (solid line) and a loaded belt (dotted line).



**Figure 8.26:** Actual safety factor during direct start-up of an unloaded belt (solid line) and a loaded belt (dashed line).

The direct start-up of an induction motor driven flywheel, where the supply frequency of the induction motor is 50 Hz, has been simulated. The reduced mass of the flywheel was equal to the total mass of the unloaded or loaded belt reduced on the drive pulley. The resistance torque on the flywheel was equal to the belt motion resistance multiplied by the drive pulley radius. The simulation of the direct start-up of the unloaded belt is referred to as simulation I, whereas the start-up of the loaded belt is referred to as simulation II.

Figure 8.23 shows the belt speed versus time in both cases. The start-up time of the unloaded belt is 5.3 s and of the loaded belt 27.8 s. Figure 8.24 shows the motor torque during the start-up. The start-up drive force can be calculated from the

motor torque by multiplying the motor torque by the reduction factor, 17.99, and dividing the result by the drive pulley radius, 0.6 m. This yields a drive force of 44.7 kN at  $t=0$  which is half the start-up drive force used in the foregoing calculation. The maximum drive force, which is equal to 140.5 kN, can be calculated from the maximum drive torque, which in case of a direct start is equal to the tilting couple of the induction motor. The start-up time of the loaded conveyor is longer than estimated by the calculation II caused by the lower start-up drive force. The start-up force for the unloaded belt and the loaded belt are equal resulting in a shorter start-up time than estimated for the unloaded conveyor. Figure 8.25 depicts the motor current during both start-ups. The time during which the maximum start-up current is allowed to be present in the motor is about 10 seconds. This illustrates that a direct start-up, according to this simulation, overloads the motor. Therefore, also based on the simulation results, the conclusion would be that a slip coupling is required to drive the belt, to prevent the motor from overloading. Besides that the motor is overloaded, also the belt is overloaded. Figure 8.26 shows that the minimum safety factor is 2.2 for both the unloaded and loaded belt which is less than half the required 5.4, see Section 3.1.4. As can be learned from comparing the calculation results and the simulation results, taking the correct motor characteristics into account significantly influences the results. The influence of the belt's elastic response however is still unknown. Therefore simulations have been made of the start-up of the unloaded and loaded belt conveyor with finite element model 2, which has been described in Section 8.3. The results of these simulations are described in the first section of the next paragraph.

## 8.6 Start-up of an elastic conveyor belt

In this paragraph the results of simulations using the software system **TUDBELT** and finite element models 2 and 3 are presented. The response of the belt to a direct start-up and to velocity controlled start ups have been simulated. Based on the results of these simulations, criteria for the design of proper start procedures are listed in the last section of this paragraph.

### 8.6.1 Direct start

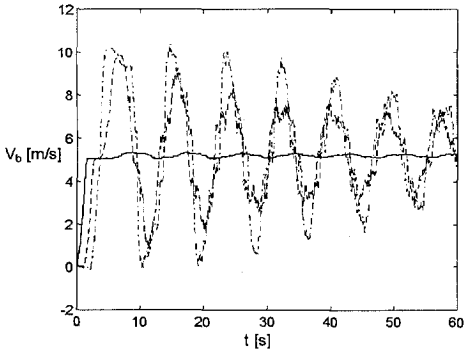
In addition to the calculations and the simulations for the unloaded and the loaded belt described in Section 8.5, four simulations of a direct start-up have been made using model 2:

simulation a: direct start-up of an unloaded belt conveyor tensioned by a winch tensioner

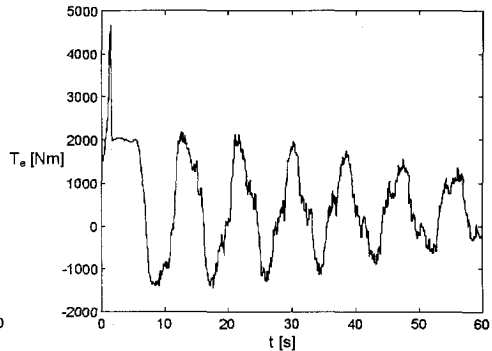
simulation b: direct start-up of an unloaded belt conveyor tensioned by a weight tensioner

simulation c: direct start-up of a loaded belt conveyor tensioned by a winch tensioner

simulation d: direct start-up of a loaded belt conveyor tensioned by a weight tensioner

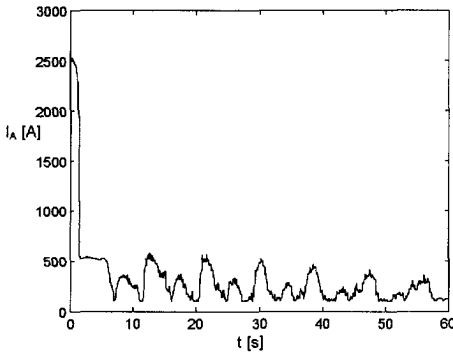


**Figure 8.27:** Belt speed at the drive pulley (solid line), the tail pulley (dashed line) and at the tensioning pulley (dash-dot line) during a direct start of the unloaded belt.

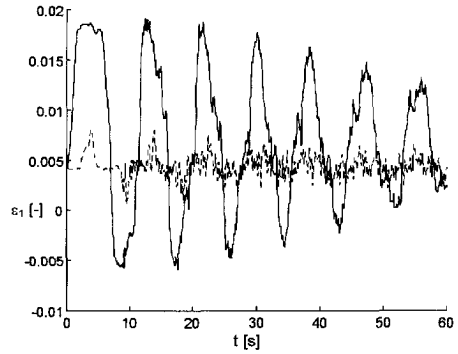


**Figure 8.28:** Motor torque during a direct start of the unloaded belt.

Figure 8.27 shows the speed of the belt at three sections in the conveyor during the start up of simulation a: the drive pulley (node 4 of model 2), the tail pulley (node 14 of model 2) and the tensioning pulley (node 24 of model 2). At the drive pulley, the belt is accelerated within 1.6 seconds to a velocity of  $5.2 \text{ m}\cdot\text{s}^{-1}$ . In paragraph 3.1.4 the longitudinal velocity of waves in a belt has been discussed. If the distributed mass due to the idler rolls, which is different for the carrying and return part of the belt, and the mass of the belt are accounted for, then the ratio of velocity of waves, defined in Section 3.1.4,  $C_U=0.70$  for the carrying belt part and  $C_U=0.81$  for the return part. The average ratio of velocity of waves is  $C_U=0.75$  resulting in an average longitudinal wave velocity of  $c_l=408.95 \text{ m}\cdot\text{s}^{-1}$ . With this velocity, the lowest natural frequency of longitudinal vibration of the total belt is 0.102 Hz. The corresponding period of vibration is 9.78 seconds which can clearly be recognised in Figure 8.27. The amplitude of vibration is different for the three different belt sections. It is small for the belt on the drive pulley where the motion of the belt is governed by that pulley, whereas it is large for the belt in the free-moving tensioning system. Figure 8.28 shows the drive torque during a direct start-up of the unloaded belt conveyor. The first peak in this figure, of about 4750 Nm, is the tilting couple which the drive torque passes during acceleration of the induction motor, see also Figure 6.4. Since the belt speed vibrates around the nominal speed, also the angular velocity of the motor shaft varies around its nominal value. This results in the motor torque and



**Figure 8.29:** Motor current during a direct start of an unloaded belt.



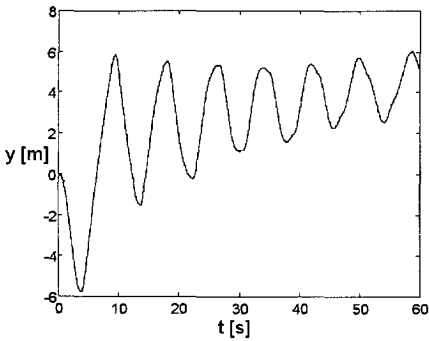
**Figure 8.30:** Variation of the axial strain  $\epsilon_1$  in the belt after the drive pulley (solid line) and before the tensioning pulley (dashed line) during a direct start of an unloaded belt.

current as shown in the Figures 8.28 and 8.29 respectively. The period of motor torque and current variation is the same as the period of the longitudinal belt vibration.

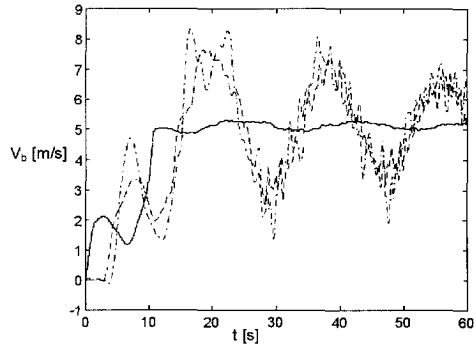
The alternating motor torque results in an alternating belt tension. Figure 8.30 shows the variation of the axial strain  $\epsilon_1$ , see equation (7.13), in two different belt segments: the segment right after the drive pulley (element 4 of model 2) and just before the tensioning system (element 23 of model 2). As can be seen in that figure, the variation of the axial strain of the belt on the drive pulley is smaller than zero during a part of the cycle. However, it should be realised that even if  $\epsilon_1$  is smaller than zero, the total belt strain  $\epsilon_1^*$  is positive and the belt is still tensioned.

Finally, the belt sag in the carrying belt part influences the motion of the tensioning weight. If the belt is driven and the belt tension increases, also the total belt length increases. Therefore normally the average vertical displacement of the tensioning weight,  $y$ , is downwards ( $y < 0$ ). However due to the non-linear effect of belt sag in the carrying part of the belt, the tensioning weight is lifted ( $y_{\text{average}} > 0$ ) as can be seen in Figure 8.31. This figure also shows that the maximum vertical displacement of the tensioner weight is 11.80 m which is not acceptable. Figure 8.32 shows the belt speed during the direct start-up of simulation c. The head of the belt reaches a speed of  $5.2 \text{ m}\cdot\text{s}^{-1}$  in 10.7 seconds. The motor torque and current are shown in the Figures 8.33 and 8.34. The ratio of velocity of longitudinal waves, defined in Section 3.1.4, for the loaded carrying part  $C_L=0.30$  whereas it is 0.81 for the unloaded return part. With the average ratio of 0.55 the average velocity of the longitudinal waves is  $299.11 \text{ m}\cdot\text{s}^{-1}$ .

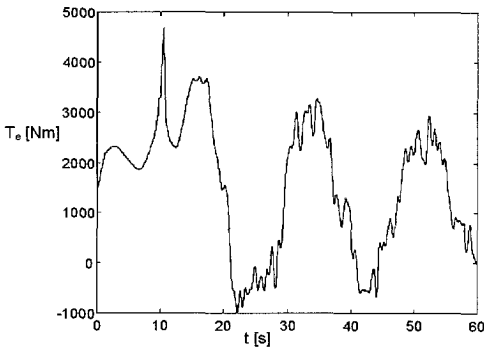




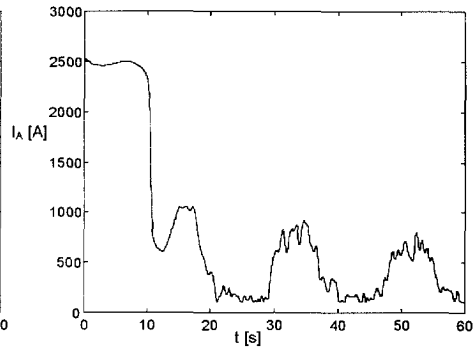
**Figure 8.31:** Vertical displacement of the tensioning pulley during a direct start of an unloaded belt (winch tensioner).



**Figure 8.32:** Belt speed at the drive pulley (solid line), the tail pulley (dashed line) and at the tensioning pulley (dash-dot line) during a direct start of the loaded belt.

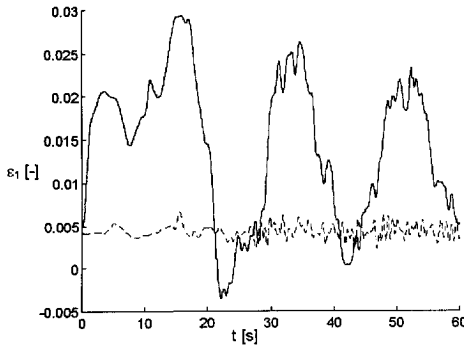


**Figure 8.33:** Motor torque during a direct start of the loaded belt.

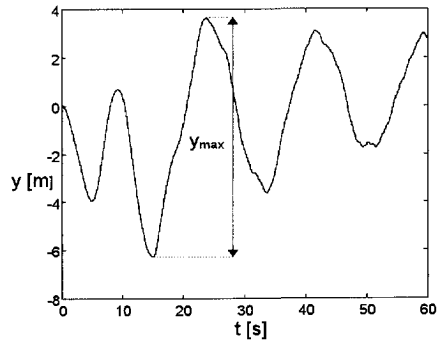


**Figure 8.34:** Motor current during a direct start of the loaded belt.

With this velocity, the lowest frequency of axial vibration of the belt is 0.07 Hz and the period of vibration 13.37 seconds. The variation of the belt strain  $\varepsilon_1$  in the carrying side is only occasionally negative, see Figure 8.35. Therefore the positive vertical displacement of the tensioning pulley is smaller than during the direct start-up of the unloaded belt, see Figure 8.36. The results of the simulations b and d are not shown in detail since the differences between a and b, and between c and d are small. The results of the simulations a-d and those of the calculations and simulations of Section 8.5 are summarised in Table 8.6. In this table the loading degrees, the type of tensioning system, the start-up times, the maximum vertical displacement of the tensioning pulley  $y_{\max}$ , see Figure 8.36, the maximum strain  $\varepsilon_{1,\max}^*$  and the actual safety factors of the belt during the start-up are given.



**Figure 8.35:** Variation of the axial strain in the belt after the drive pulley (solid line) and before the tensioning pulley (dashed line) during a direct start of a loaded belt.



**Figure 8.36:** Vertical displacement of the tensioning pulley during a direct start of a loaded belt (winch tensioner).

Start-up procedure	Loading degree	Tensioning system	$y_{max}$ [m]	$c_{l,max}^*$ [-]	$S_{min}$	Start-up time [s]
calculation I	0 %	-	-	0.0088	12.2	21.8
calculation II	100 %	-	-	0.0314	3.4	19.2
simulation I	0 %	-	-	0.0485	2.2	5.3
simulation II	100 %	-	-	0.0485	2.2	27.8
simulation a	0 %	winch	11.802	0.0195	5.5	1.58
simulation b	0 %	weight	11.925	0.0191	5.6	1.61
simulation c	100 %	winch	9.934	0.0306	3.5	10.65
simulation d	100 %	weight	9.753	0.0294	3.6	10.75

**Table 8.6:** Calculation and simulation results.

As can be seen from Table 8.6, the start-up times obtained from the calculations I&II and simulation I&II are longer than the start-up times obtained from the simulations a-d. The safety factors obtained from the simulations I&II are smaller than the safety factors obtained from the simulations a-d.

From the results of the simulations a-d it follows that the belt is always in tension during a direct start-up. However, the maximum vertical displacement of the tension pulley is about 10 m. Therefore, the performance of the belt conveyor during direct start-up is not acceptable. From the results of the simulations c and d it follows that a direct start-up of the loaded conveyor is also not admissible since the minimum safety factor on the belt tension during start-up is smaller than the prescribed 5.4. Also the time, during which the maximum start-up current is present in the motor of the loaded belt conveyor, is critical. Therefore, the start-up of the belt conveyor has to be controlled to decrease the acceleration of the belt in order to increase the minimum safety factor. In the next section the attention is focused on the velocity controlled start-ups of a loaded belt conveyor.

## 8.6.2 Velocity controlled start

In Section 8.6.1 it was shown that a direct start-up of the loaded belt conveyor overloaded the belt and heavily loaded the motor. Also the performance of the belt conveyor during start-up, see the definition in Section 8.5, was unacceptable. Therefore a start-up procedure should be chosen which:

- lowers the maximum motor torque
- limits the motor current
- enables the control of the start-up time and trajectory of the belt speed

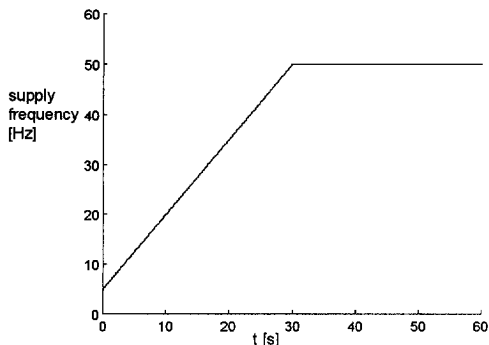
To satisfy these requirements an SPC is chosen to control the supply frequency of the motor. By controlling the supply frequency, the motor torque is controlled indirectly whereas the belt speed on the drive pulley is controlled directly as will be shown in the next section.

### 8.6.2.1 Linear offset start-up procedure

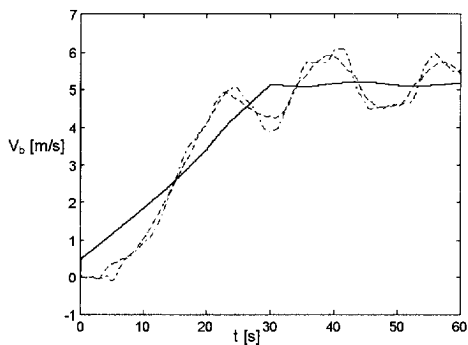
As a start, a linear offset start-up procedure is chosen with a start-up time of 30 seconds. The velocity profile of a linear offset procedure is:

$$V_{ba}(t) = \frac{(V_b - V_{b,0})}{T_a} t + V_{b,0}, \quad 0 \leq t \leq T_a \quad (8.35)$$

where  $V_{b,0}$  is the initial speed at  $t=0$  s. For a linear start-up the initial speed is zero. To produce a break-away couple and obtain an initial belt speed, the supply frequency of the motor is given a start value of 5 Hz, see also Figure 6.4. From the start value the frequency is linearly increased to 50 Hz. Figure 8.37 shows the variation of the supply frequency with time for this start-up procedure. Figure 8.38 shows the belt speed at three belt sections in the conveyor during the start-up. Comparison of the Figures 8.37 and 8.38 learns that in this case controlling the supply frequency implies that the belt speed at the drive pulley is controlled. Linearly increasing the supply frequency in 30 seconds from 5 Hz to 50 Hz results in a linear increase of the belt speed at the drive pulley from an initial speed to the stationary speed in 30 seconds. It turned out that similar conclusions hold for all the following (simulated) velocity controlled start-ups.



**Figure 8.37:** Motor frequency supplied by the SPC during a start-up of 30 s.

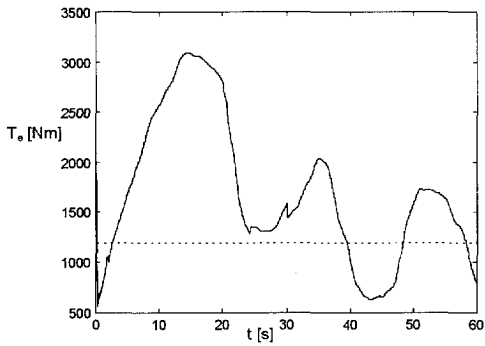


**Figure 8.38:** Belt speed on the drive pulley (solid line), the tail pulley (dash-dot line) and tensioning pulley (dashed line) during a velocity controlled start-up of 30 s.

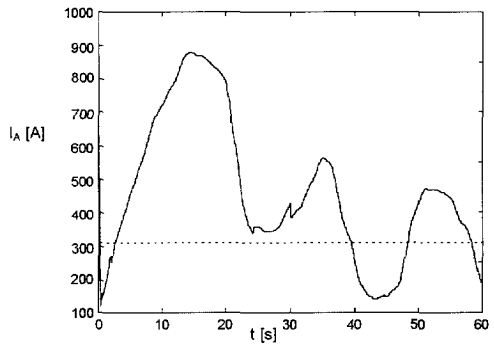
The motor couple during the start-up is depicted in Figure 8.39. Comparing this figure with Figure 8.33 shows that the maximum motor couple is much lower in case of a velocity controlled start-up. The same holds for the motor current which can be seen from comparison of the Figures 8.40 and 8.34. The lower motor couple results in lower belt tensions and smaller axial belt strains.

Figure 8.41 shows the variation of the axial strain of the belt. If the belt sag is small then the total axial strain  $\epsilon_1^*$  and the variation of the axial strain  $\epsilon_1$  are equal, see Section 7.2.1.2. The maximum axial strain  $\epsilon_1^* = 0.0238$  which implies a minimum safety factor of 4.5. In case of a direct start up the maximum strain  $\epsilon_1^*$  and the minimum safety factor were 0.0298 and 3.6 respectively. From Figure 8.41 it also follows that the axial strain  $\epsilon_1$  is always larger than zero. Therefore it may be expected, as was explained in Section 8.5.1, that the vertical displacement of the tensioning pulley is downwards resulting in negative values of the displacement parameter  $y$  of the tensioning pulley. This is confirmed by Figure 8.42 which shows the vertical displacement of the tensioning pulley.

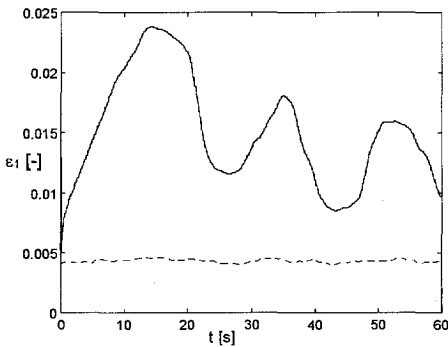
The transverse displacement of the belt can be determined from the ratio between the vertical belt load and the belt tension, see equation (3.14). Only transverse belt vibrations caused by belt tension variations are determined. Figure 8.43 shows the belt sag ratio of a belt segment right after the drive pulley and just before the tensioning pulley.



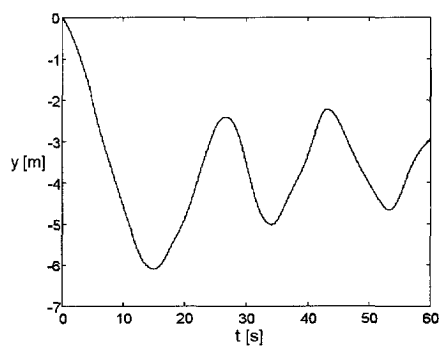
**Figure 8.39:** Motor torque during a velocity controlled start-up of 30 s (solid line). The dotted line indicates the stationary torque.



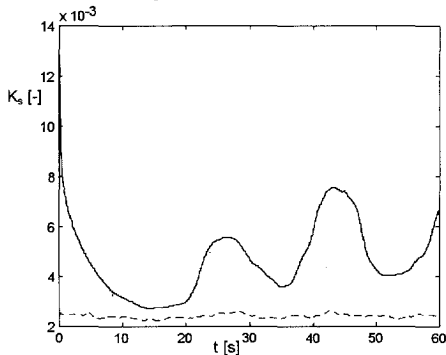
**Figure 8.40:** Motor current during a velocity controlled start-up of 30 s (solid line). The dotted line indicates the stationary motor current.



**Figure 8.41:** Variation of the axial strain in the belt on the drive pulley (solid line) and on the tensioning pulley (dashed line) during a velocity controlled start-up of 30 s.



**Figure 8.42:** Vertical displacement of the tensioning pulley during a velocity controlled start-up of 30 s.



**Figure 8.43:** Belt sag ratio of belt segment right after the drive pulley (solid line) and just before the tensioning pulley (dashed line) during a velocity controlled start-up of 30 s.

### Start-up time

From the results of the simulation of the linear offset start-up of 30 seconds, it follows that, compared to the results of a direct start-up, the motor is no longer overloaded, the axial belt strain is always positive and the maximum belt strain is lower. However, the minimum safety factor of 4.5 is still below the required 5.4 and the maximum vertical displacement of the tensioning weight (6m) is still considerable. To find the influence of the start-up time on the safety factor, four additional simulations have been made of a linear offset start-up of the loaded belt in which the start-up time was 10, 20, 40 and 50 seconds respectively, and the offset frequency 5 Hz. Since the performance of the belt conveyor was already acceptable in case of a direct start-up, the question is which start-up time results in an admissible maximum belt tension.

Figure 8.44 shows the maximum total axial belt strain as a function of the start-up time. This curve is used to calculate the minimum safety factor versus start-up time (Figure 8.45). From this figure it follows that the start-up time should be at least 40 seconds to keep the minimum safety factor above the required 5.4. In that case also the maximum vertical displacement of the tensioning weight is acceptable, see Figure 8.46. The start-up times  $T_a$  obtained in Section 6.1.1 are 11.4 seconds according to equation (6.3), and 60 seconds according to the rule of one-minute-per-km-conveyor-length. According to the results of the simulations, the start-up time which follows from equation (6.3) yields an unacceptable short start-up time as was expected whereas the rule of one-minute-per-km-conveyor-length, yields an acceptable start-up time for this specific conveyor. The start-up time which can be determined from equation (6.6) is discussed at the end of this section.

To complete the information of the velocity controlled start-ups, Figure 8.47 shows the minimum belt strain  $\epsilon_1$  as a function of the start-up time and Figure 8.48 shows the belt sag ratio. Besides the minimum safety factor also the maximum belt sag is normally prescribed for design purposes. The maximum belt sag ratio for this conveyor was set to 0.015. Before the start-up, the belt sag ratio of the carrying part of the loaded conveyor is 0.013. As can be seen in Figure 8.48 the belt sag ratio decreases with increasing start-up time. For a start-up times larger than 30 seconds, the initial belt sag is not exceeded. The minimum start-up time based on this information is therefore 30 seconds. Finally, the Figures 8.49 and 8.50 show the maximum motor torque and the maximum motor current respectively as a function of the start-up time. From Figure 8.50 it can be seen that the maximum motor current is constant above a start-up time of 30 seconds. The motor current of 905.2 A at the beginning of the start-up procedure, where the supply frequency is 5 Hz, is then also the maximum.

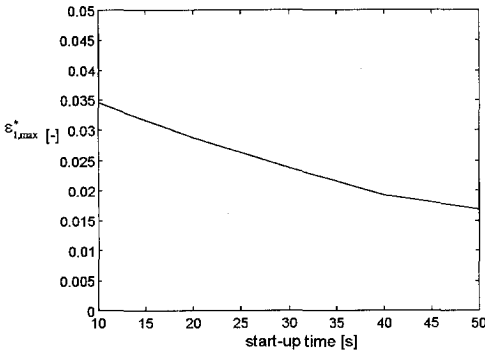


Figure 8.44: Maximum total belt strain  $\epsilon_1^*$  during velocity controlled start-ups.

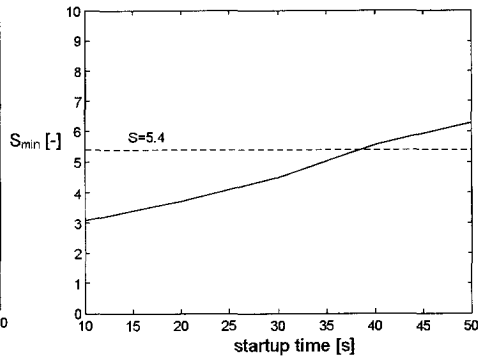


Figure 8.45: Minimum safety factor during velocity controlled start-ups.

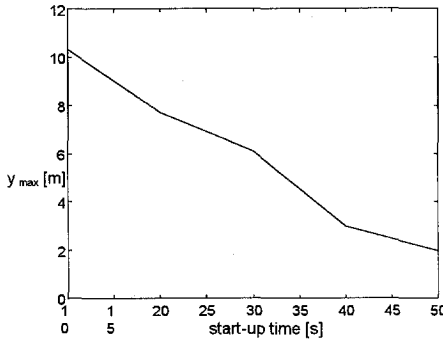


Figure 8.46: Maximum vertical displacement of the tensioning pulley during velocity controlled start-ups.

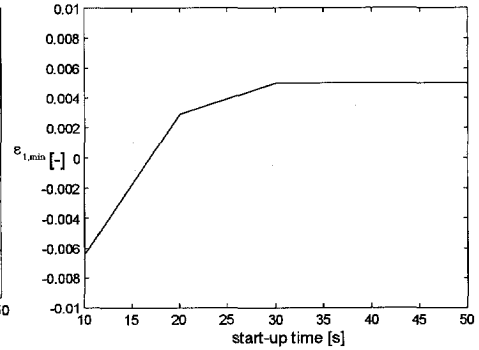


Figure 8.47: Minimum belt strain  $\epsilon_1$  during velocity controlled start-ups.

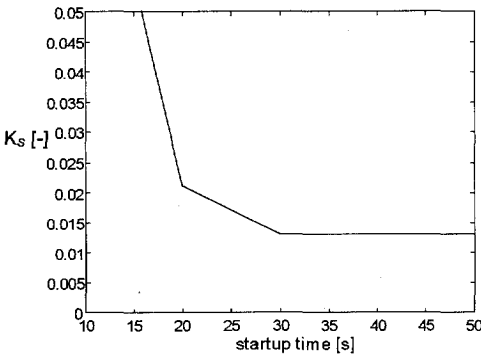


Figure 8.48: Maximum belt sag ratio during velocity controlled start-ups.

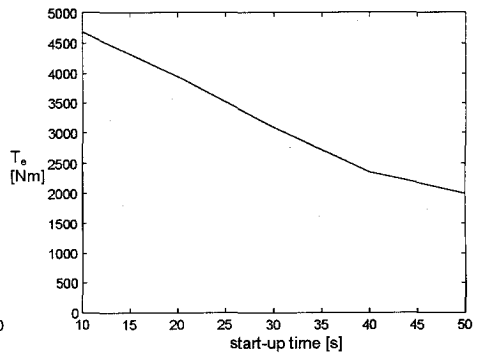
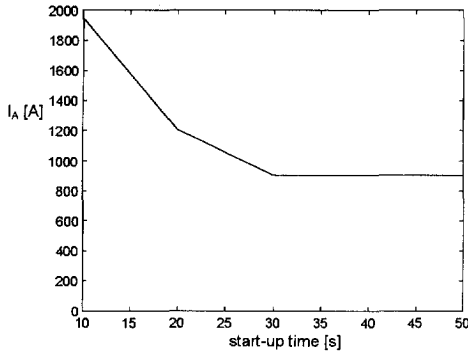
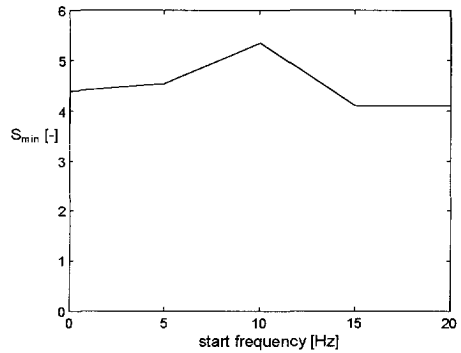


Figure 8.49: Maximum motor torque during velocity controlled start-ups.



**Figure 8.50:** Maximum motor current during velocity controlled start-ups.



**Figure 8.51:** Minimum safety factor versus start frequency for velocity controlled start-ups of 30 s.

### Start-up frequency of the SPC

From the above consideration it can be concluded that the linear offset procedure, during which the belt speed is linearly increased, is a suitable start-up procedure. The question however is which start frequency should be used. The start frequency directly influences the belt acceleration. To determine the relation between the start frequency and the minimum safety factor, three additional simulations of a linear offset start-up have been made. During these simulations the start-up time was 30 s and the start frequencies were 10, 15 and 20 Hz. The results for a start frequency of 0 and 5 Hz being known. Figure 8.51 shows the minimum safety factor as a function of the start frequency. From that figure it follows that the highest (minimum) safety factor is obtained for a start frequency of about 5-10 Hz, which is 10-20 % of the maximum supply frequency. In that case the maximum vertical displacement of the tensioning weight is 2.96 m whereas it is 7.63 m and 8.45 m respectively for a linear offset start-up with start frequency of 15 and 20 Hz. It should be noticed that the offset frequency directly determines the start-up current which is normally restricted to 1.4-1.5 times the stationary current. According to the results of the simulations, an offset frequency of 5-10 Hz is therefore admissible.

#### 8.6.2.2 Alternative velocity controlled start-ups

In Section 6.1.1 three alternatives were given for the linear offset speed increase used in the start-up procedures mentioned above. Besides the speed trajectories proposed by Harrison, equation (6.1), and Nordell, equation (6.2), also a variant with a delay period was mentioned. The velocity profile of this procedure is:



$$\begin{aligned}
 V_{ba}(t) &= \frac{V_b}{T_a} t, \quad 0 \leq t \leq T_r \\
 V_{ba}(t) &= \frac{V_b}{T_a} T_r, \quad T_r \leq t \leq T_r + \Delta T_a \\
 V_{ba}(t) &= \frac{V_b}{T_a} (t - \Delta T_a), \quad T_r + \Delta T_a \leq t \leq T_a + \Delta T_a
 \end{aligned}
 \tag{8.36}$$

where  $T_r$  is the time at which the rest period starts and  $\Delta T_a$  the rest time. Note that the total start-up time in this case is  $T_a + \Delta T_a$ .

To determine the minimum safety factors which result from a start-up procedure with velocity profile according to the equations (6.1), (6.2) and (8.36), four additional simulations have been made. The basis of comparison is the linear offset start-up procedure with the start frequency of 5 Hz, linear speed increase and start-up time of 30 seconds. To quantify the influence of the offset frequency, an extra simulation has been made of a linear start-up, where the initial frequency is zero, with a start-up time of 30 seconds. The influence of the delay period has been determined from a simulation where, after 5 seconds ( $T_r = 5$  s), a delay period of 5 seconds ( $\Delta T_a = 5$  s) is inserted during which the supply frequency is kept constant. The supply frequency trajectories of the other two simulations correspond to the speed trajectories of the procedures described by Harrison and Nordell. Remember that the trajectory of the belt speed at the drive pulley follows the trajectory of the supply frequency, see Figure 8.38. The supply frequencies as a function of the start-up time of the five procedures are shown in Figure 8.52.

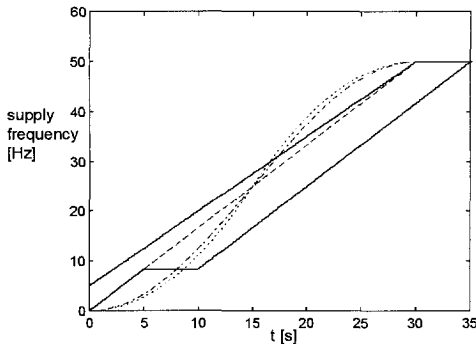


Figure 8.52: Supply frequency during five simulations. Linear offset (solid line left), linear (dashed line), linear delayed (solid line right), Harrison (dash-dot line) and Nordell (dotted line).

	$y_{\max}$ [m]	$K_{s,\max}$ [-]	$\epsilon_{1,\max}$ [-]	$S_{A,\min}$ [-]	$a_{\max}$ [m.s <sup>-2</sup> ]	T [Nm]	I [A]
linear offset	6.101	0.0130	0.0238	4.5	0.155	3095.4	905.2
linear	6.292	0.0130	0.0246	4.3	0.170	3229.9	927.9
linear delayed	5.148	0.0130	0.0236	4.5	0.170	3094.2	869.0
Harrison (6.1)	9.345	0.0301	0.0303	3.5	0.268	4132.4	1282.8
Nordell (6.2)	10.748	0.0382	0.0382	2.8	0.341	4291.2	1365.5

Table 8.7

The results of the simulations are summarised in Table 8.7. Compared with the linear offset procedure, it can be seen that the linear delayed procedure yields an equal safety factor whereas for all other procedures it is lower. This is caused by differences in maximum acceleration at the head of the belt. In the start-up procedures of Harrison and Nordell, the maximum acceleration appears in the middle of the start-up. The transient phenomena are not yet damped out by the time the start-up procedure ends. The belt acceleration during the linear procedure is higher than during the linear offset procedure. This explains why the safety factor of the linear procedure is lower than that of the linear offset. The insertion of a delay period seems to be useful when comparing the safety factors, however, in case of the linear delayed procedure the total start-up time is 35 seconds. From Figure 8.45 it follows that the minimum safety factor of a linear offset procedure with a start-up time of 35 seconds is 5.0. Therefore, if 35 seconds are available, the linear offset procedure is preferable. The maximum vertical displacement of the tensioning weight of a linear offset start-up of 35 s is comparable to that of the linear delayed start-up of 35 s.

### 8.6.3 Estimation of the start-up time

Equation (6.6) [Harrison and Roberts, 1984] describes the required safety factor on the belt tension during stationary operation  $S_B$ . In equation (6.6) the minimum safety factor on the belt tension during non-stationary operation is assumed to be 3. If this value is replaced by  $S_{A,\min}$ , then the following equation for the minimum safety factor can be obtained:

$$S_{A,\min} = S_B \left( \frac{F_1}{F_1 + F_{ac}} \right) \quad (8.37)$$

where  $F_1$  is the maximum belt force during stationary operation and  $F_{ac}$  the maximum acceleration force. The maximum stationary belt force of the considered conveyor  $F_1$  can be written as:

$$F_1 = \left( \frac{e^{\mu\alpha}}{e^{\mu\alpha} - 1} \right) F_d = C^* F_d \quad (8.38)$$

Substituting equation (8.6) in (8.38) yields:

$$F_1 = C^* C f g L_{\text{conv}} (m'_{\text{roll}} + 2m'_{\text{belt}} + m'_{\text{bulk}}) \quad (8.39)$$

Substituting equation (6.5) and (8.39) in (8.37) yields the following approximation for the minimum safety factor on the belt tension during non-stationary operation:

$$S_{A,\text{min}} = S_B \left( 1 + \frac{1/4 \dot{V}_{b,\text{max}}}{C^* C f g} \right)^{-1} \quad (8.40)$$

Another more accurate approach is as follows. Assume that the start-up of the belt is controlled by a velocity and that the belt speed is increased linearly. In that case the acceleration of the belt on the drive pulley is constant. To accelerate the belt, bulk and idlers, an extra drive force  $F_{\text{ac}}$  is required which can be estimated by:

$$F_{\text{ac}} = (m'_{\text{roll}} + 2m'_{\text{belt}} + m'_{\text{bulk}}) L_{\text{conv}} \dot{V}_b \quad (8.41)$$

The extra drive force yields an extra belt tension  $F_{\text{1ac}}$  which is equal to:

$$F_{\text{1ac}} = C^* F_{\text{ac}} \quad (8.42)$$

With this extra belt tension due to the acceleration of the belt, equation (8.37) can be rewritten to:

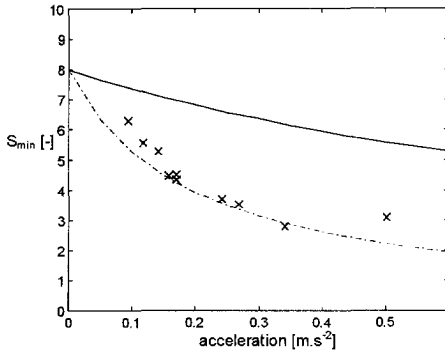
$$S_{A,\text{min}} = S_B \left( \frac{F_1}{F_1 + F_{\text{1ac}}} \right) \quad (8.43)$$

Substitution of equation (8.39) and (8.42) in (8.43) yields:

$$S_{A,\text{min}} = S_B \left( 1 + \frac{\dot{V}_b}{C f g} \right)^{-1} \quad (8.44)$$

The crosses in Figure 8.53 depict the maximum accelerations and the minimum safety factors of the simulations of the velocity controlled start-ups described in this section.

---



**Figure 8.53:** Minimum safety factor versus maximum belt acceleration. Crosses indicate the simulation results, the solid line equation (8.38) and the dash-dot line equation (8.42).

In the calculation of paragraph 8.1 the safety factor on the belt tension during stationary operation  $S_B$  was taken 8.0. The solid line depicts the minimum safety factor on the belt tension during non-stationary operation as a function of the maximum acceleration according to equation (8.40). The dash-dot line depicts this variation according to equation (8.44). As can be seen in Figure 8.53, the solution according to equation (8.44) seems to be a lower limit of the safety factors as a function of the maximum acceleration of the belt.

In case of a linear increase of the belt speed, the belt acceleration is:

$$\dot{V}_b = \frac{V_b}{T_a} \tag{8.45}$$

The minimum required safety factor during non-stationary operation is  $S_A$ . Therefore, after substitution of equation (8.45) in equation (8.40), the following expression for the start-up time can be obtained:

$$T_A = \frac{1/4 V_b}{C^* C f g} \left( \frac{S_A}{S_B - S_A} \right) \tag{8.46a}$$

Substitution of equation (8.45) in (8.44) yields:

$$T_A = \frac{V_b}{C f g} \left( \frac{S_A}{S_B - S_A} \right) \tag{8.46b}$$

Equation (8.46a) yields a start-up time of 9.4 seconds whereas according to equation (8.46b) the start-up time is 56.1 seconds. Considering the results of the simulations, the start-up time calculated with equation (8.46a) is not acceptable whereas application of equation (8.46b) results in a smooth start-up. Table 8.8 summarises the start-up times predicted by the different criteria and indicates whether or not these start-up times lead to a smooth start-up.

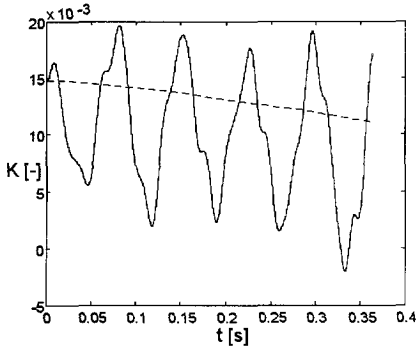
Start-up time according to:	start-up time [s]	yields smooth start-up
equation (6.3)	11.4	no
one minute per km rule	60.0	yes
equation (8.46a)	9.4	no
equation (8.46b)	56.1	yes
simulations	38.5	yes

Table 8.8: Summary of the start-up times.

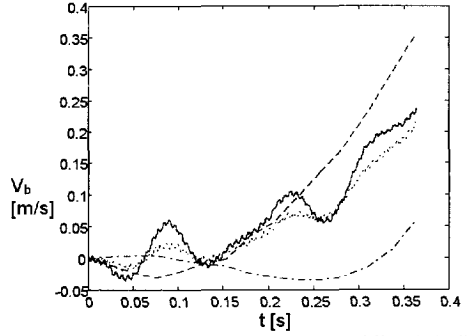
### 8.6.4 Application of beam elements

In Section 8.6.1 the direct start-up of the belt conveyor was discussed. During the simulations described in that section model 2 has been used. The belt sag ratio of the belt segment just after the drive pulley, modelled by element 4, was determined from equation (3.14) using the local dynamic belt tension. To determine directly the belt sag ratio, a simulation of a direct start-up of the unloaded belt conveyor is made using model 3. In that case the belt sag ratio can be determined from the transverse displacement of a belt segment between two idlers. In terms of model 3, this implies that the belt sag ratio is calculated by dividing the vertical displacement  $v$  of nodal point 8 by the idler spacing  $L=1.5$  m. Figure 8.54 shows the belt sag ratios obtained from both simulations. As can be seen in this figure, the belt sag ratio is equal to about 0.015 for the non moving belt in both cases. If the belt sag ratio is calculated from an actual vertical belt displacement, then positive vertical belt displacements, which result in negative values of the belt sag ratio, can be detected. This is not possible when the belt sag is calculated from the belt tension.

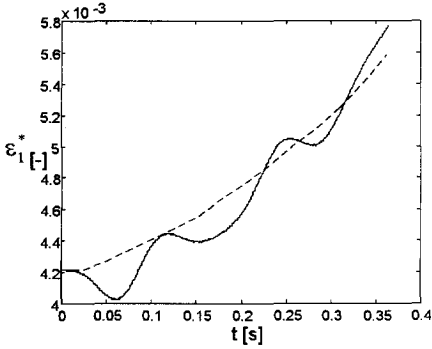
The average belt tension during the time interval from  $t=0$  to  $t=0.4$  s was 21.18 kN. With the density of the belt of  $1155.34 \text{ kg}\cdot\text{m}^{-3}$  and the carrying idler distance of 1.5 m, the average frequency and period of transverse vibration are 12.8 Hz and 0.077 s respectively. This period of vibration can be recognised in Figure 8.54. It can also be found in the transverse vibrations of the adjacent nodal points of node 8 which are shown in Figure 8.57 (dashed line) and in Figure 8.58 (solid line). Analysis of the data of the vertical displacements of nodal points 7-9 with Matlab<sup>®</sup>, shows that, besides the frequency of 12.8 Hz, also a frequency of 9.0 Hz is apparent in that data. This frequency can also be recognised in the variation of the total axial strain as is shown in Figure 8.56. This frequency is the natural frequency of axial vibration of the belt segment of 25 m, modelled by truss element 4 of model 3, preceding the considered belt segment. In Section 8.6.1 it was explained that the average longitudinal velocity of waves in the unloaded belt was  $408.95 \text{ m}\cdot\text{s}^{-1}$ .



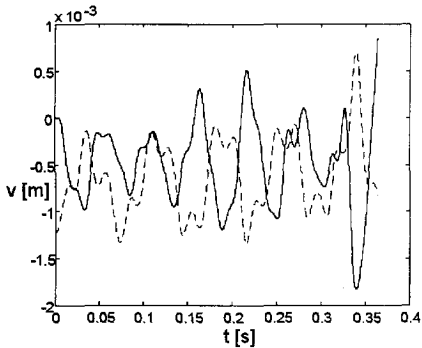
**Figure 8.54:** Belt sag ratio of element 4 of model 2 (dashed line) and of the node 8 of model 3 (solid line) as a function of time for a direct start-up of the unloaded belt conveyor.



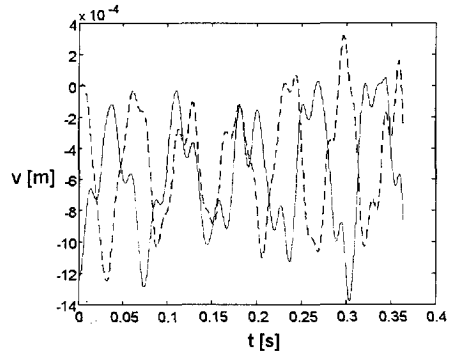
**Figure 8.55:** Belt speed on top of the idler 1 (solid line), idler 2 (dotted line), at the drive pulley (dashed line) and 100 m after the drive pulley (dashdot line).



**Figure 8.56:** Total axial strain in the sagged belt segment modelled by beam elements (solid line) and truss elements (dashed line).



**Figure 8.57:** Transverse displacement of the belt just before (node 6, solid line) and just after (node 7, dashed line) idler 1 of model 3.

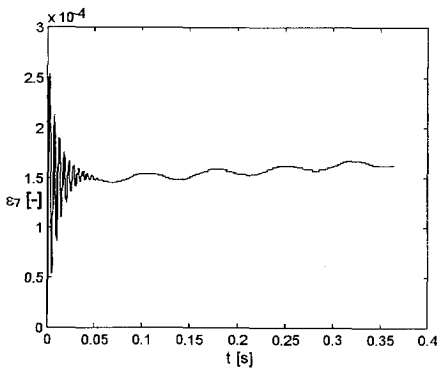


**Figure 8.58:** Transverse displacement of the belt just before (node 9, solid line) and just after (node 10, dashed line) idler 2 of model 3.

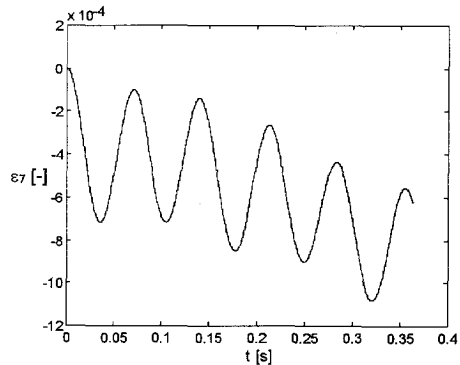
Substitution of this velocity and the belt length of 25 m in equation (8.21) yields the natural frequency of axial vibration of 9.0 Hz and the period of vibration of 0.11 seconds. This period of vibration can also be recognised in the variation of the belt speed as is shown in Figure 8.55. As was already discussed in Section 8.4.3, the natural frequency of axial vibration of the total belt can normally be found in the variation of the belt speed of real belt conveyors. The high frequency of 9 Hz, however, which is caused by the application of only one truss element to model the belt segment preceding the considered segment, will not appear in the belt speed variation of real belt conveyors.

Figure 8.55 shows the belt speed at the drive pulley, 100 m after the drive pulley and the belt speed on top of the two idlers of the considered belt segment. The belt speed at the drive pulley and 100 m after the drive pulley are respectively the axial velocities of the nodal points 4 and 5 of truss element 4 of model 2. The belt speeds on top of the idlers are the axial velocities of the extra displacement parameters  $\xi$  of the idler supported beam elements 6 and 9 of model 3. Apart from the belt speed variation, the belt speeds on top of the idlers, which are placed about 25 m after the drive pulley, lay between the belt speed at the drive pulley and 100 m after the drive pulley.

Finally, the Figures 8.59 and 8.60 show the angle of twist in the two shafts of the drive system as a function of time. The high frequency vibration of the motor shaft, which can be seen in Figure 8.59 right after  $t=0$  s, is caused by the natural vibration of that shaft.



**Figure 8.59:** Angle of twist of the shaft between the induction motor and the reduction box (element 0 of model 3).



**Figure 8.60:** Angle of twist of the shaft between the reduction box and the drive pulley (element 2 of model 3).

## 8.7 Conclusions

Based on the results of the calculations and simulations as described in the Sections 8.4-8.6, the following conclusions can be listed:

1. The bending stiffness of the belt used in the considered belt conveyors is low. Therefore, as can be seen in Section 8.4.2, the influence of the bending stiffness on the lowest frequency of transverse vibration of the pre-stressed belt can usually be neglected. In such a case, truss elements instead of beam elements can be used to determine the transverse vibration of an idler supported belt segment. However, when it is required to model accurately the bending of the belt on top of an idler, this can only be done by beam elements.
2. The application of 20 truss elements in a model of a 1 kilometre long belt conveyor, that take approximately into account the effect of belt sag, enable an accurate calculation of the low frequency axial vibrations and the average belt sag between the idlers. The local application of beam elements and of special idler supported beam elements to model a specific belt span supported by idlers, enable the accurate calculation of the axial strain and the belt sag between the idlers. An important drawback of the local application of beam elements is that their application slows down the calculation process for two reasons. Firstly this is caused by the smaller step-size that is required for a stable integration of the equations of motion. Secondly this is caused by the application of special idler supported beam elements which require every time-step a check whether or not a nodal point passes an idler and, if necessary, the termination and restart, after rebuilding the finite element model, of the simulation process.
3. Application of the DIN procedure, to calculate the maximum stationary belt tension and introduction of a drive system dependent multiplication factor to estimate the maximum tension during start-up giving the minimum safety factor on that tension, showed that a direct start-up of the specific belt conveyor under consideration results in an inadmissible maximum belt tension as expected. Based on the required minimum safety factor, it was then calculated that the average acceleration of the belt during a non-direct start-up should be limited to  $0.10 \text{ m}\cdot\text{s}^{-2}$  which will result in a start-up time to reach a speed of  $5.2 \text{ m}\cdot\text{s}^{-1}$  which is 50.8 s. Using these start-up data, it was shown that this can for example be achieved by the application of a drive system with a fluid coupling. Comparing the start-up time of 50.87 s with the minimum required start-up time of 40 s, obtained from the results of the finite element simulations, shows that, for the considered belt conveyor system, application of a velocity controlled start-up with linear speed increase and the start-up time of 50.8 s will yield a smooth start-up. Application of the DIN procedure to analyse a direct start-up results in overestimation of the start-up time.



4. Based on the results obtained from the finite element simulations, it can be concluded that calculations where the belt is assumed to be inextensible, the inertia is taken into account by a flywheel and the real (ideal) motor characteristic is taken into account (method II), result in overestimation of both the maximum belt tension and the start-up time. Application of this method does not yield a more accurate analysis of the start-up than the DIN procedure. It is therefore not useful to use this method to calculate the belt tension during non-stationary operation of a belt conveyor system.
5. Based on the results of the finite element simulations, it can be concluded that, to minimise the belt tension during start-up, the maximum acceleration of the belt should be minimised. It was shown that the best option to minimise the belt acceleration is the application of a start-up procedure, either velocity controlled or torque controlled, with constant acceleration. In case of a velocity controlled start-up it turned out that the lowest belt tension during start-up was obtained in case the start supply frequency of the induction motor was about 10-20 % of the stationary supply frequency. It also turned out that all other performance characteristics of the considered conveyor, including the vertical displacement of the take-up pulley, were acceptable if the maximum belt tension during start-up was admissible.
6. The software system **TUDBELT** is not optimised to time but to efficiency of storage of variables. Due to the small torsion elements used to model the shafts in the drive system, simulation of a start-up of a belt conveyor using a finite element model is time-consuming. However, if it is used to calculate accurately the maximum belt tension during non-stationary operation, to determine the minimum required belt strength, application of this method is worth the effort, since the belt is the most expensive component of long belt conveyor systems.
7. The required belt strength can be calculated using either the stationary belt tension or the non-stationary belt tension multiplied by their respective safety factors. Since the non-stationary operation of a belt conveyor system can be influenced by the choice of the start-up or stopping procedure, it should be realised that a reduction of the required belt strength, and thus a reduction of the investment, can only be achieved if the non-stationary belt tension and the corresponding safety factor are used to calculate the minimum required belt strength.
8. Compared to the safety factors obtained from the finite element simulations, a good estimation of the minimum safety factor can be achieved by using the maximum acceleration of the belt, the safety factor on the belt tension during stationary operation, the effective friction coefficient and the ratio between the total motion resistances and the main resistances. Application of the start-up time, calculated with that method in case of a start-up procedure with constant acceleration, results in a smooth start-up of the considered belt conveyor.

9. Models based on the finite element method, like the simulation software system **TUDBELT**, are most suitable to analyse the dynamics of belt systems since they provide a flexibility that models based on other methods do not provide. In particular the procedure of accounting for constraints by using zero-prescribed deformation parameters is very effective.
10. The object-oriented structure of **TUDBELT** enables an efficient and easy accessible storage structure of the model and calculation parameters which enables an easy maintenance and development of the model components. An important drawback of the object-oriented structure is that it slows down the calculation process due to the overhead of the three decomposition structures.

### 8.8 References

Harrison, A. and Roberts, A.W. (1984), "Technical requirements for operating conveyor belts at high speed", *Bulk Solids Handling* 4, pp. 99-104.

Hartog, J.P. den (1956), *Mechanical Vibrations*, McGraw Hill Book Company, New York.

Kuhnert, G. and Schulz, G. (1995), "L. Euler or J.A. Eytelwein ? The origin of the rope friction equation", *Bulk Solids Handling* 15, pp. 261-263.

Lodewijks, G. (1990), *Stageverstag Dunlop-Enerka B.V.* (in Dutch), Department of Transportation and Storage of Bulk Solids, Twente University.

Roberts, A.W. , Hayes, J.W. and Scott, O.J. (1981), "Optimal design of continuous conveyors", *Bulk Solids Handling* 1, pp. 255-264.

Simonson , H. (1987), *Conti Fördergurt-Berechnung*, Continental Fördergurt.

## Chapter 9

# Experimental analysis of transverse belt vibrations

---

In this chapter an experimental analysis of transverse vibrations of a stationary moving flat belt span supported by two idlers is considered. These experiments have been performed to evaluate the approximate analytical models as described in Chapter 4, see also [Van den Dool and Otto, 1993], [Dijkstra and Stelwagen, 1993], [Van Ammers and Timp, 1994], [Weijgand, 1995] and [Wit, 1995]. In Section 9.1 an introductory experiment performed with a real full-scale belt conveyor is discussed. The components of the test facility used for the other experiments, as discussed in Section 9.3, are described in Section 9.2. The results obtained are given in Section 9.4 whereas their applications are discussed in Section 9.5.

### 9.1 Introductory experiment

Geometric imperfections of idler rolls and pulleys, or the passage of a belt splice over an idler roll or pulley, cause an excitation, yielding a transverse vibration in a belt. An introductory experiment has been performed to investigate whether or not the frequencies of excitation and the first natural frequency of transverse vibration of a particular belt span between two idlers can be obtained from a measurement of the transverse displacements. The excitation frequency of, for example, an eccentric idler roll depends on its angular speed, and thus on the belt speed  $V_b$ . The excitation frequency,  $f_i$ , of an idler roll with eccentricity is equal to:

$$f_i = \frac{V_b}{\pi D_r} \quad (9.1)$$

where  $D_r$  is the diameter of the idler roll. The belt is also excited by the passage of a belt splice over an idler. The frequency of belt splice passage,  $f_s$ , depends on the belt speed, the belt length and the number of splices. For a belt with endless length  $L_{\text{belt}}$  and one belt splice the important frequencies are:

$$f_s = \frac{V_b}{L_{\text{belt}}} \text{ and } f_s^* = \frac{V_b}{L} \quad (9.2)$$

where  $L$  is the idler spacing. Assume that the description of the transverse displacement of a supported belt span can be approximated by the linear differential equation (4.39). In that case, and neglecting the bending stiffness, the lowest natural frequency of small amplitude transverse vibration in case of a simply supported belt is given by (also see Section 4.2.4.3,  $\kappa=1$ ):

$$f = \frac{c_2}{2L} \sqrt{1 - \beta^2} \quad (9.3a)$$

where  $\beta = V_b/c_2$ . In case of a belt span where one end is subjected to harmonic vertical displacement (eccentric idler roll), this frequency is given by (see Section 4.2.3.2):

$$f = \frac{c_2}{2L} (1 - \beta^2) \quad (9.3b)$$

Resonance will occur when a natural frequency of transverse vibration of the belt is approached by either the excitation frequency of an idler or an excitation frequency of belt splice passage. As follows from the equations (9.1), (9.2) and (9.3), to design belt supports that prevent excitation in the first natural frequency, the so-called resonance free belt supports, the idler spacing  $L$ , and the belt speed, are subjected to the following conditions:

$$f_s \neq f \Rightarrow L \neq \frac{L_{\text{belt}}}{2\beta} \sqrt{1 - \beta^2} \quad (9.4a)$$

$$f_s^* \neq f \Rightarrow V_b \neq \sqrt{\frac{1}{3}} c_2 \quad (9.4b)$$

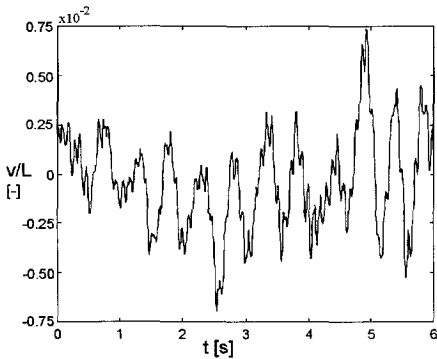
$$f_i \neq f \Rightarrow L \neq \frac{\pi D_r}{2\beta} (1 - \beta^2) \quad (9.4c)$$

The maximum production length of conveyor belts is about 100 till 400 m. With a maximum belt speed of 10 m/s, the maximum frequency of the primary belt splice excitation is 0.1 Hz. Since the frequencies of transverse vibration are always higher, condition (9.4a) is always satisfied. The second and third condition however should be considered during the design stage of a belt conveyor. To illustrate that all the frequencies, given in the equations (9.1), (9.2) and (9.3), can be determined, the transverse displacement of a stationary moving supported belt span has been measured

using an acoustic distance meter (ADM), which will be discussed in Section 9.2.1, and recorded on a PC, see Section 9.2.5.

The considered conveyor belt, an unloaded EP 250/2, has a belt width of 0.6 m, a thickness of 7.3 mm, a density of  $1197.2 \text{ kg}\cdot\text{m}^{-3}$  and one belt splice. The endless belt length is 52.7 m, the considered idler spacing is 3.66 m and the idler rolls have a diameter of 0.108 m. The belt tension force during the experiment was about 1.1 kN as could be learned from the static belt sag ratio  $K_s=0.021$ . The longitudinal velocity of transverse waves  $c_2=14.6 \text{ m/s}$  which was calculated from the square root of the ratio between the belt stress and the belt density. With a stationary belt speed  $V_b=3.57 \text{ m/s}$ , the dimensionless speed ratio  $\beta$  was 0.24. With these data the following frequencies can be calculated:

$$f_s = 0.067 \text{ Hz}, f_s^* = 0.98 \text{ Hz}, f = 1.88 \text{ Hz}, f_i = 10.52 \text{ Hz}$$

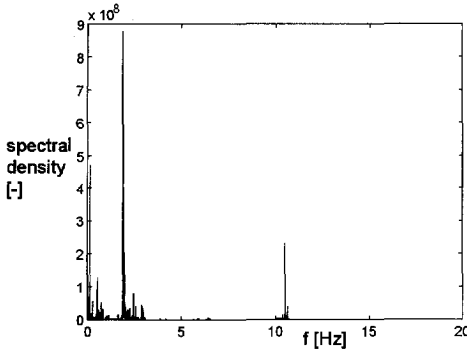


**Figure 9.1:** Ratio between the measured transverse displacement and the idler spacing of a stationary moving belt span supported by two rolls.

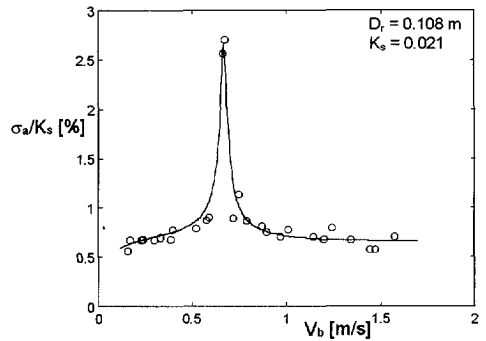
Figure 9.1 shows the ratio between the measured transverse displacement  $v$  and the idler spacing  $L$  as a function of time. After processing of this signal by a Fast Fourier Technique (FFT) the spectral density of Figure 9.2 was obtained. In this figure all four frequencies can be recognised. The first frequency, which appears at 0.067 Hz, is caused by the passage of the belt splice through the considered belt span. The second, at 0.98 Hz, is caused by passage of the belt splice over the idler stations. The third frequency, which appears at 1.91 Hz, is the first natural frequency of transverse vibration of the belt span. The fourth

frequency, at 10.5 Hz, is caused by the rotation of the idlers. The difference between the calculated and measured natural frequency of the transverse belt vibration will be clarified in Section 9.4. Due to the motion resistances, the dynamic belt tension is higher than the pre-tension which explains part of the difference. From equation (9.4b) it can be learned that resonance may be expected when the belt speed is approximately 0.67 m/s. Since the belt speed was 3.57 m/s, no resonance phenomena occurred during the experiment.

To illustrate that resonance phenomena due to idler excitation can occur, the transverse displacement of the considered belt span has been measured during an SPC controlled start-up of the belt conveyor. The belt speed was increased step-wise.



**Figure 9.2:** Spectral density of transverse vibration of a stationary moving belt span supported by two rolls.



**Figure 9.3:** Measured ratio of the standard deviation of the amplitude of transverse vibration and the static belt sag .

After every step the belt speed was kept constant and the transverse displacement of the belt was measured after a stationary state had been reached. As can be seen in Figure 9.1, the amplitudes of transverse vibration over a time interval were not constant. Therefore the standard deviation was calculated. The mean amplitude of vibration can be approximated by  $\sqrt{2}$  times the standard deviation assuming that the belt vibrates harmonically. Figure 9.3 shows the measured ratio between the standard deviation of the amplitude,  $\sigma_a$ , and the static belt sag ratio  $K_s$  for different belt speeds. This figure shows that indeed resonance occurs around a belt speed of 0.67 m/s as was expected.

Severe transverse belt vibrations not only cause extra wear of the conveyor components, but also dissipate a part of the drive power. To estimate the power dissipated in the transverse vibration of belt parts, it is assumed that the transverse displacement is described by the linear solution of the equation of transverse motion in the first vibration mode:

$$v(x,t) = a \sin\left(\frac{\pi x}{L}\right) \cos(\omega t) \tag{9.5}$$

where  $a$  is the vibration amplitude of the middle of the belt part. The kinetic energy of the transverse motion of the belt is maximum for  $v(x,t)=0$ . In that case it is equal to:

$$K_{\max} = \frac{1}{2} \int_0^L (\rho A |v_{,t}|^2) dx \tag{9.6a}$$

From equation (9.5) it can be seen that  $v(x,t)=0$  for  $\omega t = (1+2n)\pi/2$ . Differentiation of  $v$  with respect to time yields the transverse belt speed  $v_t$ . Substitution in equation (9.6a) yields:

$$K_{\max} = \frac{1}{4} \rho A_b a^2 \omega^2 L \quad (9.6b)$$

Due to the damping of the belt material and bulk solid material on the belt, the amplitude of transverse vibration will decrease. The amplitude reduction within one vibration period :

$$t_p = \frac{2\pi}{\omega_d} = \frac{2\pi}{\omega \sqrt{1-\zeta^2}} \quad (9.7)$$

where  $\omega_d$  is the damped natural frequency and  $\zeta$  the damping factor, is equal to:

$$\frac{a_{t+t_p}}{a_t} = \exp\left(\frac{-2\pi\zeta}{\sqrt{1-\zeta^2}}\right) \quad (9.8)$$

With this amplitude reduction, the energy dissipated in one vibration period  $t_p$ , which should be supplied to the belt to maintain a transverse vibration with amplitude  $a$ , is:

$$U_{\text{dis}} = \frac{1}{4} \rho A_b (a_{t+t_p}^2 - a_t^2) \omega^2 L \quad (9.9)$$

This corresponds to the power:

$$P_{\text{dis}} = \frac{U_{\text{dis}}}{t_p} = \frac{1}{8\pi} \rho A \omega_1^3 a^2 L \left[ 1 - \exp\left(\frac{-4\pi\zeta}{\sqrt{1-\zeta^2}}\right) \right] \quad (9.10)$$

According to Otto and Van den Dool (1993) the damping factor of conveyor belts is about 0.02 to 0.04. Therefore the required power can be simplified to:

$$P_{\text{mt}} \approx \frac{1}{8\pi} \rho A \omega_1^3 a^2 L [1 - \exp(-4\pi\zeta)] \quad (9.11)$$

According to Harrison (1994) the amplitude of vibration in belt spans of the return part is approximately 1% of the idler spacing. This is confirmed by Figure 9.1. If the

horizontal belt conveyor considered in Section 8.1 is used as an example, then the power required to maintain natural transverse belt vibrations of all the belt spans of the return part of the belt is equal to 11.5 kW which is about 5.6% of the total drive power. In case of resonance the amplitudes of vibration are even larger. However the situation that all the belt spans of the return part vibrate with the same amplitude is rare.

From the foregoing considerations it follows that transverse belt vibrations can considerably affect the operational behaviour of a belt. However, they also enable the determination of the magnitude of the belt tension. Therefore, experiments have been performed on a special test facility to determine which of the models, as described in Chapter 4, most accurately predicts the finite amplitude natural frequency of transverse vibration. In particular, this is important to determine what safety margin should be accounted for in the design of resonance free belt supports and to evaluate whether or not the frequencies of transverse vibrations can be used in a belt monitoring system. The equipment used in these experiments is described in the next section.

### 9.2 Test facility

The main purpose of the test facility, which is depicted in the Figures 9.4 and 9.5, is to enable the determination of transverse vibrations of an idler supported, stationary moving, belt span. To control the belt speed an SPC is applied on the 1.5 kW induction motor. The conveyor structure is stiff and isolated from the ground by four thin rubber foundation sheets to eliminate environmental influences and noise. In the design special attention is given to an easy replacement of the endless belt. The belt is supported by seven aluminium pulleys and two aluminium idlers. The drive, tail, and tension pulleys have a diameter of 0.150 m and for the bend pulleys and the idler rolls it is 0.100 m. The drive pulley is crowned to track the belt. If the tracking is not sufficient then also the tail pulley and the bend pulleys can be adjusted to track the belt. The conveyor has been designed to support an endless belt with a length of about 7 m. To prevent the belt from being lifted off the idlers, the belt is installed under the idler rolls instead of on top of the rolls. In the Figures 9.4 and 9.5 three parts can be distinguished: an SPC, a belt conveyor and a data recording and processing unit.



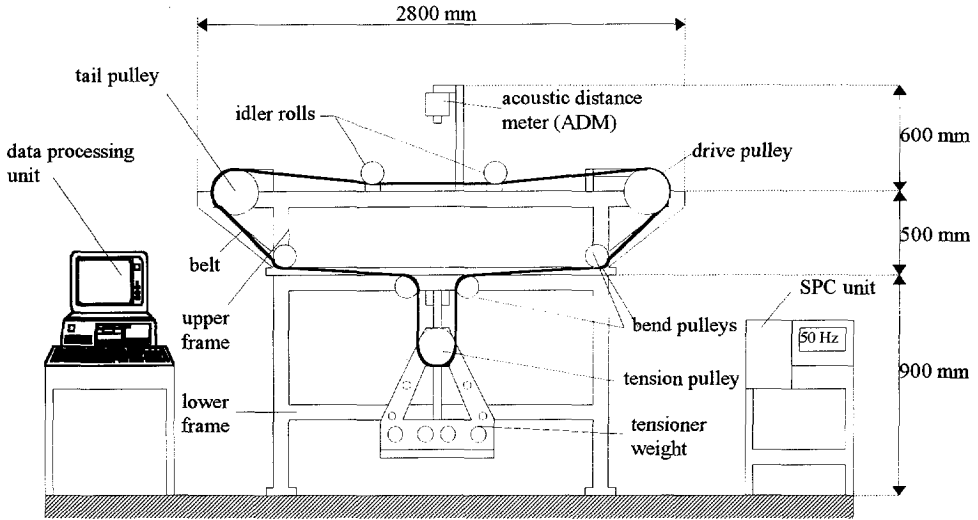


Figure 9.4: Schematic presentation of the dynamic test facility.



Figure 9.5: The dynamic test facility (Photograph courtesy of Facilitair Bedrijf TU Delft).

From Chapter 4 it is clear that the following data are required to describe accurately the transverse vibration  $v(t)$  of a belt span by a non linear model:

1. the idler spacing:  $L$
2. the belt tension:  $T$
3. the belt speed:  $V_b$
4. the specific belt mass:  $m'_b$
5. the effective bending stiffness:  $(EI)_{\text{eff}}$
6. the effective normal stiffness of the belt:  $(EA)_{\text{eff}}$

The specific belt mass and also the effective normal and bending stiffness are determined by the selected belt type. The belt conveyor is designed to enable the measurement of the transverse displacement of the belt in the middle of the span; the idler spacing, the belt tension and belt speed can be adjusted. The components and the signal processing will be discussed in the following sections.

### 9.2.1 Acoustic displacement meter

To measure the transverse displacement of the idler supported belt span, an acoustic displacement meter, or ADM, is used. The ADM, type "Ultrasonic Ranger HE-501", is placed above the middle of the supported span and is used to measure contactlessly the distance to the belt. It is provided with two transducers. The first one emits a sound wave which, after reflection against the belt surface, is received by the second transducer. The delay time between transmission and arrival is a measure for the distance between the ADM and the belt.

### 9.2.2 Idler spacing adjustment

To enable a quick and accurate adjustment of the idler spacing, the two beams of the upper frame that carry the idlers are provided with holes over a length of 2 m. The distance between adjacent holes is 50 mm. Also the idler frames are provided with two holes. The idler spacing can be adjusted between 100 mm and 2000 mm by fixing the idlers to the structure with fitted dowels. During the experiments three idler spacings have been used: 800, 1200 and 1600 mm.

### 9.2.3 Belt tension adjustment

To pre-tension the belt, the conveyor is provided with a weight tensioner. The tensioner is built up of a tension pulley and a container which are bolted together. The tensioner can move along two guide bars which prevent the container from swinging.

The mass of the tension pulley and the container is 38.6 kg. Special blocks with a mass of about 12 kg are available to be put into the container to increase the mass of the tensioner. During the experiments 0, 2, 4 or 6 blocks were added which resulted in pre-tensions of the belt as is summarised in Table 9.1. With increasing pre-tension the energy loss due to bending of the belt increases. Due to the limited motor power of 1.5 kW, the maximum tensioner mass turned out to be about 120 kg.

To excite the moving belt, a small block is dropped in the container. To guide this block, a shaft is mounted on the bottom of the container. The transverse vibration of some belts was governed by a strong low frequency excitation caused by the belt splice. In those cases the excitation provided by the tensioner weight was not enough to enable the determination of the first natural frequency of transverse vibration. These belts were therefore excited by hand between the idlers.

Number of blocks [-]	0	2	4	6
Tensioner mass [kg]	38.6	65.5	89.8	113.9
Belt pre-tension force[N]	189.27	321.29	440.20	558.35

Table 9.1

Due to the motion resistances, the belt tension is not equal to the pre-tension. The drive force  $F_d$  is equal to the sum of the motion resistance forces. All the idlers and pulleys are, related to the position of the ADM, symmetrically placed in the conveyor. It is assumed that the motion resistances are equally distributed over the conveyor. This assumption holds if the conveyor is well aligned and the resistance to rotation of the bearings of two identical idlers or pulleys is equal. In that case the belt tension of the idler supported segment,  $F_s$ , is approximately equal to the sum of the pre-tension,  $F_v$ , and half the drive force, see also Figure 9.6:

$$F_s = F_v + \frac{1}{2} F_d \tag{9.12}$$

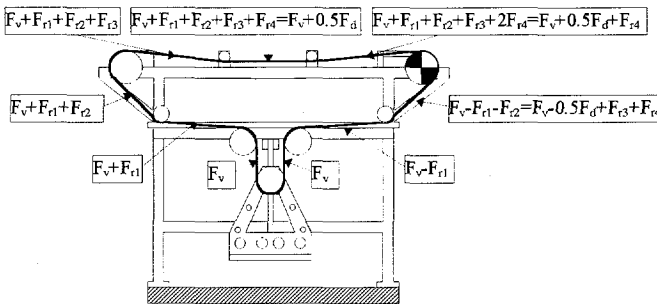


Figure 9.6: Belt tensions.

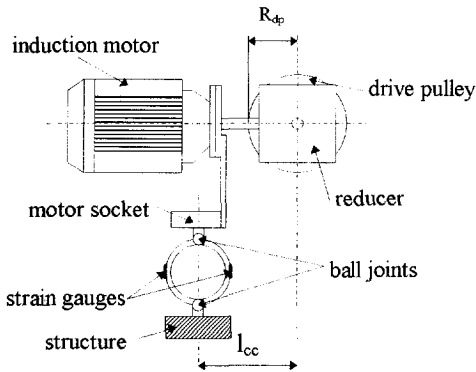


Figure 9.7: Force measuring device.

The drive force can be measured with the dynamometer shown in Figure 9.7. This device is mounted directly under the induction motor. Two strain gauges are placed on a ring which is connected to the motor socket and the structure by two ball joints. These joints ensure that only forces and no moments are measured. The dynamometer measures not only the drive force but also a static force due to the weight of the motor. To exclude this weight, the output signal of the dynamometer is put to zero in case of the belt at rest by fine tuning the device. If  $l_{cc}$  is the distance between the centre line of the drive pulley shaft and the centre line of the measuring ring and  $R_{dp}$  is the radius of the drive pulley then the drive force can be calculated from, see also Figure 9.7:

$$F_d = \frac{l_{cc} F_m}{R_{dp}} \quad (9.13)$$

### 9.2.4 Belt speed adjustment

The shaft of the induction motor, type SEW Dft 90 L4, and the drive pulley shaft are connected by a bevel gear box, type Graessner 07 H 13R, with reduction ratio 1. The nominal number of revolutions of the motor is 1420 rpm. With a reduction ratio of 1.0 and the diameter of the drive pulley of 0.15 m, this results in a nominal belt speed of  $11.15 \text{ m}\cdot\text{s}^{-1}$ . Higher belt speeds can be achieved by supplying the SPC controlled motor with frequencies above the 50 Hz. The angular speed of the drive pulley shaft is measured by a tachometer which is mounted directly on the shaft. The tachometer has a range of 0 to 2500 rpm which is enough considering the nominal number of revolutions of the shaft of the motor. To control the angular speed of the motor shaft, and thus the belt speed, an SPC, type Hitachi J100-015 HFT, supplies the motor with variable voltage and frequency. Seven different belt speeds have been used during the experiments: 0.0, 2.0, 4.0, 6.0, 8.0, 10.0 and 12.0 m/s.

Both idler rolls are provided with a digital incremental shaft encoder type Tekel TKW 6162 3600. These encoders give a discrete time series of the mechanical position of the idler roll shaft for direct display and processing. The encoder has 3600 increments per revolution which implies that an angular displacement of  $0.1^\circ$  can be

detected. The purpose of the encoders is to find out whether or not they can be used to detect severe transverse belt displacements. Assume that the start position for both encoders is the same. If the transverse displacement of the stationary moving belt between the idler rolls is small then the difference of the output signals of the encoders is small. If the transverse displacement is large then this difference is significant. The output from the encoders can also be used to determine the (local) belt speed.

### 9.2.5 Signal processing

During an experiment five analogue signals come available: the transverse displacement of the belt, the belt speed, the drive force and the angles of the two idler roll axes. The two signals of the incremental encoders are collected in a collector box which subtracts both signals and raises the difference with an offset value. The remaining four cables carrying the signals are collected in a cable collector which is directly connected to a personal computer. A trigger, which activates the PC to record the signals and which has a sample frequency of 200 Hz, is mounted in the cable collector. Also an amplifier and a filter, which are used to transform the ADM signal, are mounted in the cable collector. The software program SPEEDCON [Wit, 1995] is used to process the signals. The FFT procedure of the software package Matlab<sup>®</sup> is used to find the frequency spectrum of the displacement signal.

## 9.3 Experimental program

In this paragraph the experiments are discussed. Also the relevant properties of the conveyor belts which have been used are given.

### 9.3.1 Experimental data

Prior to an experiment the idler spacing, belt tension and belt speed have been adjusted. The transverse displacements of a stationary moving belt have been measured at seven different speeds, three different idler spacings and four different pre-tensions which yields 84 combinations. For each parameter combination two experiments have been performed; one with and one without excitation by the tensioning mass. Therefore 168 experiments have been performed for each conveyor belt. Since four different belts have been used, 672 experiments have been carried out altogether. During a series of 7 experiments the pre-tension and idler spacing were kept constant and the belt speed was decreased from 12 m/s to 0 m/s. To enable the accurate determination of the frequency of transverse vibration, the transverse displacement of the belt has been measured during 10 seconds for an experiment with

excitation and 30 seconds for an experiment without excitation. From an experiment the following data are obtained:

- *average belt speed*, which is directly obtained from the signal of the tachometer.
- *average drive force*, which is obtained from the signal of the dynamometer. From the experiments it follows that after a series of 7 experiments a residual drive force remained in the belt which was caused by the break away friction of the bearings of the idlers and pulleys. This residual drive force is subtracted from drive forces measured during the other 6 experiments [Wit, 1995].
- *average belt sag*, which is the average transverse displacement of the belt measured during an experiment without excitation. From the experiments it follows that the belt sag ratio could be accurately predicted by equation (3.14). However, for small idler distances or high pre-tensions the natural curve of the belt, caused by the manufacturing and by differences in upper and lower belt cover thicknesses, significantly influences the measured belt sag which results in significant differences between the measured and calculated belt sag.
- *standard deviation of the transverse displacement*, which is calculated, for the experiments without excitation only, to get an idea of the average amplitude of vibration. Since the transverse displacement of the supported belt part is about sinusoidal, the amplitude of transverse vibration can be estimated by multiplication of the standard deviation by a factor  $\sqrt{2}$ . The average amplitude of vibration could also have been determined directly from the measured transverse displacement signal. However, due to noise in the signal this results in an overestimation of the amplitude. The differences of the standard deviations found during the experiments without excitation is significant. This is due to the low level random excitation of the vibrations and to direct excitation of the transverse displacement by passage of the belt splice.
- *minimum and maximum transverse displacement*, which is analysed, for the experiments with excitation only, to check the amplitude of vibration.
- *damping factor*, which is calculated for the experiments with excitation only from the decrease of the amplitude of vibration.
- *frequency spectrum of transverse vibration*, which is calculated with use of the FFT procedure. The spectrum is obtained from the signals with excitation which yields the most accurate results.
- *idler spacing*, which is adjusted prior to an experiment.
- *pre-tension*, which is also adjusted prior to an experiment.

The data obtained from the experiments are listed in Appendix B.

### 9.3.2 Installed conveyor belts

For the experiments four different EP belts, as indicated in the Tables 9.2 and 9.3, have been used. The conveyor belt sizes and parameters given in Table 9.3 are provided by the conveyor belt manufacturers. More information can be found in Appendix D. The belts all had a width of 200 mm.

Belt code	Manufacturer	Manufacturer code	Cover material
EP 120/1	Fabreeka Bandtransport B.V.	11-11	PVC
EP 200/2	Dunlop Enerka B.V.	SL 200/2 RA	rubber
EP 240/2	Fabreeka Bandtransport B.V.	21-18	PVC
EP 360/3	Fabreeka Bandtransport B.V.	31-11	PVC

Table 9.2: Conveyor belt description.

	$d_b$ [mm]	$m'$ [kg.m <sup>-1</sup> ]	$(EA)_{eff}$ [10 <sup>3</sup> N]	$(EI)_{eff}$ [N.m <sup>2</sup> ]
EP 120/1	1.80	0.409	1.681	0.041
EP 200/2	5.59	1.297	2.616	0.822
EP 240/2	4.45	1.063	1.682	0.278
EP 360/3	4.24	0.964	1.815	0.272

Table 9.3: Conveyor belt sizes and parameters.

## 9.4 Results of the experiments

In this section the results of the experiments described in Section 9.3 are discussed. The main objective of the experiments is to evaluate the analytic approximations as given in Chapter 4 for the first natural frequency of transverse vibration of an axially moving belt.

Three analytical approximations are used. The linear speed independent frequency of a string,  $f_{ss1}$ , see also equation (4.50), the linear speed dependent frequency,  $f_{mb1}$ , taking into account the bending stiffness and neglecting the coriolis term, see also equation (4.65), and the non-linear frequency according to Korde (1985)  $f_1^k$ , see also equation (4.105):

$$f_{ss1} = \frac{1}{2L} \sqrt{\frac{T}{\rho A}} \quad (9.14a)$$

$$f_{mb1} = \sqrt{\frac{(1-\beta^2)^2}{4L^2} \frac{T}{\rho A} + \frac{\pi^2}{4L^4} \frac{EI}{\rho A}} \quad (9.14b)$$

$$f_1^k = \frac{1}{2L} \sqrt{\frac{T}{\rho A}} \sqrt{1-\beta^2} \sqrt{1 + \frac{9\pi^2 P_1^2 a^2}{32(1-\beta^2)}} \left[ 1 + \frac{1}{48} \left( 1 + \frac{32(1-\beta^2)}{9\pi^2 P_1^2 a^2} \right)^{-2} \right]^{-1} \quad (9.14c)$$

Besides the analytical approximations, a discrete approximation of the non linear frequency of an axially moving belt according to Thurman and Mote (1969),  $f_{nl}$ , is used. For this purpose a computer program developed by Serckx (1995) and based on the finite difference method is used. In the solution process, terms up to the order  $O(\mu^2)$ , where  $\mu$  is a small perturbation parameter used in Section 4.2.4, are taken into account. Serckx (1995) performed 13 experiments to verify his numerical model. Although his results are not discussed in detail in this chapter, they are taken into account when drawing conclusions at the end of this paragraph.

The total number of experiments was 672. To limit the number of calculations required to determine the non-linear frequency according to Thurman and Mote (1969), only combinations of the lowest or highest pre-tension and the smallest or largest idler spacing are considered for four different belt speeds. This results in 16 combinations for each conveyor belt and 64 in total. The experimentally obtained frequencies and the frequencies obtained from the three analytical and the discrete approximations for these combinations, are given in Appendix C. These frequencies are also shown in the Figures 9.8-9.11 as a function of the dimensionless speed ratio  $\beta$ . These figures show the linear speed independent frequency (dashdot line), the linear speed dependent frequency (solid line), the non linear frequency according to Thurman and Mote (dashed line), and the non linear frequency according to Korde (dotted line) as a function of the speed ratio  $\beta$ . The frequencies obtained from the experiments are indicated by circles. The amplitudes of transverse vibration used to calculate the non-linear frequencies are obtained from the experimental data.

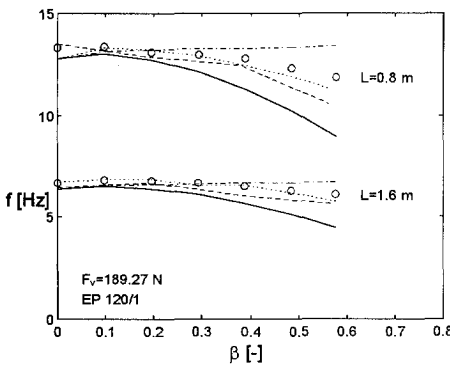


Figure 9.8a

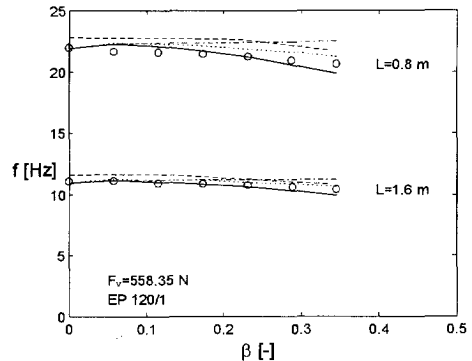


Figure 9.8b



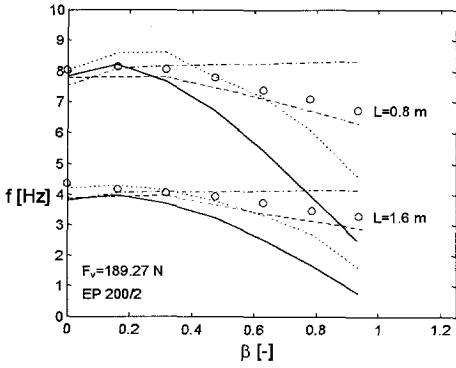


Figure 9.9a

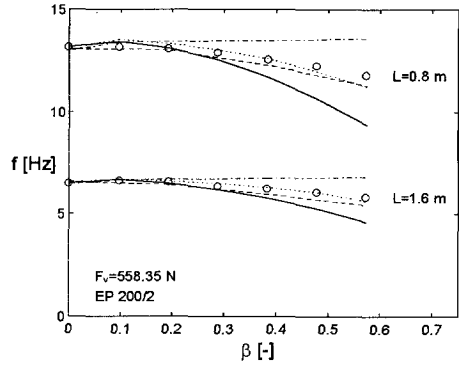


Figure 9.9b

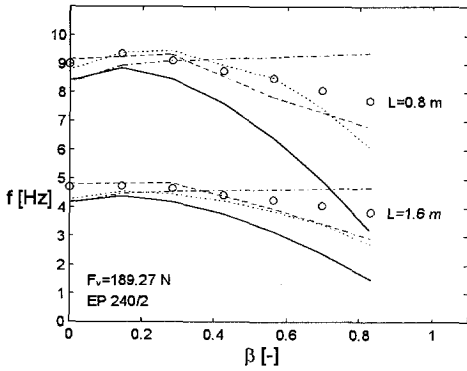


Figure 9.10a

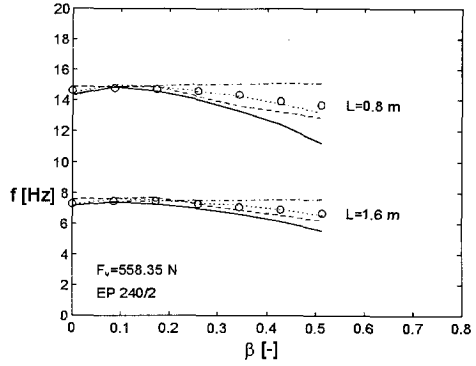


Figure 9.10b

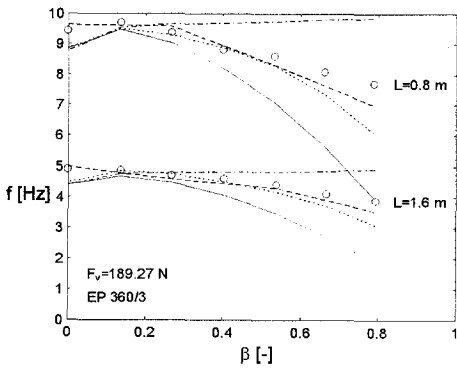


Figure 9.11a

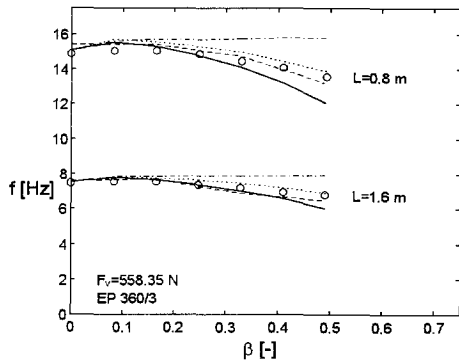


Figure 9.11b

To be able to evaluate the approximations for the frequency of transverse vibration, the basic assumptions of these approximations have to be considered. Three assumptions are relevant for this chapter:

1. In all cases terms of the order  $O(v/L)^2$ , and  $O(u/L)=O(v/L)^2$  are neglected with respect to unity.
2. In the application of the perturbation method terms of  $O(\mu^3)$  are neglected where the small parameter  $\mu = P_1^2 a^2$  where  $P_1^2 = E_b A / T_0$  and  $a$  the dimensionless amplitude of vibration.
3. Korde (1985) neglects the non-linear coupling between the transverse and the axial motion of the belt.

From the experiments the following conclusions can be drawn:

1. The dimensionless amplitude  $a$  is equal to the maximum transverse displacement  $v$  divided by the idler spacing  $L$ . During an experiment without excitation, this amplitude was not constant just as in the introductory experiment, see also Figure 9.1. In that case the average amplitude was approximated by the standard deviation of the amplitudes multiplied by  $\sqrt{2}$ . Also during an experiment with excitation, the amplitude was not constant. However, it turned out that after a few vibrations the amplitude reduced to about one third of the amplitude of the first vibration of the belt. The signal with reduced amplitudes was used to determine the frequency of transverse vibration. That reduced amplitude was also used to calculate the non-linear frequency according to Thurman and Mote (1969) and according to Korde (1985). The amplitudes of the different experiments were comparable. The average amplitude  $a$  is about  $1.5 \cdot 10^{-2}$  whereas the maximum amplitude is  $5 \cdot 10^{-2}$ . Therefore the terms  $O(v/L)^2$  and  $O(u/L)$  may indeed be neglected with respect to unity.
2. As can be seen in the figures 9.8-9.11, the linear speed independent approximation (dashdot lines) overestimates the frequency whereas the linear speed dependent approximation (solid lines) underestimates the frequency. The trends of both nonlinear approximations follow the trend of the frequency versus  $\beta$  as obtained from the experiments. The nonlinear frequencies are mostly slightly lower than the experimentally obtained frequencies. This result could be observed during all the experiments.
3. The influence of the bending stiffness of the belt on the frequency of transverse vibration is small in most cases. The maximum error made by neglecting the bending stiffness is 1.5 % in case of belt EP 200/2; the minimum error is 0.2 % in case of belt EP 120/1.
4. During the experiments the maximum value of the parameter  $\mu \approx 0.25$ . The nonlinear analytical approximations of the (small amplitude) frequency of

transverse vibration of an axially moving belt deviates maximal  $\pm 2.5\%$  from the frequency obtained from the experiments for  $\mu < 0.1$  and  $\beta < 0.9$ . For  $\mu > 0.1$  (and  $\beta < 0.9$ ), this deviation is maximal  $10\%$ . This is confirmed by the experiments of Serckx (1995). These deviations are partly caused by errors in measuring. Wit (1995) found that even after measuring in threefold the relative error is still about  $2.5\%$ . The small deviations are mainly caused by the assumption that (1) the belt behaves like an axially moving uniform string or beam and that (2) the belt is simply supported by the idler rolls. Due to the non-homogenous belt material and the imperfections in the belt caused by the production process, which can cause a non-homogenous stress distribution, the belt's behaviour can differ significantly from the behaviour of a homogeneous and uniform string or beam. The assumption of a simply supported belt includes that both belt ends can rotate freely but not move in the axial direction. In the test-facility, however, the motion of the supported belt part is constrained by the motion of the idler rolls which is governed by the friction in the bearings and its inertia. This results in under-estimation of the frequencies. Large deviations are caused by (3) taking only terms of  $O(\mu)$  and  $O(\mu^2)$  into account. Deviation due to the third approximation occurs when  $\mu > 0.10$  and for large values of  $\beta$ . In that case also terms of order  $O(\mu^3)$  should be taken into account.

5. The contribution of the non-linear terms in the equation of motion of an axially moving belt significantly increases as the belt speed increases. As already stated by Thurman and Mote (1969), the results of a linear approximation are poor for  $\beta > 0.3$ . This is confirmed by the experiments where the perturbation parameter  $\mu < 0.15$  and the static belt sag smaller than the amplitude of vibration. In case of  $\beta > 0.3$  the linear frequency deviates from the non-linear frequency by a percentage between  $10$  and  $75\%$  depending on the magnitude of  $\mu$ .
6. To estimate the natural frequency of transverse vibration of an axially moving belt the approximation of Korde (1985) is useful. Under normal operational circumstances ( $\mu < 0.05$  and  $\beta < 0.5$ ) the maximum deviation from the measured frequency is  $\pm 5\%$ . During the experiments of Serckx (1995) the parameter  $\mu > 0.05$ . His results confirm that in this case the approximation according to Korde (1985) overestimates the frequency where the approximation according to Thurman and Mote (1985) yields accurate results.
7. During the experiments only flat belts have been used. However, also the frequencies of transverse vibration of a troughed belt can be determined from its transverse displacement signal. The frequencies of transverse vibration of the troughed belt mentioned in Section 9.1 are above  $100$  Hz [Wit, 1995]. Determination of these frequencies requires a sample frequency of at least  $200$  Hz. Since the sample frequency of the ADM used during the experiments was only  $60$  Hz these frequencies could not be detected.

8. In order to obtain accurately values for the lowest frequency of transverse vibration from the transverse displacement of a belt, a measurement of at least 10 seconds was required during the experiments. Therefore, the belt tension could only be calculated from this frequency for a stationary moving belt. Determination of the belt tension during non-stationary operation is not possible.
9. Due to dominant noise in the signal, the frequency of transverse vibration of the considered belt span could not be determined from the signals of the digital incremental shaft encoders.

### 9.5 Application of the experimental results

In the experiments described in this chapter the frequency of transverse vibration of an axially moving belt was obtained from the measured transverse displacements of the belt to evaluate three analytic approximations and one discrete approximation of that frequency. It turned out that transverse vibrations of a belt span supported by two idlers without special excitation are noticeable under all operational circumstances.

The nature of these excitations is often rather random which results in considerable vibration amplitude fluctuations. The transverse displacement of a belt span is excited by the periodic passage of the belt splice and by the rotation of the supporting idlers. In the frequency spectrum, which is obtained from the measured displacement signal after transformation from the time to the frequency domain, at least three peaks are noticeable. These peaks indicate the frequency of passage of the belt splice, the first natural frequency of transverse vibration of the belt and the frequency of excitation of the idlers. Normally the spectral density at the first natural frequency of transverse vibration of the belt is far larger than the spectral densities at the other frequencies. However, due to the random character of the excitation, this spectral density varies and can sometimes be smaller at the first natural frequency than the spectral densities at other frequencies. This implies that the frequency of transverse vibration of the belt can not always automatically be found from the results of one experiment by searching for the frequency with the largest spectral density.

The relation between the belt tension and the frequency of transverse vibration can be used to design resonance free belt supports, to monitor the maintenance condition of belt conveyor components other than the belt and to monitor the conveyor belt to determine belt damage.

In the introduction to this chapter an example is given of the three frequencies that can be determined from the transverse displacement signal of an axially moving belt. Resonance phenomena may be expected when the excitation frequency of an idler roll, or a multiple of this frequency, approaches the lowest natural frequency of transverse vibration of the belt. In equation (9.4) three conditions are given that constrain the idler spacing to prevent resonance. From Section 9.4 it follows that the

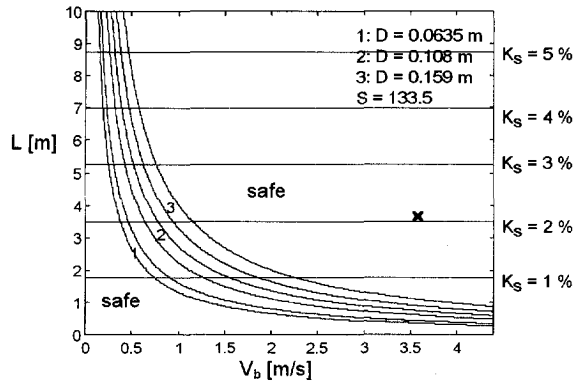
Korde (1985) approximation can be used to determine accurately the frequency of small amplitude transverse vibration. Resonance free support is ensured if a safety margin of  $\pm 10\%$  is held. The idler spacing is then subjected to the following condition:

$$f_i \neq f_i^k \Rightarrow L \leq 0.9 \frac{\pi D_i}{2\beta} \sqrt{1-\beta^2} \text{ or } L \geq 1.1 \frac{\pi D_i}{2\beta} \sqrt{1-\beta^2} \quad (9.15)$$

This equation can be used to define idler spacing zones in which resonance phenomena may be expected and that should therefore be prevented. This is illustrated in Figure 9.12 where six lines, based on this equation, are drawn. These lines bound the potential resonance zones for the conveyor described in Section 9.1. The three zones, indicated by numbers 1, 2 and 3, hold for three different idler diameters. The lines that bound the resonance zones for multiples of the idler frequency, and which are not drawn, lay between the indicated zones and the axes. The combination of the idler spacing and belt speed used in the introductory experiment is indicated by a cross mark. From this figure it can be concluded that during stationary operation no resonance is to be expected from the idler/belt span interaction.

The determination of the maintenance condition of belt conveyor components can be illustrated by inspection of the idlers. Idler wear expresses itself in idler cover wear and an increase of the motion resistance of the idler as a result of bearing wear. The idler frequency, see equation (9.1), can be determined very accurately from the transverse displacement signal of the belt. If the cover of the idler mentioned in section 9.1 reduces 2 mm then the idler frequency increases with 4 % from 10.53 Hz to 10.93 Hz. This increase can easily be detected. By determination of the belt tension for adjacent belt parts using the tension/frequency relation the motion resistance of each idler set can be determined. Although the accuracy in this case is lower than the accuracy of the cover wear determination, it gives a clear indication which idlers should be replaced to decrease the total motion resistance of the belt. This procedure is only reliable if the vertical belt load is exactly known to determine the belt tension accurately. Since the bulk material loading degree is normally not constant, this procedure can not be used for a loaded belt.

Conveyor belt damage can be determined by considering the spectral density of for example the frequency of belt splice passage. If a belt splice is damaged then the spectral density at the frequency of splice passage will increase compared to the spectral densities of other frequencies. Ageing can affect the material parameters of the belt which affect its bending stiffness. Since the influence of the bending stiffness is hardly noticeable in the frequency of transverse vibration, it is not possible to detect ageing of the belt.



**Figure 9.12:** Calculated resonance zones for different idler diameters  $D$ . Cross indicates belt speed and idler space during introductory experiment.

## 9.6 References

- Ammers, P.S. van and Timp, P.H.W. (1994), *Transversale trillingen in een transportbandsysteem, een kwantitatief onderzoek* (in Dutch), Reportno. 94.3.TT.4275, Section Transporttechnology, Delft University of Technology.
- Dijkstra, P.T.S. and Stelwagen, J.C. (1993), *Transversale trillingen in een lopende transportband* (in Dutch), Reportno. 93.3.TT.4225, Section Transporttechnology, Delft University of Technology.
- Dool, A.A. van den and Otto, J.F. (1993), *Transversale trillingen in een transportband* (in Dutch), Reportno. 93.3.TT.4165, Section Transporttechnology, Delft University of Technology.
- Harrison, A. (1994), "Belt vibration and its influence on conveyor reliability", *Bulk Solids Handling* 14, pp. 723-727.
- Korde, K.R. (1985), "On nonlinear oscillation of moving strings", *Journal of Applied Mechanics* 52, pp. 493-494.
- Lodewijks, G. (1991), *Experimenteel onderzoek van transportbandmonsters ter determinatie van de dynamische eigenschappen* (in Dutch), Reportno. 91.3.TT.2916, Section Transporttechnology, Delft University of Technology.
- Serckx, T. (1995), *Non-linear vibrations of an axially moving strip*, Faculty of Applied Sciences, Department of Mechanical Engineering, Catholic University of Louvain.
- Thurman, A.L. and Mote, C.D. (1969), "Free, periodic nonlinear oscillation of an axially moving strip", *Journal of Applied Mechanics* 36, pp. 83-91.
- Weijgand, M. (1995), *Transversale trillingen in transportbanden* (in Dutch), Reportno. 95.3.TT.4441, Section Transporttechnology, Delft University of Technology.
- Wit, J. (1995), *Het transversale trillingsgedrag van transportbanden* (in Dutch), Reportno. 95.3.TT.4442, Section Transporttechnology, Delft University of Technology.

## Chapter 10

# Design aspects, conclusions and recommendations

---

**T**o describe mathematically the dynamics of belt systems, it is useful to distinguish between the stationary and the non-stationary operation of a system. During stationary operation the dynamic behaviour of a belt system is mainly controlled by the interaction between the belt and the belt supports, and by the interaction between the belt and the belt tensioner. During non-stationary operation it is mainly controlled by the starting and stopping procedures, which are specified by velocity profiles and duration of the procedures, and by the velocity of the longitudinal wave propagation through the belt.

### 10.1 Stationary operation

During stationary operation all belt spans supported by two idlers vibrate transversely in a natural frequency due to low level random excitation and usually the amplitudes remain small. The amplitude increases considerably when a belt span is excited in the first resonance frequency. This excitation can be direct, caused by idler roll eccentricity or passage of belt splices over a supporting idler, or parametrical, caused by belt tension variation due to tensioner vibration or passage of belt splices over pulleys. To prevent that the belt speed approaches the critical speed, the belt tension should be high enough to ensure that the longitudinal velocity of transverse waves is much higher than the maximum belt speed. During stationary operation of belt conveyor systems this condition is normally fulfilled. If the dynamic behaviour of one belt span is of interest and the source, frequency and amplitude of excitation are known in advance, then it is often sufficient to consider that span isolated from the rest of the system to analyse the response to the excitation. However, in belt systems that contain many belt spans, like long belt conveyor systems, the interaction between adjacent spans and especially the interaction between longitudinal and transverse belt vibrations is important. In that case a global analysis should be considered.

## 10.2 Non-stationary operation

To analyse the dynamic behaviour of a belt system during non-stationary operation, the entire belt system should be considered and not just one belt segment. The starting and stopping procedure, which are not standardised, should be chosen in such a way that the transient belt tension does not exceed the maximum belt tension, prescribed by design standards, and that the performance of the belt system during starting and stopping is acceptable.

The transient belt tension during start-up is determined by the start couple of the drive system, the inertia and acceleration of the belt, the reflection and interference of stress waves, and the damping in the belt system.

The damping in the belt system is determined by the selected belt and its supports and can hardly be influenced since the choice of a belt is determined by its application and price.

Stress waves can reflect against pulleys. In case of a pulley that can only rotate, wave reflection occurs when the rotation of the pulley is constrained by for example the motion of components connected to that pulley like in case of a drive pulley. In case of a pulley that can both rotate and move laterally, wave reflection does always occur except when the rotation of the pulley is free and the lateral motion is constrained as for example in the belt tensioner. In case of a screw tensioner, which is used to pre-tension the belt, stress waves never reflect since the tension pulley can rotate freely and can not move laterally. However, most belt systems are fitted with a winch or weight tensioner to maintain a minimum belt tension. In that case the tension pulley can rotate and move laterally which causes reflection of stress waves. If reflection yields unacceptable stress levels then the lateral motion of the tension pulley should be prevented or constrained during start-up.

The influence of stress waves on the total belt tension is significant in case of a high start couple or a step-wise increased drive couple. To minimise the influence of travelling stress waves, the belt tension should be increased slowly and continuously. The initial value of the start-up drive force should be such that it just exceeds the total break-away resistance force.

By far the most important parameter which influences the transient belt tension is the acceleration of the (loaded) belt. The maximum allowable acceleration force is limited by the belt tension during stationary operation and the ratio between the safety factors on the tension in a moving belt during stationary operation and non-stationary operation. Given the inertia of the (loaded) belt this prescribes the maximum belt acceleration which is governed by the velocity profile and duration of the start-up procedure. From this point of view it is recommended to choose a constant belt acceleration, and thus a linearly increasing belt velocity, which will minimise the start-up time as has been explained in Chapter 8. A linearly increasing belt velocity requires a controlled start-up. In this thesis only the dynamic behaviour of static



power converter (SPC), velocity controlled start-ups have been analysed by simulation using the simulation software system **TUDBELT**. However, a linearly increasing local belt velocity can also be achieved by the application of a controlled fluid coupling or a controlled start transmission (CST). Since the belt speed turned out to increase linearly with the (electrical) supply frequency of the SPC, a control algorithm has not been designed. However, the application of a fluid coupling or a CST requires a control algorithm to ensure a linear speed increase. To test this algorithm, a simulation software system like **TUDBELT** is necessary. To prevent peak loads on the belt, the control algorithm should ensure a constant acceleration instead of forcing the belt speed to follow a predetermined velocity profile as has been explained in Chapter 6.

The performance of a belt system is acceptable if the belt is always in tension, if it remains on the supports and, in case of belt conveyors, the bulk solid material remains on the belt. It is desirable that the amplitudes of transverse vibration of the belt segments are small to reduce the energy consumption of the system, and that the displacement of the belt tensioner during non-stationary operation is small to minimise its size. Although the dynamics of a belt system can only be analysed by simulation of the dynamic behaviour of the entire system, it is sufficient to analyse only those sections in detail where operational problems like a lift off of the belt from the supports can be expected to determine whether or not the operational behaviour of the system is acceptable.

### 10.3 Calculation methods

In this thesis a number of approximation methods to analyse the dynamics of belt systems have been discussed. Some of these methods are relatively simple and can for example be used to find out whether or not resonance phenomena may be expected, as discussed in the Chapters 4 and 9, or to estimate the belt tension during non-stationary operation, as discussed in Chapter 8. Other methods, like those discussed in the Chapters 5-7, are relatively complex and enable the analysis of the dynamics of entire belt systems. It is important for an engineer in the design stage of a belt system, to use those methods that provide relevant and sufficient information. In general it can be said that complex methods are applied in case of belt systems which require a precise knowledge of the belt motion, for example in case of digital audio and video systems, or the belt tension, for example in case of belt systems with expensive tension carrying members like long belt conveyor systems.

In Chapter 4 the equations of motion of a stationary moving belt span have been derived. Depending on the amplitude of transverse vibration, either the simple linear solution or the more complex nonlinear solution of these equations can be used to determine the motion of the belt.

From experiments, described in Chapter 9, it was found that the frequency of transverse vibration of a stationary moving belt span can accurately be obtained by a perturbation method taking terms of  $O(\mu)$  and  $O(\mu^2)$  into account, where  $\mu$  is the ratio of the square of the dimensionless amplitude of vibration and the initial strain which is used as a small perturbation parameter. The nonlinear analytical approximation of the frequency deviates maximal  $\pm 2.5\%$  from the frequency obtained from the experiments for  $\mu < 0.1$  and  $\beta < 0.9$ , where  $\beta$  is the ratio between the belt speed and the longitudinal velocity of transverse waves. For  $0.1 < \mu < 0.25$ , this deviation is maximal  $10\%$  depending on the magnitude of  $\beta$ . In that case also terms of order  $O(\mu^3)$  should be taken into account. The contribution of the non-linear terms in the equation of motion significantly increases when the belt speed increases. In case of for example  $\mu = 0.15$  and  $\beta > 0.3$ , the minimum deviation of the linear frequency from the non-linear frequency is  $10\%$ . However, the same accuracy can be reached in case of smaller values of  $\beta$  and larger values of  $\mu$ , for example  $\mu = 0.22$  and  $\beta = 0.1$ . Under normal operational circumstances, where  $\mu < 0.05$  and  $\beta < 0.5$ , the approximation of Korde, neglecting the coupling between transverse and axial displacements, can be used to estimate the frequency of transverse vibration of an axially moving conveyor belt. In that case the maximum deviation from the measured frequency is  $\pm 5\%$ .

The response to direct excitation by the idlers can be determined through prescription of the time-dependent motion of the belt on the supports, whereas the response to parametric excitation can be determined approximately through prescription of the time-dependent pre-tension of the belt.

In Chapter 8 four methods have been used to analyse the dynamic behaviour of the belt, in particular to calculate the belt tension, during start-up.

In the first method, discussed in Section 8.5, the belt is assumed to be inextensible and the stationary belt tension is obtained by calculating the required stationary drive and tensioning force with a design standard. To approximate the transient belt tension, the stationary belt tension is multiplied by a factor that estimates the ratio between the start-up couple and the stationary couple of the drive system. However, this factor is only a rough approximation of the real ratio between the maximum drive couple during start-up and the stationary drive couple. The acceleration of the belt can be calculated from the constant transient belt tension and the constant total mass of the belt conveyor system. With this (constant) acceleration and the stationary belt speed, the start-up time can be calculated. Application of this procedure leads to overestimation of the start-up time since the real belt is elastic and the transient belt tension is not constant.

In the second method, also discussed in Section 8.5, the belt is still assumed to be inextensible. However, the real drive characteristics, as has been discussed in Chapter 6, are taken into account by application of a model where the drive system is

modelled correctly and where the belt is modelled by a flywheel which accounts for the inertia but not for the elasticity of the (loaded) belt, see also the equations (6.13) and (6.55). Based on the results obtained from the simulations using the third method, it can be concluded that application of this method to analyse a direct start-up results in overestimation of both the maximum belt tension and the start-up time. It is therefore not recommended to use this method since it does not yield more accurate results of a start-up than the previous method.

In the third method, as discussed in Section 8.6, belt elements as discussed in Chapter 7, which model the axial elastic response of the belt to general excitation, are introduced. To obtain accurate results from calculations with this model, a precise description of the motion resistances is required as has been discussed in Chapter 5. The most accurate model is achieved when finite elements that model both the axial and transverse elastic response of the belt are applied. From the simulations, described in Chapter 8, it was found that the application of nonlinear truss elements to model a belt segment enables an accurate calculation of the average axial strain and the average belt sag in that segment. The application of beam elements and of special idler supported beam elements to model a specific belt span supported by two idlers, enable the accurate calculation of the axial strain and the belt sag in that span.

The fourth method, discussed in Section 8.6.3, is used to approximate the minimum safety factor on the belt tension during start-up. Application of the start-up time, calculated with this method in case of a start-up procedure with constant acceleration of the considered 1 km long horizontal belt conveyor system, results in a smooth start-up.

### 10.4 Belt parameters

The belt parameters that govern the dynamic behaviour include the density of the belt material, Young's modulus, the flexural rigidity and the visco-elastic properties of the cover material.

The velocity of longitudinal waves is determined by Young's modulus and the density of the belt material. To reduce the influence of longitudinal waves on the dynamic behaviour of a belt system, the propagation speed should be as high as possible which can be achieved by application of a belt with a high stiffness, a low specific mass of the cover material and a low specific mass per unit strength of the carcass material. A high stiffness of a belt also reduces the size of the belt tensioner whereas a low specific mass reduces the motion resistances, in particular that of the unloaded return part.

To further reduce the motion resistances, in particular the indentation rolling resistance, the cover material of the selected belt should have a low loss factor.

In case of long belt conveyor systems, conveyor belts are selected not only on a low energy consumption of the belt, governed by the visco-elastic properties of the belt cover and the specific mass of the belt material, but on the splice efficiency as well.

### 10.5 Conclusions on the developed software system

Based on the experiences with the simplified methods to analyse the dynamics of belt systems and with the software system **TUDBELT**, the following conclusions can be drawn:

1. Complex finite element models, like used in **TUDBELT**, are most suitable to analyse accurately the non-linear dynamics of belt systems since they provide a flexibility that models based on other methods do not provide.
2. Belt segments can be modelled by truss or by beam elements. If an accurate calculation of the average axial strain and the average belt sag in a belt segment is required then the application of truss elements suffices. If an accurate calculation of the axial strain and the belt sag in a specific belt span supported by two idlers is required then the application of beam elements is necessary. The application of beam elements has three consequences that considerably increase the calculation time. Firstly, it requires the application of idler supported beam elements. This implies that on every time-step the model has to be reviewed to check whether or not a beam element leaves or enters the considered supported belt span and whether or not the belt is lifted off of the idlers. If that happens then the simulation is terminated and restarted with a rebuilt model. Secondly, application of beam elements decreases the step-size of the calculation process when an explicit routine is used for integration, due to the high natural frequencies of transverse vibration of beam elements, compared to the step-size of calculations with a model that consists only of truss elements. Thirdly, with the application of beam elements the number of degrees of freedom increases considerably and thus the size of all matrices and vectors. Therefore, beam elements should only locally be applied.
3. Although it is very useful to include a model of the complete drive system in the model of a belt system, the drive system should be modelled carefully to ensure that the calculation process is not unnecessarily slowed down due to high natural frequencies of drive system components.
4. The handling of the constraints, which describe for example the support of the belt by idler rolls or the coupling between different components of the drive system, by application of special finite elements with zero prescribed deformation parameters is very effective. Firstly, the description of those deformation parameters is close to the physical interpretation of the real belt support or coupling between

components. Secondly, since all the boundary conditions are handled in the same way, they can be fulfilled by one effective routine.

5. The greatest advantage of application of **TUDBELT** to analyse the non-linear dynamics of a belt system is that it enables an accurate determination of the influence of the different parameters on the dynamic behaviour of an entire system by parameter variation. This considerably enlarges the insight of the influence of the different parameters on the dynamic behaviour of that system.
6. The required belt strength can be calculated using either the stationary belt tension or the non-stationary belt tension multiplied by their respective safety factors. Since the non-stationary operation of a belt conveyor system can be influenced by the choice of the start-up or stopping procedure, it should be realised that a reduction of the required belt strength, and thus a reduction of the investment, can only be achieved if the non-stationary belt tension and the corresponding safety factor are used to calculate the minimum required belt strength. Application of any complex (time-consuming) method to determine the belt tension during non-stationary operation is therefore only profitable if the safety factor on the non-stationary belt tension may be used to select the minimum belt strength. If the stationary belt tension and corresponding safety factor are used to select the minimum belt strength then a simplified method suffices to estimate the belt tension during non-stationary operation.
7. The complexity of a software system increases until it exceeds the capacity of the programmer who maintains it. Therefore it is essential to simplify the storage structure of the model and calculation parameters. In **TUDBELT**, the object-oriented structure ensures that this storage structure is efficient, easily accessible and well maintainable. An important drawback of the object-oriented structure is that it slows down the calculation process due to the overhead of the three decomposition structures.
8. The accuracy of the simulations with a software system like **TUDBELT** depends on the accuracy of the required model parameters like the friction coefficients and the visco-elastic properties of the belt. It is therefore essential to perform detail experiments to determine those parameters.

## 10.6 Recommendations on model development

Based on the experiences with **TUDBELT** and the results of the simulations, the following recommendations are made:

1. To optimise the calculation process, it is useful to determine the influence of decoupling the storage of the calculation parameters from the remainder of the storage structure on the calculation speed. Coupling of the three decomposition

structures of the object-oriented structure decreases the calculation speed due to the accompanying overhead. It may be expected that decoupling will increase the calculation speed. Unfortunately it will also increase the effort required for rebuilding the model after a change in the boundary conditions.

2. For the simulation described in Section 8.6.3, a model has been built of a belt conveyor system where the belt was modelled by truss elements and beam elements (model 3 of Section 8.3). However, it may be more time-efficient to analyse first the global non-linear dynamic behaviour of the belt conveyor system and to use the results of this analysis to determine the local non-linear dynamic behaviour of idler supported belt spans. This requires a further development of **TUDBELT**.
3. The model of the indentation rolling resistance as described in Section 5.1 accounts only for the belt cover material. To be able to distinguish between belts with different carcass materials, the influence of the carcass on the indentation rolling resistance should be determined.
4. For the further improvement of the finite element model of belt conveyor systems in **TUDBELT** it is recommended, provided that it will not result in excessive long calculation times, that the following options are (locally) included:
  1. the influence of the trough shape on the dynamic behaviour of the belt by application of plate elements instead of beam elements to model the belt. Hereby the influence of the deformation of the cross sectional area of the belt during passage of an idler on the motion resistance can be included.
  2. a model of the rolling resistance of pipe belts and cable belts.
  3. a description of the motion resistances of air supported and cable supported belts.
  4. a separate model of the bulk solid material on the belt by application of special finite elements. This will enable the determination of the motion of the bulk material on the belt, in particular the coupling between the axial motion of the belt and the bulk material during non-stationary operation and in the feed chute, and also enables the determination of the influence of the deformation of the cross sectional area of the bulk material during passage of an idler on the motion resistance.
  5. the description of the drive/contact phenomena between drive pulley and belt. This will for example enable the analysis of the performance of multi-drive systems.
  6. a feedback control algorithm to control the start-up and stopping of belt systems driven by systems including a CST or fluid coupling.

# Appendix A

## Distribution of the belt and bulk mass

The motion resistances depend mainly on the idler loads, caused by the gravity load of the belt and bulk material, and the distribution of these loads over the rolls of an idler station.

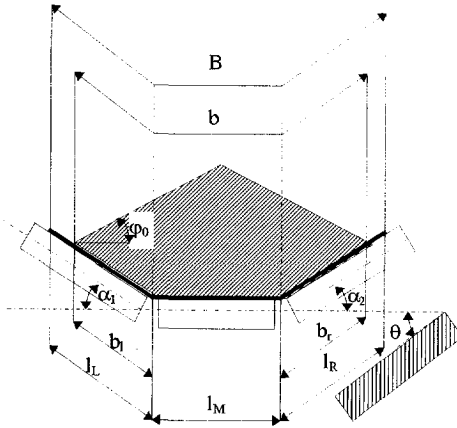


Figure A.1: Geometry of a three-roll idler station.

The total idler load caused by the weight of the conveyor belt can be calculated by multiplying the idler spacing  $L$  and the specific mass of the belt material accounting for the belt sag:

$$F_{TG,belt} = m'_{belt} g L \left( 1 + \frac{8}{3} K_s^2 \right) \tag{A.1}$$

where the specific mass is equal to:

$$m'_{belt} = B d_b \rho_{belt} \tag{A.2}$$

and the factor  $\left( 1 + \frac{8}{3} K_s^2 \right)$  accounts

for the (static) belt sag assuming the bending stiffness to be small. The forces normal to the left, middle and right roll of a three-roll idler station, as shown in Figure A.1, denoted by subscript L, M and R, are:

$$F_{NG,beltL} = \frac{l_L}{B} \cos(\alpha_1 + \theta) F_{TG,belt} \tag{A.3a}$$

$$F_{NG,beltM} = \frac{l_M}{B} \cos\theta F_{TG,belt} \tag{A.3b}$$

$$F_{NG,beltR} = \frac{l_R}{B} \cos(\alpha_2 - \theta) F_{TG,belt} \quad (A.3c)$$

where  $l_L$ ,  $l_M$  and  $l_R$  are the widths of the belt parts supported by the indicated rolls,  $B$  the total belt width,  $\theta$  the super-elevation angle of the idler station, and  $\alpha_1$  and  $\alpha_2$  the trough angles.

The calculation of the idler load caused by the weight of the bulk material is more complicated. The cross sectional area of the bulk material can be calculated from the capacity  $C$  [ $\text{kg}\cdot\text{s}^{-1}$ ]:

$$A_{\text{bulk}} = \frac{C}{V_b \rho_{\text{bulk}}} \quad (A.4)$$

Starting from a known belt speed  $V_b$ , the capacity of a belt conveyor is limited by the maximum of the cross sectional area of the bulk material on the belt. This maximum is prescribed by standards like DIN 22101. For a three-roll idler station this standard maximises the bulk solid width on the belt to  $b = 0.9B - 0.05$  [m]. Accounting for this maximum width and with use of Figure A.1 the following maximum cross sectional area can be obtained for a symmetrical idler station ( $\alpha_1 = \alpha_2 = \alpha$ ,  $b_r = b_l = b_z$ ,  $\theta = 0$ ):

$$A_{\text{bulk,max}} = (l_M + b_z \cos \alpha) b_z \frac{\sin(\alpha + \varphi_0)}{\cos \varphi_0} + \frac{l_M^2}{4} \tan \varphi_0 \quad (A.5)$$

where  $\varphi_0$  is the so-called angle of surcharge of the bulk material; it is the angle between the horizontal and the surface of the material while it is at rest on a moving belt conveyor. For the capacity of profiled conveyor belts see for example Lodewijks (1995). With the bulk solid area (A.5) the maximum idler load due to the mass of the bulk solid material is:

$$F_{TG,bulk} = m'_{\text{bulk}} g L \quad (A.6)$$

where the specific mass of the bulk material is:

$$m'_{\text{bulk}} = A_{\text{bulk}} \rho_{\text{bulk}} \quad (A.7)$$

The distribution of this force over the three rolls of the idler station depends not only on the geometry of the idler station but also on the bulk material mechanics as well. During the passage of an idler station the cross sectional area of the bulk solid



material is deformed and relaxed. Due to this deformation/relaxation behaviour of the bulk material extra forces are exerted on the rolls. Krause and Hettler (1974) derived expressions for the total bulk material forces normal to the idler rolls assuming that:

1. one idler supports a bulk solid material segment of length  $L/2$  ahead of the idler which is relaxing and a segment of length  $L/2$  in front of the idler which is deforming.
2. the bulk solid material is cohesionless and granular
3. the deformation and relaxation of the bulk material cause internal shear
4. the cross sectional area of the bulk material is symmetrical

The force normal to the left, middle and right roll are according to Krause and Hettler (1974):

$$F_{NG,bulkL} = F_{NG,bulkR} = \frac{1}{4} g \rho_{bulk} L b_z^2 (\lambda_o + \lambda_c) \cos\varphi_w$$

$$F_{NG,bulkM} = F_{TG,bulk} - \frac{1}{2} L \rho_{bulk} g b_z^2 \left[ \begin{array}{l} \lambda_c \cos(\alpha + \varphi_w) + \lambda_o \cos(\alpha - \varphi_w) \\ -(\lambda_c + \lambda_o) \sin\varphi_w \sin\alpha - (\lambda_c + \lambda_o) \mu_{br} \cos\varphi_w \sin\alpha \end{array} \right]$$

(A.8)

where

$$\lambda_o = \left( \frac{\sin(\alpha + \varphi)}{\sqrt{\sin(\alpha - \varphi_w)} + \sqrt{\frac{\sin(\varphi_w + \varphi)\sin(\varphi - \varphi_o)}{\sin(\alpha + \varphi_o)}}} \right)^2$$

(A.9a)

$$\lambda_c = \left( \frac{\sin(\alpha - \varphi)}{\sqrt{\sin(\alpha + \varphi_w)} - \sqrt{\frac{\sin(\varphi_w + \varphi)\sin(\varphi + \varphi_o)}{\sin(\alpha + \varphi_o)}}} \right)^2$$

(A.9b)

In the equations (A.8) and (A.9),  $\varphi$  is the internal friction angle of the bulk material,  $\varphi_w$  the friction angle between the bulk material and the belt,  $\mu_{br}$  the friction factor between the belt and the roll and  $\lambda_o$  and  $\lambda_c$  are the bulk solid resistance ratios. The

equations (A.8) and (A.9) are only valid if  $\varphi_0 \leq \varphi$  and  $\alpha \geq \varphi_w$  and, in case of relaxation of the cross sectional area [Krause and Hettler, 1974], for internal shear angles:

$$\varphi_s < \operatorname{atan} \left( \frac{K_o \sin \varphi_0 - \sin \varphi}{K_o \cos \varphi_0 - \cos \varphi} \right) \quad (\text{A.10a})$$

where

$$K_o = \frac{\sqrt{\lambda_o \sin(\alpha - \varphi_w)}}{\sin(\alpha + \varphi_0)} \quad (\text{A.10b})$$

In case of deformation of the cross sectional area,  $\varphi_s$  should satisfy the inequality:

$$\varphi_s < \operatorname{atan} \left( \frac{K_c \sin \varphi_0 + \sin \varphi}{K_c \cos \varphi_0 - \cos \varphi} \right) \quad (\text{A.11a})$$

where

$$K_c = \frac{\sqrt{\lambda_c \sin(\alpha + \varphi_w)}}{\sin(\alpha + \varphi_0)} \quad (\text{A.11b})$$

For a non-symmetrical cross sectional area similar expressions can be derived.

## References

Krause, F. and Hettler, W. (1974), "Die Belastung der Tragrollen von Gurtbandförderern mit dreiteiligen Tragrollenstationen infolge Fördergurt unter Beachtung des Fördervorganges und der Schüttguteigenschaften", *Wissenschaftliche Zeitschrift der Technische Hochschule Otto von Guericke Magdenburg* 18, pp. 667-674.

Lodewijks, G. (1995), "De capaciteit van geprofileerde transportbanden (in Dutch)", *BULK* 3(3), pp. 42-47.

## Appendix B

# Experimental data

---

In this appendix the data obtained from the experiments as discussed in Chapter 9 are given. The Tables B.1-B.12 present the data obtained from experiments with the belts EP 120/1, EP 200/2, EP 240/2 and EP 360/2. In the tables the following parameters are given:

$L$	the idler spacing	[m]
$F_v$	the pre-tension force	[N]
$V_b$	the belt speed	[m.s <sup>-1</sup> ]
$F_d$	the drive force	[N]
$\sigma_a$	the standard deviation of the amplitudes of transverse vibration	[m]
$\delta$	the belt sag	[m]
$a^*L$	the difference between the maximum and minimum vertical displacement $v$ of the first vibration cycle	[m]
$\zeta$	the damping factor	[-]
$f$	the measured frequency of transverse vibration	[Hz]

**B.1 Experimental data conveyor belt EP 120/1**

L [m]	F <sub>v</sub> [N]	V <sub>b</sub> [m/s]	F <sub>d</sub> [N]	σ <sub>a</sub> [mm]	δ [mm]	a L [mm]	ζ [%]	f [Hz]
0.8	189.27	11.99	57.69	0.28	1.95	37.46	2.65	11.88
		10.00	52.56	0.31	1.92	36.26	1.12	12.32
		8.00	50.38	0.30	1.92	33.72	1.34	12.80
		6.01	48.20	0.29	1.86	39.33	2.29	12.96
		3.99	44.44	1.25	1.95	39.36	4.11	13.10
		2.00	40.21	0.30	1.96	37.27	2.91	13.39
		0.00	17.20	0.08	2.11	12.89	1.08	13.31
L [m]	F <sub>v</sub> [N]	V <sub>b</sub> [m/s]	F <sub>d</sub> [N]	σ <sub>a</sub> [mm]	δ [mm]	a L [mm]	ζ [%]	f [Hz]
0.8	321.29	12.01	49.55	0.23	1.52	25.20	2.31	15.68
		10.01	46.13	0.25	1.46	19.52	1.21	15.91
		8.01	44.49	0.28	1.48	21.00	1.73	16.13
		6.00	39.21	0.40	1.44	23.61	3.06	16.28
		4.00	37.91	0.28	1.38	25.72	1.67	16.36
		1.99	31.89	0.27	1.52	27.91	1.98	16.41
		0.00	-2.03	0.08	1.55	23.13	1.71	16.70
L [m]	F <sub>v</sub> [N]	V <sub>b</sub> [m/s]	F <sub>d</sub> [N]	σ <sub>a</sub> [mm]	δ [mm]	a L [mm]	ζ [%]	f [Hz]
0.8	440.20	12.00	67.43	0.20	1.34	21.84	1.07	18.50
		9.99	61.15	0.26	1.27	26.30	1.17	18.97
		8.00	55.55	0.30	1.29	35.65	2.44	19.25
		6.00	51.71	0.45	1.24	29.63	2.05	19.36
		3.99	49.41	0.31	1.20	31.54	3.05	19.40
		2.00	44.76	0.30	1.24	29.11	2.39	19.45
		0.00	5.57	0.07	1.29	27.61	1.14	19.40
L [m]	F <sub>v</sub> [N]	V <sub>b</sub> [m/s]	F <sub>d</sub> [N]	σ <sub>a</sub> [mm]	δ [mm]	a L [mm]	ζ [%]	f [Hz]
0.8	558.35	12.00	61.84	0.23	1.04	32.52	1.79	20.69
		10.00	58.15	0.28	1.05	28.65	1.63	20.94
		8.00	52.69	0.30	1.05	24.02	2.13	21.26
		6.00	49.53	0.35	0.99	29.09	1.51	21.51
		4.00	48.48	0.33	0.94	28.21	1.81	21.60
		2.00	43.13	0.31	1.04	22.31	1.90	21.73
		0.00	0.73	0.08	1.02	18.36	1.44	21.98

**Table B.1:** Experimental data of belt EP 120/1 with idler spacing L=0.8 m.

L [m]	F <sub>v</sub> [N]	V <sub>b</sub> [m/s]	F <sub>d</sub> [N]	σ <sub>a</sub> [mm]	δ [mm]	a L [mm]	ζ [%]	f [Hz]
1.2	189.27	11.99	57.96	0.38	3.10	50.85	3.05	8.16
		10.00	51.02	0.37	3.25	40.69	5.13	8.43
		8.00	48.71	0.41	3.31	41.13	7.20	8.61
		6.00	45.14	0.44	3.24	47.45	4.79	8.84
		3.99	42.43	0.40	3.26	52.01	5.91	8.97
		2.00	38.01	0.37	3.31	52.29	2.80	8.98
		0.00	8.09	0.07	3.82	44.63	3.18	8.87
L [m]	F <sub>v</sub> [N]	V <sub>b</sub> [m/s]	F <sub>d</sub> [N]	σ <sub>a</sub> [mm]	δ [mm]	a L [mm]	ζ [%]	f [Hz]
1.2	321.29	11.99	52.40	0.30	2.04	51.83	2.10	10.40
		9.99	48.08	0.31	2.05	48.50	2.62	10.70
		7.99	44.28	0.32	2.06	42.38	1.86	10.80
		5.99	42.11	0.32	2.07	44.79	2.18	11.04
		4.00	40.81	0.49	2.12	45.94	3.03	11.06
		2.00	35.74	0.33	2.07	48.79	2.60	11.12
		0.00	7.43	0.06	2.45	51.69	1.86	11.33
L [m]	F <sub>v</sub> [N]	V <sub>b</sub> [m/s]	F <sub>d</sub> [N]	σ <sub>a</sub> [mm]	δ [mm]	a L [mm]	ζ [%]	f [Hz]
1.2	440.20	12.00	63.03	0.33	2.50	50.94	3.43	12.23
		10.00	55.92	0.34	2.75	32.26	2.84	12.39
		8.00	51.87	0.43	2.90	42.31	4.96	12.71
		6.00	49.20	0.34	3.01	44.66	2.65	12.77
		3.99	44.17	0.62	2.99	41.45	3.21	12.87
		2.01	39.04	0.29	3.20	37.95	0.94	12.93
		0.00	8.89	0.06	3.34	30.78	3.04	12.66
L [m]	F <sub>v</sub> [N]	V <sub>b</sub> [m/s]	F <sub>d</sub> [N]	σ <sub>a</sub> [mm]	δ [mm]	a L [mm]	ζ [%]	f [Hz]
1.2	558.35	12.00	46.76	0.26	2.66	38.61	2.12	13.82
		10.01	41.85	0.33	2.66	38.82	1.67	13.94
		8.00	37.41	0.30	2.63	39.49	2.24	14.06
		6.00	36.25	0.34	2.60	35.37	1.41	14.15
		3.99	31.92	0.38	2.59	36.32	2.93	14.44
		2.00	27.49	0.34	2.55	40.28	2.95	14.70
		0.00	-11.09	0.05	2.60	36.98	2.40	14.62

Table B.2: Experimental data of belt EP 120/1 with idler spacing L=1.2 m.

L [m]	F <sub>v</sub> [N]	V <sub>0</sub> [m/s]	F <sub>a</sub> [N]	σ <sub>a</sub> [mm]	δ [mm]	a L [mm]	ζ [%]	f [Hz]
1.6	189.27	12.01	67.90	0.41	6.45	59.90	5.75	6.10
		10.00	63.03	0.45	6.44	61.11	4.28	6.27
		8.00	60.31	0.46	6.46	69.37	5.64	6.51
		5.99	58.63	0.51	6.34	46.73	3.96	6.67
		3.99	54.30	0.51	6.40	66.77	3.70	6.79
		2.00	48.58	0.60	6.53	61.57	3.31	6.81
		0.00	24.97	0.06	6.88	66.04	2.86	6.70
L [m]	F <sub>v</sub> [N]	V <sub>0</sub> [m/s]	F <sub>a</sub> [N]	σ <sub>a</sub> [mm]	δ [mm]	a L [mm]	ζ [%]	f [Hz]
1.6	321.29	12.00	56.73	0.36	4.36	51.61	3.00	7.95
		10.00	50.84	0.32	4.38	51.14	2.55	8.12
		8.00	46.54	0.46	4.41	54.63	2.72	8.28
		6.00	45.58	0.33	4.40	56.84	2.54	8.43
		4.00	42.50	0.40	4.44	48.06	1.57	8.47
		1.99	36.18	0.24	4.48	65.26	2.34	8.50
		0.00	6.47	0.07	4.20	65.95	1.88	8.56
L [m]	F <sub>v</sub> [N]	V <sub>0</sub> [m/s]	F <sub>a</sub> [N]	σ <sub>a</sub> [mm]	δ [mm]	a L [mm]	ζ [%]	f [Hz]
1.6	440.20	12.01	60.44	0.28	3.59	53.68	2.12	9.32
		10.00	55.67	0.31	3.57	62.14	2.06	9.52
		8.00	50.94	0.34	3.61	54.62	1.80	9.67
		6.01	47.53	0.33	3.64	61.22	2.87	9.78
		4.00	44.24	0.39	3.60	62.48	2.37	9.81
		2.00	38.07	0.34	3.61	61.67	2.65	9.84
		0.00	-0.53	0.05	3.36	43.76	1.55	9.45
L [m]	F <sub>v</sub> [N]	V <sub>0</sub> [m/s]	F <sub>a</sub> [N]	σ <sub>a</sub> [mm]	δ [mm]	a L [mm]	ζ [%]	f [Hz]
1.6	558.35	12.01	59.21	0.29	2.90	40.99	2.58	10.43
		10.00	54.06	0.37	2.92	39.86	2.21	10.64
		7.99	49.85	0.33	2.96	39.90	2.41	10.81
		6.01	47.62	0.36	2.93	43.01	2.27	10.88
		4.01	44.66	0.42	2.97	26.14	4.51	10.94
		1.99	38.60	0.35	2.97	52.21	5.44	11.13
		0.00	-1.67	0.06	3.17	36.14	1.96	11.04

Table B.3: Experimental data of belt EP 120/1 with idler spacing L=1.6 m.

**B.2 Experimental data conveyor belt EP 200/2**

L [m]	F <sub>v</sub> [N]	V <sub>b</sub> [m/s]	F <sub>d</sub> [N]	σ <sub>s</sub> [mm]	δ [mm]	a L [mm]	ζ [%]	f [Hz]
0.8	189.27	12.01	84.02	0.61	3.32	35.08	5.56	6.75
		9.99	78.72	0.45	3.46	32.68	4.96	7.11
		8.00	72.09	0.74	3.23	32.59	2.84	7.39
		6.00	69.45	0.53	3.21	30.70	3.18	7.79
		4.00	65.73	0.87	3.18	38.91	2.43	8.05
		2.01	58.26	0.54	3.34	32.44	3.65	8.14
		0.00	0.35	0.19	3.71	28.14	3.79	8.03
L [m]	F <sub>v</sub> [N]	V <sub>b</sub> [m/s]	F <sub>d</sub> [N]	σ <sub>s</sub> [mm]	δ [mm]	a L [mm]	ζ [%]	f [Hz]
0.8	321.29	12.01	99.11	0.66	1.44	23.27	3.44	8.76
		10.01	91.08	0.43	1.34	31.17	2.62	9.24
		8.00	86.10	0.50	1.31	32.91	3.14	9.61
		5.99	82.21	0.63	1.30	25.81	2.57	9.98
		3.99	77.75	0.93	1.29	16.80	1.35	10.19
		2.00	70.56	0.43	1.21	22.92	2.08	10.32
		0.00	19.15	0.08	0.86	22.99	1.64	10.41
L [m]	F <sub>v</sub> [N]	V <sub>b</sub> [m/s]	F <sub>d</sub> [N]	σ <sub>s</sub> [mm]	δ [mm]	a L [mm]	ζ [%]	f [Hz]
0.8	440.20	12.00	106.32	0.69	1.00	27.45	2.41	10.37
		10.01	99.61	0.36	0.85	25.29	2.27	10.81
		8.00	93.93	0.42	0.83	26.67	1.85	11.21
		6.01	89.37	0.79	0.80	28.60	1.69	11.49
		3.99	84.51	0.43	0.69	25.87	1.85	11.76
		2.02	79.15	0.41	0.59	24.39	1.84	11.94
		0.00	10.65	0.07	0.31	18.33	1.39	11.93
L [m]	F <sub>v</sub> [N]	V <sub>b</sub> [m/s]	F <sub>d</sub> [N]	σ <sub>s</sub> [mm]	δ [mm]	a L [mm]	ζ [%]	f [Hz]
0.8	558.35	12.01	110.07	0.39	0.58	16.61	2.23	11.79
		9.99	102.05	0.46	0.45	14.45	1.61	12.21
		8.00	95.13	0.43	0.49	20.22	1.66	12.54
		5.99	90.87	0.50	0.46	19.48	1.30	12.88
		3.99	86.17	0.61	0.48	20.52	2.81	13.08
		2.00	77.74	0.45	0.25	23.01	2.26	13.14
		0.00	6.42	0.10	0.37	19.23	1.21	12.95

Table B.4: Experimental data of belt EP 200/2 with idler spacing L=0.8 m.

L [m]	F <sub>v</sub> [N]	V <sub>b</sub> [m/s]	F <sub>d</sub> [N]	σ <sub>s</sub> [mm]	δ [mm]	a L [mm]	ζ [%]	f [Hz]
1.2	189.27	12.01	94.14	0.45	7.74	19.57	2.79	4.48
		10.01	88.21	0.85	7.84	23.24	2.63	4.68
		8.01	83.50	0.88	7.89	24.99	2.84	4.99
		6.01	80.24	1.35	8.24	30.21	3.09	5.16
		4.00	78.02	1.24	8.91	30.63	3.71	5.41
		2.00	71.22	0.72	8.06	32.08	3.08	5.51
		0.00	10.92	0.09	9.11	28.36	3.08	5.63
L [m]	F <sub>v</sub> [N]	V <sub>b</sub> [m/s]	F <sub>d</sub> [N]	σ <sub>s</sub> [mm]	δ [mm]	a L [mm]	ζ [%]	f [Hz]
1.2	321.29	12.01	100.48	0.62	4.45	20.61	3.60	5.62
		10.00	95.35	1.15	4.46	17.61	5.04	5.97
		8.00	88.58	0.55	4.38	18.83	2.52	6.29
		6.00	82.21	0.59	4.31	18.21	3.40	6.56
		4.00	79.29	0.61	4.47	22.90	2.41	6.73
		2.00	72.13	1.90	4.39	21.33	3.10	6.84
		0.00	8.90	0.07	4.33	21.99	1.71	6.86
L [m]	F <sub>v</sub> [N]	V <sub>b</sub> [m/s]	F <sub>d</sub> [N]	σ <sub>s</sub> [mm]	δ [mm]	a L [mm]	ζ [%]	f [Hz]
1.2	440.20	12.00	115.78	0.50	2.94	22.05	3.10	6.70
		10.00	111.22	0.45	2.78	28.75	3.46	7.05
		8.00	105.29	0.65	2.72	42.84	2.15	7.39
		6.00	101.64	0.44	2.80	19.28	1.28	7.55
		4.00	97.76	1.66	2.74	28.22	1.52	7.76
		1.99	90.28	0.58	2.73	32.33	1.56	7.87
		0.00	27.35	0.078	2.53	12.16	0.85	7.86
L [m]	F <sub>v</sub> [N]	V <sub>b</sub> [m/s]	F <sub>d</sub> [N]	σ <sub>s</sub> [mm]	δ [mm]	a L [mm]	ζ [%]	f [Hz]
1.2	558.35	11.99	116.66	0.37	2.03	22.50	1.39	7.67
		10.00	111.09	0.44	1.95	40.03	2.02	7.99
		8.01	102.40	0.62	1.93	19.70	1.36	8.23
		6.00	96.08	0.43	1.92	22.17	1.43	8.44
		4.00	92.20	0.63	1.92	20.71	2.28	8.65
		2.01	84.46	0.51	1.92	22.69	1.45	8.73
		0.00	11.95	0.10	1.50	16.54	1.06	8.72

Table B.5: Experimental data of belt EP 200/2 with idler spacing L=1.2 m.



L [m]	F <sub>0</sub> [N]	V <sub>0</sub> [m/s]	F <sub>d</sub> [N]	σ <sub>a</sub> [mm]	δ [mm]	a L [mm]	ζ [%]	f [Hz]
1.6	189.27	12.00	85.12	0.75	15.84	14.87	2.85	3.28
		10.00	79.73	0.67	15.94	18.65	3.08	3.47
		8.00	76.02	0.99	15.95	19.39	2.79	3.72
		6.00	71.94	0.74	15.94	24.20	2.95	3.92
		3.99	67.57	2.38	16.13	30.31	3.09	4.05
		2.02	62.02	3.53	16.37	32.27	1.99	4.16
		0.00	7.12	0.09	17.03	37.38	2.65	4.13
L [m]	F <sub>0</sub> [N]	V <sub>0</sub> [m/s]	F <sub>d</sub> [N]	σ <sub>a</sub> [mm]	δ [mm]	a L [mm]	ζ [%]	f [Hz]
1.6	321.29	12.00	87.55	0.64	9.66	16.37	2.03	4.34
		10.00	80.64	1.23	9.91	22.25	2.29	4.56
		8.01	76.53	2.14	9.91	23.26	2.02	4.81
		6.00	71.87	0.75	9.83	23.52	2.09	4.93
		4.00	69.70	0.756	10.00	26.93	2.12	5.10
		1.99	61.79	1.29	9.88	45.77	2.14	5.15
		0.00	-6.79	0.08	9.82	21.81	2.16	5.18
L [m]	F <sub>0</sub> [N]	V <sub>0</sub> [m/s]	F <sub>d</sub> [N]	σ <sub>a</sub> [mm]	δ [mm]	a L [mm]	ζ [%]	f [Hz]
1.6	440.20	12.00	106.59	0.59	7.17	17.14	2.09	5.14
		10.01	100.49	0.63	7.19	21.25	2.15	5.35
		8.01	94.49	0.63	7.10	17.69	1.78	5.56
		6.00	89.16	0.79	7.17	18.75	1.21	5.74
		4.00	84.90	1.75	7.03	20.44	1.88	5.95
		1.99	75.85	1.25	7.04	23.03	3.08	6.00
		0.00	10.63	0.09	6.88	20.70	1.49	5.94
L [m]	F <sub>0</sub> [N]	V <sub>0</sub> [m/s]	F <sub>d</sub> [N]	σ <sub>a</sub> [mm]	δ [mm]	a L [mm]	ζ [%]	f [Hz]
1.6	558.35	12.00	109.67	0.48	5.54	13.27	1.32	5.85
		10.01	103.24	1.37	5.52	25.23	1.20	6.06
		7.99	97.81	0.61	5.53	11.42	1.91	6.26
		6.00	91.93	1.73	5.60	15.84	1.00	6.39
		4.00	87.70	1.86	5.62	10.42	2.45	6.58
		2.00	77.19	2.44	6.09	14.38	1.11	6.64
		0.00	-1.65	0.21	6.06	18.65	1.10	6.52

Table B.6: Experimental data of belt EP 200/2 with idler spacing L=1.6 m.

**B.3 Experimental data conveyor belt EP 240/2**

L [m]	F <sub>v</sub> [N]	V <sub>b</sub> [m/s]	F <sub>d</sub> [N]	c <sub>s</sub> [mm]	δ [mm]	a L [mm]	ζ [%]	f [Hz]
0.8	189.27	12.01	114.86	0.33	3.69	44.45	9.78	7.70
		10.00	104.10	0.45	3.76	48.93	6.78	8.06
		8.00	96.84	0.67	3.70	55.32	6.78	8.47
		6.01	91.37	0.89	3.57	48.54	5.99	8.74
		3.99	85.31	0.46	3.73	52.78	9.41	9.11
		2.00	70.97	0.47	3.67	45.80	4.84	9.37
		0.00	13.72	0.07	4.07	41.11	3.19	8.99
0.8	321.29	12.01	114.27	0.35	2.78	40.00	2.80	10.39
		10.01	106.61	0.74	2.67	39.86	2.31	10.59
		8.00	101.72	0.54	2.66	37.43	3.36	10.92
		6.00	93.33	0.71	2.60	29.77	3.24	11.22
		3.99	86.55	0.57	2.73	33.99	3.62	11.50
		1.98	73.66	0.44	2.58	32.80	2.03	11.75
		0.00	-5.32	0.08	2.95	38.14	2.02	11.31
0.8	440.20	12.01	126.16	0.30	2.31	35.72	1.83	12.05
		10.02	117.93	0.74	2.35	31.12	3.24	12.31
		8.01	109.10	0.36	2.27	34.36	1.81	12.61
		6.00	101.74	0.48	2.25	30.58	3.78	13.08
		4.00	97.08	1.06	2.27	35.00	2.61	13.33
		2.00	83.69	0.45	2.52	38.64	1.56	13.37
		0.00	-3.12	0.07	2.40	42.02	2.77	12.23
0.8	558.35	12.00	134.67	0.33	2.04	36.27	3.22	13.73
		10.00	127.06	0.70	2.03	30.06	1.91	13.98
		8.01	118.62	0.38	2.00	32.47	1.40	14.39
		6.00	110.80	0.36	1.98	27.55	2.28	14.63
		4.00	104.41	0.49	1.89	29.81	4.03	14.75
		1.99	92.91	0.41	1.93	34.16	4.11	14.79
		0.00	0.69	0.09	1.92	31.43	1.32	14.64

**Table B.7:** Experimental data of belt EP 240/2 with idler spacing L=0.8 m.

L [m]	F <sub>v</sub> [N]	V <sub>b</sub> [m/s]	F <sub>d</sub> [N]	σ <sub>s</sub> [mm]	δ [mm]	a <sup>*</sup> L [mm]	ζ [%]	f [Hz]
1.2	189.27	12.00	102.45	0.50	7.10	57.27	3.58	5.11
		10.00	95.53	0.50	7.09	59.71	5.02	5.39
		7.99	89.16	0.67	7.15	56.12	5.51	5.68
		6.00	85.58	0.80	7.16	63.29	3.77	5.81
		4.00	78.38	0.75	7.31	46.79	3.13	6.14
		2.00	67.84	0.76	7.28	54.12	4.30	6.22
		0.00	9.37	0.10	8.88	53.48	5.22	5.98
L [m]	F <sub>v</sub> [N]	V <sub>b</sub> [m/s]	F <sub>d</sub> [N]	σ <sub>s</sub> [mm]	δ [mm]	a <sup>*</sup> L [mm]	ζ [%]	f [Hz]
1.2	321.29	12.00	117.69	0.43	4.96	33.20	4.96	6.75
		9.99	108.93	0.45	4.95	38.14	3.31	7.06
		7.99	99.95	0.63	5.06	44.62	5.09	7.29
		5.99	93.65	0.56	5.01	42.89	2.16	7.51
		4.00	87.42	1.76	4.96	40.93	1.36	7.62
		1.98	74.19	0.69	5.05	54.25	3.66	7.74
		0.00	-3.33	0.09	6.10	51.23	4.70	7.39
L [m]	F <sub>v</sub> [N]	V <sub>b</sub> [m/s]	F <sub>d</sub> [N]	σ <sub>s</sub> [mm]	δ [mm]	a <sup>*</sup> L [mm]	ζ [%]	f [Hz]
1.2	440.20	11.99	149.10	0.49	4.46	51.70	3.74	8.02
		10.00	139.44	0.69	4.43	51.36	3.99	8.29
		7.99	131.11	0.68	4.40	55.47	3.34	8.55
		5.99	125.20	0.48	4.41	53.66	4.61	8.73
		3.99	117.71	0.70	4.45	44.41	4.82	8.84
		1.99	103.68	0.49	4.29	37.24	1.72	9.01
		0.00	12.15	0.10	4.78	47.26	1.18	8.65
L [m]	F <sub>v</sub> [N]	V <sub>b</sub> [m/s]	F <sub>d</sub> [N]	σ <sub>s</sub> [mm]	δ [mm]	a <sup>*</sup> L [mm]	ζ [%]	f [Hz]
1.2	558.35	12.01	144.06	0.62	3.88	37.80	1.36	9.05
		10.00	138.05	0.40	3.92	43.40	1.72	9.33
		8.01	128.91	0.47	3.99	31.77	3.44	9.48
		6.01	122.56	0.69	3.99	36.71	1.14	9.75
		4.00	116.06	0.45	4.11	36.58	2.56	9.89
		1.98	103.15	0.53	3.91	37.99	1.64	10.00
		0.00	8.61	0.06	4.18	38.90	1.62	9.65

Table B.8: Experimental data of belt EP 240/2 with idler spacing L=1.2 m.

L [m]	$F_t$ [N]	$V_b$ [m/s]	$F_d$ [N]	$\sigma_a$ [mm]	$\delta$ [mm]	a L [mm]	$\zeta$ [%]	f [Hz]
1.6	189.27	12.01	109.36	0.80	14.59	21.85	2.48	3.85
		9.99	102.13	0.62	14.68	22.33	3.23	4.05
		8.00	95.97	0.83	14.79	21.95	4.34	4.27
		6.00	91.69	1.48	14.83	22.17	2.38	4.43
		4.00	85.40	1.61	14.95	27.01	1.97	4.64
		1.99	70.71	0.90	14.98	28.91	2.30	4.74
		0.00	12.96	0.10	17.52	30.48	3.00	4.70
L [m]	$F_t$ [N]	$V_b$ [m/s]	$F_d$ [N]	$\sigma_a$ [mm]	$\delta$ [mm]	a L [mm]	$\zeta$ [%]	f [Hz]
1.6	321.29	12.01	122.24	0.73	10.22	15.08	2.25	5.04
		10.01	115.49	0.76	10.25	19.16	2.04	5.29
		8.01	107.96	0.83	10.38	18.51	1.70	5.48
		5.98	101.43	0.83	10.27	21.96	1.60	5.63
		3.98	94.27	1.77	10.23	21.24	2.59	5.82
		1.98	81.54	1.15	10.39	21.46	1.85	5.89
		0.00	14.27	0.10	9.99	19.35	1.59	5.73
L [m]	$F_t$ [N]	$V_b$ [m/s]	$F_d$ [N]	$\sigma_a$ [mm]	$\delta$ [mm]	a L [mm]	$\zeta$ [%]	f [Hz]
1.6	440.20	12.00	143.05	0.57	8.18	51.90	3.53	5.97
		10.01	134.02	0.75	8.17	47.68	3.66	6.14
		8.01	128.26	0.57	8.11	47.83	4.15	6.35
		6.00	121.40	0.72	8.06	50.25	3.17	6.52
		4.00	115.16	1.40	8.14	53.67	3.61	6.68
		1.98	102.89	2.25	8.21	48.67	3.77	6.72
		0.00	16.41	0.10	8.37	54.68	3.01	6.45
L [m]	$F_t$ [N]	$V_b$ [m/s]	$F_d$ [N]	$\sigma_a$ [mm]	$\delta$ [mm]	a L [mm]	$\zeta$ [%]	f [Hz]
1.6	558.35	12.01	133.66	0.76	7.07	29.07	1.85	6.71
		10.00	127.30	1.13	7.19	34.33	2.36	6.93
		7.99	119.44	0.45	7.09	39.99	2.45	7.11
		6.01	111.07	0.67	7.07	38.41	2.61	7.28
		3.99	104.59	0.85	7.06	41.15	1.85	7.42
		1.96	92.33	1.26	7.15	56.35	1.96	7.46
		0.00	6.25	0.07	7.07	28.36	1.78	7.30

Table B.9: Experimental data of belt EP 240/1 with idler spacing  $L=1.6$  m.

**B.4 Experimental data conveyor belt EP 360/3**

L [m]	F <sub>v</sub> [N]	V <sub>b</sub> [m/s]	F <sub>d</sub> [N]	σ <sub>a</sub> [mm]	δ [mm]	a L [mm]	ζ [%]	f [Hz]
0.8	189.27	12.01	98.64	0.36	2.74	7.45	1.80	7.72
		10.01	92.25	0.41	2.80	6.33	0.00	8.09
		7.99	86.12	0.51	2.87	12.60	0.00	8.61
		5.99	80.41	0.53	2.99	7.63	0.00	8.83
		4.00	77.38	0.72	2.90	6.43	0.00	9.37
		2.00	68.44	0.56	2.95	12.18	2.55	9.71
		0.00	-2.97	0.08	4.07	18.85	2.75	9.43
L [m]	F <sub>v</sub> [N]	V <sub>b</sub> [m/s]	F <sub>d</sub> [N]	σ <sub>a</sub> [mm]	δ [mm]	a L [mm]	ζ [%]	f [Hz]
0.8	321.29	12.02	112.99	0.41	1.51	22.12	2.42	10.20
		10.00	104.10	0.46	1.53	30.36	3.19	10.76
		8.00	97.25	0.44	1.64	20.54	1.89	11.14
		6.01	88.90	1.19	1.72	22.05	2.50	11.54
		3.98	85.61	0.86	1.68	22.16	2.12	11.76
		1.98	74.40	0.44	1.64	28.88	3.06	11.89
		0.00	5.15	0.06	1.82	3.96	2.05	11.52
L [m]	F <sub>v</sub> [N]	V <sub>b</sub> [m/s]	F <sub>d</sub> [N]	σ <sub>a</sub> [mm]	δ [mm]	a L [mm]	ζ [%]	f [Hz]
0.8	440.20	12.00	136.72	0.43	1.02	15.40	1.92	11.88
		9.99	135.71	0.57	1.10	14.72	2.76	12.41
		8.01	128.24	0.54	1.15	18.73	2.21	12.88
		6.00	121.42	0.82	1.19	15.52	1.78	13.33
		4.00	116.93	1.73	1.29	23.29	2.49	13.52
		2.00	107.37	0.38	1.37	9.44	1.53	13.56
		0.00	18.30	0.11	1.46	15.57	1.65	13.42
L [m]	F <sub>v</sub> [N]	V <sub>b</sub> [m/s]	F <sub>d</sub> [N]	σ <sub>a</sub> [mm]	δ [mm]	a L [mm]	ζ [%]	f [Hz]
0.8	558.35	12.02	135.54	0.48	0.58	25.38	2.27	13.60
		9.99	132.20	0.39	0.53	19.46	1.57	14.09
		8.01	123.51	0.44	0.65	21.98	2.32	14.49
		6.00	116.85	0.76	0.83	19.82	4.55	14.89
		4.00	113.28	0.58	0.73	20.32	1.50	15.03
		2.00	102.64	0.37	0.95	26.88	2.53	15.06
		0.00	15.59	0.09	0.79	13.45	1.55	14.89

**Table B.10:** Experimental data of belt EP 360/1 with idler spacing L = 0.8 m.

Appendix B

L [m]	F <sub>v</sub> [N]	V <sub>b</sub> [m/s]	F <sub>a</sub> [N]	σ <sub>a</sub> [mm]	δ [mm]	a L [mm]	ζ [%]	f [Hz]
1.2	189.27	12.01	120.36	0.47	6.52	15.52	1.56	5.07
		10.02	113.77	0.30	6.58	15.94	1.67	5.41
		7.99	107.92	0.64	6.79	22.48	3.08	5.67
		6.00	104.50	0.77	6.89	20.13	2.12	6.10
		3.99	98.99	0.85	7.07	47.37	3.72	6.28
		1.99	94.30	1.64	6.84	22.00	2.54	6.50
		0.00	34.48	0.09	8.10	22.58	3.64	6.31
L [m]	F <sub>v</sub> [N]	V <sub>b</sub> [m/s]	F <sub>a</sub> [N]	σ <sub>a</sub> [mm]	δ [mm]	a L [mm]	ζ [%]	f [Hz]
1.2	321.29	11.99	136.83	0.33	4.30	8.24	1.94	6.83
		9.99	130.51	0.41	4.40	7.65	3.61	7.22
		8.01	124.31	0.49	4.50	8.49	1.93	7.46
		6.00	122.76	0.42	4.71	9.29	2.67	7.67
		4.00	116.79	0.86	4.65	9.06	2.80	7.93
		1.98	108.94	0.61	4.58	8.17	1.73	8.00
		0.00	30.05	0.06	4.78	16.05	1.55	7.87
L [m]	F <sub>v</sub> [N]	V <sub>b</sub> [m/s]	F <sub>a</sub> [N]	σ <sub>a</sub> [mm]	δ [mm]	a L [mm]	ζ [%]	f [Hz]
1.2	440.20	12.00	128.14	0.39	2.87	4.82	0.00	7.99
		10.00	120.77	0.39	2.95	4.52	0.00	8.36
		8.02	114.24	0.46	3.00	5.91	0.00	8.56
		6.00	113.44	0.60	3.22	5.97	1.70	8.82
		4.00	102.46	1.02	3.09	5.98	0.00	8.87
		1.98	92.478	0.69	3.02	4.96	2.61	9.20
		0.00	2.35	0.07	2.96	7.12	1.95	9.10
L [m]	F <sub>v</sub> [N]	V <sub>b</sub> [m/s]	F <sub>a</sub> [N]	σ <sub>a</sub> [mm]	δ [mm]	a L [mm]	ζ [%]	f [Hz]
1.2	558.35	12.00	140.47	0.61	1.89	4.31	2.24	9.16
		10.00	133.22	0.40	1.85	3.79	1.92	9.45
		8.02	127.10	0.42	1.94	3.90	1.78	9.68
		6.00	118.72	0.68	2.06	5.45	1.76	9.90
		3.99	113.69	1.08	2.10	5.40	1.55	10.09
		1.99	100.84	0.52	2.03	3.28	1.58	10.17
		0.00	10.70	0.12	1.63	4.03	2.99	10.31

Table B.11: Experimental data of belt EP 360/1 with idler spacing L=1.2 m.

L [m]	F <sub>v</sub> [N]	V <sub>b</sub> [m/s]	F <sub>a</sub> [N]	σ <sub>a</sub> [mm]	δ [mm]	a L [mm]	ζ [%]	f [Hz]
1.6	189.27	12.01	101.44	0.32	12.58	18.54	4.74	3.87
		9.99	91.92	0.39	12.71	18.55	2.97	4.12
		7.98	86.55	0.37	12.81	23.30	2.81	4.39
		5.99	85.21	0.60	13.06	22.94	3.17	4.59
		3.97	81.03	1.15	13.11	31.11	2.70	4.68
		2.01	73.54	1.42	13.36	30.18	3.13	4.86
		0.00	5.75	0.06	14.00	24.28	2.46	4.90
1.6	321.29	11.99	120.63	0.34	8.04	13.43	1.38	5.06
		9.99	114.55	0.30	8.20	15.90	1.60	5.28
		7.99	108.03	0.40	8.29	16.84	1.58	5.51
		5.98	107.66	0.49	8.36	20.13	1.74	5.74
		3.98	100.33	0.84	8.34	22.65	2.22	5.81
		2.00	94.36	0.88	8.44	21.88	1.61	6.02
		0.00	12.19	0.06	9.25	19.84	1.81	5.89
1.6	440.20	12.00	132.68	0.91	5.72	9.84	0.88	5.95
		9.99	129.87	0.59	5.89	9.11	1.71	6.16
		7.99	122.24	0.44	5.99	8.00	1.45	6.44
		5.97	116.58	0.62	6.08	10.59	1.64	6.59
		3.59	109.07	0.99	6.11	13.05	0.93	6.73
		1.98	102.80	1.20	6.14	15.60	1.39	6.84
		0.00	18.66	0.06	6.68	12.16	1.12	6.72
1.6	558.35	12.02	137.92	0.29	4.56	7.79	3.02	6.80
		10.01	133.39	0.39	4.54	5.85	1.36	7.00
		8.00	126.84	1.34	4.64	11.29	1.16	7.23
		5.99	121.78	0.54	4.73	7.24	2.19	7.37
		3.98	113.03	1.10	4.68	13.18	1.31	7.54
		2.01	107.44	0.84	4.79	7.35	2.22	7.56
		0.00	12.15	0.06	4.95	11.76	1.53	7.47

Table B.12: Experimental data of belt EP 360/1 with idler spacing L=1.6 m.





## Appendix C

# Computational data

---

In this appendix the three analytical and the discrete approximations of the first frequency of transverse vibration of a stationary moving, idler supported, belt span, as discussed in Chapter 9, are given. The Tables C1-C4 present the data of belts EP 120/1, EP 200/2, EP 240/2 and EP 360/3. In the tables the following parameters are given:

$L$	the idler spacing	[m]
$F_v$	the pre-tension force	[N]
$V_b$	the belt speed	[m.s <sup>-1</sup> ]
$f_m$	the measured frequency	[Hz]
$f_{nl}$	the nonlinear frequency according to Thurman and Mote	[Hz]
$f_{ss1}$	the linear speed independent frequency	[Hz]
$f_{mb1}$	the linear speed dependent frequency	[Hz]
$f_1^k$	the nonlinear frequency according to Korde	[Hz]

## Appendix C

L [m]	F <sub>v</sub> [N]	V <sub>b</sub> [m/s]	f <sub>m</sub> [Hz]	f <sub>n</sub> [Hz]	f <sub>st</sub> [Hz]	f <sub>mt1</sub> [Hz]	f <sub>t</sub> <sup>*</sup> [Hz]
0.8	189.27	0	13.31	13.50	12.76	12.78	12.78
		4	13.10	12.88	13.21	12.73	13.22
		8	12.80	12.45	13.20	11.32	12.46
		12	11.88	10.54	13.42	8.97	11.23
L [m]	F <sub>v</sub> [N]	V <sub>b</sub> [m/s]	f <sub>m</sub> [Hz]	f <sub>n</sub> [Hz]	f <sub>st</sub> [Hz]	f <sub>mt1</sub> [Hz]	f <sub>t</sub> <sup>*</sup> [Hz]
0.8	558.35	0	21.98	22.81	21.91	21.92	21.94
		4	21.60	22.76	22.37	22.08	22.30
		8	21.26	22.63	22.41	21.23	21.86
		12	20.69	21.74	22.50	19.84	21.33
L [m]	F <sub>v</sub> [N]	V <sub>b</sub> [m/s]	f <sub>m</sub> [Hz]	f <sub>n</sub> [Hz]	f <sub>st</sub> [Hz]	f <sub>mt1</sub> [Hz]	f <sub>t</sub> <sup>*</sup> [Hz]
1.6	189.27	0	6.70	6.46	6.34	6.38	6.75
		4	6.79	6.69	6.62	6.37	6.87
		8	6.51	6.07	6.67	5.67	6.57
		12	6.10	5.68	6.73	4.49	5.76
L [m]	F <sub>v</sub> [N]	V <sub>b</sub> [m/s]	f <sub>m</sub> [Hz]	f <sub>n</sub> [Hz]	f <sub>st</sub> [Hz]	f <sub>mt1</sub> [Hz]	f <sub>t</sub> <sup>*</sup> [Hz]
1.6	558.35	0	11.04	11.57	10.95	10.96	11.02
		4	10.94	11.68	11.18	11.03	11.11
		8	10.81	11.27	11.20	10.61	10.98
		12	10.43	10.84	11.25	9.91	10.64

Table C.1: Computational data of belt EP 120/1.

L [m]	F <sub>v</sub> [N]	V <sub>b</sub> [m/s]	f <sub>m</sub> [Hz]	f <sub>n</sub> [Hz]	f <sub>st</sub> [Hz]	f <sub>mt1</sub> [Hz]	f <sub>t</sub> <sup>*</sup> [Hz]
0.8	189.27	0	8.03	7.79	7.55	7.87	8.03
		4	8.05	7.83	8.17	7.69	8.63
		8	7.39	7.14	8.23	5.46	7.15
		12	6.75	6.30	8.34	2.50	4.59
L [m]	F <sub>v</sub> [N]	V <sub>b</sub> [m/s]	f <sub>m</sub> [Hz]	f <sub>n</sub> [Hz]	f <sub>st</sub> [Hz]	f <sub>mt1</sub> [Hz]	f <sub>t</sub> <sup>*</sup> [Hz]
0.8	558.35	0	12.95	13.08	12.97	13.15	13.10
		4	13.08	13.01	13.42	13.12	13.32
		8	12.54	12.27	13.47	11.70	12.59
		12	11.79	11.28	13.55	9.37	11.22
L [m]	F <sub>v</sub> [N]	V <sub>b</sub> [m/s]	f <sub>m</sub> [Hz]	f <sub>n</sub> [Hz]	f <sub>st</sub> [Hz]	f <sub>mt1</sub> [Hz]	f <sub>t</sub> <sup>*</sup> [Hz]
1.6	189.27	0	4.13	3.88	3.77	3.82	4.19
		4	4.05	3.96	4.06	3.70	4.13
		8	3.72	3.38	4.10	2.53	3.32
		12	3.28	2.87	4.15	0.76	1.63
L [m]	F <sub>v</sub> [N]	V <sub>b</sub> [m/s]	f <sub>m</sub> [Hz]	f <sub>n</sub> [Hz]	f <sub>st</sub> [Hz]	f <sub>mt1</sub> [Hz]	f <sub>t</sub> <sup>*</sup> [Hz]
1.6	558.35	0	6.52	6.60	6.48	6.51	6.55
		4	6.58	6.48	6.74	6.51	6.63
		8	6.26	5.99	6.77	5.81	6.28
		12	5.85	5.44	6.80	4.62	5.62

Table C.2: Computational data of belt EP 200/2.

L [m]	F <sub>v</sub> [N]	V <sub>b</sub> [m/s]	f <sub>m</sub> [Hz]	f <sub>nl</sub> [Hz]	f <sub>st</sub> [Hz]	f <sub>mb1</sub> [Hz]	f <sub>1</sub> <sup>*</sup> [Hz]
0.8	189.27	0	8.99	9.17	8.34	8.43	8.80
		4	9.11	9.32	9.09	8.46	9.44
		8	8.47	7.84	9.21	6.43	8.51
		12	7.70	6.82	9.39	3.21	6.09
L [m]	F <sub>v</sub> [N]	V <sub>b</sub> [m/s]	f <sub>m</sub> [Hz]	f <sub>nl</sub> [Hz]	f <sub>st</sub> [Hz]	f <sub>mb1</sub> [Hz]	f <sub>1</sub> <sup>*</sup> [Hz]
0.8	558.35	0	14.64	14.89	14.32	14.38	14.48
		4	14.75	14.87	14.97	14.58	14.89
		8	14.39	13.69	15.06	13.34	14.32
		12	13.73	12.91	15.16	11.25	13.26
L [m]	F <sub>v</sub> [N]	V <sub>b</sub> [m/s]	f <sub>m</sub> [Hz]	f <sub>nl</sub> [Hz]	f <sub>st</sub> [Hz]	f <sub>mb1</sub> [Hz]	f <sub>1</sub> <sup>*</sup> [Hz]
1.6	189.27	0	4.70	4.80	4.17	4.18	4.30
		4	4.64	4.85	4.55	4.20	4.46
		8	4.27	3.96	4.60	3.17	3.88
		12	3.85	2.89	4.67	1.47	2.70
L [m]	F <sub>v</sub> [N]	V <sub>b</sub> [m/s]	f <sub>m</sub> [Hz]	f <sub>nl</sub> [Hz]	f <sub>st</sub> [Hz]	f <sub>mb1</sub> [Hz]	f <sub>1</sub> <sup>*</sup> [Hz]
1.6	558.35	0	7.30	7.57	7.16	7.17	7.23
		4	7.42	7.68	7.47	7.25	7.49
		8	7.11	6.92	7.52	6.64	7.19
		12	6.71	6.23	7.56	5.57	6.56

Table C.3: Computational data of belt EP 240/2.

L [m]	F <sub>v</sub> [N]	V <sub>b</sub> [m/s]	f <sub>m</sub> [Hz]	f <sub>nl</sub> [Hz]	f <sub>st</sub> [Hz]	f <sub>mb1</sub> [Hz]	f <sub>1</sub> <sup>*</sup> [Hz]
0.8	189.27	0	9.43	9.61	8.67	8.85	8.87
		4	9.37	9.59	9.64	9.04	9.30
		8	8.61	8.32	9.73	7.11	8.30
		12	7.72	7.01	9.86	3.96	6.10
L [m]	F <sub>v</sub> [N]	V <sub>b</sub> [m/s]	f <sub>m</sub> [Hz]	f <sub>nl</sub> [Hz]	f <sub>st</sub> [Hz]	f <sub>mb1</sub> [Hz]	f <sub>1</sub> <sup>*</sup> [Hz]
0.8	558.35	0	14.89	15.39	15.03	15.09	15.07
		4	15.03	15.42	15.68	15.31	15.54
		8	14.49	14.77	15.75	14.10	14.96
		12	13.60	13.22	15.82	12.07	13.91
L [m]	F <sub>v</sub> [N]	V <sub>b</sub> [m/s]	f <sub>m</sub> [Hz]	f <sub>nl</sub> [Hz]	f <sub>st</sub> [Hz]	f <sub>mb1</sub> [Hz]	f <sub>1</sub> <sup>*</sup> [Hz]
1.6	189.27	0	4.90	4.99	4.38	4.39	4.47
		4	4.68	4.58	4.79	4.46	4.76
		8	4.39	4.28	4.82	3.46	4.17
		12	3.87	3.48	4.90	1.85	3.07
L [m]	F <sub>v</sub> [N]	V <sub>b</sub> [m/s]	f <sub>m</sub> [Hz]	f <sub>nl</sub> [Hz]	f <sub>st</sub> [Hz]	f <sub>mb1</sub> [Hz]	f <sub>1</sub> <sup>*</sup> [Hz]
1.6	558.35	0	7.47	7.60	7.52	7.53	7.53
		4	7.54	7.68	7.85	7.65	7.76
		8	7.23	6.95	7.90	7.06	7.47
		12	6.80	6.51	7.93	6.03	6.92

Table C.4: Computational data of belt EP 360/3.



## Appendix D

# Measured belt properties

To determine the material parameters of a belt, a test specimen standardised in DIN 22102 and DIN 22109 has been used, see Figure D.1. The initial gauge length  $l_0$  is 100 mm. The geometry ensures a homogenous belt stress distribution in the middle of the specimen. To determine the tensile strength and failure strain, a tensile testing machine provided with special gripping wedges, which

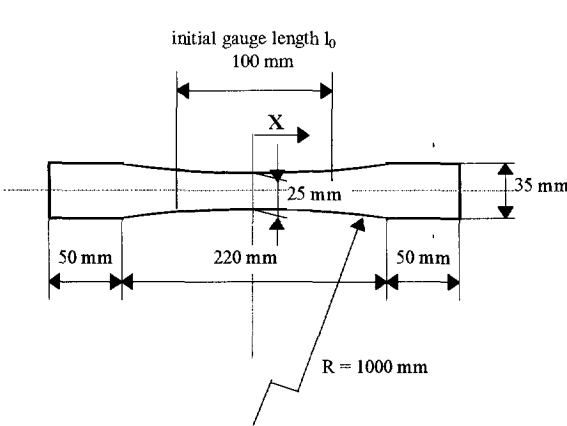


Figure D.1: Top view of DIN 22109 standard test specimen.

prevents slip of the specimen in the wedges, has been used. The rate of elongation of the specimen, standardised in DIN 22102, is 100 mm/min. To determine the influence of the strain rate on the tensile strength and failure strain also tensile tests at a rate of elongation of 50 mm/min and 200 mm/min have been performed. Besides tensile tests on the belt also tests on the belt splice have been carried out to determine the tensile strength and failure strain of the splice. Each test has been performed in threefold. For each belt the following data have been obtained:

- failure strain:  $\epsilon_b = \Delta l / l_0$
- failure stress:  $\sigma_b$
- tensile strength per unit width:  $k$
- effective (static) Young's modulus:  $E_b$
- failure stress of the belt splice:  $\sigma_{b,splice}$
- splice strength efficiency:  $\eta_{splice} = \sigma_{b,splice} / \sigma_b$

These data are listed in Table D.1.

	EP 120/1	EP 200/2	EP 240/2	EP 360/3
$\epsilon_b$ [%]	18.21	17.87	20.13	18.64
$\sigma_b$ [MPa]	60.61	44.09	58.24	80.53
$k$ [N.mm <sup>-1</sup> ]	109.10	246.49	259.15	341.46
$E_b$ [MPa]	319.71	210.28	294.80	390.26
$\sigma_{b,splice}$ [MPa]	12.99	23.74	17.95	34.96
$\eta_{splice}$ [%]	21.43	53.84	30.82	43.41

**Table D.1:** Conveyor belt data obtained from tensile test.

From the tensile tests the following conclusions can be drawn:

1. Performing the tensile test in threefold results in a standard deviation of the tensile strength of maximal 2.5 %. This accuracy is sufficient for this application.
2. The belts EP 120/1 (one fabric ply), EP 240/2 (two fabric plies) and EP 360/3 (three fabric plies) are provided with finger splices whereas belt EP 200/2 (two fabric plies) is provided with an overlap splice. The splice efficiency of an overlap splice is about  $n/n-1$ , where  $n$  is the number of carcass plies;  $\eta_{splice}$  is about 50 % for belt EP 200/2. The splice efficiency of a one-ply finger spliced belt (EP 120/1) is about 20 %. Every additional carcass ply in a finger spliced belt increases the splice efficiency with a factor 1.5;  $\eta_{splice}$  is about 30 % for belt EP 240/2 and about 45 % for belt EP 360/3. The splice efficiency of a finger splice is lower than the splice efficiency of an overlap splice.

To determine the relevant visco-elastic parameters, hysteresis experiments have been performed. The loading conditions during these experiments should include the loading conditions in the test facility. The four pre-tensions used during the experiments are given in Table 9.1. As follows from the tables in Appendix B, the maximum drive force is about 150 N. Adding half this maximum drive force to the pre-tension yields the belt tension in the idler supported belt part. Since the belt width is 200 mm, the belt force per unit width during the hysteresis experiments must be 1.3, 2.0, 2.6 and 3.2 [N/mm]. Two loading cycles can be distinguished. The first loading cycle is due to the motion of the belt through the conveyor. With a maximum belt speed of 12 m/s and an average belt length of 7 m this cycle has a frequency of 1.7 Hz. The second loading cycle originates from the transverse vibration of the belt during passage of the idler supported section. Due to the transverse displacement in this section an extra load is applied to the belt. The maximum measured frequency of the first transverse vibration is 22 Hz, see Appendix B. The additional belt strain due

to the transverse displacement can be estimated by using equation (7.11) where the maximum transverse displacement must be used instead of the belt sag. From Appendix B it follows that the average transverse displacement is about 1.5 % of the idler spacing for the first vibration. In that case the additional belt strain is about 0.06 %. With Young's modulus of the belt material and the given cross sectional area, the additional belt force is between 80 and 200 N. This is of the same order of magnitude as the drive force. However, after reduction of the amplitude of vibration to about one third of the amplitude of the first vibration, the additional belt strain is 0.0067 % and the additional belt force is between 9 and 22 N. Depending on the amplitudes of vibration either the frequency of drive force variation or the frequency of variation of the belt force due transverse vibration determines the frequency of the major load cycle. The amplitudes of vibration are large with respect to the belt sag and the frequency of the tension variation is twice the frequency of transverse vibration. Therefore the maximum frequency of the tension variation will be 44 Hz. Unfortunately, the maximum frequency of the tensile testing machine is 20 Hz. To determine the frequency dependency of the visco-elastic belt properties, hysteresis experiments have been performed at frequencies of 1, 10 and 20 Hz. Since the pre-stress of the belt is approximately equal to the minimum belt stress, the minimum belt stress during the hysteresis experiments was taken equal to the pre-stress. The maximum belt stress was equal to the sum of the pre-stress and the additional stress due to the transverse displacements. From the stress-controlled hysteresis experiments the following data are obtained:

- the loss angle  $\delta$
- the dynamic Young's modulus  $E_d$
- the storage modulus  $E'$
- the loss modulus  $E''$

See also Section 3.1.2. These data are listed in the Tables D.2 and D.3.

## Appendix D

EP 120/1				
f = 1 Hz				
pre tension [N/mm]	± 1.3	± 2.0	± 2.6	± 3.2
δ [rad]	0.0864	0.0789	0.0801	0.0744
E <sub>a</sub> [MPa]	413.47	441.19	483.70	505.09
E' [MPa]	411.93	439.82	482.15	503.70
E'' [MPa]	35.69	34.74	38.65	37.53
f = 10 Hz				
pre tension [N/mm]	± 1.3	± 2.0	± 2.6	± 3.2
δ [rad]	0.0908	0.0828	0.0771	0.0761
E <sub>a</sub> [MPa]	461.51	480.14	494.00	515.85
E' [MPa]	459.61	478.50	492.52	514.36
E'' [MPa]	41.85	39.72	38.06	39.20
f = 20 Hz				
pre tension [N/mm]	± 1.3	± 2.0	± 2.6	± 3.2
δ [rad]	0.0902	0.0878	0.0823	0.0787
E <sub>a</sub> [MPa]	479.40	510.22	520.41	547.30
E' [MPa]	477.41	508.63	518.64	545.61
E'' [MPa]	43.13	44.83	42.67	42.99
EP 200/2				
f = 1 Hz				
pre tension [N/mm]	± 1.3	± 2.0	± 2.6	± 3.2
δ [rad]	0.0963	0.0910	0.0875	0.0817
E <sub>a</sub> [MPa]	252.47	284.74	296.90	309.17
E' [MPa]	251.05	283.29	295.67	308.14
E'' [MPa]	26.76	28.69	26.94	25.23
f = 10 Hz				
pre tension [N/mm]	± 1.3	± 2.0	± 2.6	± 3.2
δ [rad]	0.1005	0.0894	0.0723	0.0622
E <sub>a</sub> [MPa]	265.60	282.14	313.23	355.78
E' [MPa]	264.26	281.09	307.42	355.09
E'' [MPa]	26.65	24.35	22.24	22.09
f = 20 Hz				
pre tension [N/mm]	± 1.3	± 2.0	± 2.6	± 3.2
δ [rad]	0.1008	0.0894	0.0735	0.0670
E <sub>a</sub> [MPa]	279.46	310.98	345.36	370.03
E' [MPa]	278.03	309.74	344.43	369.18
E'' [MPa]	28.15	27.76	25.31	24.74

**Table D.2:** Visco-elastic properties of conveyor belt EP 120/1 and EP 200/2 obtained from hysteresis tests.



EP 240/2				
f = 1 Hz				
pre tension [N/mm]	± 1.3	± 2.0	± 2.6	± 3.2
δ [rad]	0.1132	0.1087	0.1058	0.1030
E <sub>d</sub> [MPa]	321.76	363.77	394.12	418.46
E' [MPa]	319.70	361.63	391.91	416.24
E'' [MPa]	36.35	39.45	41.65	43.01
f = 10 Hz				
pre tension [N/mm]	± 1.3	± 2.0	± 2.6	± 3.2
δ [rad]	0.1198	0.1130	0.1063	0.1031
E <sub>d</sub> [MPa]	343.20	403.48	431.62	449.76
E' [MPa]	340.75	400.90	429.18	447.37
E'' [MPa]	40.99	45.51	45.80	46.35
f = 20 Hz				
pre tension [N/mm]	± 1.3	± 2.0	± 2.6	± 3.2
δ [rad]	0.1299	0.1213	0.1106	0.1127
E <sub>d</sub> [MPa]	361.57	425.59	445.61	468.60
E' [MPa]	358.51	422.46	442.88	465.63
E'' [MPa]	46.80	51.48	49.19	52.65
EP 360/3				
f = 1 Hz				
pre tension [N/mm]	± 1.3	± 2.0	± 2.6	± 3.2
δ [rad]	0.1035	0.0980	0.0942	0.0960
E <sub>d</sub> [MPa]	411.27	419.41	439.36	646.65
E' [MPa]	409.07	417.39	437.41	462.51
E'' [MPa]	42.48	40.95	41.31	44.54
f = 10 Hz				
pre tension [N/mm]	± 1.3	± 2.0	± 2.6	± 3.2
δ [rad]	0.1121	0.1042	0.1034	0.1034
E <sub>d</sub> [MPa]	424.89	439.91	468.14	484.17
E' [MPa]	422.15	437.52	465.63	481.57
E'' [MPa]	47.57	45.80	48.27	49.98
f = 20 Hz				
pre tension [N/mm]	± 1.3	± 2.0	± 2.6	± 3.2
δ [rad]	0.1104	0.1078	0.1090	0.1063
E <sub>d</sub> [MPa]	425.12	453.08	477.44	496.74
E' [MPa]	422.53	450.45	474.60	493.94
E'' [MPa]	46.71	48.71	51.94	52.70

Table D.3: Visco-elastic properties of conveyor belt EP 240/2 and EP 360/3 obtained from hysteresis tests.

From these experiments the following conclusions can be drawn:

1. Due to the low minimum belt strains of about 0.22 % till 0.67 %, and thus low belt stresses, the dynamic Young's modulus increases with increasing average belt stress. Above a belt strain of about 1.5 %, however, it decreases with increasing average belt stress, see also Figure 3.7.
2. Due to the visco-elastic character of the belt material, the dynamic Young's modulus increases with increasing strain rate or loading frequency.
3. The loss angle is small and decreases with increasing average belt stress. Therefore it is profitable, from an energy point of view, to have a high belt stress and a small cross section. The loss angle increases with increasing strain rate.
4. The relation between the dynamic Young's modulus, the loading frequency and the belt tension is almost linear within the indicated strain and frequency range.

To determine whether or not the loading conditions of the belts during the experiments are comparable to the normal loading conditions during stationary operation, the static belt sag ratio  $K_s$  and the actual safety factor  $S$  can be used. Normally the maximum static belt sag ratio  $K_s=1.5$  % and the maximum safety factor  $S=10$ . The minimum and maximum values of these parameters during the experiments are listed in Table D.4. The parameters in this table are calculated with use of the data given in the tables of Appendix B.

	$K_{s,min}$	$K_{s,max}$	$S_{min}$	$S_{max}$
EP 120/1	0.0003	0.0111	65.2	211.3
EP 200/2	0.0007	0.0088	115.5	380.4
EP 240/2	0.0024	0.0110	76.7	253.6
EP 360/3	0.0012	0.0043	40.8	126.8

Table D.4: Belt tension related conveyor belt parameters.

As can be seen in Table D.4, the belt sag ratio is lower than 1.5 %. However, the actual minimum safety factor is much higher than 10. The minimum safety factor is governed by the maximum belt tension which was limited by the drive power as stated in Section 9.2.3.

# Acknowledgements

---

**F**inishing a doctorate project like this is not possible without the encouragement and help of many people.

In particular I would like to thank the following people:

- My father, Johan Lodewijks, for teaching me the basic principles of transport engineering, encouraging me to continue studying as a graduate student and giving me the opportunity to use my skills in practice during the last ten years (without being fired).
- Professor dr. ir. F.J.C. Rademacher for teaching me the scientific approach of storing, handling and transporting bulk solid and his encouragement and assistance to find a position as a graduate student.
- Professor ir. M. van Holst for granting me a position as a graduate student in the section of Transport Technology, his amiable way of being a supervisor and for his confidence in a successful ending of this project.
- Professor dr. ir. P. Meijers for his valuable and much appreciated contribution to the project and for his meticulous reading of the manuscript.

I would also like to thank BANZO B.V., Dordrecht, Dunlop-Enerka B.V., Drachten, and FABREEKA Bandtransport b.v., Uitgeest, the Netherlands, for the free deliverance of components for the test facility; Sytze Brouwers and Hans de Vries of Dunlop Enerka B.V., Drachten, the Netherlands, for the interesting discussions we had during the last six years and their personal interest in my project; Arie Klein, Clemens van der Snoek, Rene de Jong and Jochem Wit, for all their assistance to the performance of the experiments; Arnold Gerstel, for his encouragement to publish the results of the project; Karel Drenth, for the valuable discussions we had on several belt conveyor related topics; Jacqueline Kalkman, for her secretarial support and her assistance to the organisation of the journeys I made last year; Josephine Spoek, for her secretarial support; Dick Buitenhek, Frans van der Meijden and Joop de Bruin,

---

for their support on the computational side of the project; Jan v.d. Maas; my roommates Shi Wei Tong and Hans Mascini; my paranimphs Wendy Mackus and Gerben Helder; my family and friends for their interest in my work and support in their own way.

Last, but certainly not least, I would like to thank my wife Katja for her encouragement and support to the completion of my project, her support to continue working in the field of transportation of bulk solids wherever that may be, and providing me with the best atmosphere to forget everything and just relax whenever that was necessary.

# Curriculum Vitae

---

**G**abriël Lodewijks was born in Apeldoorn, the Netherlands, on September 5, 1969. After graduating from the pre-university education (VWO) at the Christelijk Streeklyceum Ede in May 1987, he studied Mechanical Engineering at the University of Twente. In 1991 he continued this study at Delft University of Technology, from which he graduated in June 1992 (with honour). He continued his studies as a graduate student at the section of Transport Technology of Delft University of Technology where he wrote a thesis on the dynamics of belt systems and supervised a number of students on belt conveyor related subjects. He also was a lecturer of three industrial seminars and contributed to a number of international conferences. Since 1989 he co-operated as a consultant in several Dutch consultancies in the field of the development of bulk material handling systems and equipment. He will be employed as a project engineer at Conveyor Dynamics, Inc., Bellingham, Washington, USA.

---



---